University of Alberta

High Temperature Thermal Cracking of Heavy Oils

by

Kourosh Vafi

A thesis submitted to the Faculty of Graduate Studies and Research
in partial fulfillment of the requirements for the degree of

Doctor of Philosophy

Department of Chemical and Materials Engineering

Fall 2012
Edmonton, Alberta

Abstract

Thermal cracking of the vacuum residue fraction of bitumen and petroleum is an important feature of several refinery processes. At normal process temperatures, this fraction remains liquid, which favors coke formation. In order to understand the reaction yields and intrinsic reaction kinetics of this important material at temperatures above 600°C, innovative reactor designs and techniques were developed.

First, a microstructured mixer was used to rapidly heat reactants to nearly constant reaction temperatures in a few milliseconds. The reactor was tested by studying of the rate of the thermal cracking of n-hexadecane temperatures ranging from 600 to 750°C, at atmospheric pressure, and mean residence time of 110 to 170 milliseconds. The apparent activation energy and pre-exponential factor for the over all first order reaction was calculated as 235 kJ/mol and 1.1×10^{13} s^{-1} respectively, consistent with the majority of previous studies in the literature.

In order to minimize the role of the liquid phase in cracking of vacuum residue, an aerosol reactor was designed and constructed. Thermal cracking of Athabasca vacuum residue was studied at temperatures of 700 to 800°C at atmospheric pressure and residence time of 100 to 115 milliseconds. The feed was introduced as submicron droplets into the reactor. Alkenes were the dominant components among the gas products, with total yield of ethene and propene ranging from 5 to 18 wt %.The yield of coke was 6.3 wt% on average, and was insensitive to conversion of the vacuum residue. Both these observations were consistent with

the predominance of vapour-phase reactions. , The molar ratio of hydrogen to carbon decreased monotonically with conversion from 1.4 for unconverted feed to 0.98 at 78% conversion, consistent with high yields of hydrogen-rich gas products.

Acknowledgement

National Sciences and Engineering Research Council of Canada and Syncrude Research Ltd. were sponsors of this research. Dr. M.R. Gray was the supervisor of my PhD program. Dr. McCaffrey and Dr. Wanke were members of the supervisory committee. I had the benefit of consultation with Dr. Carlos Lange from the Department of Mechanical Engineering and with Dr. Vinay Prasad. Dr. Pfeifer helped with the design of the micro-structured mixer. Institute for micro-process engineering fabricated and supplied this device. During a course named advanced topics in chemical engineering, I used a software which was provided by Dr. Hayes to do some simulation case studies which gave me insight for reactor design for my PhD research work. The contribution of the chemists, technicians and technologist of the Department of Chemical and Materials Engineering, Department of Chemistry and the Department of Earth and Atmospheric Sciences should also be acknowledged. I would like to appreciate the quality of the consultation and services provided by the application engineering departments of Alpha Omega Technologies Inc. and Agilent Company (USA) with regard to instructions for diagnosis and repair of the gas chromatography instruments.

Table of Contents

List of Tables

Chapter 2

Chapter 3

Chapter 4

Chapter 5

Chapter 6

Chapter 7

Appendix D

Appendix F

List of Figures

Chapter 2

Chapter 3

Chapter 4

Chapter 5

Chapter 6

Chapter 7

residue is defined as the fraction with boiling point of 650°C+ and light residue by the fraction with boiling point range of 524 to 650°C. (Page 269)

Appendix A

Appendix B

Appendix C

Appendix D

List of Symbols, Nomenclature, and Abbreviations

The symbols, nomenclature and abbreviations are given in the body of the dissertation wherever they are used. However, the followings are given here for the convenience.

AVR Athabasca Vacuum Residue
BP Boiling point
MFC Mass Flow Controller
PAH Poly Aromatic Hydrocarbon
SSR Sum of Square of Residues
TGA Thermal Gravimetric Analysis
TRT Temperature Rise Time
$t_{0.5}$ Half-life of the reaction
VR Vacuum Residue

Chapter 1

Introduction

The western Canadian sedimentary basin contains 27.4 billion cubic meters (173 billion barrel) of crude bitumen reserves, which is the largest bitumen reserve in the world [1] and comparable in size with the oil reserves of major petroleum exporting countries. Increasing prices of conventional and lighter crude oil, together with anticipation of higher demand for energy and slow progress in exploration of new reserves [2] have made production and upgrading of heavier oils more economically attractive. Consequently, the oil industry has become interested in development of related processes and particularly refining processes of bitumen and residue fractions.

When organic compounds are heated to high temperatures, the carbon-carbon bonds break to give smaller fragments. This thermal cracking reaction is at the heart of all commercial technologies for upgrading or converting the heaviest fractions of petroleum, heavy oil, and bitumen. An equivalent term for this reaction is pyrolysis, from the Greek, while thermal decomposition has a similar usage. The term "thermal cracking" will be used throughout this thesis to describe the complex set of non-catalytic reactions that occur in oils at high temperatures, in excess of 350-400^{o}C.

The widely used commercial non-catalytic thermal cracking processes in upgrading of bitumen are visbreaking, delayed coking and fluid coking. Visbreaking is a thermal viscosity reduction process and is limited in the level of conversion of the feed. Delayed coking and fluid coking are coking processes which are designed to convert the residues to lighter products and coke. Introduction of hydrogen into residue conversion processes helps to suppress formation of coke. In presence of catalyst, hydrogenation of aromatics and olefins and removal of sulphur and nitrogen become possible.

Maximizing the quantity and quality of the liquid products together with minimizing the capital investment and operating costs have been a demand in upgrading of bitumen. Compared with hydroconversion processes, the coking processes require lower investment cost but their products are lower in quality and give high yields of coke. Since the commercialization of fluid coking, the goal for most of the next generation of these processes has been to reduce the vapor-phase residence time. Shorter residence time in the vapor phase reduces formation of light ends, which remove the hydrogen that is much more required for the liquid products. Residence time of the vapor phase can be reduced by making the reactors more compact. Compact reactor design can help to make the process commercially feasible, especially for upgrading at remote field locations.

The short-residence time approach requires higher reaction temperatures, above the upper end of the fluid-coking range and beyond. As the temperature is increased and the reactions in the liquid residue accelerate, the distribution of products is more ruled by the rate of heat transfer into the liquid feed and the rate of transport of cracked liquid products out of the liquid phase. The length of diffusion path of the cracked products in the liquid phase affects the product distribution and the yield of coke. The influence of heat and mass transfer processes prevent accurate prediction of liquid yield and quality as the reaction temperature increases and the residence time is reduced, because of the complex coupling of reaction kinetics and transport processes.

Developing higher temperature conversion reactors requires a knowledge of the kinetics of bitumen reactions and product distributions. This should be studied in absence of the masking influence of transport processes. Despite the attention which is paid and the interest in high temperature short residence time thermal cracking, few published reports have appeared in which the researchers tried to study the intrinsic kinetics of thermal cracking of bitumen and residues at such severe operating conditions. The kinetic studies in which the researchers considered the effect of heat and mass transfer were carried at temperatures below

550ºC. Other researchers who considered higher temperatures in their thermal cracking studies focused on reporting the product distribution without considering the effect of transport phenomena and the phase in which cracking occurred on their results or without reporting kinetic parameters for the rate of thermal cracking.

At high temperatures above 600ºC, the rate of thermal cracking is fast and the reactant should be brought to the desired reaction temperature before a significant portion converts to products. This has been a common challenge for most of the researchers who studied high temperature thermal cracking of heavy oils. A review of the works of previous researchers (Chapter 2) defines two major challenges in the study of high-temperature short-residence time thermal cracking:

- Minimization of the effect of heat and mass transfer in kinetic studies
- Fast rate of heat-up of the reactant to reaction temperature

This research work was intended to develop the required technologies to study thermal cracking of heavy oils by a combination of high temperatures, above 600°C, and short residence times in the order of 100 milliseconds. An experimental approach is adopted, however whenever it was required, appropriate theoretical tools were used to design the equipment or to interpret the results. The philosophy of the reactor design is explained in Chapter 3. The technology of micro-structured mixers and the concept of multi-lamination of the flow were used to meet the requirement for fast heat-up of the reactant to reaction temperature (Chapter 4). An innovative reactor was designed and constructed to bring the reactant to reaction temperature in a few milliseconds and for a close to ideal isothermal operation in a continuous flow reactor. The reactor was tested by measuring the rate of thermal cracking of n-hexadecane and comparing these data with the published results in the literature.

In order to minimize the interfering effects of mass and heat transfer with the kinetic studies of heavy oils with fractions which remained in the liquid phase at reaction temperature, a continuous flow aerosol reactor was designed , built and tested (Chapter 5). Aerosolization of feed to submicron feed particles was the main idea used to minimize the mass transfer resistance and consequently to minimize formation of the yield of coke and to maximize the conversion of the residue. Generation of such fine particles and introduction of these particles into the reactor became the most challenging part of this research work. The experimental efforts to achieve this goal were summarized in Chapter 5. In Chapter 8, the advantages and limitations of the current approach and design are discussed and technical recommendations for future studies or continuation of this research are given.

Chapter 2
Literature Survey

The focus of this research is on developing required technologies to study thermal cracking of heavy oils by a combination of high temperatures, above 600°C, and short residence time. This chapter, first reviews the free radical chain reaction of thermal cracking of hydrocarbons. The mechanism and kinetics of coke formation are then considered. Minimization of the yield of coke in favor of increasing the quantity of the liquid products has been always an important topic in upgrading of heavy oil. The commercial processes which use non-catalytic thermal cracking are then briefly reviewed to highlight the backgrounds for the industrial interest in short-contact time processes. The experimental reactors and the efforts of the previous researchers in the area of high temperature thermal cracking are reviewed to understand the challenges that they faced in the way of their studies and the limitations or benefits of their design for potential application to the reactor design in this research (design philosophy, Chapter 3). The reported data on the distribution of the products, yield of coke and rate of thermal cracking is also considered in the design philosophy. In a bench scale reactor atomization of vacuum residue without adding any solvent to reduce the viscosity is very challenging. Therefore, the reported interaction of the aromatic solvents with the feed in the thermal cracking reactions has also been reviewed.

2.1 Mechanisms and kinetics of thermal cracking

The description of thermal decomposition of *n*-alkanes by a chain mechanism of free radical reactions goes back to the publications of Rice and Herzfeld in 1934 [3] and Kosiakoff and Rice in 1943 [4]. The chain of free radical reaction in pyrolysis of *n*-alkanes in a very simplified form can be written as the following [5]:

Initiation:

$$M \xrightarrow{k_1} 2R^{\cdot} \quad (2.1)$$

Propagation:

Hydrogen abstraction $R^{\cdot} + M \xrightarrow{k_2} RH + M^{\cdot}$ (2.2)

β-scission $M^{\cdot} \xrightarrow{k_2} R^{\cdot} + A$ (2.3)

Termination: $Radical + Radical \xrightarrow{k_3} Products$ (2.4)

In which M and $M^{\cdot}$ represent the parent alkane and the corresponding radical respectively. RH and $R^{\cdot}$ are the lower alkanes and the corresponding alkyl radicals. A demonstrates an olefin.

Most pyrolysis reactions involve radicals but some purely molecular reactions may play a significant role. Neglecting of molecular reactions that occur simultaneously with radical reactions can result in misleading conclusion of the rate parameters, especially for olefins and diolefins [6] . Dente and Ranzi [6] categorized the elementary reactions of pyrolysis of hydrocarbons.

1. Chain-initiation reactions

   unimolecular:

   $R — R' \rightarrow R^{\cdot} + R'$ (2.5)

   example: $C_2H_6 \rightarrow 2\ CH_3^{\cdot}$ (2.6)

   Bimolecular (R′H is an unsaturated hydrocarbon)

   $RH + R'H \rightarrow R'' + R'''$ (2.7)

   example: $C_2H_6 + C_2H_4 \rightarrow 2\ C_2H_5^{\cdot}$ (2.8)

2. Hydrogen-abstraction (metathesis) reactions

$R^{\cdot} + R'H \rightarrow RH + R'$ (2.9)

Example: $CH_3^{\cdot} + C_2H_6 \rightarrow CH_4 + C_2H_5^{\cdot}$ (2.10)

3. Radical- decomposition reactions

$R^{\cdot} \rightarrow R'H + R''$ (2.11)

Example: $n\text{-}C_3H_7^{\cdot} \rightarrow C_2H_4 + CH_3^{\cdot}$ (2.12)

4. Radical - addition reactions to unsaturated molecules

$R^{\cdot} + R'H \rightarrow R''$ (2.13)

Example : $CH_3^{\cdot} + C_2H_4 \rightarrow n\text{-}C_3H_7^{\cdot}$ (2.14)

5. Chain-termination reactions

by recombination of radicals:

$R^{\cdot} + R' \rightarrow R — R'$ (2.15)

Example : $CH_3^{\cdot} + C_2H_5^{\cdot} \rightarrow n\text{-}C_3H_8$ (2.16)

By disproportionation of radicals:

$R^{\cdot} + R' \rightarrow RH + R''H$ (2.17)

Example : $C_2H_3^{\cdot} + C_2H_5^{\cdot} \rightarrow 2\ C_2H_4$ (2.18)

6. Purely molecular reactions

$RH + R'H \rightarrow R''H + R'''H$ (2.19)

Examples:

$C_2H_6 \rightarrow C_2H_4 + H_2$ (2.20)

1-pentene $\rightarrow C_2H_4 + C_3H_6$ (2.21)

1-3 hexadiene $\rightarrow$ *2-4 hexadiene (isomerization)* (2.22)

cyclohexane $\rightarrow C_2H_4 + C_4H_6$ (Diels-Alder dissociation) (2.23)

7. Radical isomerization

$R' \rightarrow R''$ (2.24)

Example: $CH_3CH_2CH_2CH_2^{\cdot} \rightarrow CH_3CH_2C^{\cdot}HCH_3$ (2.25)

Reaction (2.23) is reversible depending on the conditions. An additional class of intermolecular reactions is Diels–Alder cyclization reactions which are an important non-free radical pathway for addition-cyclization of dienes [7]. Although thermal cracking of bitumen and vacuum residue consist of a complex network of free radical reactions between a large numbers of molecules, experiments show that the over all thermal cracking reaction follows an apparent first-order kinetics [8].

2.2 The effect of phase in distribution of products in thermal cracking reactions

Khorasheh and Gray [9] studied the distribution of products of thermal cracking of *n*-hexadecane in a tubular flow reactor at 380 to 450°C and 13.9 MPa. They found that under high-pressure conditions, radical addition to α-olefins became significant. They reported the following products of addition reactions:

1. Formation of alkyl hexadecanes in the C_{18} to C_{31} range by addition of parent hexadecyl radicals to α-olefin.
2. Formation of higher *n*-alkanes by addition of lower primary alkyl radicals to α-olefins including *n*-C_{15} and n-C_{17}.
3. Addition of lower secondary alkyl radicals resulted in the formation of C_7 to C_{17} branched alkanes.

Wu et al. [10] compared product distribution and rate of thermal cracking in liquid and gas phase at low temperatures rangin from 330 to 375ºC. They used glass ampoule as the reactor with estimated initial pressure of 2 atmospheres. At this low range of temperature the rate of the reaction was low; therefore they applied long reaction times from 2 to 90 hours. In the gas phase cracking, they only found products of scission with carbon number less than 16. In liquid phase cracking, both scission and addition products were observed. The products in

either case were reported to be *n*-alkanes and 1-alkenes. In liquid phase cracking at low conversion an equimolar distribution of alkanes and alkenes were reported. As conversion increased in the liquid phase, the proportion of alkanes increased while the proportion of alkenes decreased. In gas phase a larger proportion of alkenes was always detected both at low and high conversions. They explained the difference in the selectivity of products in gas and liquid as the following: In liquid phase, free radicals which are produced from decomposition of the parent radicals are stabilize by hydrogen abstraction much faster than decomposition via β-scission mechanism therefore the yield of light products (C_1 to C_4) is low. In gas phase, β-scission reactions are dominant which produce many light products. These researchers detected addition products in the range of C_{18} to C_{30} in liquid-phase cracking.

Wu et al. stated that the over all rate of thermal cracking of *n*-hexadecane could be described by a first-order rate. The activation energy which they were reported for liquid and gas phase cracking were 290 kJ/mol and 270 kJ/mol, respectively. The difference between the rate of thermal cracking in liquid and gas phase were not found to be significant. At a reaction temperature of 330ºC, the rate constant of reaction was 2.2×10^{-4} in liquid phase and 2.1×10^{-4} in gas phase. At 375 ºC the rate constant of reaction was 1.15×10^{-2} in liquid phase and 8.6×10^{-3} in gas phase.

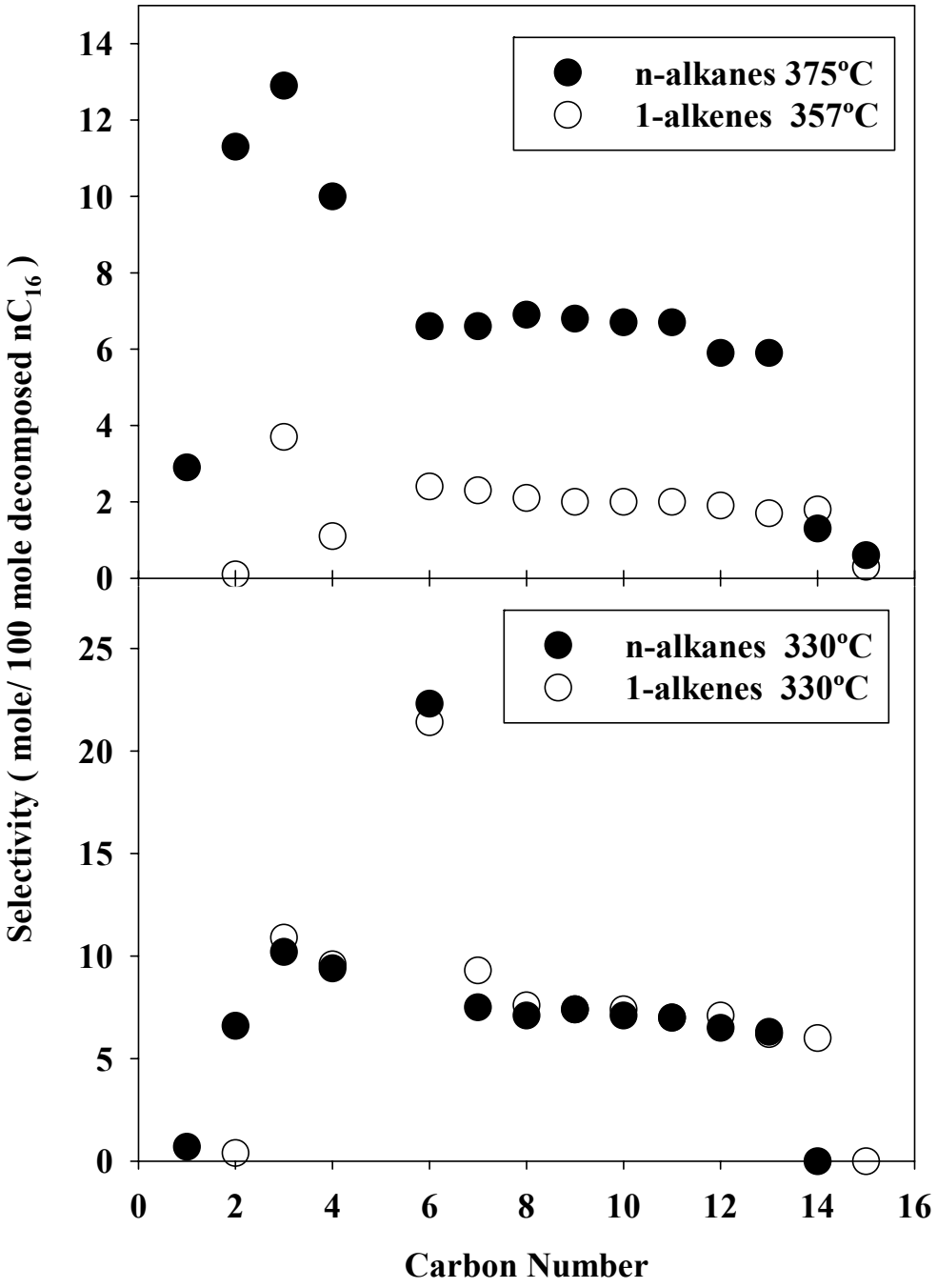

Figure 2.1 Selectivity in thermal cracking of *n*-hexadecane in liquid phase. Data from Wu et al. [10]

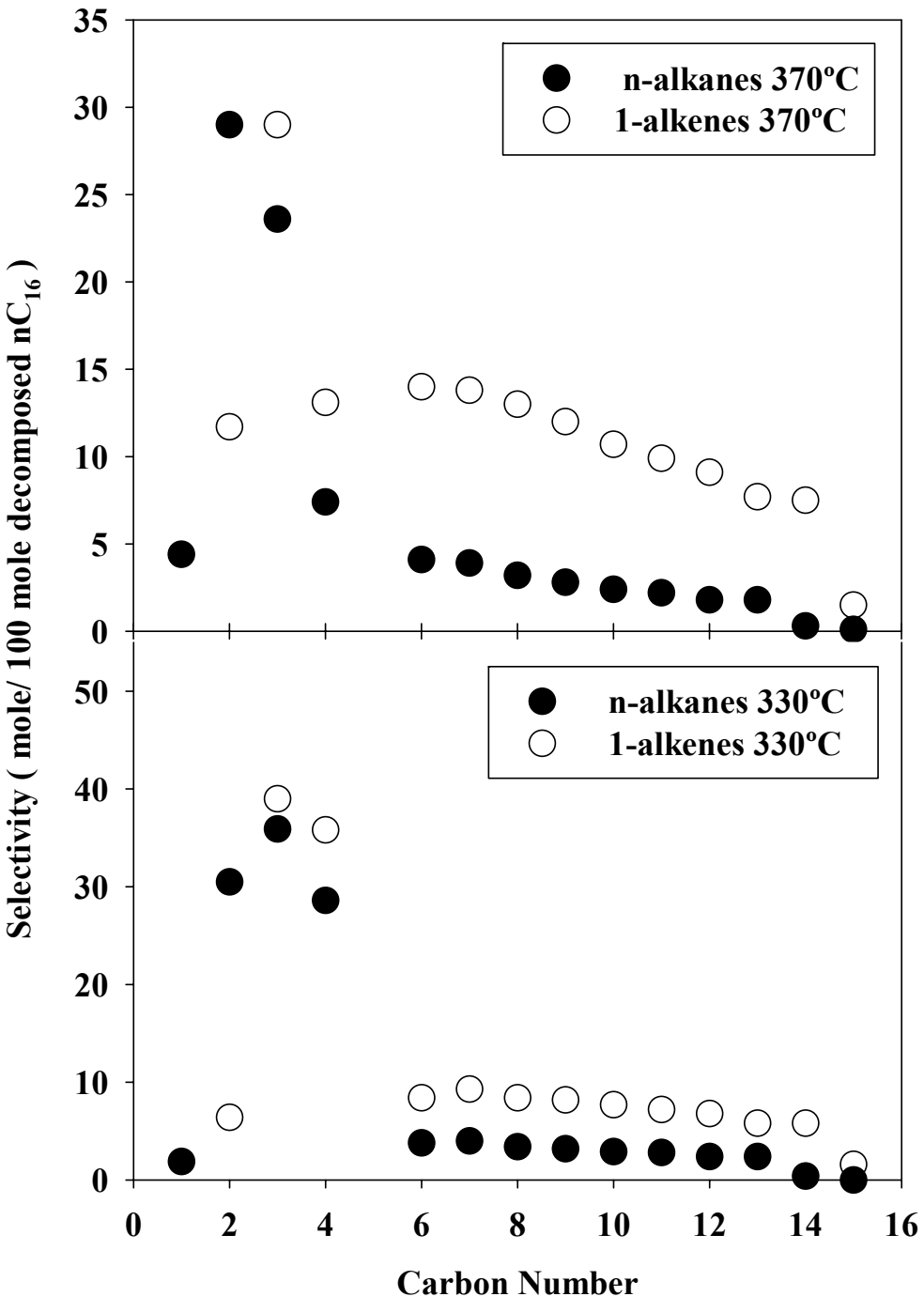

Figure 2.2 Selectivity in thermal cracking of *n*-hexadecane in gas phase. Data from Wu et al. [10]

2.3 Formation of coke

Formation of coke affects the yield of liquid products in upgrading processes of heavy oil as well as the operability of these processes. Coke can form both in gas and liquid phases; however, in short residence time reactors formation of coke in the gas phase is insignificant compared with the liquid phase. Higher molecular weight fractions and higher asphaltene content in a feed give higher coke yield [8]. Goncalves et al. [11] studied the influence of asphaltenes on coke formation during thermal cracking of different Brazilian distillation residues. They concluded that asphaltenes are the main contributor to coke formation during thermal cracking of different Brazilian atmospheric distillation residues.

2.3.1 Formation of coke by liquid-liquid phase separation

Wiehe [12] suggested a kinetic model based on the postulation that formation of coke occurs by a mechanism that involves liquid-liquid phase separation. Asphaltenes react and form a phase which is lean in abstractable hydrogen. When these components reach a critical concentration, they separate from the main liquid phase and coke forms immediately. The infinite reaction rate which they assumed for coke formation reaction indicates that this reaction is controlled by phase equilibrium:

$$H^{+} \xrightarrow{k_H} aA^{*} + (1-a)V \tag{2.26}$$

$$A^{+} \xrightarrow{k_A} mA^{*} + nH^{*} + (1-m-n)V \tag{2.27}$$

Solubility limit: $A^{*}_{max} = S_L\,(H^{+} + H^{*})$ (2.28)

$$A^{*}_{ex} = A^{*} - A^{*}_{max} \tag{2.29}$$

$$A^{*}_{ex} \xrightarrow{\infty} (1-y)TI + y\,H^{*} \tag{2.30}$$

In which:

H^+ reactant (nonvolatile heptane solubles)

H^* product (nonvolatile heptane solubles)

A^+ reactant (asphaltenes)

A^* asphaltene cores

A^*_{max} maximum asphaltene cores that can be held in the solution

A^*_{ex} excess asphaltene cores that are beyond what can be held in the solution

V volatiles

TI toluene insoluble coke

S_L solubility limit (wt % / wt %)

k_A first-order reaction rate constant for reactant asphaltene thermolysis (min^{-1})

k_H first-order reaction rate constant for the thermolysis reactant which are heptane soluble (min^{-1})

a , m and n stoichiometric coefficients

2.3.2 Formation of coke by addition reaction

Alshareef et al. [13] studied the importance of addition reactions in thermal cracking of heavy oils in liquid phase. They selected a series of model compounds for the large components in petroleum with molecular weights from 534 to 763 g/mol which they cracked thermally using a batch reactor at 365 to 420°C. Thermal cracking in liquid phase in all cases of their studies gave significant yield of addition products larger than the starting compounds ranging from 26 to 62 wt%. They reported that the molecular structure of the addition products were consistent with addition reactions between alky groups rather than the formation of aryl-aryl linkages or larger fused-ring products. They found that the yield of addition products from bridged pyrene compounds were much larger than from the corresponding phenyl analogous.

Khorasheh and Gray [14] studied thermal cracking of *n*-hexadecane at high pressure (13.9 MPa) and a temperature range of 380 to 450ºC. They stated that at

such conditions olefins could undergo addition reactions in the liquid phase. These addition products of the olefins could be continued and by further polymerization that would generate larger molecules with higher molecular weight or coke. Gray et al. [5] suggested that a reasonable mechanism for coke formation from hydrocarbons is free-radical chain polymerization following by rearrangement to give a more thermally stable product. Lu and Mulholland [15] studied growth of aromatic compounds in thermal cracking of a mixture of naphthalene, indene and cyclopentadiene**.** Their experiments were carried in a laminar flow reactor at the temperature range of 700 to 850ºC. The reaction was in the vapor phase and they used helium as the carrier gas. The molar concentration of the mixture in helium was 0.04%, 0.07% and 0.01% for cyclopentadiene, indene and naphthalene respectively. The major products of thermal cracking of this mixture include benzene, fluorene, two $C_{14}H_{10}$ isomers, anthracene and phenanthrene, two $C_{17}H_{12}$ isomers (benzo[a]fluorene and benzo[b]fluorene) were three $C_{18}H_{12}$ isomers (chrysene, benz[a]anthracene and benzo[c]phenanthrene). The $C_{14}H_{10}$ isomers were the most abundant components of the products. They studied the mechanism of reaction of indene and cyclopentadiene with naphthalene and with each other; they explained that due to the lack of resonance stabilization, the aryl-aryl addition to naphthyl radicals results in much shorter reaction chains, less reaction channels, and no subsequent rearrangements. The lower stability of naphthyl radicals also results in reactant fragmentation. They concluded that, comparing the fuels with and without cyclopentadienyl in thermal cracking reactions, the resonance stabilized radicals results in more PAH growth and higher soot tendencies.

Gray et al. [5] suggested that intermolecular addition reactions are responsible for formation of stable toluene insoluble material. If a part of a molecule which is already attached by one bond undergoes intermolecular addition, then the resulting double-bonded molecular fragment can be retained much more strongly in the liquid phase or by the coke material. The aromatic groups which are linked

by more than one bond to a larger molecule or matrix are much less probable to be released as products of thermal cracking.

2.3.3 The contribution of mass transfer resistance to the coking mechanism

Gray et al. [16] used a Curie point reactor to study coupling of mass transfer and reaction in coking of thin films of Athabasca vacuum residue. They studied mass transfer through diffusion and bubbling in a liquid film and examined the hypothesis that reduction of the liquid film thickness and hence the diffusion resistance would result in reduction of the coke yield and increasing of the yield of liquid products. Thin films of Athabasca bitumen vacuum residue ranging from 10 to 75μm were placed on the inside wall of stainless tube which were inductively heated. A stream of nitrogen swept the products which evaporated into the vapor phase out of the tube and were condensed in a cryogenic trap filled with glass wool. The time to reach the reaction temperature at 530ºC was reported 7 to 20 seconds from the ambient temperature and 3 to 8 seconds from 350ºC. The reaction temperature was maintained at 240 seconds to ensure that the ultimate yield of coke had been reached. Figure 2.3 demonstrates the measured yield of coke versus the initial film thickness. The yield of coke was the most sensitive to the film thickness between 20 to 50 μm, above 50 μm the yield of coke was rather constant at about 17.5 %. These researchers stated that below the liquid thickness of 20μm the error of the technique became significant and the trend of the coke yields were difficult to measure.

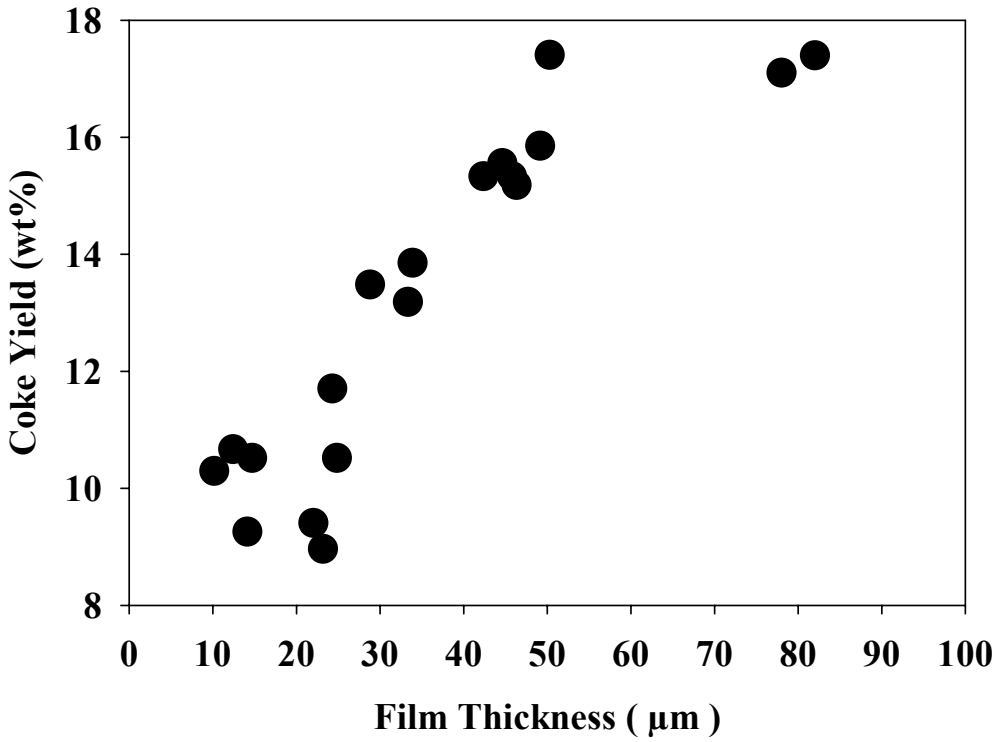

Figure 2.3 Yield of coke versus initial liquid film thickness at 530ºC reproduced from [16]

Gray et al. [16] suggested the importance of the retrograde reactions during coke formation. These reactions can trap the potential volatile products which otherwise could leave the liquid film and move to the vapor phase. As the reaction progresses the liquid phase transforms from liquid to close to solid, the high viscosity liquid can physically trap the volatile products. In summary, the yield of coke may be due to combination of immobilization or retrograde reactions, which trap the volatile products. These researchers suggested that more efficient removal of products from the liquid films by decreasing the film thickness below 20µm would minimize retention of the products by either of the mechanism and reduce the yield of coke.

2.3.4 A more general description of coking mechanism

Wiehe's model does not consider the contribution of two important mechanisms on the yield of coke which are described in the literature:

1. Addition reactions through free radical chain reactions.
2. The effect of resistance to diffusive mass transfer due to the thickness and viscosity of the liquid film.

The higher is the mass transfer resistant, the longer the volatile fragments remain in the liquid phase. Higher residence time in the liquid phase gives higher chance to the products of cracking to undergo the addition reactions which contribute to formation of molecules with higher molecular weight and oligomerization reactions which are precursors for coke formation. Low mass transfer resistance enhances release of the volatile products of thermal cracking into the vapor phase where the rate of coking is much smaller than liquid.

Figure 2.4 illustrates the combination of the theory of Wiehe and the hypothesis of the effect of mass transfer resistance on the yield of coke due to the thickness of the liquid film. The fragments of cracked products diffuse through the liquid film toward the vapor phase. In their pathway to reach the vapor phase they can undergo addition reactions and form larger molecules. Accumulation and addition of these larger molecules eventually lead to appearance of a second liquid phase in which coke forms very fast. The reduction of liquid film thickness reduces the diffusion path of the volatile products toward the vapor phase. This change decreases the chance for addition reactions to occur and lets more of volatile products leave the liquid phase and enter the vapor phase before undergoing such reactions. Reduction of the liquid film thickness also decreases the volume of the second liquid phase in which formation of coke takes place. While reduction of this volume does not necessarily change the rate of coke formation, it can decrease the total yield of coke.

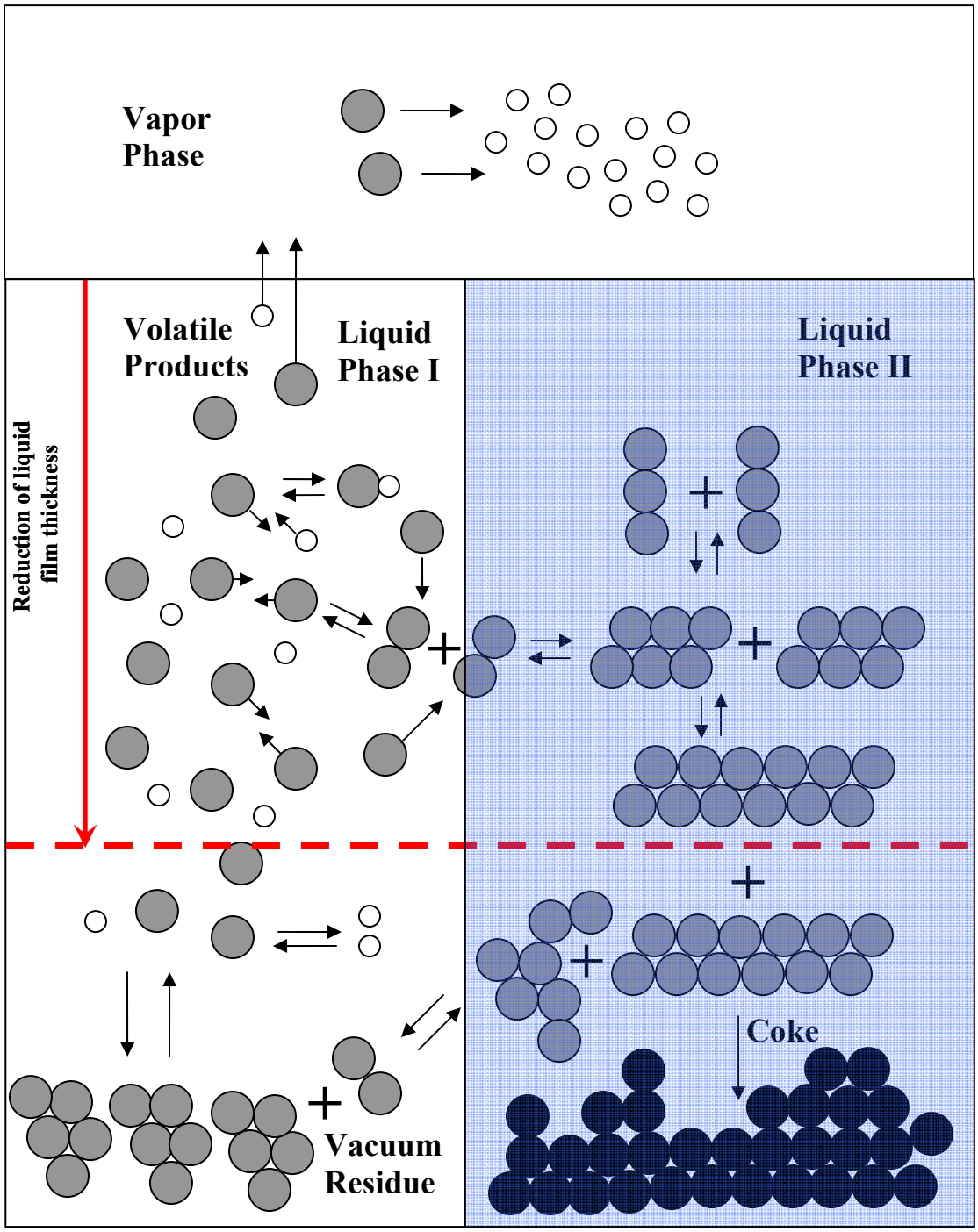

Figure 2.4 Mechanism of coke formation; reduction of liquid film thickness decreases the diffusion path of the volatile products and volume of the liquid phase in which formation of coke takes place.

Zou et al. [17] used a tubular continuous flow reactor to study kinetic of gas oil pyrolysis and coke deposition. The boiling point range of the feed was 372 to 641ºC and the reaction temperature was 790 to 935ºC at atmospheric pressure. They reported ethylene and aromatics as the coke precursors. The formation of coke from aromatics was found to be predominant. However, the Zou et al. study focused on coke formation on walls of the reactor, which is normally the reaction of adsorbed species, either with each other or with gas phase components.

2.4 Commercial processing of vacuum residue

The major non-catalytic thermal cracking processes which are used in upgrading of heavy oils are designed for reaction temperatures below 550°C. Three major commercially used non-catalytic thermal cracking processes are visbreaking, delayed coking and fluid coking.

2.4.1 Visbreaking

Visbreaking is the most broadly used residue conversion process. This process is used to produce 15 to 20 % of atmospheric distillates with a proportional reduction in production of heavy fuel oils [18]. The main goal of Visbreaking is to reduce the viscosity by a mild thermal decomposition. This is a simple process and is available in two versions; coil cracker and soaker cracker. The coil cracker is operated at 450 to 500°C with the residence time of about one minute. The entire conversion occurs inside a heater. The heat flux across the tube walls ranges from 25 to 30 kW/(m^2.h). In the soaker cracker, the heater is followed by a soaking drum to complete the conversion. The reaction temperature is 30 to 40°C lower than the coil cracker but the residence time is much longer, that is from 10 to 20 minutes [18]. After the desired conversion are achieved the products are quenched by gas oil to stop the reaction and prevent coking [19].The operating pressure varies from about 0.3 to 2.5 MPa [19, 20].The conversion in this process is limited to avoid deposition of coke inside the heater tubes. Increasing the conversion can result in more sediment deposition. The instability of the products of visbreaking is a disadvantage of this process. The composition of the feedstock

can increase the tendency to yield coke and unstable visbroken fuels. Therefore different feedstock cannot be treated with the same severity using visbreaking process [18].

2.4.2 Delayed coking

Close to 90 % of the petroleum coke which is produced around the world comes from processes of the delayed-coking type. The feed is first preheated by exchanging heat with coking gas oil then mixed with the fraction from the bottom of the fractionating column. The feed which is a combination of the fresh feed and the recycle stream is heated up to about 500°C in a heater at a short residence time and then is sent to the coking drum where the coking continues [18]. The residence time of the vaporized phase in the coking drum is at most a few minutes. The liquid fraction stays in the reactor until it either turns to coke and vapor or to the end of the drum cycle [8]. The operation pressure of the coking drum is between 0.2 to 0.4 MPa. The coking drums operate in cycles and are switched periodically to remove the coke from the suspended drum [18]. The disadvantage of delayed coking is high yield of coke and low yield of liquid products, nevertheless this processes has been frequently preferred by refiners for residue processing because of its inherent flexibility in handling any kind of residue [19].

2.4.3 Fluid Coking

Exxon developed fluid coking, in order to enhance the yield of distillate products and minimize yield of coke by reducing the residence time of the cracked product vapors in the reactor [8]. The fluidized bed is formed by the coke particles which are produced through coking reaction. The preheated feed is sprayed onto the coke particles. The average temperature of the reactor is between 500 to 550°C. The residence time is between 15 to 20 seconds. The volatile fraction flashes before the cracking and condensation take place at the surface of the coke particles. Coke deposits in onion-skin form on the supporting coke particles. The coke particles then are sent to the burners where a part of the coke in proportion to

5 % of the carbon in the feed is burned to maintain the energy requirement of the process. The rest of the hot coke particles are recycled from the burner to the fluidized-bed reactor [18].

2.4.4 Short-contact time processes

The delayed coking and fluid coking technologies have been developing to increase the yield or to improve the quality of liquid products. Comparing to high pressure hydro- cracking processes, the low capital cost of coking processes due to low pressure operation has been attractive [8]. There is significant interest in improving the coking technology in order to increase the yield and to achieve higher quality of the liquid products. The current approaches to this purpose can be summarized as the following [25]:

- Developing new reactor technologies to shorten residence time of the vapor phase in the reactor to minimize over cracking and loss of hydrogen content of liquid products into hydrogen-rich light ends.
- Design and adjustment of liquid recycle in delayed and fluid coking to raise the yield and quality of the liquid products. The quality and yield of liquid products are entangled. Achieving higher quality of liquid products is coupled by higher yield of undesirable 524ºC+ fraction.
- Enhancement of introduction of feed in fluid coking to minimize the mass transfer resistance and to reduce the reaction temperature. Lower reaction temperatures favors lower yield of high-hydrogen content light ends and thus higher quality of the liquid products.
- Control the reactor composition in order to reduce or modify formation of coke (e.g. use of steam , additives or hydrogen donors)

In delayed coking and fluid coking vapor products can undergo over-cracking before they are cooled off. In short-contact time coking processes, the goal is to minimize cracking of desirable product to the light ends which remove hydrogen from the liquid products and lower their yield and quality. The following features are common in short contact time coking design [8]:

- The heat carrier is hot solid particles like sand, alumina, silica or coke which are mixed with the feed in the reactor.
- Rapid separation of vapors from solid particles and quenching to stop the reaction
- Burning the solid particles to achieve partial or complete conversion of coke materials.
- Return of hot solid particles to the reactor

Lurgi-Ruhrgas (LR) and ART processes are examples of short contact time reactors which were constructed at a commercial scale. LR process was developed by Lurgi and has been used on a commercial scale for olefin production [8]. LR coker is based on the same principal as the fluid coker. The difference is in the method of mixing of the fresh feed with the heat carrier. The mixing device in this process consists of two rotating screws which engage and clean each other. It guarantees very good dispersion of the heat carrier solids in the feed. The reactor can be considered in plug flow regime in which all the particles have the same residence time. The products in the vapor phase are withdrawn and condensed and fractionated. This system can handle very viscous feeds and even solids. The temperature in LR process is 500°C and the residence time is 2 to 10 seconds [18]. ART process was developed by Engelhard. This process is based on fluid catalytic cracking but instead of using a catalyst, an inert solid is used as the heat carrier. Coke, metals and sediments from the feed are deposited on these inert particles. In this process, the feed and the heat carrier particles are mixed and pass through a riser reactor [8]. The temperature in ART process ranges 500 to 540°C and the residence time ranges between 0.1 to 2 seconds [18]. Severe fouling of the reactor led to decommissioning of the one commercial scale unit built in the US [8]. Other variations of these reactors for short contact time and operation at higher temperatures are not yet industrialized and have only been tested in demonstration units [18]. Vogiatzis et al. [21] investigated combination of shorter residence times and high temperature in pyrolysis of heavy oils by using a mini-pilot plant reactor which will be reviewed in section 2.5.2 in more detail.

2.5 Experimental reactors for high-temperature thermal cracking studies

In this section, the experimental reactors which the previous researchers used to study high temperature thermal cracking of *n*-alkanes, bitumen and vacuum residues are reviewed. The suggested technologies with the potential to provide a fast rate of heat transfer to heat up the feed are also reviewed.

2.5.1 Low pressure and high temperature thermal cracking of *n*-hexadecane

Laidler et al. [22] used a batch reactor to study pyrolysis of propane at 530 to 670°C and pressures up to 600 mmHg (80 kPa). The reaction vessel was a quartz cylinder, 15 cm long and 4.6 cm internal diameter which was placed inside a furnace**.** The large size of this batch reactor and high ratio of the internal diameter to the length of the vessel raise the question of temperature homogeneity inside the reactor. They did not elaborate on the operation of the reactor with regard to the reaction time and temperature rise time. They used both an unpacked and packed reaction vessels. The packed reaction vessel was filled with quartz tubing to increase the surface to volume ratio. In the unpacked vessel the reaction was found to be of the first order at lower temperatures and higher pressures. At higher temperatures and lower pressures a transition to 3/2 order was observed. They reported that the rates were reduced in the packed reaction vessel and an apparent order of 1.25 was calculated. They did not assign any real significance for this reaction order, and the kinematic parameters were calculated for the results which were obtained from the unpacked reaction vessels. This indicates that the design of the reactor had an impact on their kinetic studies. They reported the activation energy for first order reaction and 3/2 order reaction, 281 and 228 kJ/mol, respectively. Thus at lower range of reaction temperature they found the reaction be first order and with higher value of activation energy and at higher range of the reaction temperature they obtained higher order of reaction and lower value for activation energy [22, 23].

Kershenbaum et al. [24] used a flowing annulus reactor to study the kinetics of non-isothermal pyrolysis of propane at 800 to 1000 ºC. They stated that the rate

of reaction at these temperatures is so high that batch or even an isothermal flow experiment was impossible. The reactor was an annulus with both surfaces made from Vitreos Refractory Mullite ($Al_6O_{13}Si_2$). The ID of the outer tube was ¼ inch (6.3 mm) and the O.D of the inner tube was 7/32 in (5.6 mm). This reactor was placed inside an electric heated reactor. They demonstrated that the error due to neglecting the longitudinal diffusion in the flowing reactor was negligible. These researchers did not mention if they operated the reactor at higher pressure than atmospheric, but their kinetic model includes the pressure profile along the reactor as well as the non-isothermal temperature profile. They did not consider the method of equivalent reactor volume satisfactory. They measured the non-isothermal temperature profile along the reactor with a thermocouple and solved a mathematical model to calculate the kinetic parameters. They calculated activation energy and the pre-exponential factor of Arrhenius equation for a first order reaction as 218 kJ/mole and 2.40×10^{11} s^{-1}, respectively. They reported a decrease in activation energy with increasing reaction temperature. They explained this effect by the fact that at higher reaction temperatures the yield of olefins are higher, and they suggested that olefins inhibit the rate of reaction [24].

Depeyre et al. [25] studied steam thermal cracking of *n*-hexadecane in temperature range of 600 to 850°C and atmospheric pressure. They used two concentric tubular reactors. The outer tube of one reactor was made of Incoloy 800 and the inner tube from quartz. The second reactor was made of all quartz. The reaction tubes were placed inside an electrical furnace. Steam and *n*-hexadecane were separately introduced into the pre-heating section of the reactor. The temperature of *n*-hexadecane would reach to 480°C in the pre-heating section. The temperature profile of inside the reaction tube was measured by inserting and sliding a thermocouple inside the inner quartz tube while the fluid was flowing through the annulus. They did not report any heat transfer model to correct the temperature reading from the thermocouple. The thermocouple faced to the furnace wall. Considering that quartz did not absorb all of the radiation energy, the temperature of the tip of the thermocouple would likely be different

from the temperature of the quartz wall and the fluid which was flowing behind it. The assumption that the reading from the thermocouple was equal to the temperature of the fluid could be a source of error especially in the non-isothermal section of the reactor where the fluid temperature was much below the furnace temperature. The pre-heaters for *n*-hexadecane and steam were not placed external to the reaction furnace but internally connected in one furnace body. Including the pre-heating section inside the reactor can significantly help to minimize the heat losses that usually occur from the area between an external pre-heater and the reaction furnace. They reported a catalytic effect of the Incoloy 800 reactor walls. In the experiment that they carried at 700°C, they detected a large amount of hydrogen and aromatic compounds, 6 wt% and 4 wt% of the feed, respectively. Therefore, they used a quartz reactor to avoid catalytic effects for the rest of the study.

They did not detect any paraffins higher than propane. All olefins from pentane to pentadecene were reported as α-olefins. They reported that steam enhanced ethene, propene butene, and butadiene production while it reduced the formation of hydrogen, methane, ethane and aromatics at high temperature. The explained that the steam lowered the partial pressure of *n*-hexadecane and the residence time, consequently this delayed dehydrogenation and aromatic production which would lead to formation of coke deposits.They calculated the residence time of the non-isothermal reactor based on the Hougen and Watson and Hirato et al. reactor equivalent volume principal [25]. The equivalent reactor volume is defined as the volume which gives the same conversion as the non-isothermal reactor with its temperature profile. The reported residence time was 0.3 to 1 second. They observed that the overall kinetics of the pyrolysis of *n*-hexadecane were first-order and calculated the activation energy and pre-exponential factor in the Arrhenius equation 239 kJ/mol and 9.6×10^{13} s^{-1} respectively. The range of measured activation energies in the preceding studies by other researcher were 230 to 250 kJ/mol and the pre-exponential factors from 3×10^{13} to 1×10^{15} s^{-1} [25].

Bajus et al. [26] used a design which is similar to the Depeyre et al. reactor to investigate pyrolysis of heptane at temperature range of 680 to 760 ºC and atmospheric pressure. However, their concentric reaction tubes were made all of stainless steel, both the inner and outer tube, and they used an external pre-heater. They introduced the mixture of heptane and steam into the same pre-heater. The mass ratio of steam to heptane was 3 to 1. They followed the same procedure to measure the residence time as Depeyre et al. [25]. They found that the overall reaction kinetics were first-order. The calculated activation energy and pre-exponential constant of the Arrhenius equation were reported as 195.5 kJ/mol and 1.34×10^{11} s^{-1}, respectively.

Bartekova et al. [27] used the reactor which was designed by Bajus et al. to investigate pyrolysis of *n*-hexadecane with the same mass ratio for steam. They carried out the experiment over a temperature range of 700 to 780°C and at atmospheric pressure. For the overall kinetics, they considered a first-order reaction and they reported activation energy and the pre-exponential factor for Arrhenius equation 162 kJ/mol and 3.5×10^{9} s^{-1}. They noted that the activation energy that they have calculated based on their experimental data was lower than most of other investigators [25, 27]. The major alkane products were methane, ethane and small amount of propane. The major alkene products were ethene and propene, and their yield increased with temperature and residence time. The products were dominantly 1-alkenes. The 1-alkenes higher than 1-pentene were reported to decrease with conversion that indicated their instability comparing to lighter 1-alkenes. They reported an unexpectedly higher content of 1-hexene in the product comparing to other 1-alkenes which they believe was caused by isomerization of alkyl radicals.

Billaude et al. [28] used a continuous flow reactor to study high temperature steam thermal cracking of a mixture of *n*-paraffins from C_{11} to C_{20} with C_{14} to C_{16} as the major components They experimentally demonstrated the advantage of using high temperature and short residence time in minimization of production of

aromatics and selective production of α-olefins. The reactor consisted of Incoloy 800 tubes, O.D. 6 mm and I.D. of 2 and 4 mm which were wound around a graphite core and was heated by high-frequency induction. The temperature range was 640 to 820°C. This reactor was also used to study pyrolysis of vacuum residue. More details about their reactor design is given in Section 2.5.2. They reported hydrogen, methane, ethene, propene, 1-butene, 1-pentene, 1-hexene, 1-heptene,1-octene and 1-nonene as the major product of the pyrolysis of n-hexadecane.

Rastogi et al. [29,30] designed a micro-reactor to study thermal cracking of propane at 600 to 900 ºC with pyrolysis time of up to 2 seconds for temperature range of 600 to 800º C and up to 1 second at 900ºC. Methane, ethene, hydrogen and propene were the major reported products. They emphasized the requirement of accurate knowledge of the time in which the reactant would reach the reaction temperature in the study of fast kinetics of hydrocarbon pyrolysis reactions. An important question in any reactor design is to what extent the reaction may progress before the reactant reaches the reaction temperature. There are different methods that can provide a rapid rate of heating, e.g. shock-tube, laser, arc, filament-resistive heating and high- frequency induction heating. While the temperature rise time of the shock-tube,laser and arc pyrolysis are shorter than other methods, the measurement and verification of the equilibrium temperature could be a serious issue [30]. Rastogi et al. [30] criticized inaccuracy of the residence time determination (5 to 10 %) and the temperature. In the laser, arc or plasma jet pyrolyzer the reaction temperature is an approximate value. Therefore, they recommended that these methods should not be used for quantitative kinetic measurements. The filament pyrolyzer which works based on the electric resistance of a platinum foil and application of high voltage can provide rapid rate of heating. However, Rastogi et al. criticized the application of this technology. Significant temperature differences can be detected along the filament based on its geometry. If the same filament is used repeatedly, carbon is dissolved in the platinum foil and changes its characteristic. Such change in physical property of

filament change the equilibrium temperature and this is not desirable in quantitative kinetic studies.

Curie-point alloys give rapid heating of small size samples in an electrical induction field. This principal has been used in commercial pyrolysis-gas chromatography and to study chemical reaction kinetics [16]. Rastogi et al. [29] selected a Curie-point approach and made a glass microreactor which encapsulates a ferromagnetic heating filament and the reactant. The distance between the wall of the microreactor and the ferromagnetic heating element was 55 μm. Their simulation for the worst case scenario, in which heat transferred only by conduction, indicated that in less than 0.2 ms the gas and the element could reach thermal equilibrium. They measured the temperature rise time for temperatures at 700 , 800 and 900 ºC. At these temperature the temperature rise time were 46 , 65 and 84 milliseconds respectively from an ambient temperature of 300ºC. The capsule containing the element were released and passed inside an inductively heated furnace through a free fall under gravitation field. At the bottom a hammer broke the capsule and a stream of helium quenched and carried the products directly into a gas chromatograph for analysis. For a first order thermal cracking reaction of propane, they calculated a value of 136 kJ/mol for the activation energy, which was significantly lower than the range of 210 to 290 kJ/mole which was reported by other researchers. They discussed that this low value for the activation energy could be through inhibition of the free radical reactions by olefins and specially propene. When they limited the calculation to use the data which were obtain at the temperature range of 600ºC to 700ºC , the calculated activation energy of 210 kJ/mol was obtained which was closer to the reported range by the other researchers. Ratsogi et al. stated that they used pure propane with no inert gas. They did not keep the conversion low, and given the fact that they used a batch reactor, they concluded that the inhibition effect in their case should expectedly be higher than that observed by other researchers [29].

The reported half time of the thermal cracking reaction of propane can be seen in

Table 2.1. As it can be seen in this table, at temperatures 800 and 900 ºC, the temperature rise time is significant comparing with half-life of the reaction at 600 to 700°C. The removal of data points related to the temperature range of 800 to 900°C at these two temperatures increased the calculated value of the activation energy. This observation suggests that the temperature rise time can still be an issue in this design for the higher temperatures at the range of their study.

Table 2.1 Half lives of the pyrolysis of propane reported by Ratsogi et al. [29]. (TRT = Temperature Rise Time)

T (ºC)	$t_{0.5}$ (ms)	TRT (ms)
600	14270	-
700	663	46
800	422	65
900	88	84

Rastogi et al. [29] summarized that for thermal cracking reaction of hydrocarbons at temperatures below 500 ºC, it is reasonable to ignore the temperature rise time. For temperatures up to 650 ºC, temperature rise time could be neglected if apparatus with short temperature rise time like Curie-point reactor is used. At temperatures above 750 ºC the rate of thermal cracking is very fast and a significant portion of the reactant may crack during the heat-up period and this issue should be considered in the kinetic study.

Fairburn et al. [31], who criticized use of externally heated tubular reactors , used the Curie point concept and the reactor which was designed by Rastogi [29] to study thermal cracking of *n*-hexadecane at temperature range of 576 to 842°C and 1 to 2 atm pressure. In their work, which is cited frequently in the literature, the researchers reported a significantly different activation energy and pre-exponential factor and to justify their results they highly criticized the reactor design, product analysis and arithmetic calculation of the previous researchers.

Therefore, their work particularly should be reviewed in more detail. They used the same of batch micro-reactor of Rastogi et al. which consists of a ferromagnetic alloy wire coated with n-hexadecane and encapsulated in glass. The size of this reactor was 12 mm long and 0.7 mm in diameter, contained a 0.4 mm diameter ferromagnetic wire coated with approximately 15 μg of *n*-hexadecane. The volume of gas inside the glass was 3.11 μL. The sample size and the reactor were kept small to ensure minimum heat and mass transfer gradients. A dilute *n*-hexadecane – carbon disulfide solution was used to apply the reactant on the wire. The carbon disulfide quickly evaporated, leaving a thin *n*-hexadecane layer on the wire. The amount of *n*-hexadecane was then determined by weighing. The wire then was inserted into a Pyrex capillary tube and quickly flame-sealed under vacuum. Evacuation was necessary since no air was acceptable to be present in the micro-reactor. At such small mass of reactant, 15 μg , the weighing procedure is very important and although the boiling point of *n*-hexadecane , 281°C, is not low the evaporation of the reactant at high ratio of surface to volume on the wire should be considered. Later this reactant on the wire is inserted in the glass micro-reactor and flame sealed under vacuum. Higher temperature and lower pressure can help with evaporation of a portion of the reactant. It is a question now using such a procedure how the accuracy of the initial weigh of the reactant can be ensured.

A rod-like hammer was installed above the inductive furnace chamber, which was dropped and crushed the micro-reactor at the end of the reaction and the products were quickly then mixed with helium which as the carrier gas which cooled off the products to stop further reaction and facilitated direct transfer of the products into the gas chromatograph for analysis. Fairburn et al. used a combination of several GC columns, column switching valves, two thermal conductivity detectors (TCD) and a flame ionization detector (FID) to split the light products, C_4^- from C_5^+. The C_5^+ products were separated with a column, which was capable of separating C_5 to C_{24} hydrocarbons. Through a rather complicated operation the C_4^- products were directed to the TCD detector and the heavier fraction to FID. They assumed that all the products were washed out from the crushed micro-reactor

with the helium and passed eventually through the FID. They justified this assumption by observation of a peak for pyrene, which was the heaviest reaction product that they expected, near the end of the chromatogram. It should be noted that observation of a peak of a product in the chromatogram does not mean that all the products has passed the column and reached the detector. It is possible that part of the detected products condensed on the tubing before they reached the gas chromatograph. They conducted the experiments first at 300°C and 10 ms at a condition that low conversion was expected and measured an average weight of 11.7 µg of *n*-hexadecane with standard deviation of 0.3 µg, which they interpreted as the reproducible initial mass of the reactant inside the micro-reactor. For the actual experiments, they measured 12.4 µg of n-hexadecane and a standard deviation of 1.5 µg. They used these results as a proof of the mass balance. It is notable that the measured value for *n*-hexadecane where the reactant is converted to the product is higher than the case of the run with no conversion. Fairburn et al. were not clear in reporting how this measurement and calculation were carried out. A mass balance by comparing the weight of the collected products with the weight of the initial reactant were not presented. Application of this Curie-point design to the study of kinetics of thermal cracking of liquids can cause significant problems. Especially for the heavy oils, which contains fractions, which do not evaporate at the reaction temperature, high rate of heating would cause splashing of the feed and inhomogeneity in temperature distribution inside the micro-reactor. The difference between the application of this design with the case of Rastogi is that the propane is in gas phase, so when the reactant is not actually on the wire, the heat transfer through conduction might compensate the temperature homogeneity. In the case of *n*-hexadecane, splattering the liquid reactant upon sudden temperature rise of the wire is expected and the *n*-hexadecane would evaporate on the wall of the micro-reactor. To ignore such an effect in inhomogenity of temperature and heat transfer calculation like Rastogi provided is necessary [29]. The heavy liquid products could be aerosolized in the quench system and therefore entrained with the carrier gas and later condensed before enter the GC. Observation of the peak of heavy components on the chromatogram

does not mean that all of the mass of these components passed the column and reach the detector. They reported the activation energy of 165 kJ/mol and exponential factor of 3×10^8 s^{-1}. This result can be compared with the results that are reported in the National Institute of Standard and Technology (NIST) chemical kinetics database which are given in Table 2.2. In all cases in this table, first order reaction is assumed and the reaction pressure is atmospheric.

Table 2.2 Activation energy and pre-exponential factor for thermal cracking of n-alkanes reported by the NIST chemical kinetics database [32]for reaction order 1

Researchers	*n*-alkane	Activation Energy (kJ/mole)	Pre-exponential factor (s^{-1})	Temperature (°C)
Rumyantsev et al.	*n*-pentadecane	261	2.95E+14	615-720
Kalinenko et al.	n-dodecane	221	1.58E+12	680-747
Rumyantsev et al.	n-dodecane	251	8.91E+13	600-680
Rumyantsev et al.	n-decane	260	2.19E+14	645-685
Rumyantsev et al.	n-octane	249	4.07E+13	620-720
Illes et al.	n-octane	219	1.04E+12	600-797
Pant et al.	n-heptane	251	6.03E+13	680-747
Aribike and Susu	n-heptane	206	5.79E+10	660-777
Kalinenko et al.	n-heptane	274	2.51E+15	640-727
Bajus et al.	n-heptane	195	1.30E+11	680-757
Illes et al.	n-heptane	220	1.89E+12	600-797
Levuch et al.	n-heptane	255	8.71E+13	847-1097
Zychlinski et al.	n-hexane	220	5.40E+11	680-757
Kalinenko et al.	n-hexane	275	2.51E+15	675-817
Ebert et al.	n-hexane	260	8.32E+13	377-567
Illes et al.	n-hexane	220	2.34E+12	597-747
Levuch et al.	n-hexane	259	1.00E+14	847-1097
Kalinenko et al.	n-pentane	264	3.98E+14	700-847
Zychlinski et al.	n-pentane	224	6.19E+11	687-817
Levuch et al.	n-pentane	262	7.80E+13	847-1097
Kalinenko et al.	n-butane	233	5.01E+12	700-847
Illes	n-butane	236	6.24E+12	640-787
Kalinenko et al.	n-propane	225	7.94E+11	747-847
Hautman et al.	n-propane	245	3.16E+12	837-967
Zychlinski et al.	n-propane	221	1.70E+11	727-847
Kalinenko et al.	ethane	299	1.00E+15	797-897

2.5.2 High temperature thermal cracking of bitumen and vacuum residues

There are few published reports in the literature about the kinetic study of high temperature thermal cracking of bitumen, heavy oil or vacuum residue at temperatures above 600°C. Only few attempts have been reported to measure intrinsic rate of thermal cracking at high temperature in which the coupled effect of mass and heat transfer was considered in the design of the experiment. Nevertheless, high temperature pyrolysis of petroleum fractions is not new to oil industry. Heilman reported on industrial processes and optimum operating conditions to achieve maximum yields of certain dienes or olefins from high temperature pyrolysis of naphtha and gas oil in 1947 [33]. The reported operating temperature ranged from 650 to 1040°C at near atmospheric pressures and residence times from a fraction of a second to many minutes.

The only experimental work on Alberta's heavy oils at temperature about 600°C is reported in Tan's PhD dissertation but the result was not found to be published [34]. Tan used the same reactor design of Rastogi and Fairburn to study thermal cracking of Cold Lake and Peace River. This researcher tested the reactor with *n*-hexadecane and reported a low activation energy like Fairburn et al.[31]. The work of this researcher is subject to the same criticism as the work of Fairburn et al. The result of Tan was compared to the result of this study for thermal cracking of Athabasca vacuum residue in Chapter 5. Billaud et al. [28,35] studied thermal cracking of vacuum gas oil at 780°C and residence time of 10 to 20 milliseconds.Their reactor consisted of an Incoloy 800 tube , O.D. 6 mm and I.D. 4 mm which was wound around a graphite core and was heated by high-frequency induction. The water and the vacuum gas oil was first pumped into an external pre-heater at 400°C and after vaporization , the mixture of steam and the reactant were introduced into the reactor. It was assumed that along the non-isothermal section of the reactor, reaction did not advance and reaction progressed entirely along the isothermal zone. They reported product distribution and characteristics of the products of thermal cracking of vacuum gas oil and hydrotreated vacuum distillates. The yield of gas products increased with residence time. The major gas products was ethene and propene. No study on the rate of thermal cracking of

vacuum gas oil was reported. The heaviest feed which was applied had a boiling point range of 271 to 586°C. They assumed a plug flow regime to calculate the residence time.

This reactor design can work for a feedstock, which is in the vapor phase at reaction temperature. The pre-heater is external to the reactor; therefore, very good insulation is required to keep the temperature of the mixture of steam and the feed at 400°C before it enters the reactor and avoid condensation of the reactant in the inlet tubing. If the fluid enters the reactor without any heat losses, it should still be heated up to 780°C, which is the desired reaction temperature. A key issue in this design is how long actually it takes that fluid to reach the reaction temperature and how large the non-isothermal section of the reactor is. The temperature of the body of the reaction tube is not necessarily representative of the average bulk temperature of the fluid even in a reactor. If the rate of thermal cracking is fast enough then it is possible that feed converts to products before it reaches the reaction temperature. The extent of this conversion is an important design problem, especially if the reaction is assumed to occur at constant temperature. If reaction progress is significant in the non-isothermal section, the temperature profile should also be considered in the calculation of the residence time and in the kinetic model.

Vogiatzis et al. [21] conducted an experimental study of pyrolysis of Cold Lake bitumen at 500 to 900°C and short residence times ranged 70 to 500 milliseconds by using a mini-pilot plant reactor at the University of Western Ontario. They claimed that “the rationale for ultrarapid pyrolysis (Ultrapyrolysis) lies in the fact that molecular structure of natural heavy, carbonaceous fuels is not strongly cross-linked. If appropriately hit by a high temperature thermal shock (fast pyrolysis), these feedstocks will shatter and disintegrate into smaller reactive molecular fragments before the structure has time to become cross-linked and refractory. On the contrary slow pyrolysis would leave enough time for the structure to become cross-linked and refractory thus leading to a lot of worthless tar and coke.” As the preceding review of mechanisms shows, this claim has merit to the extent that

rapid transfer to the vapor phase will serve to minimize any addition reactions. Vogiatzis et al. used a jet impact reactor at mini-pilot plant scale. In this design a jet of heat carrier impacts onto a jet of atomized liquid feedstock. They described the reactor design as the following: The heat carrier is at a temperature higher the reaction temperature. The feedstock is preheated to 200°C to reduce its viscosity. The heat carrier gas is nitrogen to which 100 μm sand particles may be added. The reaction temperature ranges from 500 to 950°C. The initial temperature rise time to the reaction temperature is achieved through direct contact of the atomized liquid and the heat carrier in a device which they named thermovortactor. The thermovortactor has two opposing tangential inlets. One tangential stream effectively destroys the momentum of the other causing severe turbulence. The liquid feedstock are injected from the top of the thermovortactor through and air cooled tube into the turbulent region where mixing occurs within 30 milliseconds. The reaction continues in the reaction section which is a tube which is kept under isothermal condition inside a furnace [21].The products are cooled to less than 300°C with a stream of cold nitrogen downstream of the reactor. The products streams passed a water- cooled cyclonic condenser, a cold trap, an electrostatic precipitator and a porous metal filter cartridge, so that only the non-condensable products could reach the gas collection bags. In their mass balance they had a mass recovery of more than 92 wt% of the bitumen feed. They found that at 900°C and 331 milliseconds the total gas product was rich in olefins, and 51 wt% of the bitumen converted to gas products. Under this operation condition, more than 18 wt% of the bitumen was converted to ethene as the major gas product component.The rate of injection of feedstock into this reactor was 0.5 kg/hr which was significantly larger than the feasible range which can be applied to a bench scale reactor. Consequently, the flow rate of nitrogen as carrier gas and the hot stream should be proportionally high compared with the bench scale reactors. Use of an external furnace as a source of a hot stream of the inert gas is possible when the ratio of the mass flow rate of the hot stream to the mass of the tubing and the insulation between the external furnace and reaction furnace is high enough so that the heat losses stay reasonably low in this section. However, in a bench scale

laboratory reactor where mass flow rate of the hot stream is low, the heat losses between the external furnace and the reaction furnace can be so high that makes such a design is impractical. In a bench scale design when the flow rate is low (compared with a pilot plant) the ratio of the mass flow rate of gas to the mass of the tubing and insulation is an important design factor in control of the heat losses between the external pre-heater and the reactor. Depending on the size of the tubing and flow rates, use of an external source of generation of hot stream of inert gas and conduction into the reactor may not possible due to severe heat losses no matter how good the insulation is.

The study of Vogiatzsis et al. focused in reporting the yield and distribution of the products versus temperature and residence time. They did not report on any measurement of rate of thermal cracking. They observed occurrence of secondary cracking reactions at temperatures above 650°C. At temperatures of 850 to 900°C for all residence times (70–400 milliseconds) they reported secondary cracking reactions. According to Vogiatzis et al., the mixing time between the hot stream and the cold stream which carried the feed was about 30 milliseconds and the subsequent reactor was assumed to be isothermal. In order to use such a design to study rate of thermal cracking, the conversion of bitumen should not be significant in the first 30 milliseconds of the total residence time.

Gray et al. [16,36] used a Curie point reactor which was described in Section 2.3.3 to study rate of thermal cracking of Athabasca vacuum residue in temperature range of 457 to 530°C and atmospheric pressures. They reported activation energy and pre-exponential factor of 218 kJ/mole and 1.2 × 1013 s^{-1} respectively for cracking of heavy residue (650°C +) to light residue (524 to 650 °C)and gas oil (343 to 524°C). The lumped kinetic model that they have suggested considered the mass transfer resistance and they calculated the value for mass transfer coefficients for the heavy residue and its cracked products in the liquid film. This type of reactor operated with very low gas-phase temperatures, so that products were effectively quenched upon exiting the thin liquid film.

Consequently, this reactor type is unsuitable for study of vapor-phase reactions at high temperatures.

2.5.3 Pyrolysis gas chromatography

Temperature rise time in the range of 30 to 85 milliseconds was reported to be achievable by using jet impact and Curie point reactors. It will be explained in Chapter 3 that the half time of reaction in thermal cracking of heavy oils like vacuum residue is estimated to be less than 30 milliseconds at 700°C. Technologies that are based on concentrating energy at a small spot or area can achieve very shorter temperature rise times.

Fanter et al. [37] used a beam of focused laser light in pyrolysis gas chromatography to heat up the sample to a high temperature within a short temperature rise time. Temperature rise time was estimated to be 100 to 300 μs, however they did not present any direct measurement of rate of heating and temperature of the sample. Levy et al. [38] reported a method to measure the reaction temperature for the pyrolysis gas chromatography method with application to Curie-point reactor and filament pyrolyzers as well. In their method they considered the fact that the thermocouples which were arc-welded to the filament or ferromagnetic wire would indicate the temperature of themselves and not necessarily the samples. They have measured the temperature of the filament (or the ferromagnetic wire) in the cases in which they held the sample and in cases that they did not hold the samples and observed a significant difference.

Obtaining enough mass of products to meet the minimum weight requirement of the samples for product analysis is a problem with such techniques. Although the technology of analytical instruments has been advancing toward using smaller amounts of samples, practically a minimum of 1 gram or more is required for product analysis of petroleum fractions, and to obtain a mass balance around the reactor. Beside the problem with accuracy of temperature measurements in such

methods, such batch systems cannot convert enough mass of feed to products due the small volume of the spot or area where the feed is applied.

2.5.4 Laminar entrained flow reactor for thermal cracking of polymers and coal

Westerhout et al. modeled and evaluated a laminar entrained flow reactor for the determination of the thermal cracking kinetics of polymers. They reported deposition of polymer on the reactor wall as a major problem and that operation under a laminar regime could solve the problem [39].

Chen et al. described a tubular flow reactor for high temperature reactivity studies of pulverized solids [40]. The reactor consisted of a quartz tube which was placed inside an inductively heated furnace. At the top of the vertical reactor, a feeder dumped the pulverized particles into an entrainment stream. The temperature profile of the wall and fluid flowing inside the reactor was non-isothermal. The thermal and residence time history of the particles along the reactor were calculated for kinetic studies. They have used this reactor to study coal devolatitization during rapid transient heat transfer at furnace temperature of 1567°C and residence times of 56 to 90 milliseconds [41].The feed particle size distribution was not reported but a range of 50 to 100 μm was mentioned for the feed particles. They maintained the mixture as an optically-thin suspension which flowed downward into the inductively heated section of the furnace. The optically thin suspension ensured that the radiant heat flux to individual particles at any axial position was uniform and the macroscopic effects could be interpreted in terms of single-particle phenomena. The entrainment gas was transparent to radiation therefore the only means of heating was by convection from the tube wall and particles. The thin suspension of pulverized coal had little interfacial surface area for heat transfer so the entrainment gas remained relatively cool and quenched the primary products, and the components that evaporated from the coal or were expelled out of the particles. To study the secondary reactions of the vapor phase components, these researchers increased the loading of suspension

and increased the residence time by using a longer furnace. The thermal history of the gas and the particles was calculated; the maximum reported temperature of the particles was below 730°C. The temperature of the entrainment stream was from 200°C to more than 400°C below the temperature of the particles. The maximum reported temperature of the gas was about 330°C. In order to increase the entrainment gas temperature, they increased the concentration of the particles to 1200 particles/cm^3 when they considered the suspension not to be optically thin in all directions and at which the radiation absorption became significant [42]. The furnace was set from 1207°C to 1467°C and residence times varied from 156 to 174 milliseconds. Temperature of the gas profiles were from 120°C to 200°C lower than the temperature of particles. The maximum temperature of the entrainment stream ranged from 527 to 847°C. These researchers reported complications in gas temperature measurements by the intense radiation and by deposits of heavy hydrocarbons onto the thermocouples.

Calculation of thermal history and residence time can be complicated in such multi-phase mixtures. The particles absorb radiation from the furnace while part of this thermal radiation is absorbed by quartz wall (reaction tube). Particles also absorb radiation energy from the quartz wall. When the suspension is not optically-thin, then scattering of electromagnetic waves by particles should be considered. In both cases of an optimally thin and higher concentration of particles in suspension, the temperature of gas phase was either so low that the reaction did not progress, or the temperature of the vapor phase was significantly different from the particle. This significant temperature difference between solid, liquid and vapor phase makes the system more complicated for kinetic studies. Depending on the nature of the feed the coalescence of the feed particles and formation of liquid-solid agglomerates can be a problem or may not be observed. These researchers did not report on such a problem. Depending on the type and rank of the coal, the coalescence of the pulverized solids which generate particles of larger sizes may or may not be a concern in the pyrolysis of coal by these researchers, however, as it can be seen later in Chapter 3, it is a crucial factor in

any design for aerosolization of bitumen or in a commercial fluididized bed reactor. High concentration of the particles in carrier gas can intensify the rate of coalescence and deposition of feed on wall of the reactor.

2.5.5 Use of thermal-gravimetric analyzer (TGA)

Zhao et al. used a thermal- gravimetric analyzer to study thermal cracking of bitumen in a range of temperature from 30 to 600°C. They reported overall activation energy of 79 kJ/mole [43]. Using this design, volatile fractions of bitumen can evaporate but do not undergo a cracking reaction. Therefore, the overall activation energy is expectedly to be low. The temperature versus –mass loss that these researchers reported demonstrates that more than 50% of mass loss happens below 350°C which supports the idea of significant evaporation without involvement in thermal decomposition. Olmstead and Freund [44] used very high boiling fractions to obtain useful cracking data for vacuum residues, but the limit of their method was circa 500-550^{o}C. At higher temperatures, volatilization would inevitably compete with cracking at the time scale required to heat the TGA samples.

2.5.6 Use of fluidized bed reactors

Widely used coking processes are complex systems where phase behavior, heat, mass and momentum transfer combine with the reaction kinetics of coking processes. In fluid coking the heavy oil is sprayed into a bed of fluidized coke particles. The heavy liquids react on the surface of coke particles. The behavior of the wet particles depends on the Stokes number of the particles, the thickness of liquid films and diameter and surface roughness of the particles [45].

In kinetic studies, it is desirable and necessary that to either avoid the effects of heat and mass transfer or design the system of study in a way that these effects can be accurately modeled. In delayed coking the reaction takes place in a pool of liquids at a temperature range of 430 to 490°C. The reaction temperature of this process is much lower than the desired range in this research. Moreover, much higher yield of coke is expectable if such a process would be run at higher

temperatures due to much longer mass transfer path that the cracked products need to travel to move out of liquid phase. In contrast, in fluid-bed coking the reacting phase is a thin liquid film of liquid which are distributed on the hot surface of coke particles at temperature range of 510 to 540°C. The liquid feed is injected into the reactor by means of two fluid-phase nozzles with steam as the atomization gas and bitumen as the liquid phase. Formation of solid liquid agglomerates makes this system very complex for kinetic studies. When liquid products get trapped between coke particles, the mass transfer resistance against the volatile products of cracking which are moving out toward the vapor phase is increased. They will undergo more addition reactions and eventually all the liquids which are caught between the coke particles turn to coke. The heat transfer resistance should also be considered in addition of mass transfer resistance in modeling of fluid-bed coking that makes kinetic study of this system more complex.

Ali et al. [46] used the same reactor as Gray et al [16] and adopted the same procedure to study yield of coke and heat transfer in thermal cracking of liquid-solid agglomerates of Athabasca vacuum residue. They reported that the average coke from the agglomerates was 23% while the coke yield from thin liquid films of 20μm thickness was 11%. They developed a heat transfer model to calculate the thermal diffusivity of the agglomerates. They also found that in reaction of the thin liquid films, the rate of heating in the range of 14.8 to 148 K/s did not affect the yield of coke significantly. They observed that the concentration of liquids in the agglomerates does not make a significant difference in the yield of coke, and the yield of coke was insensitive to the agglomerate thickness. The reduction of the agglomerate thickness from 4 to 2 mm did not change of the yield of coke. This result suggested that such a reduction in size of the agglomerates did not reduce the mass transfer resistance in the liquid within the agglomerate, which is consistent with control of diffusion within the local environment of the liquid film, rather than with porous agglomerate. Thus a fluidized-bed reactor, due to the aforementioned complexity of the reaction and transport processes, is not an

appropriate choice for a study of intrinsic kinetics (unaffected by transport processes) to measure the rates of thermal cracking at high temperature.

2.6 Effect of solvent on the rate of thermal cracking

The over all rate of thermal cracking of *n*-alkanes are generally regarded to be a first order reaction. For a first order reaction, the rate constant is not a function of the initial concentration of the feed. Khorasheh and Gray studied high pressure thermal cracking of *n*-hexadecane in aromatic solvents [47]. They considered the possible impact of the dilution of the feed on the measured apparent kinetics of the reaction. They used a tubular flow reactor at 398 to 451°C and 13.9 MPa. The initial mole fraction of *n*-hexadecane in feed was 0.01, 0.03 and 0.05. For thermal cracking in benzene they had the following observations and conclusions:

- C_1 to C_{14} *n*-alkanes and C_2 to C_{15} α-olefins were produced
- Biphenyl was produced as a major product. They concluded that benzene cannot be considered as an inert diluent in thermal cracking of alkanes at the temperature range of their experiments.
- Low temperatures and higher initial concentrations of feed favoured higher molar selectivities for C_5 to C_{13} n-alkanes
- Increasing the reaction temperature and decreasing the initial concentration of n-hexadecane in feed resulted in a shift in distribution of *n*-alkanes in products toward lower carbon number and increase in total molar selectivity for α-olefins as major reaction products.
- They also found that the apparent first-order rate constants for overall conversion of *n*-hexadecane increased with increasing the initial concentration of *n*-hexadecane in feed. The increase in apparent first order rate constants with initial mole fraction of *n*-hexadecane in feed was an indication that the over all reaction order with respect to *n*-hexadecane was greater than one.
- The calculated activation energy were about 272 kJ/mole which was slightly above 256 kJ/mole for thermal cracking of pure *n*-hexadecane.

The difference in activation energy that these researchers reported for thermal cracking of *n*-hexadecane in benzene and the case of thermal cracking of pure n-hexadecane was within the range of experimental uncertainty of the activation energy.These researchers studied thermal cracking of *n*-hexadecane in toluene and ethylbenzene as well with the following results:

- Higher alkylbenzenes as major reaction products
- Lighter *n*-alkanes and olefins in the products
- Cracking in toluene and ethylbenzene was slower than cracking of pure n-hexadecane and in both case slower than cracking in benzene
- Equimolar distribution of n-alkanes was observed.
- They explained the inhibition of the cracking rate and product distribution by abstraction of benzylic hydrogens from the solvents. The dominance of benzylic radicals would account for the significance of selectivities for alkylbenzenes, formed by addition to α-olefins. The product distribution and the conversion -dependent kinetics were explained by the model they developed.

In toluene, alkyl radicals which are generated from the parent hexadecyl radicals would likely participate in hydrogen abstraction primarily from the solvent. Benzylic hydrogens of toluene were readily abstractable and were present at high concentrations:

$$R^{\bullet} + n - C_{16} \rightarrow RH + n - C_{16}^{\bullet} \quad (2.31)$$

$$R^{\bullet} + toluene \rightarrow RH + benzyl \quad (2.32)$$

$$benzyl + n - C_{16} \rightarrow toluene + n - C_{16}^{\bullet} \quad (2.33)$$

in which $R^{\cdot}$ is an alkyl radical. Reaction (2.32) is much faster than reaction (2.31). Reaction (2.32) would inhibit conversion of *n*-hexadecane since reaction (2.33) is much slower than reaction (2.31) due to the stability of the benzyl radicals. The alkyl radicals react with olefins and generate less reactive radicals. These

researchers suggested the probability that the inhibition of rate of thermal cracking of *n*-hexadecane was due to reaction of solvents radicals with α-olefins. In thermal cracking of *n*-hexadecane in toluene, the main propagation reaction that resulted in consumption of *n*-hexadecane was hydrogen abstraction from *n*-hexadecane by benzyl radicals (reaction 2.33), followed by β-scission. Benzyl radicals could react with α-olefins (radical addition reaction) and produce *n*-alkylbenzene radicals, which could eventually produce *n*-alkylbenzne by abstracting a hydrogen.

$$benzyl\ radical + \alpha - olefin \rightarrow n - alkylbenzene\ radical \qquad (2.34)$$

The inhibition can occur if the n-alkylbenzene radicals which are produced in Reaction (2.34) are stable radicals. These researchers stated that the activation energies for overall conversion of *n*-hexadecane could not be evaluated since the inhibition effects decreased the first-order rate constant with increasing conversion. The approximate activation energies which were estimated by these researchers for thermal cracking of *n*-hexadecane in ethylbenzene and toluene were 289 and 243 kJ/mole, respectively. The uncertainty in this estimation and the data should be considered in comparing in these two activation energy values. Nevertheless, the reported estimated activation energy for thermal cracking in toluene is noticeably lower than that in ethylbenzene solvent, while the reported data indicated that toluene is more rate inhibitory compared with ethylbenzene solvent. They suggested a mechanistic reaction model for thermal cracking of *n*-hexadecane in toluene which consists of 14 reactions. These mechanisms did not predict formation of benzene and ethylbenzene as major by products. However, it should be noted that the operating condition of their experiment covered a low range of temperature and was at high pressure as mentioned earlier.

Lannuzel et al. [48] studied kinetic influence of toluene on *n*-alkane pyrolysis and suggested the mechanisms of inhibition of rate of thermal cracking at temperatures in the range of 350 to 600°C and pressure range of 0.001 bar to 700 bar. They experimentally measured the inhibition of the rate of thermal cracking

of n-octane at high pressure and low temperature and compared it with thermal cracking data at low pressure and high temperature thermal cracking from the literature. Figure 2.5 demonstrate these comparisons. The molar mixture of *n*-octane/toluene is 9:1. The inhibition factor is defined as the following:

$$\text{Inhibition Factor} = \frac{\text{conversion of reactant without additive}}{\text{conversion of reactant with additive}} \qquad (2.35)$$

Figure 2.5 suggests that above 30 % conversion of *n*-octane and higher at the given dilution ratio, inhibition of the rate is insignificant for both high pressure-low temperature and low pressure - high temperature cases. Furthermore, the inhibition factor is much larger at the high temperature and low pressure operating condition compared with the case of high pressure - low temperature. They suggested a mechanism for such behavior by suggesting a kinetic model for suppression of the rate of thermal cracking and comparing the results of the model with the experimental data. The kinetic models consisted of elementary reactions of thermal cracking of pure n-octane, pure toluene and the suggested cross-reactions of n-octane/toluene mixture. The thermal cracking of *n*-octane is described by a free- radical mechanism. At low conversion the elementary reactions include initiation, hydrogen transfer, radical decomposition by β-scission, addition to double bonds and termination. In this model the organic compound which is subjected to pyrolysis was called μH. A radical which undergoes a monomolecular reaction is named $\mu^{\cdot}$ and a radical that reacts through bimolecular reactions is named $\beta^{\cdot}$. The inhibitor is a co-reactant in the case of chain reactions which can easily convert a chain carrier radical into a less reactive radical and causes new termination reactions. The symbols μH and YH represents the alkane and the inhibitor of toluene type respectively. YH contains a mobile H atom and yields a thermally stable and less reactive $Y^{\cdot}$ radical. The new initiation reactions from YH are unimportant. The inhibitor causes new propagation and termination reactions as the following:

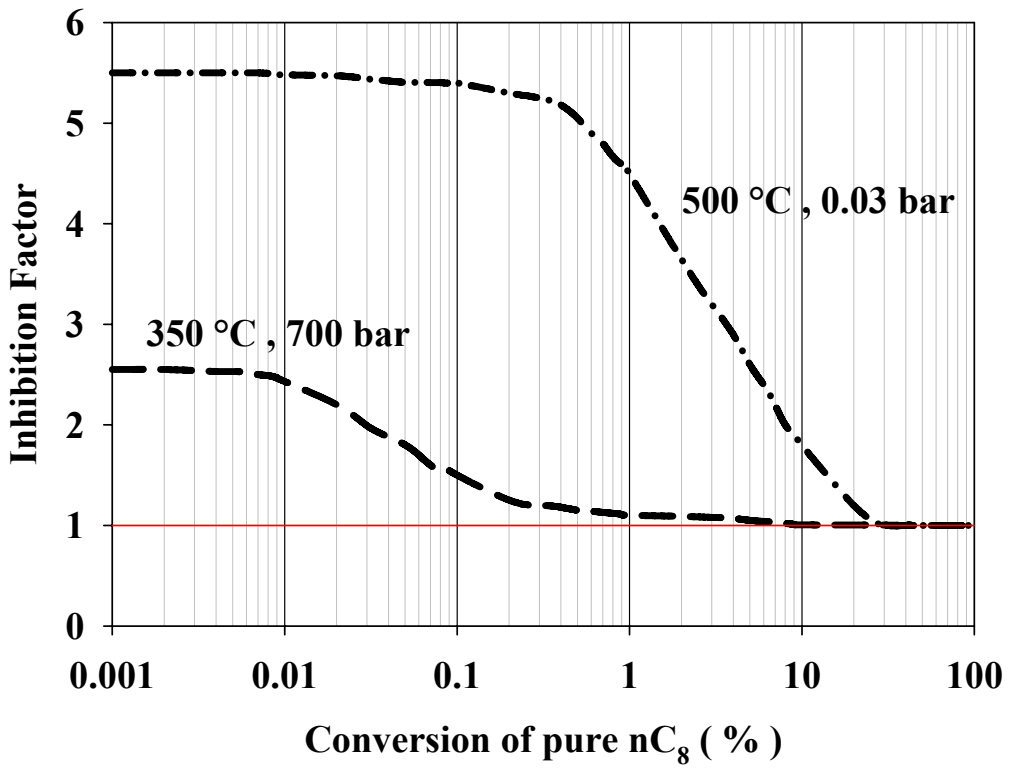

Figure 2.5 Calculated inhibition factor as a function of conversion of n-octane for the case of 700 bar and 350°C and the case of 0.03 bar and 500°C with n-octane/toluene ratio of 9:1 reproduced from [48]

Initiation :

$\mu H \rightarrow$ free radicals (β type) (2.36)

Propagation I :

$\mu^{\cdot} \rightarrow$ alkene + $\beta^{\cdot}$ (2.37)

$\beta^{\cdot} + \mu H \rightarrow \beta H$ (or alkane – minus) + $\mu^{\cdot}$ (2.38)

Propagation II :

$\mu^{\cdot}$ + alkene $\rightarrow$ heavy- radical (2.39)

heavy-radical $^{\cdot}$ + $\mu H \rightarrow$ alkane-plus + $\mu^{\cdot}$ (2.40)

Propagation III:

$\mu^{\cdot} \rightarrow$ alkene + $\beta^{\cdot}$ (2.41)

$\beta^{\cdot} + YH \rightarrow \beta H$ (or alkane-minus) $+ Y^{\cdot}$ (2.42)

$Y^{\cdot} + \mu H \leftrightarrow YH + \mu^{\cdot}$ (2.43)

Propagation IV:

$\mu^{\cdot} + YH \leftrightarrow \mu H + Y^{\cdot}$ (2.44)

alkene $+ Y^{\cdot} \rightarrow R^{\cdot}$ (2.45)

$R^{\cdot} + \mu H \rightarrow RH + \mu^{\cdot}$ (2.46)

Terminations:

$\mu^{\cdot} + \mu^{\cdot} \rightarrow$ products (2.47)

$\beta^{\cdot} + \beta^{\cdot} \rightarrow$ products (2.48)

$\mu^{\cdot} + \beta^{\cdot} \rightarrow$ products (2.49)

$Y^{\cdot} + \mu^{\cdot} \rightarrow$ products (2.50)

$Y^{\cdot} + \beta^{\cdot} \rightarrow$ products (2.51)

$Y^{\cdot} + Y^{\cdot} \rightarrow$ products (2.52)

in which the following stoichiometries are defined:

μH = alkene + alkane-minus

$RH = YH +$ alkene

YH reacts with $\mu^{\cdot}$ and $\beta^{\cdot}$ Equations (2.42), (2.43), and (2.44) and generates thermally stable $Y^{\cdot}$. This radical can react with μH (equations (2.43 and (2.45) or yield YY, $Y\beta$ and $Y\mu$ through the termination reactions. In the absence of the inhibitor, only radicals $\mu^{\cdot}$ and $\beta^{\cdot}$carry the chain reaction of μH (propagation I). YH introduces a new propagation (propagation III). The effect of YH on the kinetics of thermal composition of the alkane pyrolysis depends on the relative importance of radicals $\mu^{\cdot}$ and $\beta^{\cdot}$. At low-temperature / high-pressure conditions concentration of $\mu^{\cdot}$ is much higher than $\beta^{\cdot}$. Therefore reaction (2.37) is rate

limiting and the $r_{\mu H} = k_2 [\mu^{\cdot}]$. In presence of YH, the chain carriers $\mu^{\cdot}$ and $\beta^{\cdot}$ are consumed and $Y^{\cdot}$ is generated. $Y^{\cdot}$ reacts with $\mu^{\cdot}$ in new terminal reaction (equation (2.50) and decreased the concentration of $\mu^{\cdot}$. By reduction of the concentration of $\mu^{\cdot}$, the rate of thermal decomposition decreases. Thus the inhibition effect of *YH* takes place through the new termination reactions. At high temperature / low pressure conditions concentration of $\beta^{\cdot}$ is much higher than $\mu^{\cdot}$ therefore reaction (2.38 is rate limiting and the rate of thermal cracking is :

$$r_{\mu H} = k_3[\beta^{\cdot}][\mu H] + k_{4\beta}[\beta^{\cdot}][YH] \qquad (2.53)$$

YH affects the kinetics in two ways. It has an accelerating effect since the new propagation III generates the same products as of the reactions in propagation I. It also has an inhibition effect by consuming the chain carriers $\mu^{\cdot}$ and $\beta^{\cdot}$ (reactions (2.42, (2.43 and (2.44) and producing less reactive $Y^{\cdot}$ which eventually produce *YY* and $Y\beta$ in new termination reactions. As a consequence the concentration of $\beta^{\cdot}$ decreases and hence the rate of thermal cracking, $r_{\mu H}$, decreases. Thus, the effect of *YH* on the kinetic of the thermal cracking of n-alkanes depends on the reaction temperature and pressure.

These researchers conclude that when $Y^{\cdot}$ is not very reactive, its concentration is high and results in new important termination reactions. The overall kinetic effect in this case is inhibition of the rate. When $Y^{\cdot}$ is more reactive, its concentration is very low and the new termination reactions are not important. The over all kinetic effect can be acceleration of thermal decomposition of μH through propagation III in this case. For the case of toluene and *n*-octane the experimental results of these researchers showed a significantly lower inhibition factor at high-pressure / low-temperature conditions comparing to the case of low-pressure / high temperature conditions. Additionally in both cases, the inhibition factor tended to unity at higher conversion. These two observations can be explained by the propagation IV. They found alkylbenzenes (from propylbenzene to octylbenzene) which were

products of addition of benzyl radicals on alkenes (from ethylene to heptene). Addition of $Y^{\cdot}$ radicals to alkenes leads to formation of more reactive $R^{\cdot}$ radicals (of type $\beta^{\cdot}$) which decrease the inhibition effect. At higher conversion in both cases of high-pressure / low –temperature and low-pressure/ high temperature concentration of alkenes increases and consequently more of $Y^{\cdot}$ radicals transforms to $R^{\cdot}$ and by decrease in concentration of $Y^{\cdot}$, inhibition factor decreases as well. However, high pressure favors addition reactions and comparing to the case of low pressure, more alkenes can react with $Y^{\cdot}$ radicals and expectedly and consistent with the experimental results the inhibition effect of toluene found lower at high-pressure case. To summarize the work of these researchers, they found that toluene inhibits the pyrolysis of n-octane (presenting n-alkanes) at very low pressure regardless of the temperature (350 to 500°C). At high pressure, they did not observe a significant inhibition (350 to 450°C and 100 and 700 bar). An important conclusion from their experimental data at the range of pressure and temperature that they carried the experiments is that at conversions above 30% there is no inhibition in both case of high and low pressure.

According to the kinetic model which Lannuzel et al. proposed, in thermal cracking of pure toluene the following can be produced; bibenzyl, ethylbenzene , xylene and ethane in termination reactions and methane, hydrogen , benzene and benzylphenyl in other propagation reactions. The cross reactions in mixture of toluene and *n*-octane generates products from reaction of benzyl radical with alkane radicals which ranges from ethylbenzene to nonylbenzene in termination reactions. Ethylbenzene is the product of reaction of benzyl radical with methyl radical while nonylbenzene is the product of the reaction of octyl (n-octane radical) with benzyl radical. In propagation reactions, alkenes add to benzyl radical to produce another radical which reacts with n-octane or toluene and yield a benzylcene (benzyl radical + alkene) [48]. Hydrogen and benzene are also produced in propagation reactions. This benzene is product of reaction of phenyl radical and n-octane.

Zhorov and Volokhova [49] reported that extraction of polycyclic aromatic hydrocarbons (PAH) from kerosene - gas oil cuts could increase the yields of lower olefins during cracking, especially ethylene in pyrolysis reaction while monocyclic hydrocarbons with long side chains did not inhibit pyrolysis. To study the inhibition effect of bicyclic and tricyclic hydrocarbons on naphtha and kerosene-gasoil cuts they first selected n-hexadecane and decalin as model compounds for paraffinic and naphtenic hydrocarbons. They used naphthalene and phenathrene as the bicyclic and tricyclic aromatic hydrocarbons. They also added these PAH compounds to commercial naphtha and kerosene-gas oil fractions and measured the yield of gaseous compounds. The thermal cracking temperature was 800 to 900°C and residence time of 0.13 to 0.14 second. The feed stock was diluted with steam from 50% to 100 wt%. In thermal cracking of n-hexadecane and decalin , addition of the PAH compounds reduced the yield of gas products of thermal cracking reaction. Table 2.3 compares the results of pyrolysis of pure n-hexadecane and decalin with pyrolysis of mixtures of each of these two components with naphthalene and phenathrene. The inhibition effect of naphthalene and phenathrene on *n*-hexadecane and decalin with regard to the reduction in the yield of gas products are almost the same.

They also investigated the inhibition effect of naphthalene and decalin on a naphtha cut with initial boiling point of 150°C and 210 to 340°C kerosene – gas oil cut. The original naphtha feedstock did not contain any PAH. The kerosene-gas oil contained only bicyclic aromatics (8.6 wt%). Therefore, they added both naphthalene and phenathrene to naphtha and only phenathrene to kerosene-gas oil cut. Table 2.4 and Table 2.5 compare the result of thermal cracking of naphtha and kerosene-gas oil cuts without and with added PAHs. Both naphthalene and phenathrene had strong inhibitive effect on thermal cracking reaction and reduced the yield of gases significantly. Addition of phenethrene to kerosene-gas oil cut did inhibit the rate of thermal cracking but the reduction in yield of gas was much lower comparing to the case of naphtha. They explained this difference by the fact that there were already fairly significant amount of PAH in the original feedstock.

They concluded that presence of both bicyclic and tricyclic aromatics are not desirable in the feedstock as they reduce the yield of ethylene. They additionally reported that removal of these components from the feedstock would give a substantial decrease in the rate of coke formation on the walls of the pyrolysis coil.

Table 2.3 Effect of PAH on yield of products in pyrolysis of n-hexadecane and decalin. Data from Zhorov and Volokhova [49]

feedstock	yield wt% of the feed stock							
	total gas		methane		ethene		propene	
	800°C	900°C	800°C	900°C	800°C	900°C	800°C	900°C
n-hexadecane pure	57.8	72.2	6.3	7.7	36.3	43.5	5.6	10.0
n-hexadecane + 5 wt% naphthalene	42.5	45.4	4.5	5.3	28.3	25.0	4.5	8.3
n-hexadecane + 5 wt% phenathrene	41.0	46.2	3.9	4.9	25.3	29.3	4.6	2.4
decalin pure	29.9	51.1	4.4	11.1	16.6	25.0	3.3	7.6
decalin+ 5 wt% naphthalene	19.6	23.8	3.1	5.3	11.3	12.3	1.5	2.9
decalin + 5 wt% phenathrene	21.2	23.2	2.8	5.6	12.6	11.9	1.1	3.7

Table 2.4 Effect of PAH on yield of products in pyrolysis of naphtha . Data from Zhorov and Volokhova [49]

feedstock	yield wt% of the feed stock			
	total gas	methane	ethene	propene
	850°C	850°C	850°C	850°C
naphtha only	86.3	18.2	40.0	14.3
naphtha + 3 wt% naphthalene	72.5	11.8	30.7	13.6
naphtha + 6 wt% phenathrene	63.9	13.3	26.3	11.3

Table 2.5 Effect of PAH on yield of products in pyrolysis of kerosene-gas oil cut. Data from Zhorov and Volokhova [49]

feedstock	yield wt% of the feed stock			
	total gas	methane	ethene	propene
	900°C	900°C	900°C	900°C
kerosene – gas oil only	63.5	9.0	26.0	14.2
kerosene-gas oil + 2 wt% naphthalene	61.3	8.5	25.5	13.0
kerosene-gas oil + 4 wt% phenathrene	53.6	7.7	22.6	11.8

Zou et al. [17] reported that they observed a self-inhibition action in pyrolysis of gas oil as the conversion increased. They observed that rate constant decreased by increase of conversion. They used steam as the diluent in their experiments. No aromatic solvent was used in their experiments, nevertheless the feed consisted of 11.1 wt% of aromatic compounds. Their observations are consistent with the experimental work of Zhorov and Volokhova [49]. However, the fact that the rate constant decreased with the progress of the reaction could be due to the change of in the nature of the bonds which undergo thermal decomposition. At higher conversions, a higher percentage of the reactant consists of aromatic compounds which hardly crack under non-catalytic operation conditions. Even if there is no mechanism self-inhibition, a change in the rate constant of the reaction is expected due to such changes in the structure of the unconverted reactant components.

Herbinet et al. [50] studied pyrolysis of norborane dissolved in benzene (norbornane is solid at room temperature). They used a jet-stirred reactor at 600 to 700°C and 106 kPa. The feed mixture was 20 wt% norbornane and 80 wt% benzene. The carrier gas was helium and the molar composition of the component in the feed at the inlet of the reactor was 0.7% norborane, 3.6 wt% benzene and the balance was helium. Residence times ranged from 1 to 4 seconds. The measured conversion of norborane at these operating conditions were 0.04 to 22.6 %. They observed that benzene was very stable and its conversion was very small. Evolution of small quantities of aromatic and polyaromatic compounds were reported which were considered to be the products of cross-coupling reactions of the norbornane-benzene binary mixture. These researchers studied the possible influence of benzene on the kinetics of the pyrolysis of norbornane in benzene. They studied pyrolysis of pure benzene in a helium carrier at temperatures 640°C and 700°C at residence times ranging from 1 to 4 seconds at pressure of 106 kPa. The mole fraction of benzene was 3.6% molar in helium. The mole fraction of benzene in the helium was set to the same value as for the case of pyrolysis of the bornane – benzene mixture. The maximum measured conversion of benzene was 0.08 % at 700°C and 1 second residence time. The conversion of norbornane dissolved in benzene under the same conditions was 9.7%. The only product of pyrolysis of benzene which was detected was biphenyl. Formation of toluene, styrene, indene and naphthalene was not observed in thermal cracking of pure benzene in helium. These researchers concluded that the termination reactions between radicals derived from the two hydrocarbons could explain some products like toluene. They concluded that the overall cross-coupling reactions in the binary mixture of norbornane and benzene were rather limited because the decomposition of benzene generated only a few components in the temperature range of their study. The literature is not consistent in regarding benzene as an inert solvent for thermal cracking reactions. Khorasheh and Gray in conclusion of their study about high pressure thermal cracking of *n*-hexadecane in benzene considered the presence of biphenyl as a major reaction product as an indication that this solvent could not be an inert diluent at mild

temperatures (400 – 450°C) [47]. Herbinet et al. accepted that interactions between benzene and norbornane did occur, however they considered that presence of benzene had a negligible influence on the reactions of norbornane at temperatures less than 700°C.

2.7 Conclusions

In this chapter the work of previous researchers on high temperature thermal cracking of heavy oils is reviewed. There is no published work on intrinsic kinetics of bitumen and vacuum residue at temperatures above 600 ºC in which the effect of heat and mass transfer are considered and the rate constant of the thermal cracking are reported. The research work of Gray et al. in which the coupling of transport phenomena with the kinetics has been taken into account, was carried at temperatures below 600°C. They reported limitations of their method for kinetic studies at higher temperatures [16,36]. Nevertheless, their results especially the quantitative trends between liquid film thickness and yield of coke can be used in designing technologies for kinetic studies at higher temperatures. The researchers who studied heavy oils which are in vapor phase at the reaction temperatures faced fewer challenges; however, they frequently reported the problem of conversion of feed before reaching the reaction temperature. The reports about interaction of heavy oils with aromatic solvents and materials were also reviewed, and these results suggest that aromatic solvents may affect the apparent kinetics of bitumen conversion. These insights will be used in the interpretation of the results in Chapter 5. In summary the major reactor types which used by the previous researchers to study rate of thermal cracking of n-alkanes and heavy oils are as follows. :

1. The continuous flow reactors which are operated in non-isothermal condition and are criticized for the inaccuracy of the reaction evaluation of the temperature profile in axial and radial directions.
2. The Curie point reactors described in the literature either cannot bring the reactant rapidly to the reaction temperature for studies at temperatures above 550 °C, or the reported kinetic results were found to be inconsistent with the literature.

Chapter 3
Design Philosophy

Based on the review of the work of the previous researchers, the challenges for the kinetic study of thermal cracking of heavy oils at high temperatures can be summarized as the following:

1. The rate of thermal cracking at elevated temperatures is high. The time required for the reactants to reach the desired reaction temperature is an important design factor. A significant portion of the reactant must not convert before it reaches the reaction temperature; therefore, the rate of heat - up of the feed to the reaction temperature should be sufficiently fast.
2. For heavy oils with fractions which remain in the liquid phase at reaction temperature, the effect of heat and mass transfer must be considered for an intrinsic kinetic study. Formation of liquid solid-agglomerates gives complex coupling of mass and heat transfer with the reactions; therefore introduction of the feed must be accomplished so that the heat and mass transfer resistance can be minimized.

The focus of this research work is to develop the technologies for the study of high-temperature short-residence time thermal cracking of heavy oils by overcoming these two basic problems.

3.1 Role of heating method and phase behavior

Reaction of liquids in a fluidized or riser reactor is one method of achieving rapid heating. This method, however, gives liquid - solid agglomerates that increase the diffusion path of the volatile products of cracking toward vapor phase. Figure 3.1 illustrates how solid-liquid agglomerates change the path for mass transfer. The volatile products which are trapped between the three solid particles inside the

liquid phase stay longer in the liquid phase, and undergo more addition reactions. The mechanism of formation of coke was reviewed in Chapter 2. Higher thickness of the liquid film on the heat carrier particles results in higher yield of coke product. The work of Gray et al. demonstrated the clear relationship between thickness of liquid film and yield of coke (Figure 2.3) [16].

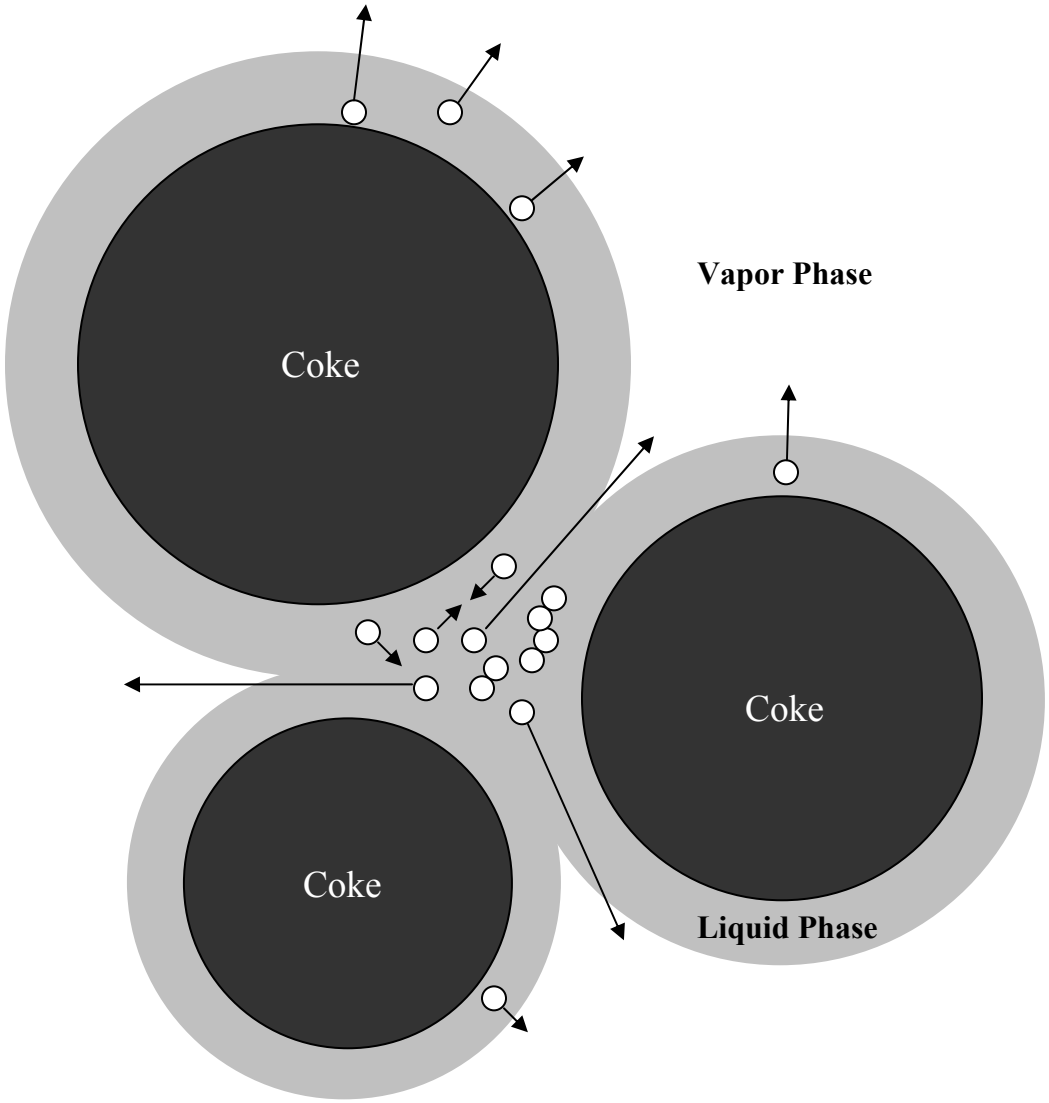

Figure 3.1 Solid-liquid agglomeration increases mass transfer resistance: More addition reactions in the area where the liquid films are shared between the particles are a consequence of the longer diffusion path. Small circles show the products of thermal cracking .

Unless the liquid is very uniformly distributed on the particles, local wet agglomerates will give slow heating and reaction at temperatures well below the surrounding vapor phase. A reduction of liquid film thickness will lead to more vaporization of the feed liquid, given a mixture with a wide range of boiling points. Thermal cracking in vapor phase favors β-scission rather than addition reactions in the free radical chain reactions. The higher the reaction temperature, relative to the boiling range of the feed, the greater the portion of the feed that can be vaporized. Therefore, the combination of a reduction of liquid film thickness and reaction at higher temperatures will give a higher yield of olefins at a given extent of conversion. Short residence time operation minimizes the progress of the addition reactions which are precursors of coke formation. Moreover, short residence times at a given temperature also reduce the cracking of components in the vapor phase to give light ends, minimizing the loss of hydrogen from the final liquid products. Consequently, a combination of high temperature, short residence and minimization of mass transfer resistance is expected to give the following results:

1. Minimization of the yield of coke
2. Maximization of the yield of olefins at a given level of conversion
3. Improvement in quantity and quality of liquid products may or may not be observed depending on the trade-off between reaction in the vapor phase and the severity in terms of the combination of reaction temperature and residence time

3.2 Required heating rate

The half-life of reaction can be used as a metric to determine the required time for the reactant to reach the reaction temperature. Table 3.1 shows the estimated of half life of thermal cracking of Athabasca vacuum residue in the temperature range of 600 to 800ºC. The half-life is estimated by extrapolation of the results of Gray et al. [36], which was obtained at a lower range of temperature (maximum temperature 530ºC). The estimated half life of the reaction for thermal cracking of

Athabasca vacuum residue is 27 milliseconds at 700°C. If the desired reaction temperature is 800°C and if the reactant spent about 27 milliseconds around 700°C before it reaches the reaction temperature, about 50% of the reactant will be converted to the products by the time the feed stream reaches the final reaction temperature.

Table 3.1 Prediction of half life of Athabasca vacuum residue in thermal cracking reaction by extrapolation of the results of Gray et al. [36]

Temperature ◦C	Half life (ms)
600	500
700	27
800	2

Extrapolation of the kinetic data to temperatures much above the range in which the data were collected does not guarantee an accurate prediction; nevertheless, it gives an estimate for the order of magnitude of the half-life of the reaction. Table 3.2 demonstrates the estimation of half-life of the reaction for thermal cracking of n-hexadecane in the same temperature range. The half-life of this reaction was calculated by interpolation and extrapolation of the results of Depyre et al. [25] which carried out their experiments at the temperature range of 596 to 698°C.

Table 3.2 Prediction of half life of n-hexadecane in thermal cracking reaction by interpolation and extrapolation of the results of Depyre et al.[25].

Temperature ◦C	Half life (ms)
600	1400
700	47
800	3

3.3 Designs of the previous researchers

The requirement for a high rate of heat-up of the feed to the reaction temperature has been considered by some of previous researchers, and they tried different designs to overcome the problem of undesirable conversion of the reactant before reaching the reaction temperature [25, 29 and 36]. Table 3.3 compares the time which is required for the feed to reach the reaction temperature in their designs. These designs were reviewed in Chapter 2. The comparison of the temperature rise time that they reported with the estimated half life of reactions which are given in Table 3.1 and Table 3.2 show that, their reactors are not suitable to study the kinetics of thermal cracking of liquids like vacuum residue or vapors of n-hexadecane at temperatures above 600°C.

Table 3.3 Reactor type and temperature rise time: Temperature rise time is the time at which the feed reaches the reaction temperature

Researchers	Reactor type	Feed	Temperature range (°C)	Temperature rise time (ms)
Vogiatzis et al. [21]	Mixing jets of hot and cold (reactant stream)	Cold Lake bitumen	500 to 900	30
Rastogi et al. [25]	Curie Point Pyrolyzer	propane	600 to 900	45-85
Gray et al. [36]	Curie point Pyrolyzer	Athabasca vacuum residue	457 to 530	3000-8000

Technologies like focused laser beam are available which can raise the temperature to such high temperatures in less than 100 μs [30]. The problem with this technology and other technologies which are based on concentrating energy at a small spot or area to provide a fast rate of heat-up were reviewed in Chapter 2 and can be summarized as the following:

1. Collection of enough mass of product for complete product analysis in a reasonable operation time is not possible.
2. Accuracy in measurement of reaction temperature is very difficult
3. At high rate of heat–up a liquid sample bubbles and splatters. This gives a lack of uniformity of temperature and reaction time of the feed material [51].
4. Homogeneity of temperature inside the sample (reactant): Even if the sample remains intact during the reaction, the temperature in the liquid versus the vapor may not be the same regardless of the mode of heating, i.e. from within the liquid or from the exterior of the liquid.

3.4 Design Objectives

The major activity in this research work was to design and construct reactors to meet the following goals:

1. Operation at atmospheric pressure and temperature range of 600°C to 800°C.
2. Flexibility for applying short residence time in the given range in Table 3.1
3. To minimize heat and mass transfer resistance so that their effects can be neglected for the intrinsic kinetic study of thermal cracking of bitumen and vacuum residue.
4. Fast heat-up of the feed to the reaction temperature and fast cool-off of the products if required, in order of few milliseconds; It is desirable to design a reactor which can be operated in very close to ideal isothermal condition.
5. Collection of enough mass of products for gas chromatography, simulated distillation, NMR, MCR and elemental analysis in a reasonable operation time. In addition, the total quantity of feed which is introduced into the reactor at each run of experiment should be sufficiently high relative to the size of the apparatus (including the product collection system) to minimize the error in mass balance due to possible losses in the recovery of products. The range of products to collect and quantify if from light gases to coke.

3.5 Selection of reactor type

In order to meet the aforementioned goals, a tubular continuous flow reactor type was selected. Stainless steel 316 was chosen as the reactor material because of the availability of the compression fittings and reasonable durability of the material at high temperature. Quartz was the preferable material as it eliminated the possibility of catalytic effects of the surface, but its fragility prevented the use of metal fittings to accomplish the required introduction of feed and recovery of products. Furthermore, attachment of thermocouples to measure the wall or fluid

temperature along the reaction tube was not feasible if the tube was made of quartz.

An electrical furnace was selected to heat the exterior of the tubular reactor. Depending on the operation (isothermal or non-isothermal) the furnace can serve to either maintain isothermal conditions or to heat the reactants up to the reaction temperature. Figure 3.2 illustrates a simplified temperature profile for a tubular reactor. The temperature profile consists of three sections. As the fluid flows inside the reaction tube inside the furnace, the feed is heated up (Section I), then it reaches the reaction temperature and is maintained at this temperature as the furnace compensates for the heat losses (Section II) and eventually the reactants cool off by means of heat losses or a quenching system at the end of the reaction tube or down stream of the reactor (section III).

An important design factor is to ensure that the extent of the reaction is insignificant in section I and section II. The reactants must be heated fast enough to the reaction temperature and at the end cooled off fast enough to quench the reaction, to give most of the conversion in the isothermal section.

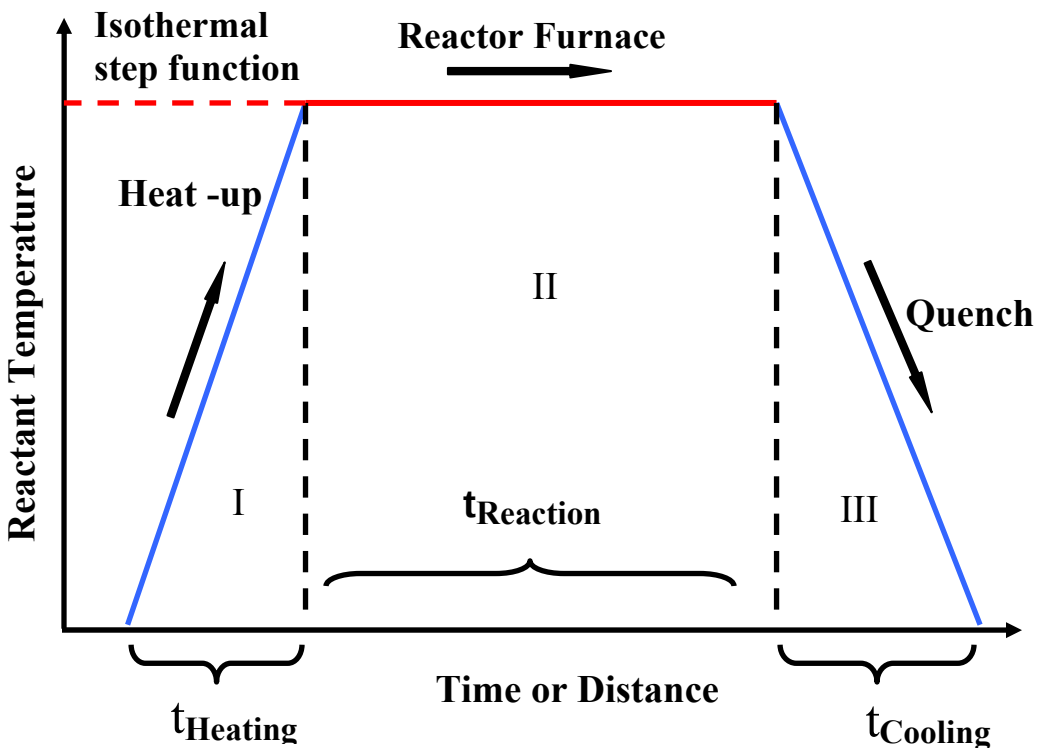

Figure 3.2 Temperature profile along a continuous flow reactor and the quench at the down stream

3.6 Micro-structured mixers for fast heat-up of the feed

In order to minimize $t_{Heating}$ so that the temperature profile along the reactor resembles an ideal step function, the technology of micro-structured mixers was selected. A hot stream of inert gas at a temperature higher than the reaction temperature is mixed effectively with a cold stream of inert gas which carries the reactant and the temperature of the mixture reaches quickly to the desired reaction temperature. Pfeifer et al. [52] described the manufacture of microstructured mixers based on the multi-lamination principle and introduced different type of these kinds of mixers which are produced by the Institute for Micro- process Engineering (IMVT). A multi-lamination process provides a very short diffusion length to achieve mixing in a very short mixing time and short mixing length in the direction of the flow. Figure 3.3 demonstrates the principle of mutlti-lamination. A microstructured mixer splits the two fluids A and B which are to be mixed into many sublayers. As the thickness of the adjacent sublayers of fluid A

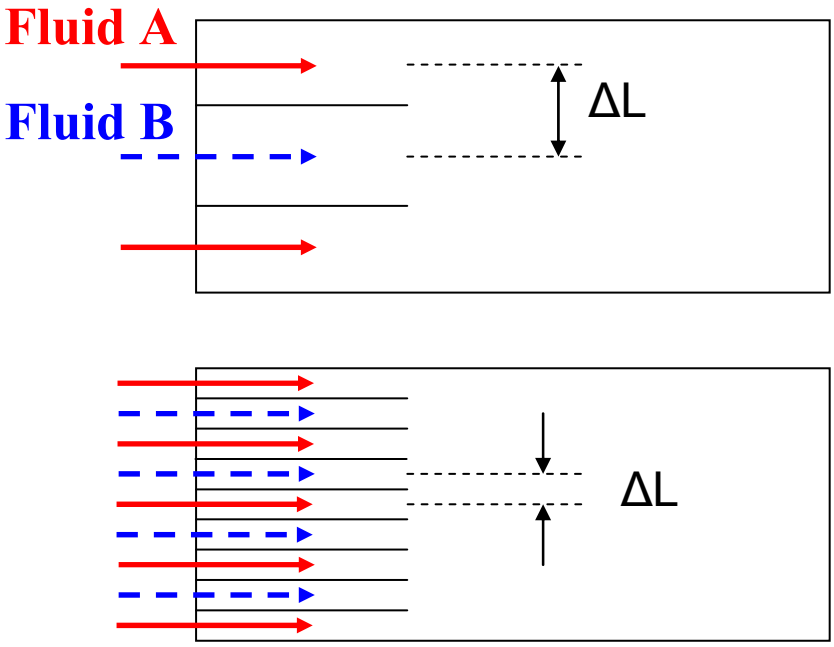

Figure 3.3 Principle of multi-lamination: As the thickness of the sublayers of the fluid A and fluid B are decreased the diffusion path for mass transfer decreases and consequently the mixing is accomplished in a shorter time and a shorter length in the direction of the flow. The drawing with modification from [52].

and B is decreased, the diffusion path for mass transfer becomes shorter. Thus the mass transfer resistance declines. Consequently mixing can be accomplished in shorter time and shorter distance from the outlet of the mixer.If the mixing is assumed to be only due to the diffusion mass transfer then the mixing time can be approximated by the following equation [53]:

$$t_{mixing} \approx \frac{\Delta L^2}{D} \tag{3.1}$$

The diffusion length ΔL is the distance between two micro-channels. Given that the diffusion constant does not change at a constant temperature, the shorter which is the diffusion length, the shorter the mixing time will be. The mixer

performance can be affected by change of the cross section of the micro-channels as well as the distance between the channels.

Haas - Santo et al. [53] studied the characterization of micro-structured mixing experimentally. They used a V-mixer in which the angle between the exiting fluid streams is 90°C. Table 3.4 describes the specification of the V-mixer. They used a capillary tube with outside diameter of 30μm and inside diameter of 20μm to take fluid samples at the outlet of the mixer. By analyzing of concentrations at different positions at the outlet of the mixers they could evaluate the mixing quality versus a variety of mixing parameters. They calculated the quality of mixing using the following equations:

$$M = 1 - \frac{S}{S_0} \tag{3.2}$$

$$s = \sqrt{\frac{1}{N-1}\sum_{i=1}^{N}(y_i - \bar{y})^2} \tag{3.3}$$

$$\bar{y} = \frac{1}{N}\sum_{i=1}^{N} y_i \tag{3.4}$$

Table 3.4 Geometry of the V-mixer used by Haas-Santo et al. [53]

Channel height	0.1mm
Channel width	0.1mm
Channel length	20.0 mm
Number of channels per foil	40
Number of foils per passage	12
Number of channels per passage	480
Foil thickness	0.2mm
Width of mixer outlet	11.2 mm
Stack height	4.8 mm
Mixing angle	90.0º

In which M is the degree of mixing, S is the standard deviation of N samples and S_0 is the standard deviation referring to the initial state. y_i and $\bar{y}$ are molar ratio and mean molar ratio of the gas component. These researchers measured the mixing length to reach a mixing degree of 95 % and showed that the mixing length at the same operation condition (temperature and flow rates) were significantly smaller when they mixed He with N_2 comparing with the case of mixing of Ar with N_2. They explained this by the difference of the binary diffusion coefficient which is 0.69 cm^2/s for He-N_2 and 0.19 cm^2/s for Ar-N_2. They also showed that for the case of V-mixer the mixing time was reduced by increasing the flow rates. They explained that this effect was caused by a non-diffusion mechanism. They suggested that the shear stress between the sub-streams of the fluid which were induced by the geometry of the mixer enhance the mixing quality. Figure 3.4 and Figure 3.5 demonstrate change of mixing length

and mixing time by temperature for the case of mixing argon and nitrogen using the V-mixer and at the flow rate of 5 SLM per each passage of the mixer.

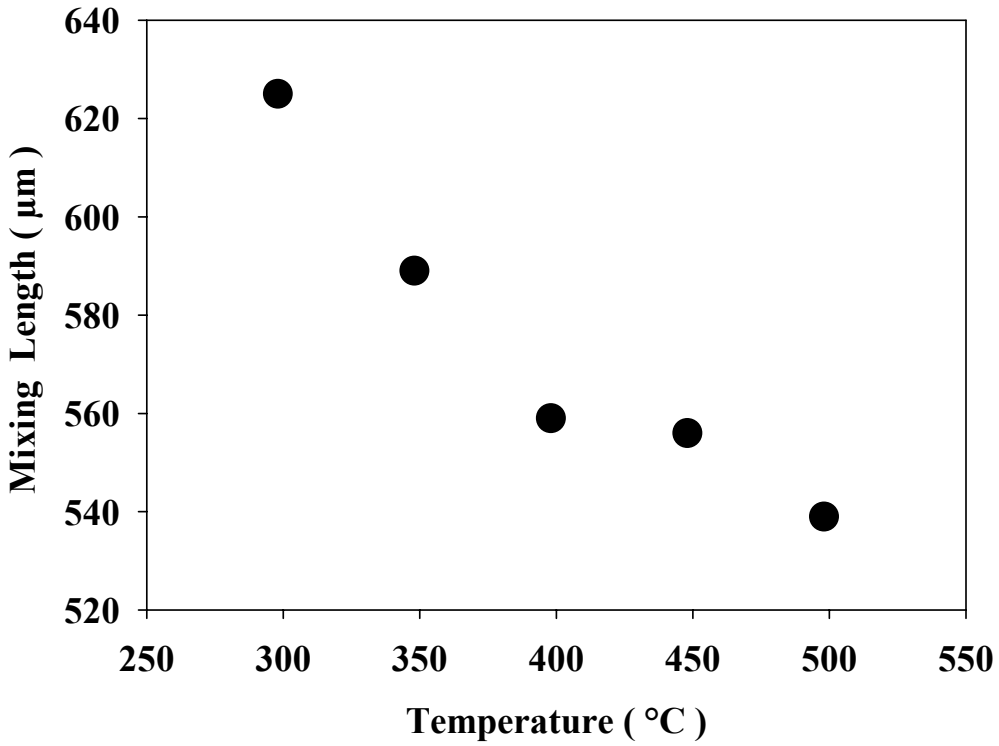

Figure 3.4 Mixing Ar and N_2 at 5 SLM/passage by the V-mixer which is described in Table 3.4. Mixing length decreases as the temperature increases. The diagram is produced based on the data from [53].

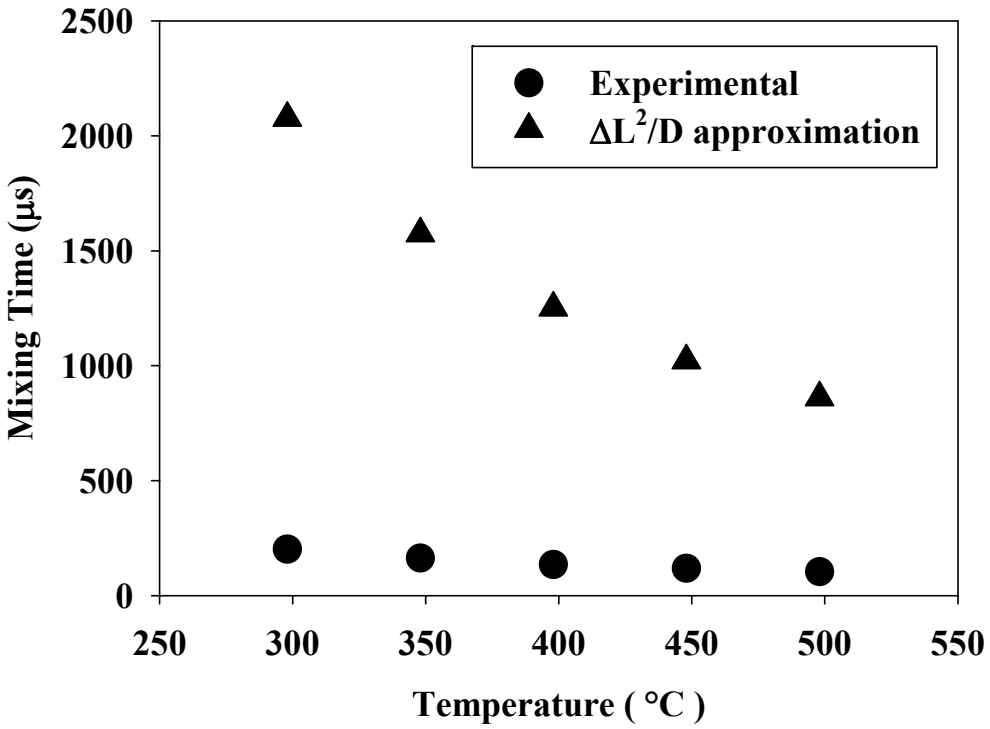

Figure 3.5 Mixing Ar and N_2 at 5 SLM/passage by the V-mixer which is described in Table 3.4 . Mixing time decreases as the temperature increases. The experimental data are compared with theoretical approximation when mixing is all through diffusion. The diagram is produced based on the data from [53].

In order to calculate the mixing time these researchers used the following formula:

$$t_{mix} = \frac{L_{mix}}{V_{out}} \tag{3.5}$$

In which L_{mix} is the diffusion length and V_{out} is the velocity of the gas in the mixing chamber.Figure 3.5 demonstrates that non-diffusion mixing mechanism reduces the mixing time by one order of magnitude. As the temperature increases the viscosity of the gas increases and this should have a negative effect on the mixing degree due to decrease in mixing by convection. However, the experimental results indicated a reduction in the mixing time, which can be explained with the effect of diffusion mixing. As temperature increases the

diffusion coefficient of the gases increases and this decreases the mixing time according to Equation (3.1).

Haas - Santo et al. [53] summarized the important design factors in construction of the micro-structured mixer that affects the efficiency of the mixer; the width and height of the channels, the distance of the channels which determine the diffusion length and the angle between the directions of the sub-streams of the fluids that exit the channels at the outlet of the mixer. The micro-structured mixer can be used to mix a cold stream of an inert gas which carriers the reactant with a stream of an inert gas at a temperature higher than the reaction temperature. It should be kept in mind that the mixing time does not necessarily equal to the time to reach thermal equilibrium. If thermal conduction is considered as the only mechanism of heat transfer between the streams then by using the analogy between heat and mass transfer the time to reach thermal equilibrium can be estimated by the following equation:

$$t_{\text{thermal equilibrium}} \approx \frac{\Delta L^2}{\alpha} \tag{3.6}$$

in which α is thermal diffusivity of the fluid. For the same geometry of the micro-channels, the higher is the thermal conductivity of the carrier gas the shorter is the time to reach thermal equilibrium. Thermal conductivity of helium is one order of magnitude larger than the thermal conductivity of nitrogen and argon. Therefore, if helium is used, thermal equilibrium by micro-mixing is expected to be one order of magnitude shorter than when argon or nitrogen is used as the carrier gas and as the hot stream. Figure 3.6 compares the order of the magnitude to reach thermal equilibrium when the heat transfer is only by means of conduction for the cases in which argon, nitrogen and helium are used. The physical properties are taken from the literature [54, 55, 56].

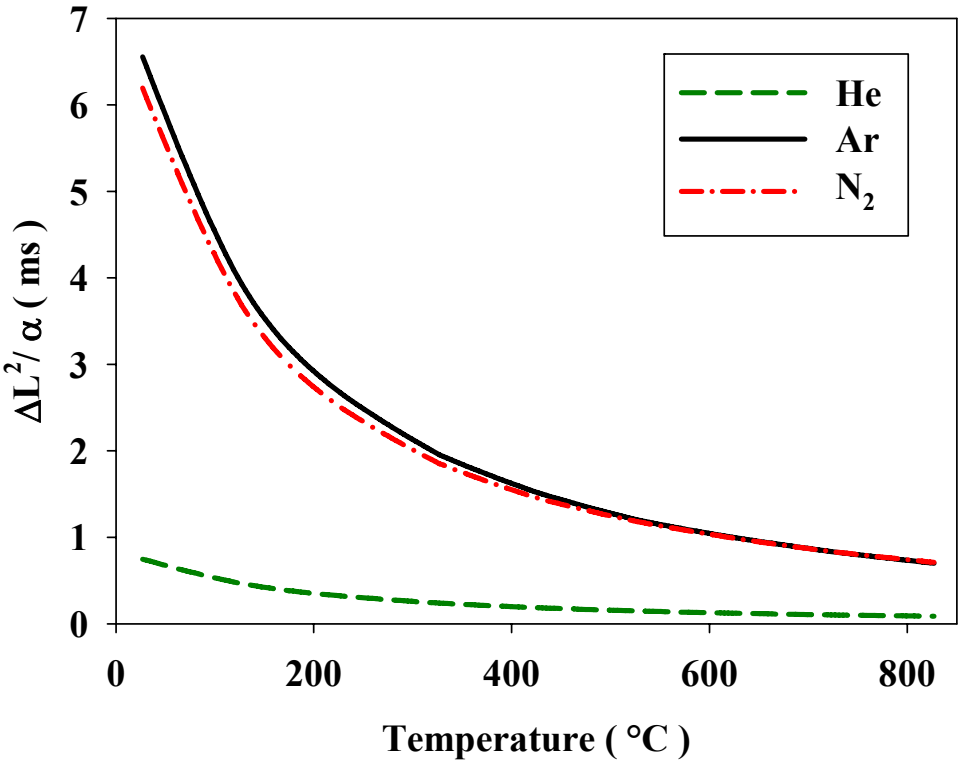

Figure 3.6 Estimation of order of magnitude of the time which is required for thermal equilibrium when a two hot and cold stream are mixed using the principle of multi-lamination of the flow. Physical data from [54,55 and 56]

The Lewis number, defined as the ratio of the thermal diffusivity and the mass diffusion coefficient, in the temperature range of 25 to 800 °C for helium and argon is 1.1 and for nitrogen very close to 1.0. Consequently, the mixing time and the time for thermal equilibrium through conduction should be in the same order of magnitude. However, it should be kept in mind that the design is not based on the mixing time but only on the thermal equilibrium time, which is short enough for the purposes of this research.

A micro-structured mixer was fabricated to be used in this research by Institute for Microprocess Engineering, Karlsruhe, Germany. A hot stream of helium gas at above the reaction temperature is mixed with a cold stream of the helium which carries the feed and reach the reaction temperature in few milliseconds as it is

estimated by the manufacturer. This design closely approximate the ideal isothermal profile by providing a fast rate of heat-up of the reactant to a constant reaction temperature. The design specifications and test of its performance are presented in Chapter 4.

3.7 Quenching the products

At the exit of the reaction tube the products and the unconverted feed must be cooled off to ensure that the reaction does not progress any further. Therefore, as it can be seen in Figure 3.2 , it is also important to minimize $t_{Cooling}$ at the end of the reaction time. A quench method was originally designed, using a microstructured heat exchanger, but experiments showed that the loss of heat downstream of the reaction furnace was so large that simple air cooling was sufficient. Indeed, some heating was used to control the condensation of products at the reactor outlet. Consequently, $t_{Cooling}$ was not a concern and the installation of a quench system was unnecessary.

3.8 Atomization of feed

Minimization of mass and heat transfer resistance can be achieved by introduction of feed as aerosol of very fine particle into the reactor. The target size for the feed particle can be determined by approximation through calculation and by consideration of the published experimental results of the previous researchers [16]. The size of the feed particles should be small enough so that mass and heat transfer residence can be ignored. Resistance to heat transfer gives particles that have a different temperature from the carrier gas. The temperature history of the feed particles can be calculated in principle, but this calculation is subjected to simplifications and is difficult to verify by direct measurement. However, calculation can help to approximate the maximum allowable size of the particle and then aim for the size which is safely smaller.

The calculation of temperature profiles is simplified by considering a single particle in a semi-infinite medium, and ignoring the enthalpy of vaporization and reaction. The calculations of Appendix A suggest that particle must be smaller than 20 μm to follow the carrier gas temperature. The vaporization of feed and the endothermic cracking reactions will tend to further cool the particle by increasing the amount of heat that must be transferred from the carrier gas. With regard to the effect of the mass transfer, the work of Gray et al. [16] studied the trend of reduction of yield of coke by reducing the liquid film thickness from 75 to 10 μm. Determining the exact limit for the film to avoid coupling of mass transfer with reaction to minimize coke formation is complex; therefore, the thickness is chosen to be one order of magnitude lower than the minimum which Gray et al. studied, that is a liquid film thickness of 1μm (particle diameter of about 2μ). The extent of the achieved reduction in mass transfer resistance can be detected by comparing the yield of coke in this research with the results of Gray et al. (Chapter 5).

A third constraint on the size of particles is deposition of liquid (feed and liquid products) and coke particles inside the reaction tube or the components of the reactor. The design criterion in this case is that particles will follow the stream lines of the flow when the Stokes number is much smaller than 1 [57], where the Stokes number is defined as:

$$St = \frac{\tau U_0}{D} \tag{3.7}$$

U_0 is the fluid velocity

τ = particle relaxation time

$$\tau = \frac{\rho_{particle}\, d^2\, C_c}{18\,\mu} \tag{3.8}$$

d = diameter of the particle

C_c = Cunningham slip correction factor

$$C_C = 1 + 2.52 \frac{\lambda}{d} \tag{3.9}$$

λ = mean free path

Detailed calculations are presented in Appendix B. To keep the Stokes number below 0.1 in the reaction tube, the diameter of feed particles should be less than 7 μm.

Overall, a maximum particle diameter of less than 2 μm is desirable in this research. The generation and conduction of such small particles of viscous fluids like vacuum residue are challenging tasks. In practice, the limited technology for atomization defines the size of the finest particle that is achievable. Thus, any more sophisticated modeling and calculation or experimentation to find a precise limit for the size of the particles to meet all the conditions was not attempted. The method which was developed to atomize the feed was explained in Chapter 5.

Chapter 4

An Innovative Isothermal Reactor to Study High Temperature Thermal Cracking

A major concern in the study of high temperature thermal cracking is the progress of the reaction before the reactant reaches the reaction temperature. With regard to this issue, a non-isothermal flow reactor can be used to study the kinetics of thermal cracking when:

1. The temperature rise time (to reaction temperature) is much smaller than the half-life of the reaction so that the progress of the reaction in the non-isothermal section of the reactor is negligible.
2. The temperature profile along the reactor can be reasonably calculated or measured and included in the kinetic model.

The latter is less desirable as this method is prone to more errors in measurement or calculation of the temperature profile. The kinetic model needs to include the temperature profile and considers a wider range of temperature. In comparison, an ideal isothermal reaction is not subject to any of the aforementioned sources of uncertainties. Development of new technologies for fast heating of the reactant to elevated reaction temperatures is a challenging and costly task. In practice, an isothermal temperature profile is a mathematical ideal, which is not fully achievable.

This chapter presents an application of the technology of micro-mixing to eliminate or significantly minimize the non-isothermal portion of the inlet temperature profile along a tubular continuous flow reactor in order to achieve a temperature profile which is as close as possible to the ideal isothermal profile. The concept of micro-mixing and its application as an efficient method to mix two streams of fluids was explained in Chapter 3. The heat and mass transfer analogy suggests that this technology can be used as an efficient heat-exchanging device as well, to bring the reactant to the reaction temperature in a very short

time. Hass-Santo et al. [53] verified the mixing performance of this technology previously, and in this work its application to chemical reaction at high temperature is demonstrated.

The objective of the experiments described in this chapter is to verify the heat transfer performance of this device and its capability to enable a practically isothermal reaction operation through micro-mixing of the reactant stream with a stream of hot inert gas. The conversion of n-hexadecane was measured at temperatures from 600 to 750ºC at atmospheric pressure, and the results are compared with the results in the literature. In order to demonstrate the advantage of using the microstructured mixer, the temperature profile during isothermal operation of the reactor with the microstructured mixer was compared with non-isothermal operation of an equivalently operated straight tubular reactor without the microstructured mixer. The temperature of the wall of the reactor was measured and compared with the temperature of the fluid at the same position along the reactor in isothermal operation to investigate the variation of temperature in the reaction tube in radial direction.

4.1 Materials and Methods

4.1.1 Chemicals

The essential chemicals which were used are as the following:

- Fisher Scientific *n*-hexadecane, purity 99.4 % from Fisher Scientific, Mississauga, Canada
- Toluene certified ACS, purity > 99.5 % from Fisher Scientific , Mississauga, Canada
- Helium with purity of 99.995 %, O_2 < 5 ppm and H_2O < 5 ppm, supplied by Praxair in Edmonton

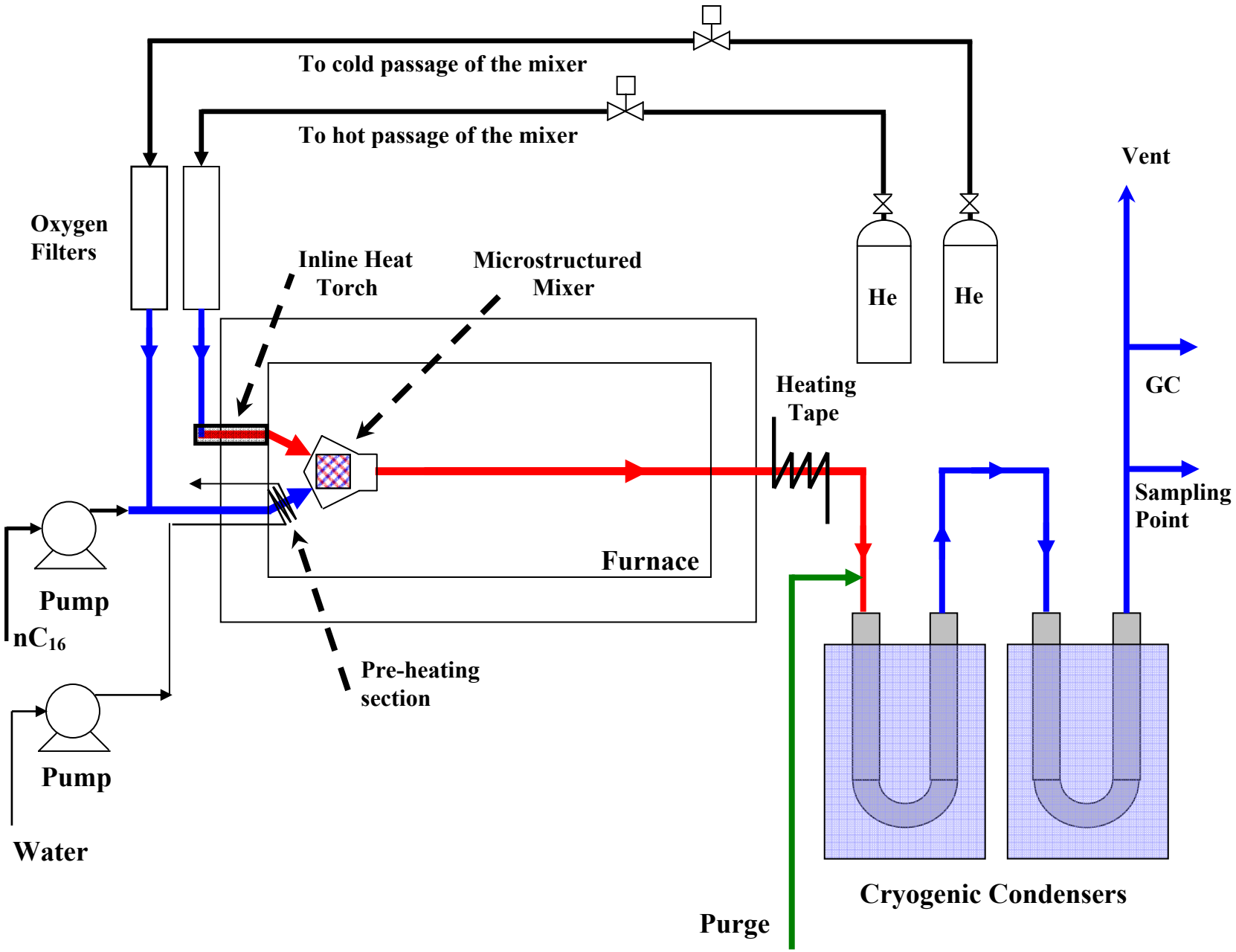

Figure 4.1 Process flow diagram of the isothermal reactor

4.1.2 Reactor apparatus

Most of the previous researchers, who used a continuous flow reactor design in their kinetic studies, applied an external furnace or a pre-heater, or a combination of both to heat up the carrier gas and the reactant before they enter the reaction section inside the reaction furnace. Application of external furnaces and pre-heaters increases the rate of heat losses through the connecting tubes with the reaction furnace, and at laboratory scale these losses are usually unacceptable. Consequently, higher quality of insulation material and a more delicate installation are required to ensure minimization of the heat losses in this area. In this research an innovative compact design is used which combine a pre-heating section for the reactant, an inline heater for the carrier gas and a microstructure mixer all fabricated in a 3 × 9 × 9 cm space including the essential tubing and with the microstructured mixer which is occupying a space less than 1 × 2 × 4 cm . This compact design of three pieces of equipment in one body is installed inside the reaction furnace as illustrated in Figure 4.1.

Figure 4.1 shows the process flow diagram of the reactor. Two streams of helium enter the microstructured mixer. The microstructured mixer has two passages. Each passage consists of an inlet tube which enters into an array of micro-channels. One stream is used to sweep the n-hexadecane which is evaporated in the pre-heating section (Figure 4.1 and Figure 4.2) into the micro-channels in the cold passage of the mixer. The pre-heating section, which is a short tube (length 2.5 cm length, ID 10 mm), passes through a coil of cooling water to prevent over-heating of n-hexadecane (Figure 4.1). The other stream passes through an inline heat torch (inline heating element) at a higher flow rate and enters the hot passage of the mixer. The two mass flow controllers (UFC 1200 A, Unit Instruments, Wichita, Kansas) have a maximum capacity of 2.9 SLM helium (stream to cold passage) and 8.6 SLM helium (stream to hot passage) respectively.

Each stream of He passes through a two-stage oxygen trap (LabClear, Oakland, California), then enters the mixer. The traps with higher capacity are followed by an indicating oxygen trap. This combination guarantees an

efficient removal of trace oxygen before the He streams enter the mixer and the reactor. The traps are capable of removing oxygen from the He to less than 5ppb. After oxygen removal, each stream passes an inline particulate filter (Swagelock, Solon, Ohio). These filters prevent any solid particles that the He streams may possibly carry from entering into the micro-channels. The innovative combination of the microstructured mixer and an inline heating element facilitated quick heat-up of the reactant to the reaction temperature. Figure 4.2 shows the micro-channeled mixer and the inline heating element and the way they were connected.

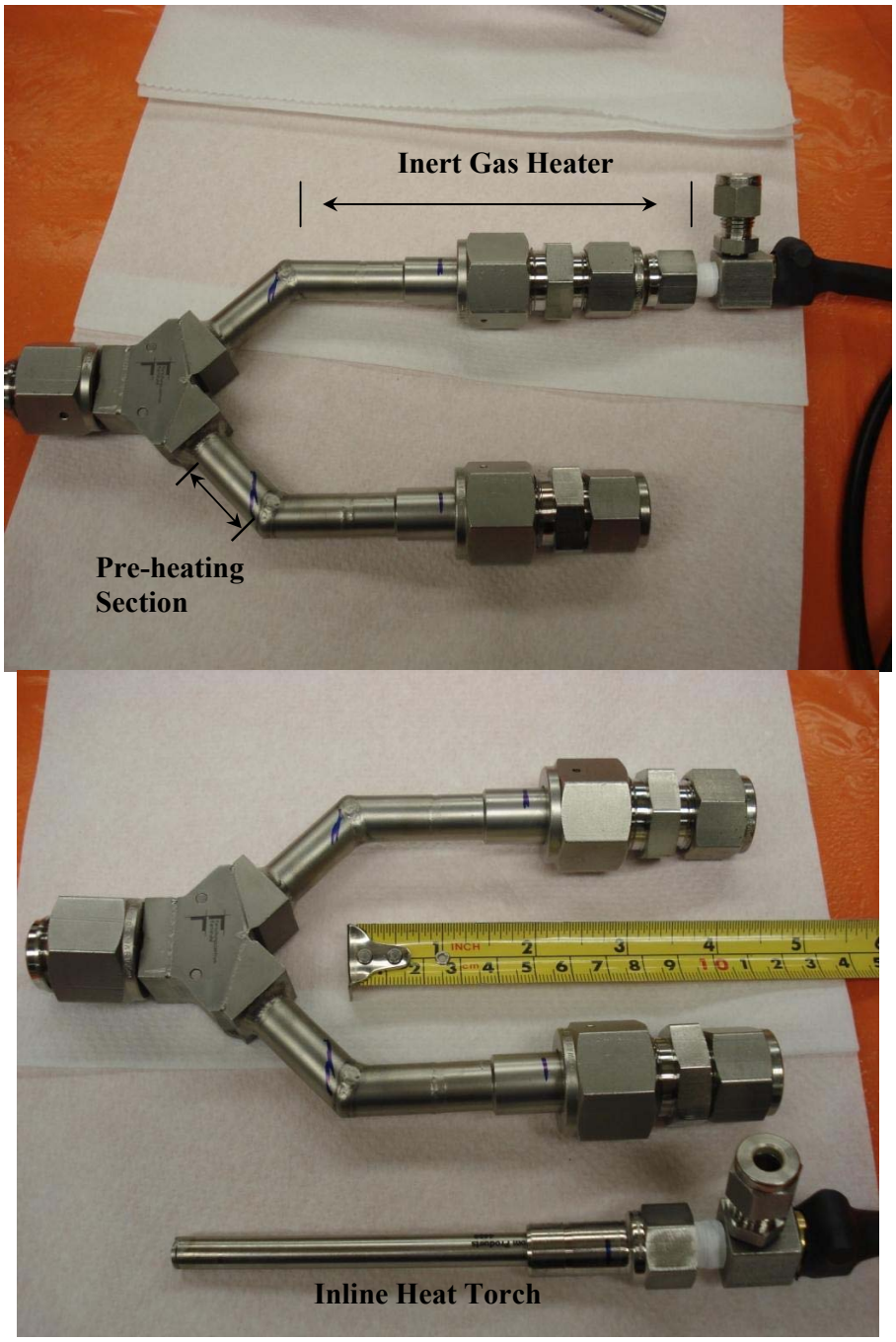

Figure 4.2 The inline heating element was installed by inserting inside the inlet tubing of the mixer. This eliminates requirement for generating and introducing an external stream of hot stream and undergoing a significant heat losses. The pre-heating section is placed inside the furnace and can be wrapped with a coil of cooling water to protect against the over-heating at higher furnace temperatures.

The inline heating element (Tutco-Farnam Heat Torch model 030 - 300W-120 V, Arden, North Carolina) had recommended minimum and maximum flow rates of 8.5 SLM (0.3 SCFM) and 28.3 SLM (1 SCFM) of air respectively. The maximum recommended temperature for operation was 704°C (1300°F). However, this device was safely operated at higher temperatures under an inert atmosphere.The microstructured mixer was fabricated by the Institute for Micro-Process Engineering in Karlsruhe, Germany. This mixer was made of alloy 800. Table 4.1 shows the technical specification of the mixer.

Table 4.1 The technical specification of the microstructured mixer (reproduced from the specification data sheet provided by the Institute for Micro-Process Engineering, Karlsruhe, Germany)

Material Data		
Foil Material	Incoloy Alloy 800 (DIN 1.4876)	
Device Body	Incoloy Alloy 800H (DIN 1.4958)	
Connectors	AISI 316L Swagelok VCR 1/2”	
Geometry		
Foil Size (mm^2)	40 × 19.6	
Total Number of Foils	26	
Stack Length (mm)	9.62	
	Passage 1	**Passage 2**
Number of Foils/Passage	13	13
Number of Channels per Foil	16,14,12,10,6	16,14,12,10,6
Foil Thickness (mm)	0.37	0.37
Channel Width (μm)	400	400
Channel Depth (μm)	200	200
Fin Width (μm)	200	200
Inspection Data		
	Passage 1	**Passage 2**
He Leak Rate in the Passage (mbar .Lit /s)	$< 1 \times 10^{-8}$	$<1 \times 10^{-8}$
N_2 Throughput (Lit/min STP) at ΔP = 100 mbar (1.45 psi)	23.0	22.9
Stacking Scheme: Passage 1 and 2 each : 2 pieces at 6 channels, 2 pieces at 10 channels , 2 pieces at 12 channels , 2 pieces at 14 channels and 5 pieces at 16 channels **Solid Particles:** The inlet should be equipped with filters with mesh size of <= 50 μm to avoid blocking of the micro-channels by solid particles.		

The heat transfer to the cold stream of the fluid which carries the reactant is achieved in three ways:

1. Micro-mixing of the cold stream and hot stream at the outlet of the microstructured mixer which is inlet of the reaction tube.
2. Heat transfer from the hot stream to the cold stream within the microstructure of the mixer by conduction. The hot and cold streams do not physically mix inside the microstructure.

3. Heat transfer from furnace to the body of the mixer by radiation and then through the microstructure to the fluid by conduction.

Figure 4.3 illustrates the path of fluids inside the mixer. The hot and cold streams do not mix inside the device, but they exchange heat by conduction through the foils body. At the outlet, the heat transfer between the two streams continues through conduction and mixing. Turbulence at the outlet of the mixer can shorten the mixing time by one order of magnitude [53]. Considering the size of the reactor and the range of required residence time, a fully turbulent regime cannot be achieved. The existence of the vortices in a laminar regime of fluid flow will change the residence time distribution away from the ideal laminar flow case in absence of such vortices. If an aerosolized stream of heavy oil is conducted into the cold passage of the mixer, then existence of vortices or a turbulent flow regime is undesirable as they intensify the tendency of the feed particles to coalesce to each other and form larger particles or deposit on the wall of the reaction tube. Thus, the microchannels of the hot and cold passages were designed to be parallel to each other at the outlet to avoid turbulence or laminar vortices at the outlet of the mixer. In order to avoid vortices, the array of microchannels at the outlet was designed to exit into a circular duct. Figure 4.5 shows internal parts of the mixer and part of the arrays of the micro-channels as viewed from the outlet port of the micro-mixer. The mixer consists of a stack of 26 micro-channeled foils, 13 foils for the cold stream and 13 for the hot stream.

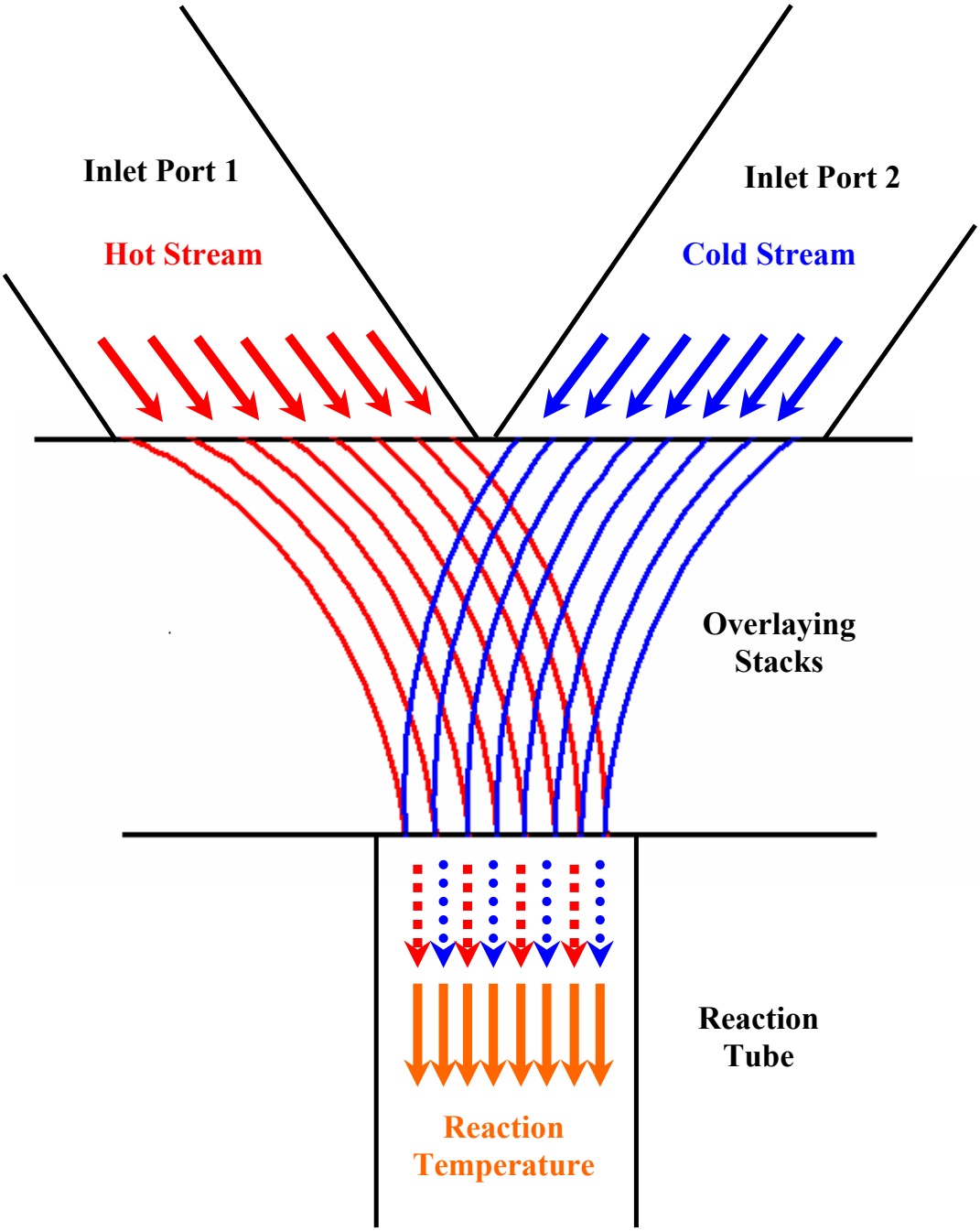

Figure 4.3 The microstructured mixer, the hot and cold stream do not mix until they exit the mixer and enter the reaction tube

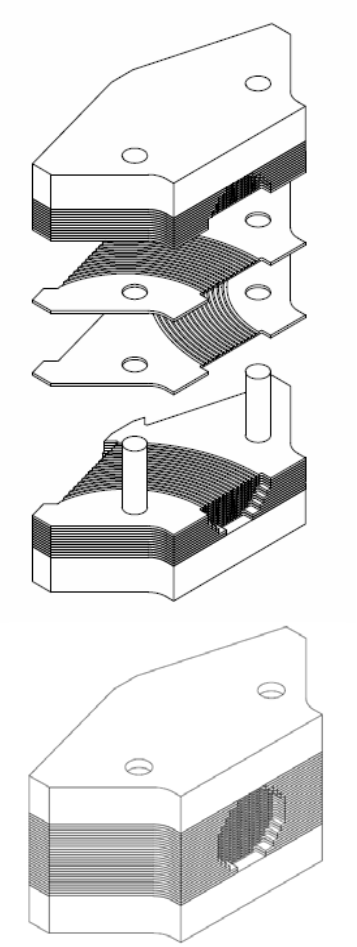

Figure 4.4 Parts of the micro-structured mixer.Courtesy Peter Pfeifer and Institute for Micro-Process Engineering

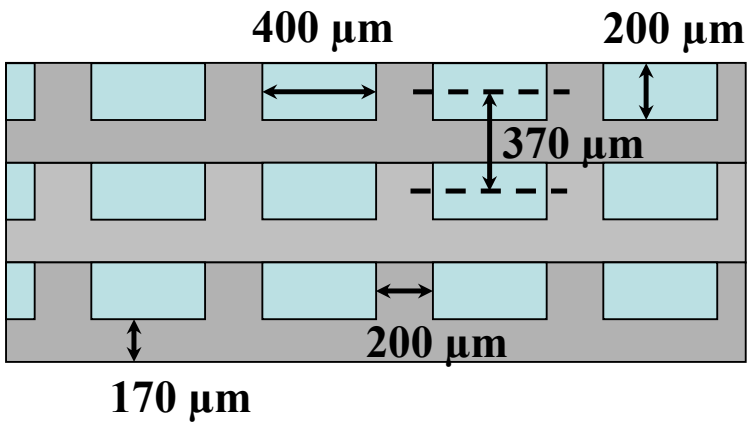

Figure 4.5 The dimensions of the micro-channels

The sizes of the channels and the foils are shown in Figure 4.5. The microstructured mixer, together with the reaction tube, which is connected to its outlet, is placed inside a 3-zone horizontal tube furnace (Model DT-22HTOS-3Z-1-36(12)-W6401, Deltech Incorporated, Denver, Colorado). The heating surface of this furnace is cylindrical. The reaction tube is placed at the centre of this cylinder (Figure 4.1). The furnace maintains the fluid at reaction temperature along the reaction tube. Table 4.2 contains the technical specification of this furnace. The placement of the microstructed mixer inside the furnace minimizes the heat loss from the hot stream inlet tubing of the mixer. The temperature differential is lower if the mixer is placed inside the furnace. Locating the mixer inside the furnace provides other advantages.

Table 4.2 Specification of the reaction furnace

Furnace	
Type	Horizontal tube furnace
Electrical	208 volts , 35 A
Number of Heating Zones	3
Maximum Power	12.6 kW
Maximum Temperature	1200 °C
Length of heating area	91.4 cm (36 in)
Diameter of heating area	30.5 cm (12 in)
Control Cabinet**:** 3-zone , 208 volts, 35 A, 3 phase	

The cold inlet of the mixer (length 2.5 cm) which is located inside the furnace is used as a pre-heater which helps to evaporate n-hexadecane, therefore installation of a more sophisticated external pre-heater to vaporize the feed outside the reactor is avoided. The feed is directly injected into the entrance of cold passage of the microstructured mixer, which is hot enough to evaporate the feed without formation of coke and plugging the micro-channels. The other advantage of locating the mixer inside the reactor is the heat transfer from the furnace into the cold stream (which carriers the reactant) through the body of the microstructure by radiation and conduction.

The reaction tube is a straight seamless tube which is made of stainless 316 with outside diameter of 0.5 inch and average wall thickness of 0.049 in (1.2 mm). The reaction tube is connected to the outlet port of the mixer by means of Swagelok VCR fittings. The length of the tubular reactor from the outlet of the micro-channels to the exit at the end of the reaction furnace (measured at the internal wall) was 86.5 cm (34 in). The reaction tube expands at high temperature and slides outside the furnace through the downstream port of the

furnace. The expansion of the tube is considered in the calculation of mean residence time. The expansion of the furnace body and insulation is insignificant. Figure 4.6 shows a modified Swagelok VCR fitting which is used to attach the thermocouples which measure the body temperature and the temperature of the fluid. The temperature of the fluid is measured at the centre of the VCR fitting which is the centre of the reaction tube as well.

A pressure transmitter (Model PX726A 0-50 psi Omega Company, Laval, Quebec) is installed upstream of the cold passage of the mixer. The flow through the cold passage in all the experiments is set at 3 SLM which is much below the design flow rate of the mixer (23 SLM). Therefore in the absence of any pressure drop due to deposition of coke inside the micro-channels, the pressures drop through the cold passage is expected to be insignificant. In the reaction experiments no pressure drop due to deposition of coke inside the micro-channels was observed. Therefore, the pressure which is measured by this pressure transmitter is a very good measure of the reactor pressure. A pressure transducer (Model C-10 0-50 psi, Wika Instrument Ltd., Edmonton) was installed at the upstream of the hot passage of the mixer to monitor pressure at the inlet of the hot passage of the microstructured mixer.

The length of the reaction tube at the exit of the furnace was wrapped with a heating tape to keep the temperature of the tube at 250-300ºC to avoid condensation of the heavy liquids and unconverted *n*-hexadecane before entering the inlet tubing of the cryogenic condenser.

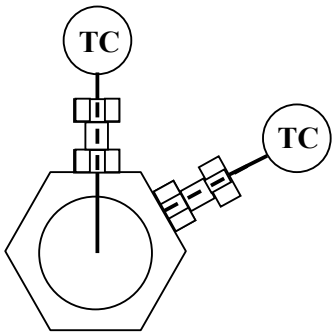

Figure 4.6 Installation of the thermocouples

The cryogenic condenser consisted of four stainless steel U-tubes. The connection between these U-tubes and the outlet of the reactor and inlet of the vent system were made by means of several stainless steel braided Teflon-lined hoses. The U-tubes were made of seamless stainless steel tube 316 with 1 inch OD and 0.083 inch average wall thickness. A 1/8 inch OD thermocouple was installed inside the U-tube at the first stage that indicated the temperature of gas at the outlet branch of the first stage of the condenser at the area where the tube was submerged inside the liquid nitrogen and above the area that the liquefied gases might build up. They were installed to form two parallel trains. Each train consisted of two U-tubes in series. The U-tubes were placed inside two buckets which were made of insulation and filled with liquid nitrogen during the operation of the reactor. The level of the liquid nitrogen were maintained manually during the operation. The boiling point of liquid nitrogen is -196 ºC. The temperature of the helium passing the condenser was -170 ºC at the first stage at the measurement point. The outlet of the U-tubes at the second stage was filled with glass wool (Fisher Scientific, Mississauga ON). The glass wool helped to capture droplets of heavy liquids, which might be entrained by the helium gas. The cryogenic condenser could be isolated by its inlet and outlet valves. A pressure transducer, Model C-10 (0-50 psi) from Wika Instruments Ltd., was installed to measure the pressure of the condenser when it was required.

4.1.1 Reactor operation

The feed was *n*-hexadecane with purity of 99.4 % from Fisher Scientific. The weight of the feed solution container was measured after filling up the tubing of the injection pump and the liquid line which entered into the inlet of the micro-mixer. The weight of the feed container was measured at the end of injection at the end of each experiment. Therefore, the total weight of injected feed and the flow rate of injection could be calculated. The feed was injected by a peristaltic pump (Masterflex, driver Model L/S 100 RPM 115/230, pump head STD #13 PPS/SS and tubing FDA Viton #13 , Cole Parmer ,Canada). This pump was able to maintain a specific flow rate consistently. It is important to maintain a constant flow rate of feed into the reactor with minimum fluctuations. When the flow rate of feed was constant, then the

concentration of the gas products in the vent stream was constant in time as well.

4.1.2 Recovery and gas chromatography of gas products

The products of the reaction were gases and liquids. The products from C_5 to C_{16} stayed inside the cryogenic condensers during operation of the reactor. Most of C_2 to C_4 gases were liquefied inside the cryogenic condenser, while almost all of the methane and a small portion of ethane and ethene escaped from the cryogenic condenser. These gases, which I call vent gases, were measured during reactor operation by using a HP 5890 II gas chromatograph, which was equipped with a 2mL sampling loop, a 6 port-manual sampling valve and an FID. The GC column was GS- Alumina 30 m × 0.535 mm from Agilent Company. The carrier gas was helium with column flow rate of 6.5 mL/min and split ratio of 10:1. The inlet port was set to 250°C, the detector at 220°C, the oven initial temperature at 75°C and initial time of 1 min and warmed up to 95°C at 5°C/min and then to 200°C at 30°C/min at stayed for 11 min at 200 °C. The GC was calibrated with two certified standard gas mixture references which were provided by Praxair Company in Edmonton and contained methane, ethane and ethene. Table 4.3 shows the concentration of the components in the gas mixture.

Table 4.3 Certified Standard for calibration of GC to measure vent gases

	Reference 1	**Reference 2**
Component	**ppm molar**	**ppm molar**
Methane	10.3	104
Ethane	10.4	104
Ethene	9.95	100

At the end of each reaction experiment, the flow of helium and injection of n-hexadecane were stopped. The cryogenic condenser was isolated by closing the inlet and outlet valves and the U-tubes were taken out of the liquid

nitrogen. When their temperature reached close to 0ºC, they were placed into water to help them reach the room temperature in a reasonable time. While the condenser warmed up, the liquefied gases evaporated and the helium density decreased. This caused a pressure build up inside the cryogenic condenser. The pressure was recorded and the trend could be monitored by using the data acquisition system in real time. The temperature of the condenser became practically constant when it reached the water temperature, which was a few degrees below the room temperature. Simultaneously, the pressure of the condenser did not increase anymore and stayed constant as well. At this time, the pressurized gas inside the condenser was emptied into a gas sample bag (Tedlar Model 231-05, 5L supplied by Concept Control Incorporated). The temperature and pressure of the condenser was recorded before and after of transferring of the gases. The change in pressure and the temperature of the condenser determined the number of the moles of gas which was collected. The condenser was purged with helium and the purged gases were also transferred to the gas sampling bags. However, no significant change of temperature that might have any effect in calculation was recorded. Samples of the collected gases were injected into the GC to measure the concentration of the gases inside the bags. Knowing the concentration and the total number of moles at each collection, the quantity of the gas component could be calculated. The GC was calibrated with a certified standard gas mixture (Praxair Company, Edmonton). Table 4.4 shows the components and the concentration in this gas mixture. The condenser was purged three to five times with helium after the first collection to collect the light gases, which stayed in the condenser and might have evaporated from the liquid.

Table 4.4 Certified standard to calibrate the GC for measuring the concentration of the liquefied gases

Component	**mole %**
Methane	15.0
Ethane	6.97
Ethylene	7.47
Acetylene	0.999
Propane	8.01
Propylene	3.01
Butane	2.51
Isobutane	2.02
cis-2-Butene	0.998
n-Pentane	0.503
Isopentane	0.500
Pentene	0.100
cis 2- Pentene	0.0988
trans-2 Pentene	0.100
Hexane	0.100
Isohexene	0.100
Carbon dioxide	3.00
Carbon monoxide	2.00
Argon	1.00
Nitrogen	4.00
Hydrogen	balance

4.1.3 Recovery and Gas Chromatography of the Liquid Products

After the collection of the gas products was completed, the liquid products were recovered. The cryogenic condenser was washed out using toluene. The collected liquids were all clear and there was no sign of coke particles. The concentrations of components in the liquid products were measured by an HP 5890 gas chromatograph equipped with an FID. The GC column was THERMO TR-1 30 m × 0.25 mm × 0.5μm (Thermo Scientific). The carrier gas was helium, column flow rate 1 mL/min and split ratio 60:1. Inlet temperature was set at 250°C , detector at 340 °C , initial temperature of oven 40°C, initial time 1 min, then from 40°C to 320°C at 32°C/min and was held at 320°C for 10 minutes.

4.1.4 Identification of the products

In order to identify the gas products a sample was injected to the HP 5890 II gas chromatograph and the residence time of the components were compared with those in the reference gas mixture.The reference gas mixture (Table 4.4) contained 16 common hydrocarbons which can be usually found in the pyrolysis products of n-hexadecane. For the products which were recovered by toluene from the condenser and were liquid at laboratory temperature a, gas chromatograph - mass spectrometer was used. The gas chromatograph was Trace GC Ultra from Thermo Scientific and the mass spectrometer, DSQII from the same company. The column was TR5MS, 15 m × 0.25 mm ID ×0.25 μm from Thermo Scientific. The method which was used is as the following. Flow rate of helium was constant at 1 mL/min. The initial oven temperature 40°C , held for 1 min then temperature was increased at 30°C /min up to 280 °C. Split ratio was 1:60. Injector was set at 250 °C, the heated zone of ion source was set at 200°C. The results were double checked by comparing the residence time of a reference mixture of the liquid n-alkanes, 1-alkenes and 2-alkenes which are injected to the HP 5890 gas chromatograph for the liquid samples in the range of C_5 to C_{16}.

4.1.5 Data acquisition system

The data acquisition system was designed to control two mass flow controllers, read up to 12 ungrounded K type thermocouples and up to three pressure transducer. The data acquisition software was LabVIEW. The control cabinet was supplied. The thermocouples were provided by OMEGA company. They were Model KMQXL-062-U-48, K type ungrounded with proprietary sheath alloys which were recommended for high temperature measurement. According to this company, this probe provided very low drift at high temperatures as compared to conventional Inconel and stainless steel sheathed probes [58]. The selection of ungrounded thermocouples was based on the electric circuitry limitation of the data acquisition system in handling the number of electrically un-isolated thermocouples. The thermocouples, with the exception of the thermocouples for cryogenic condenser, were all 1/16 inch OD. This was a practical size which worked and consistent with the mechanical design and operation procedures and provided the minimum

required resilience against the mechanical stresses beside the good features for high temperature measurements. The reaction operation took place when the system was at steady state condition, therefore a slower response of ungrounded thermocouples versus grounded thermocouples was not a disadvantage.

The furnace was equipped with 6 thermocouples which measured the temperature of the furnace atmosphere at the centre of each of the three heating zones. Two thermocouples were operated for each heating zone. One measured the temperature as a process variable to feed back the furnace temperature controller and the other which was installed close to the former one (within about 2 inch) to feed back the over temperature protection controller. In all the operation, the temperature which was measured by these two thermocouples were consistent and differed 2°C at maximum.

4.2 Results and Discussion

In this section, the heat transfer performance of the reactor which is equipped with the microstructured mixer is compared to an equivalently operated and sized non-isothermal reactor without the mixer. Then the heat transfer performance of the reactor plus microstructured mixer was investigated when the heat torch is off and compared to the case when the heat torch is on. Finally, the kinetics of n-hexadecane cracking was investigated by using the reactor with a microstructured mixer and the heat torch in the hot stream. These kinetic results were compared to the results of other researchers.

4.2.1 Performance of simple tubular reactor comparing with the reactor equipped with microstructured mixer

In order to demonstrate the efficiency of the combination of microstructured mixer and the inline heat torch in achieving a temperature profile close to an ideal isothermal profile, temperature profiles along an equivalently sized and operated tube were measured and compared with the case of a tubular reactor equipped with microstructured mixer. The heat torch was turned on and a hot stream of He was mixed with the cold stream of He. The experiments were run at 600, 650, 700 and 750°C. The operating conditions are given in Table 4.5.

Table 4.5 Flow rates of carrier gas in comparison of the simple tubular reactor with the combination of the microstructured mixer and the tubular reactor

Furnace Temperature (°C)	**Flow rate of carrier gas in reactor (mol/min)**	**Flow rate of helium at cold inlet port of the mixer (mol/min)**
600	0.371	0.134
650	0.363	0.132
700	0.512	0.134
750	0.513	0.135

The data in Figure 4.7 through Figure 4.9 demonstrate the results of this experiment at the furnace temperature of 750°C. The results of the experiments at lower temperatures are similar. The length of the heating section in the furnace is 91.4 cm (36 inches), and the simple tubular reactor has the same length, that is 91.4 cm. The microstructured mixer is placed inside the furnace at the upstream end, and its outlet is connected to a tube with the length of 86.5 cm (94 inches). Both tubes are seamless, have an OD of 0.5 inch and average wall thickness of 0.049 inch at room temperature and made from stainless steel 316. The expansion of the insulation and heating area is insignificant compared with the expansion of the stainless steel tube. The expansion of the simple tubular reactor does not change the length of the reactor which is exposed to heating within the furnace. The effects of expansion on the location of the thermocouples are considered at each experiment. For the case of the combination of the microstructured mixer and the tube, the effect of expansion on both the length of the reactor and the location of the thermocouples is considered. The dimensionless distance in Figure 4.7 to Figure 4.9 refers to the length of the tubular reactor, which is exposed to heating within the furnace in each case.

The measured wall temperature profiles for these two reactors are compared (Figure 4.7). For the case in which the microstructured mixer was used the average wall temperature along the tubular reactor was 750°C. The deviation from the average temperature ranged from -4.2 to 4.5°C which is about 0.6 % of the furnace set point. Clearly, the use of a microstructured mixer gives a temperature profile which is practically isothermal in comparison with the simple tubular reactor. The temperature profiles were compared against the furnace set point as well. At each heating zone of the furnace, there is one thermocouple which is installed by the manufacturer which measures the temperature of the furnace atmosphere to feed back to the controller of the furnace. This temperature is not necessarily the temperature of the heating elements of the furnace. The temperature of the heating elements can be more than 50°C higher than the temperature of the atmosphere of the furnace. Therefore the fact that the wall temperature of the reactor is measured a few degrees Celsius higher than the furnace temperature is not inconsistent. Furthermore, the furnaces are not in general ideally isothermal, especially near the inlet and outlet port. Given that the average temperature of the tube matches the furnace set point, and a maximum deviation of 0.6 % from the set point is measured along the reactor (case of microstructured mixer), I conclude that the reactor temperature profile is essentially isothermal.

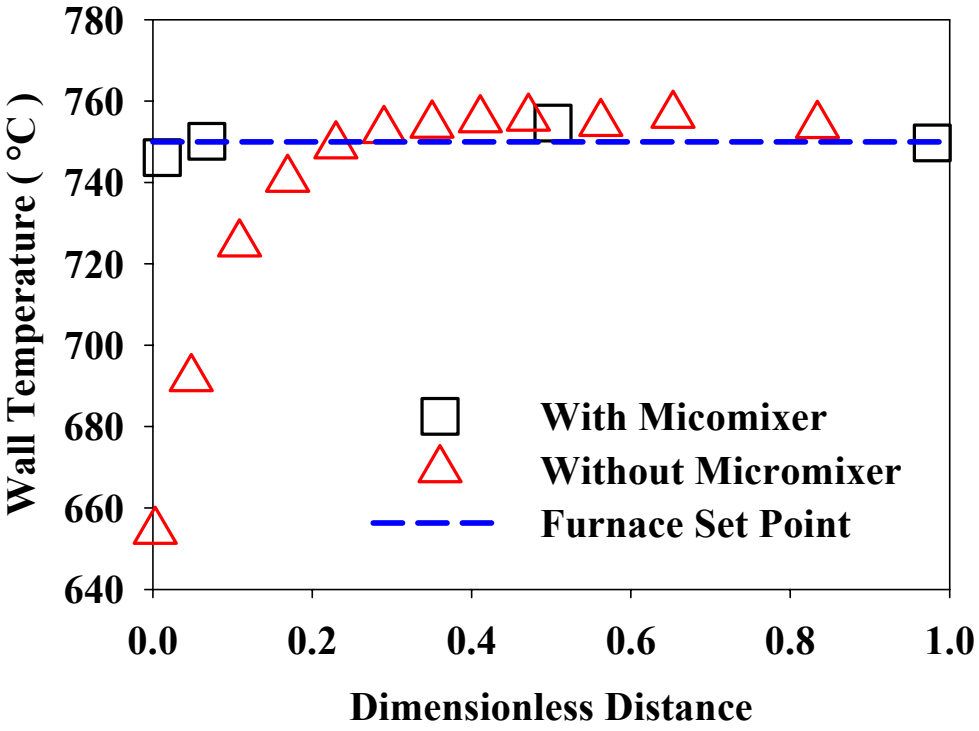

Figure 4.7 Comparison of the measured reactor wall temperatures in the cases of simple tubular reactor (no mixer) and the reactor equipped with the microstructured mixer.

Figure 4.8 demonstrates the comparison of the reactor wall temperature and the fluid temperature with the furnace set point for the case of the combination of a microstructured mixer with tubular reactor. The fluid temperature is measured directly at the center of the tubular reactor. In Appendix D, a microstructured mixer in combination with a tubular reactor was simulated by COMSOL Multiphysics, and suggest that homogeneity in temperature (radial and axial) was achieved in a few millimeters of the outlet of the microstructured mixer and a fraction of milliseconds consistent with the approximation of the manufacturer. The radial temperature profile within the reactor was not measured, however based on the earlier discussion and simulation studies of the manufacturer (and the case study given in Appendix D), the fact that the fluid temperature at the centre of the tubular reactor is very close or equal to the wall temperature indicates the uniformity of temperature in the radial direction as well.

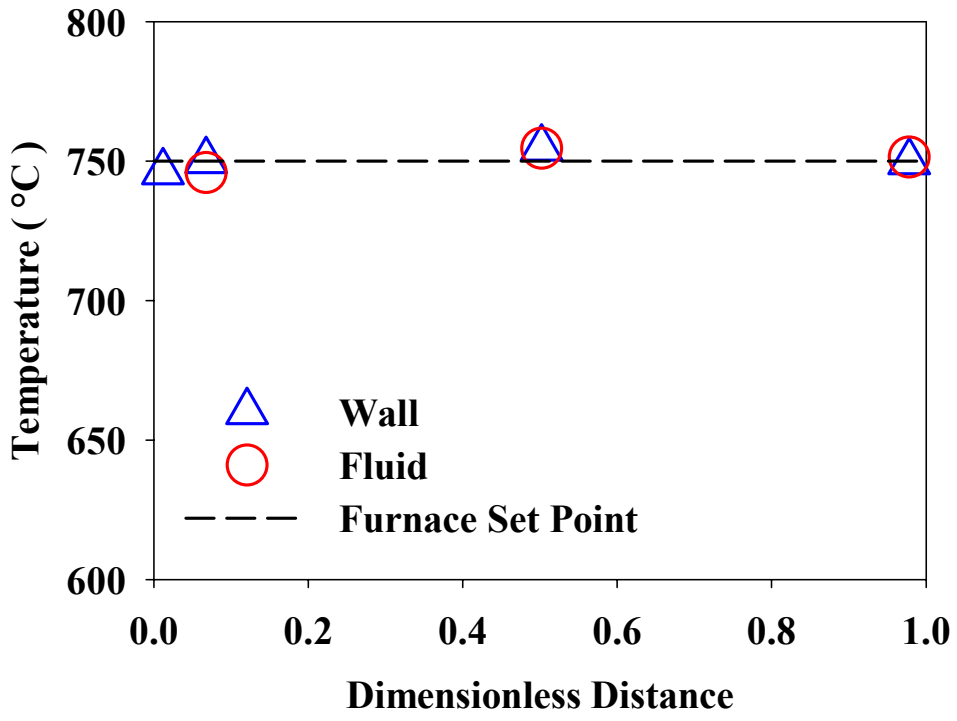

Figure 4.8 Comparison of the fluid temperature at the centre of the reaction tube and the wall temperature for the tubular reactor equipped with the microstructured mixer. Experiment at 750 °C.

Figure 4.9 compares the calculated temperature profile of the fluid along the simple tubular reactor with the measured temperature profile of the fluid along the reactor which is equipped with the microstructured mixer. Both these profiles are compared with the furnace set point. It is clear that by use of the microstructured mixer an isothermal profile is practically achieved. The average temperature fluid is 750.6°C and the deviation from the average ranges from -4.7 to 4.0 °C. That is -0.6 to 0.5 % of the set point. The heat transfer model which is used to calculate the temperature profile is explained in Appendix D.

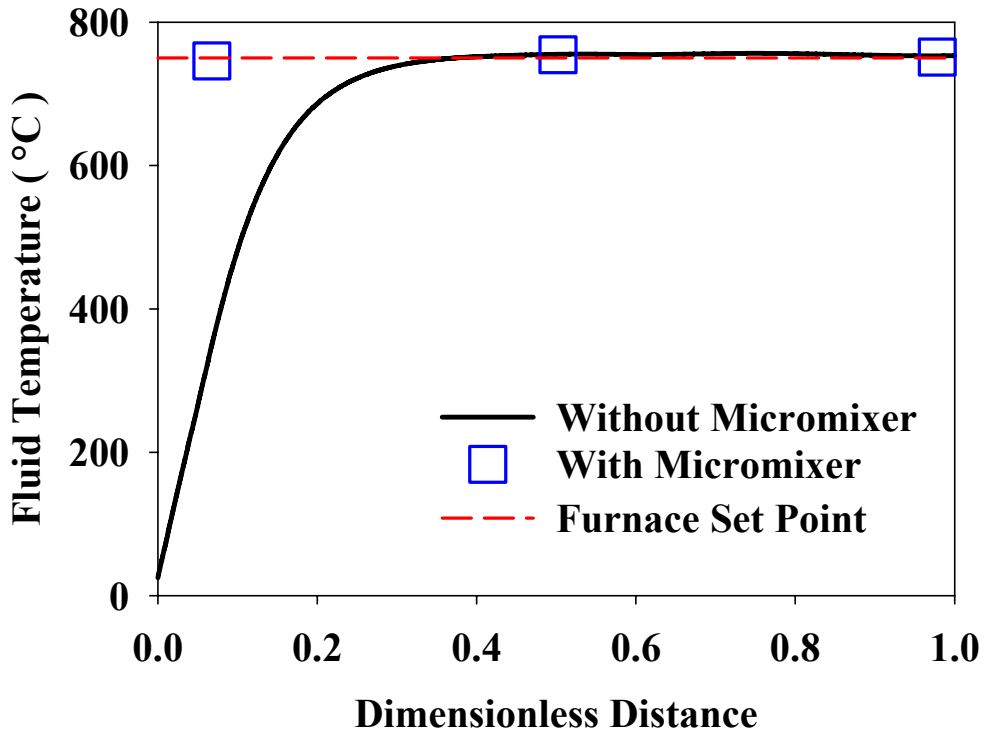

Figure 4.9 Comparison of the fluid temperatures in the cases of non-isothermal reactor and the reactor equipped with the microstructured mixer

4.2.2 Performance of the microstructured mixer when heat torch is off

As it is mentioned earlier, micro-mixing is not the only mechanism by which heat transfers to the cold stream. Heat transfers from the furnace to the body of the mixer mainly through radiation and then through the microstructures to the fluids which are flowing inside the micro-channels by conduction. In order to demonstrate the contribution of this mechanism of heat transfer, the inline heat torch was turned off (but the same molar flow rate of helium into the hot passage of the mixer was retained) and the temperature profiles along the reactor was compared with the case when the heat torch was on under the same operating condition. Figure 4.10 and Figure 4.11 demonstrate the result of this experiment. The dimensionless distance refers to the axial distance from the inlet of the tubular reactor (which is outlet of the microstructured mixer).

The contribution of the microstructure in heating up the fluid through radiation heat transfer from the furnace and conduction through the microstructure is significant, since the residence time of the cold stream inside the mixer is less than two milliseconds. The experiment was carried out at furnace set point of 750°C. Table 4.5 shows the operating flow rates for this set point. The microstructured mixer without a heat torch and without micro-mixing with a hotter stream can raise the temperature of the fluid to 97.5 % of the desired reaction temperature. The wall temperature at the same position which the fluid temperature was measured was 99.5% of the reaction temperature. The wall temperature at the very outlet of the microstructured mixer was 97.5% of the reaction temperature. At higher flow rates, this contribution is less significant and micro-mixing becomes the prevailing mechanism to heat up the reactant to the reaction temperatures. At considerably lower flow rates the microstructured mixer may heat up the fluid to the reaction temperature by itself, without requirement of mixing with a hot stream, by providing a very high surface to volume ratio for heat transfer.

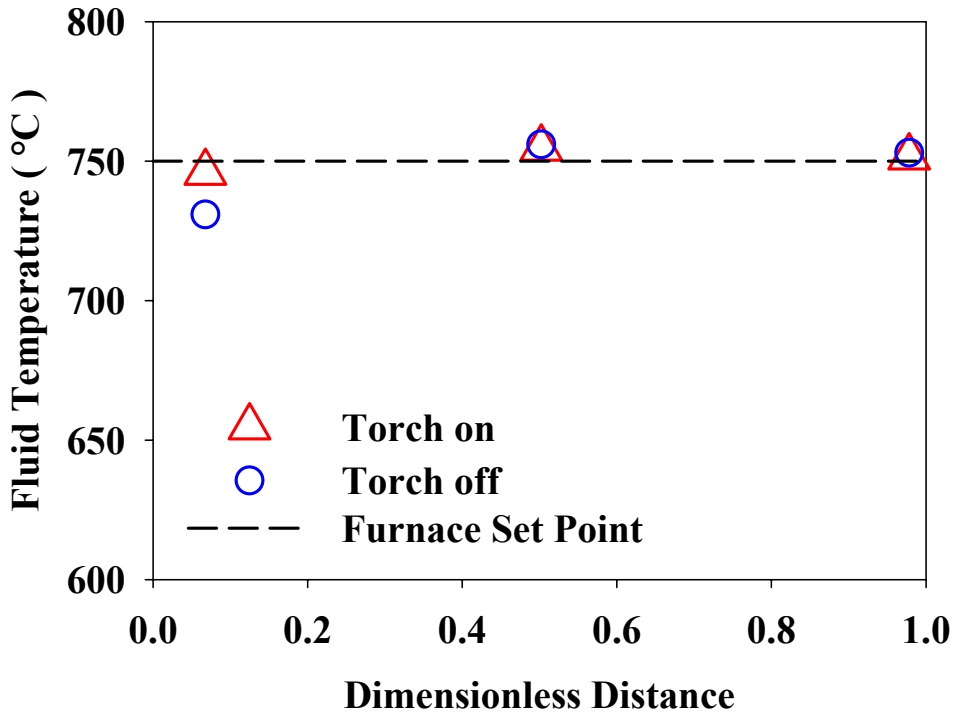

Figure 4.10 Comparison of the measured fluid temperatures in the reactor with microstructured mixer in two cases when the inline heat torch is on and off.

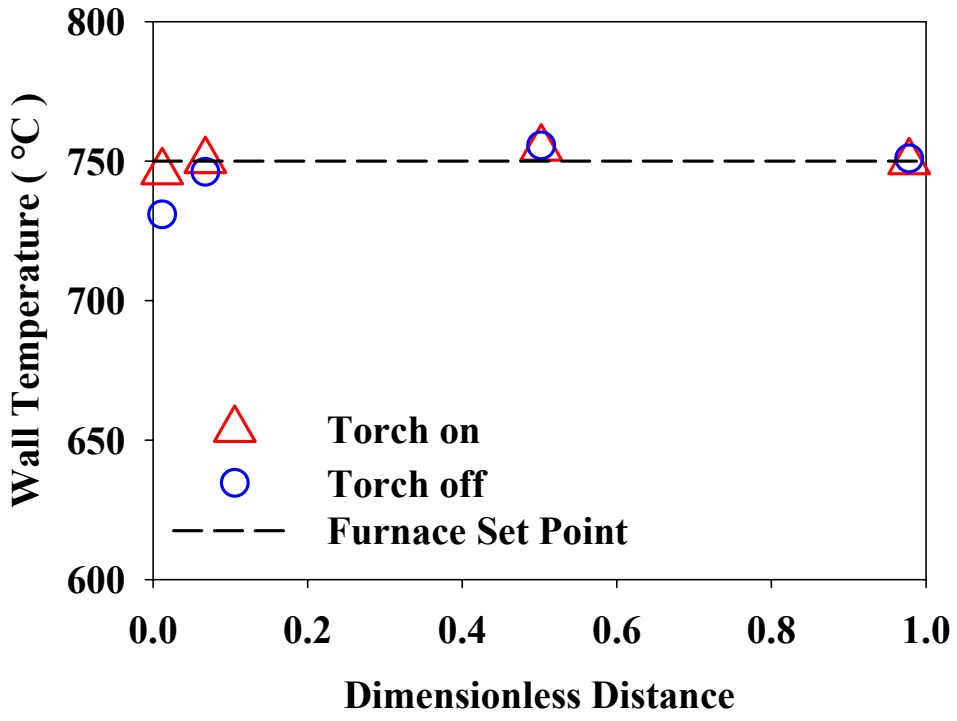

Figure 4.11 Comparison of the measured wall temperatures in the reactor with microstructured mixer in two cases when the inline heat torch is on and off.

4.2.3 Isothermal thermal cracking of n-hexadecane

The rate of the thermal cracking of n-hexadecane and the distribution of the products was measured in the tubular continuous flow reactor equipped with the combination of the microstructured mixer and heat torch. It was demonstrated earlier that by use of this technology a practical isothermal profile could be attained. The reaction temperature ranged from of 600°C to 750°C and the reactor pressure was 104 to 113 kPa The data of Table 4.6 to Table 4.9 show the operating conditions in each experiment. The mean residence time is calculated by dividing the volume of the reactor within the furnace by the volumetric flow rate of the fluid at the average reaction temperature along the reactor and at reactor pressure. Table 4.6 shows the average temperature along the reactor and the maximum deviation of temperature from the average value. The average velocity is calculated by dividing the actual volumetric flow rate of the fluid at the average fluid

temperature and the reactor pressure by the internal surface area of the tube normal to the direction of the flow.

The mean residence time in the reaction tube ranged between 110 to 170 ms and the Reynolds number ranged from 71 to 97. At room temperature, the cold stream would require about 4 ms to pass through the microstructured mixer and enter the reaction tube. When the furnace is set at reaction temperature, the temperature of the cold stream inside the mixer is in between the room temperature and the reaction temperature. A very conservative approximation is that the temperature of the reactant is at the mean of room and reaction temperatures while flowing inside the micro-channels as part of the cold stream. Thus, the residence time of the cold flow through the micro- channels can be calculated by dividing the volume of the microchannels by the actual flow rate of the cold stream at this selected temperature. Therefore, when the furnace is set at 600 to 750°C, the residence time inside the mixer is safely estimated to be less than 2 ms, which is less than 2 % of the residence time inside the reactor.

Table 4.8 shows the rate of injection of *n*-hexadecane, the concentration of n-hexadecane in the inlet of the reaction tube (at zero conversion and maximum concentration of n-hexadecane) and the concentration of the products at the end of the reaction tube (at maximum conversion and maximum concentration of products along the reactor). It is clear that the rate of injection and concentration of n-hexadecane and products are small enough that the heat of reaction of n-hexadecane and any heat effect due to different heat capacity of feed and the products can be neglected. The temperature of the fluid was not calculated, but rather is measured directly. Since the feed and product concentrations are very dilute, and their presence and their heat effect can be ignored, measurement of fluid temperature at many points along the reactor is not necessary. The temperature of the body of the reactor and the fluid were measured at three locations: at the closest distance which was physically possible at the beginning of the reaction tube (considering the limitation imposed by the size and geometry of the Swagelok VCR fittings which connected the microstructured mixer to the reaction tube), in the middle of the reaction tube and at the end of the reaction tube.

Table 4.6 Furnace and fluid temperature and reactor pressure in isothermal cracking of nC_{16}

Experiment	Furnace Temperature (°C)	Average Fluid T (°C)	Maximum Deviation from the Average T along the Reactor (°C)	Reactor Absolute Pressure (kPa)
600	600	603	+4	105.9
650-1	650	652	+4	104.9
650-2	650	652	+4	109.9
650-3	650	653	+4	105.2
700	700	702	+4.	112.8
750	750	751	+4	113.2

Table 4.7 Flow rates of carrier gas in isothermal cracking of nC_{16}

Experiment	Flow rate of carrier gas in reactor (mol/min)	Flow rate of helium at cold inlet port of the mixer (mol/min)	Molar ratio of the hot stream to cold stream
600	0.371	0.134	1.76
650-1	0.363	0.132	1.76
650-2	0.371	0.136	1.72
650-3	0.361	0.132	1.73
700	0.512	0.134	2.81
750	0.513	0.135	2.80

Table 4.8 Concentration of feed and products at inlet and at the outlet of the reactor in isothermal cracking on nC_{16}

Experiment	Flow rate of injection of nC_{16} (mol/min)	Concentration of nC_{16} at the inlet of reaction tube (mol %)	Concentration of products excluding nC_{16} at the end of reaction tube (mol %)
600	7.01E-04	0.19	1.29E-02
650-1	7.10E-04	0.20	6.69E-02
650-2	7.11E-04	0.19	4.26E-02
650-3	7.17E-04	0.20	4.88E-02
700	7.08E-04	0.14	1.59E-01
750	7.14E-04	0.14	1.57E-01

Table 4.9 Average residence time, Reynolds number, conversion and mass balance in isothermal cracking of nC_{16}

Experiment	Mean residence time (ms)	Re	Conversion (%)	Mass recovery (%)
600	168	75	1.6	100.2
650-1	161	71	11.3	98.1
650-2	165	72	11.6	96.5
650-3	163	71	9.1	100.1
700	117	97	28.5	101.6
750	112	94	69.4	97.0

At the reaction temperature, the reactant and all the products are in gas phase (no coke was found either in the products or deposited inside the reactor). However, when the products and unconverted reactant are collected from the cryogenic condenser, part of the product are in the gas phase at the laboratory temperature. The gas products are collected in dilute concentrations in helium and they range from C_1 to C_8. In gas products, both alkanes and alkenes can be detected. The liquid products are collected by washing the cryogenic condenser with toluene. C_5 to C_{16} can be detected in liquid products. All the liquid products are verified to be 1-alkenes. The verification was done both by use of a GC-MS and direct injection of 1-alkenes, 2-alkenes and n-alkanes in the desired carbon number range of interest to confirm GC peak assignments.

Figure 4.12 demonstrates the yield of collected products which are in gas phase at the laboratory temperature versus conversion. The yield was defined as the mass percent of the feed which was converted to the products. The experiment was repeated at the furnace set point of 650°C three times. The standard deviation of the yield of gas products for the three repetitions at this temperature (average conversion 10.7%) was 0.44 %. The low value of the standard deviation indicates the good repeatability of the experiments. The yield of gas products increases monotonically with conversion.

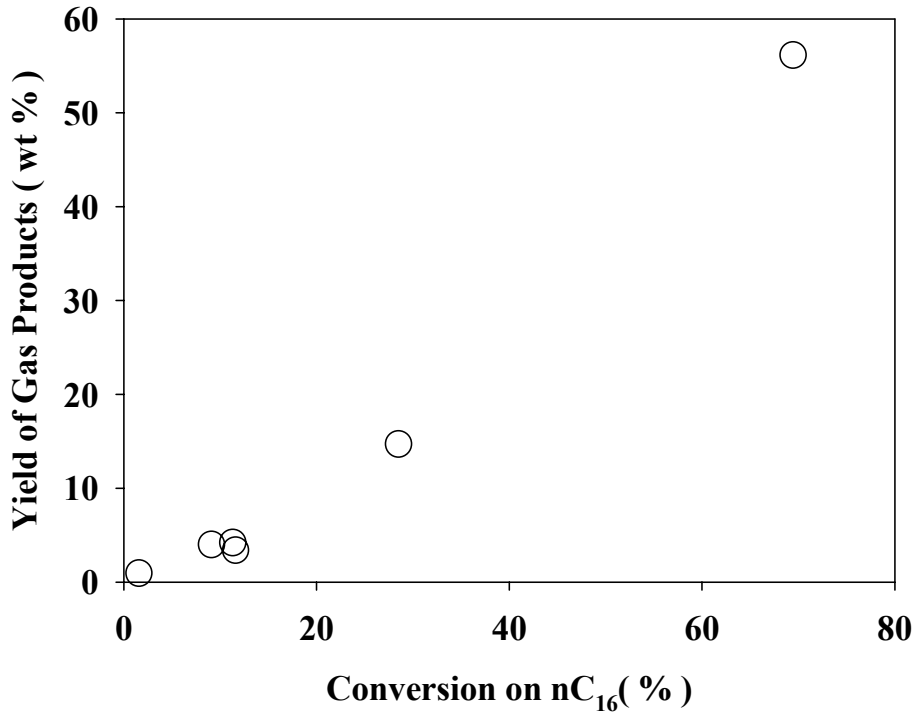

Figure 4.12 Yield of total gas products versus conversion of nC_{16}. These products were collected in gas phase in helium and ranged from C_1 to C_8. The yield is defined as the mass percent of the feed which is converted into the products. The experiment was repeated at the furnace set point of 650°C three times. The standard deviation of the three repetitions at this temperature (average conversion 10.7%) was 0.44 %.

Figure 4.13 shows the yield of products which are in liquid phase at the laboratory temperature versus conversion. The experiment at furnace set point of 650 °C (average conversion of 10.7%) was repeated. The standard deviation

for the yield of liquid products at this temperature is 0.33 % which indicates excellent repeatability of the experiments. The yield of liquids monotonically increases until conversion point of 28.5 %. The next measurement was carried out at conversion of 69.4 %. Therefore, the yield of liquid should reach a maximum value between these two conversions followed by a decrease in the yield of liquids at higher conversion. This trend is consistent with the fact that at higher conversion secondary cracking reactions convert the liquid products to gas products. This is also consistent with the accelerated increase in yield of gas products at conversion of 28.5 % as it can be seen in Figure 4.14.

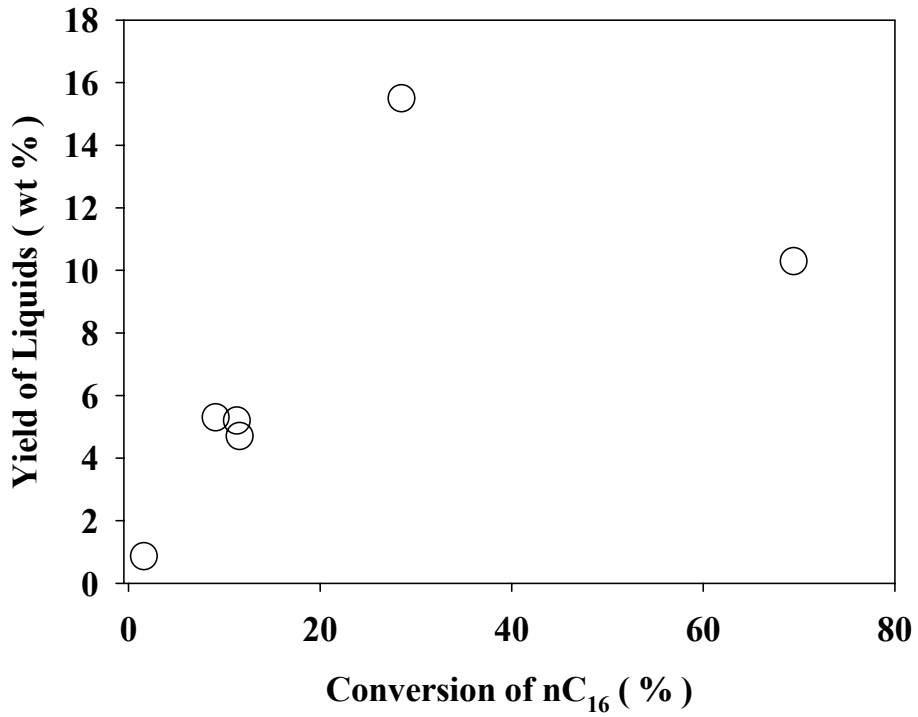

Figure 4.13 Yield of liquid products versus conversion of nC_{16}. These products were collected by washing the condenser by toluene and ranged from C_5 to C_{15} plus unconverted n-hexadecane. The yield is defined as the weight percent of feed which is converted into the products.

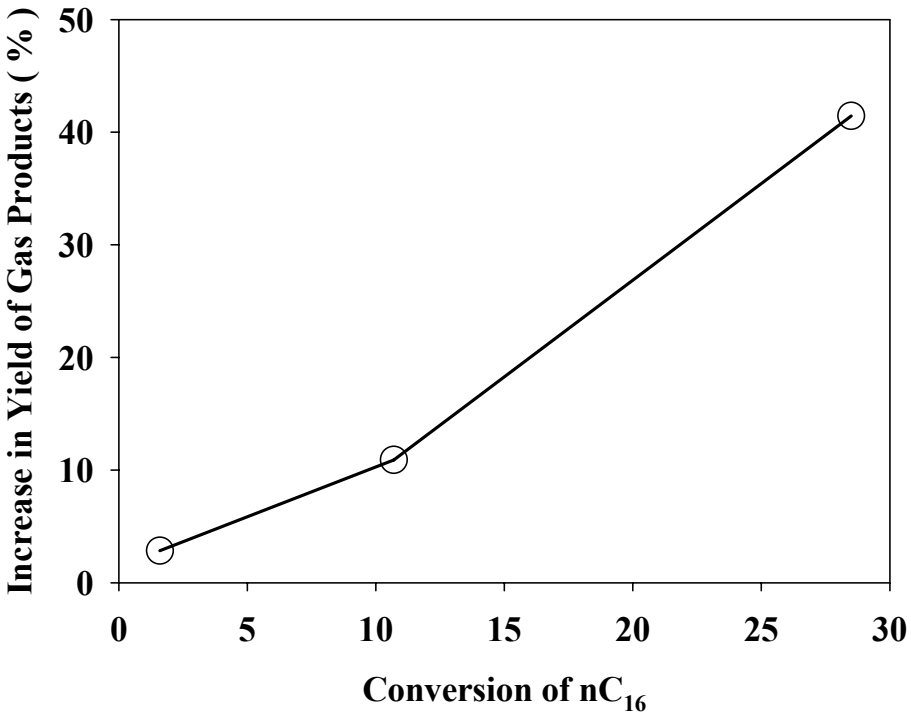

Figure 4.14 The increase in yield of gas versus conversion

The data of Figure 4.15 show the selectivity of alkanes and alkenes C_1 to C_3. The selectivity is defined as the ratio of the moles of each product to the moles of converted n-hexadecane. Alkenes are the major products of thermal cracking in vapor phase. The yield of alkanes becomes insignificant as the number of carbons increases. All the products above C_6 which were collected in liquid phase in lab temperature were 1-alkenes while some C_4 to C_6 alkanes were detected in the product which were collected in gas phase at room temperature.

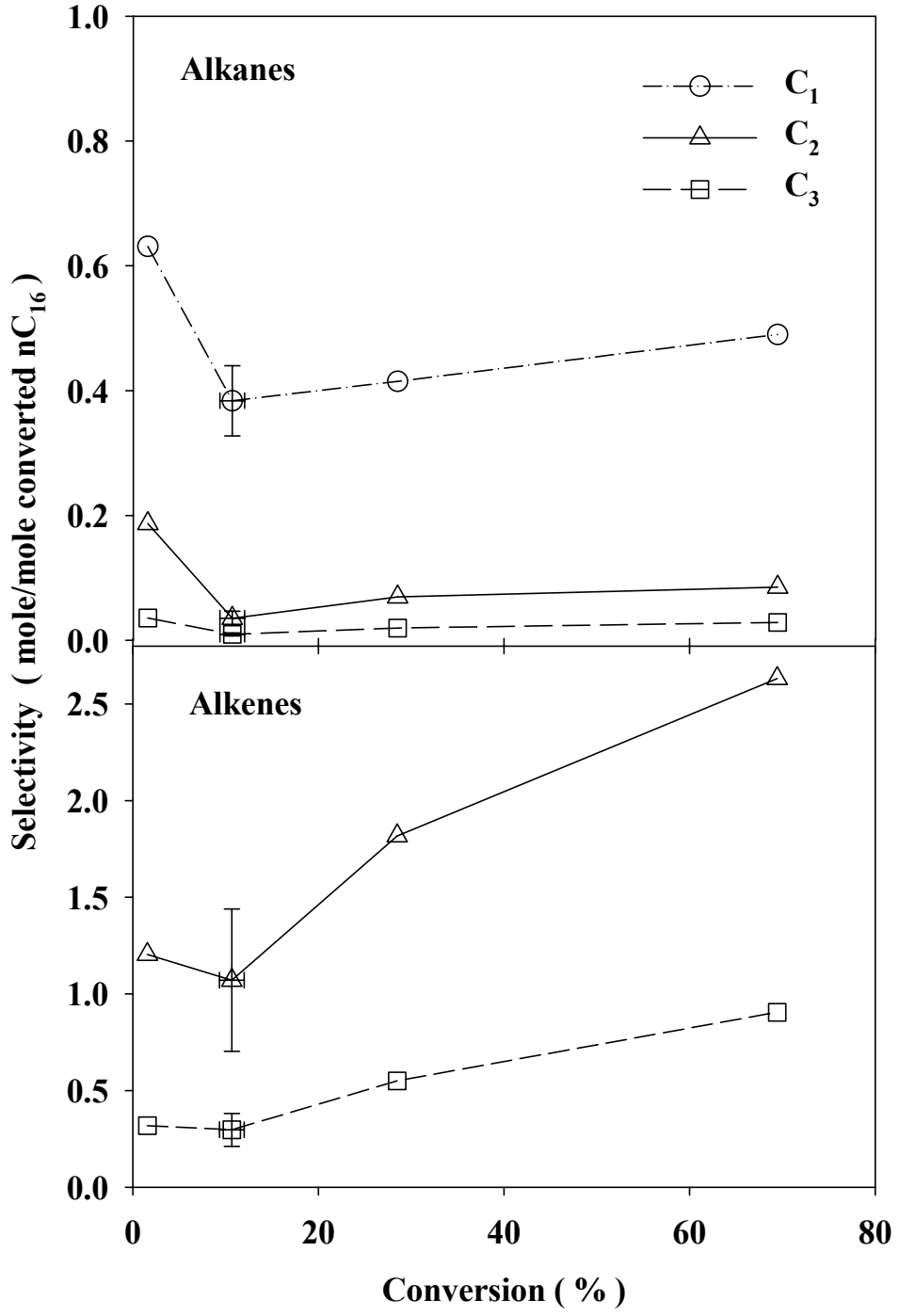

Figure 4.15 Selectivity of alkanes and alkenes from C_1 to C_3 versus conversion of nC_{16}. The error bars represents the standard deviation of the replicate experiments

The data of Figure 4.16 demonstrate the yield of products versus carbon number at different conversions. The yield of products increases with conversion. Ethene is the major product at all conversions. At all conversions, after the peak at C_2 the yield almost monotonically decreases with carbon number. At conversions of 10.7 and 28.5 % however there is a small rise in yield of C_6. Bartekova et al. [27] previously observed and reported such a local maximum of the yield at C_6.

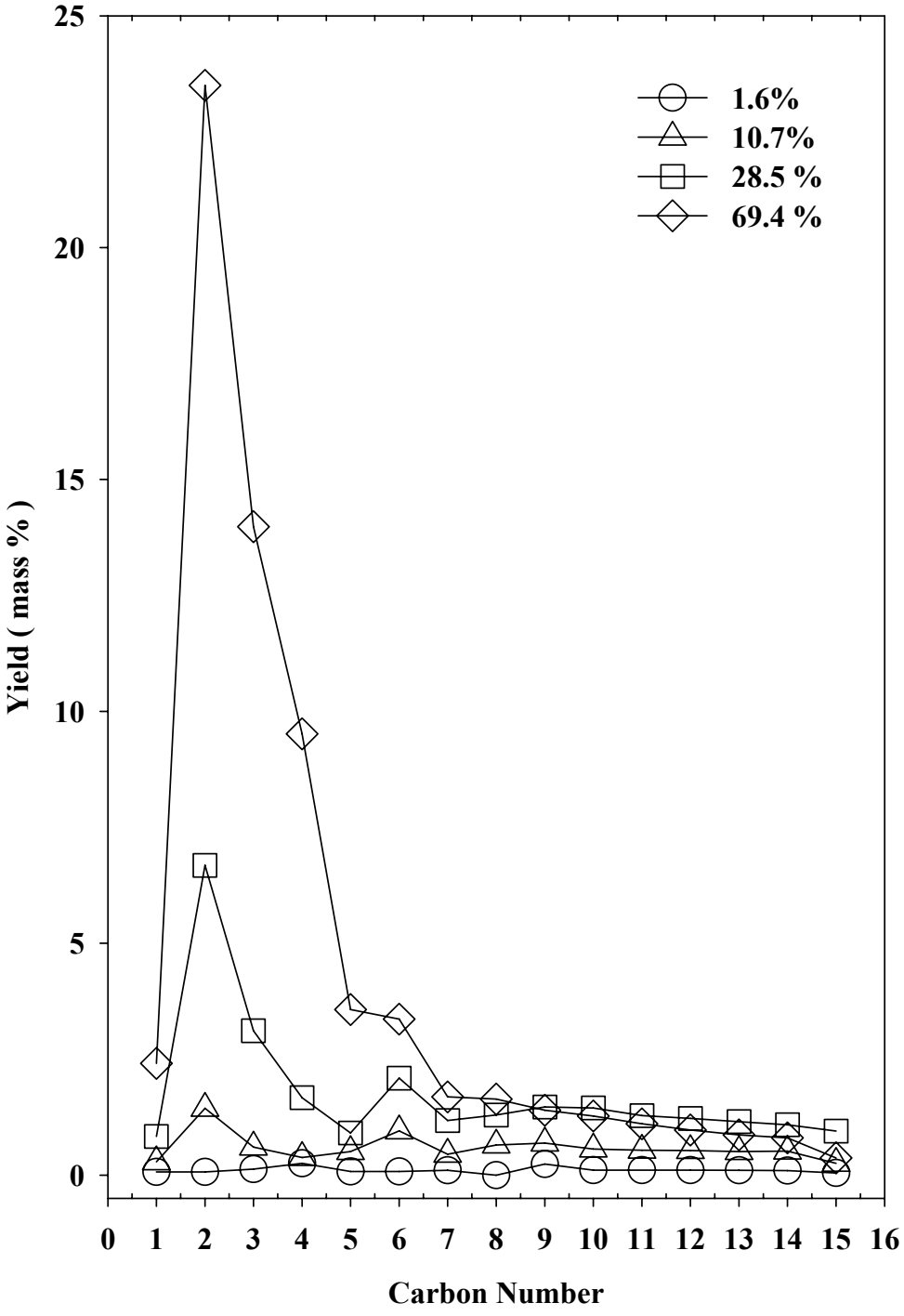

Figure 4.16 Yield of products of thermal cracking of n-hexadecane versus carbon number at different conversions from 1.6 to 69.4 %

4.2.4 Reaction kinetics of n-hexadecane conversion

Thermal cracking of n-hexadecane is a first order reaction, based on the reports of the previous researchers who studied this compound and other n-paraffins (Chapter 2). In my experiments, the reactor is practically isothermal within a narrow uncertainty band around the average fluid temperature along the reactor (maximum deviation from average is +4°C), therefore it safely can be approximated as an ideal isothermal reactor to calculate the rate constants. The residence time of the reactant in the microstructured mixer is less than 2% of the total residence time in the reaction tube. Thus, the reaction is assumed to progress only inside the reaction tube which starts at the outlet of the micromixer. The temperature of the reactant reaches the reaction temperature in a few milliseconds (see simulation case study in Appendix C for additional details). The combination of the heat transfer from the furnace to the reactant through radiation, and the exchange of heat between the cold and hot stream through the microstructure of the micro-structured mixer by conduction heat transfer, gave a time to reach reaction temperature that was much less than 1% of the mean residence time inside the reaction tube.

For a first order reaction, conversion does not depend on the concentration of the reaction molecules. As a result only the residence time distribution is required to calculate the conversion for a first order reaction in any type of reactor [59]. Levenspiel derived an equation to calculate conversion for first order reaction of a Newtonian fluid in laminar flow in a pipe and compared the ratio of the space time for this case to the case of plug flow reactors. He concluded that even at high conversions the laminar flow does not significantly reduce the conversion relative to the ideal plug flow case [60]. Figure 4.17 presents the rate constants versus the inverse of temperature. The experimentswere in the temperature range of 600 to 750°C, and were repeated three times at 650°C. The standard deviation of the calculated rate constants from the collected data at this temperature is 0.09 s^{-1}. The MATLAB *fit* function was used for linear regression. The linearized Arrhenius equation was used as the model to related the rate constants and activation energy. The R^2 of the regression is 0.99 which shows that the data are very well fit to the linear

model and is consistent with the assumption of a first order reaction. The calculated activation energy is 235 ± 31 kJ/mole (95% confidence interval) and the pre-exponential factor of the Arrhenius equation is 1.13×10^{13}. The 95% confidence bound for the natural logarithm of pre-exponential factor are ± 3.9.

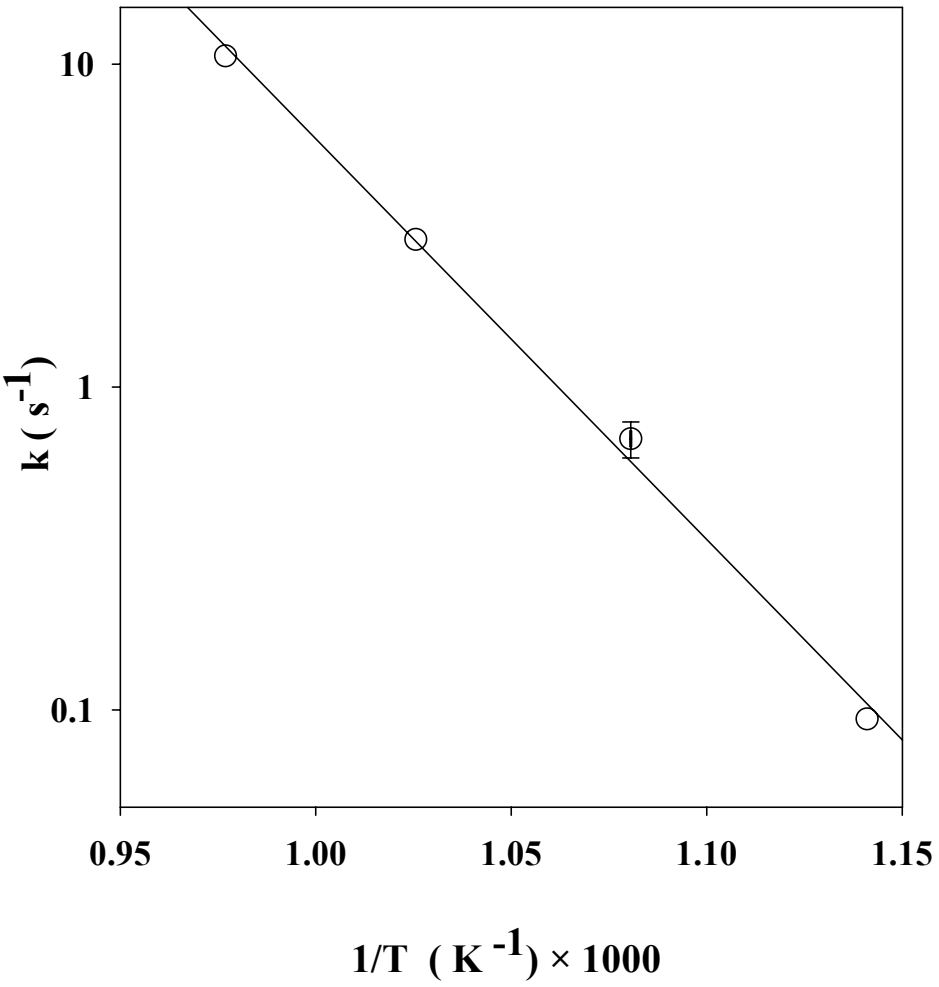

Figure 4.17 Rate constant versus temperature based on all the experimental data. The experiment was replicated three times at 652°C, standard deviation of k at this temperature is 0.09 (s^{-1})

The maximum deviation of measured temperature from the reaction temperature in all cases was + 4.5°C. Sensitivity of activation energy and pre-exponential factor to a hypothetic bias in temperature measurement of ± 5°C was calculated. This bias in measuring temperature would result in a bias of ±2 kJ/mol for activation energy and ±0.2 for natural logarithm of the pre-

exponential factor. These biases are well below the level of the uncertainty of activation energy and natural logarithm of the pre-exponential factor which were imposed by the uncertainty of the collected data.

Table 4.10 compares the values for activation energy and pre-exponential factor which were reported by previous researchers with the values which were obtained in this research. The reaction pressure is atmospheric in all cases. For the case of Fairburn et al. [31] who reported a pressure of 1 to 2 atm but used a batch micro-reactor which was under vacuum initially. The reactor design and results of these researchers were reviewed in Chapter 2.

Table 4.10 Comparison of the reported Arrhenius parameters for thermal cracking of nC_{16}

	E (kJ/mol)	**A (s^{-1})**	**T range (°C)**
Present Study	235	1.13E+13	600-750
Bartekova et al. [27]	162	3.50E+09	700-780
Fairburn et al. [31]	165	3.00E+08	576-842
Depeyre et al. [25]	239	9.60E+13	600-850
Rumyantsev et al., nC_{15} [32]	261	2.95E+14	615-720

These data are plotted in Figure 4.18 to compare the predicted rate of reaction from the different researchers for thermal cracking of n-hexadecande. The activation energy which is calculated in this study is very close to the reported value by Depeyre et al. [25]. The pre-exponential factor reported by these researchers has the same order of magnitude compared with the result of this study, yet it is higher and therefore they predicted faster rate constants as depicted in Figure 4.18. Bartekova et al. [27] and Fairburn et al. [31] both reported a significantly lower activation energy and pre-exponential factor compared with the report of all the previous researcher for thermal cracking of n-hexadecane and lower n-alkanes in general , as noted in Chapter 2 in Table 2.2.

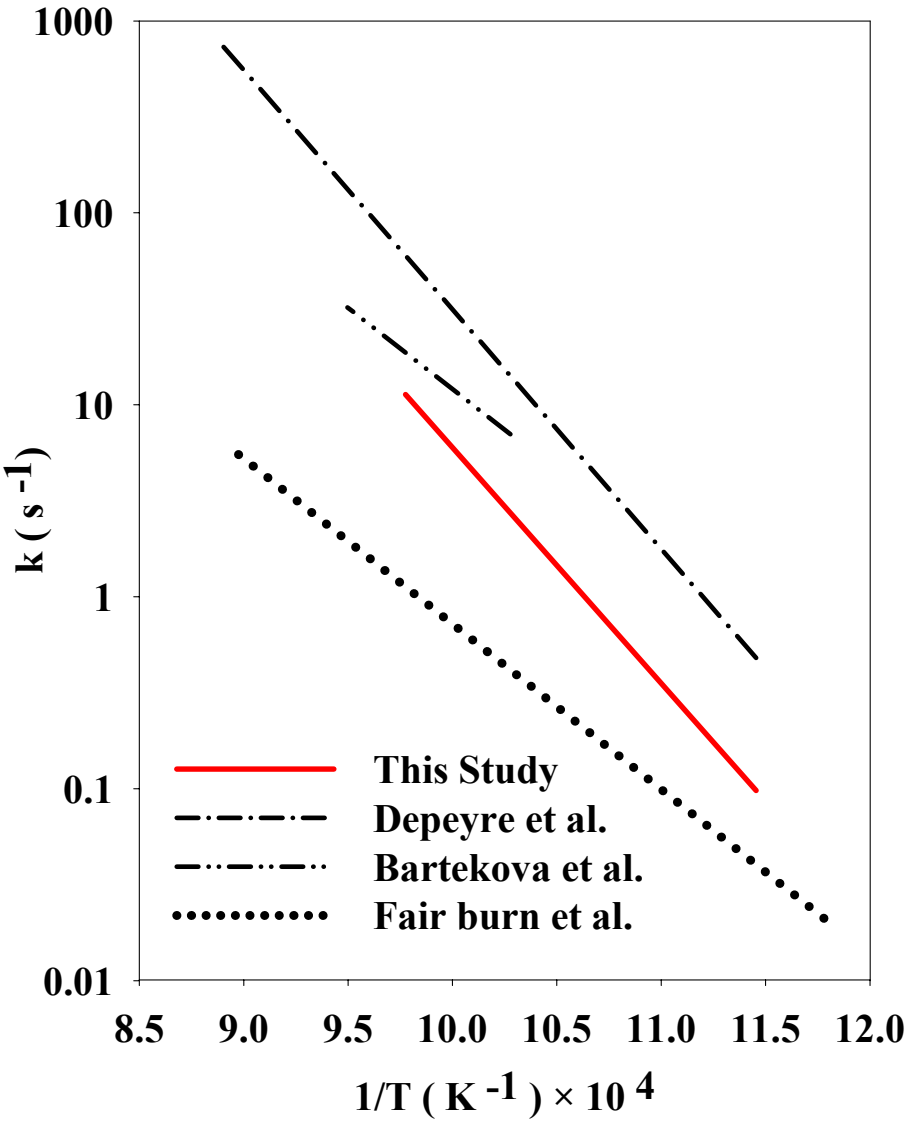

Figure 4.18 Rate constant versus temperature based on the Arrhenius' equation parameters, which are reported in literature for thermal cracking of n-hexadecane

The rate of thermal cracking reaction from this study matches very closely with the report of Rumyantsev et al. which is taken from the kinetics database of National Institute of Standards and Technology (NIST) for n-pentadecane [31]. No data were found for thermal cracking of n-hexadecane in this database. However, the overall rate of thermal cracking that they predict is closer to the results of this study. At higher temperatures, the extrapolation of

the results of this study becomes closer to the results of Bartekova et al.[27], as illustrated in Figure 4.18. Fairburn et al. reported significantly lower activation energy, and their over all prediction of the rate of thermal cracking of n-hexadecane is lower than any other studies. Figure 4.19 and Figure 4.20 illustrates the rate constants from the data of Table 2.2 to compare the activation energy and pre-exponential factor which are calculated for lower n-alkanes with the corresponding parameters which are calculated for n-hexadecane from the researchers in Table 4.10. Fairburn et al. and Bartekova et al. reported exceptionally low values for both activation energy and pre-exponential factor compared with the values which are reported for lower n-alkanes. Figure 4.21 compares the prediction of the rate constants at 700°C based on the data reported in Table 2.2. This temperature is selected since it in the temperature range of the most of the studies which are reported in Table 2.2. Fairburn et al. predicts the lowest rate constant at this temperature compared with all other researchers' reports. The exceptions in this comparison are the cases for ethane and propane with a significantly lower ratio of CH_2-CH_2 to CH_3-CH_2 bonds. Figure 4.22 demonstrates that a majority of the researchers who studied thermal cracking of lower alkanes in the range of C_7 to C_{15} predicts a very similar rate constant compared with the predictions of this study, especially the prediction of Rumyantsev et al. for n-pentadecane. This compound is the closest in carbon number and boiling point temperature to n-hexadecane. Reactor operation may account for some differences. Rumyantsev et al. used argon as the bath gas in their experiments, in contrast with Depeyre et al. [25] and Bartekova et al who used steam. Depeyre et al. used steam in thermal cracking of n-hexadecane and concluded that use of steam increases the yield of olefins. The increase in yield of olefins may be due to both a change in distribution of the products, and an increase in the conversion as well. In my study helium is used as the carrier gas.

Another factor in reactor operation is temperature measurement and control. The temperature measurement method used by Depeyre and Bartekova are subject to criticism (Chapter 2). The reactor which Fairburn et al. used was especially designed to address the issue of the slow temperature rise time in non-isothermal reactors. Their reactor required 100 ms to raise temperature of

the ferromagnetic wire which held the reactant from 270 to 842°C, while the microstructured mixer in this study can provide a temperature rise time of less than 2 ms.

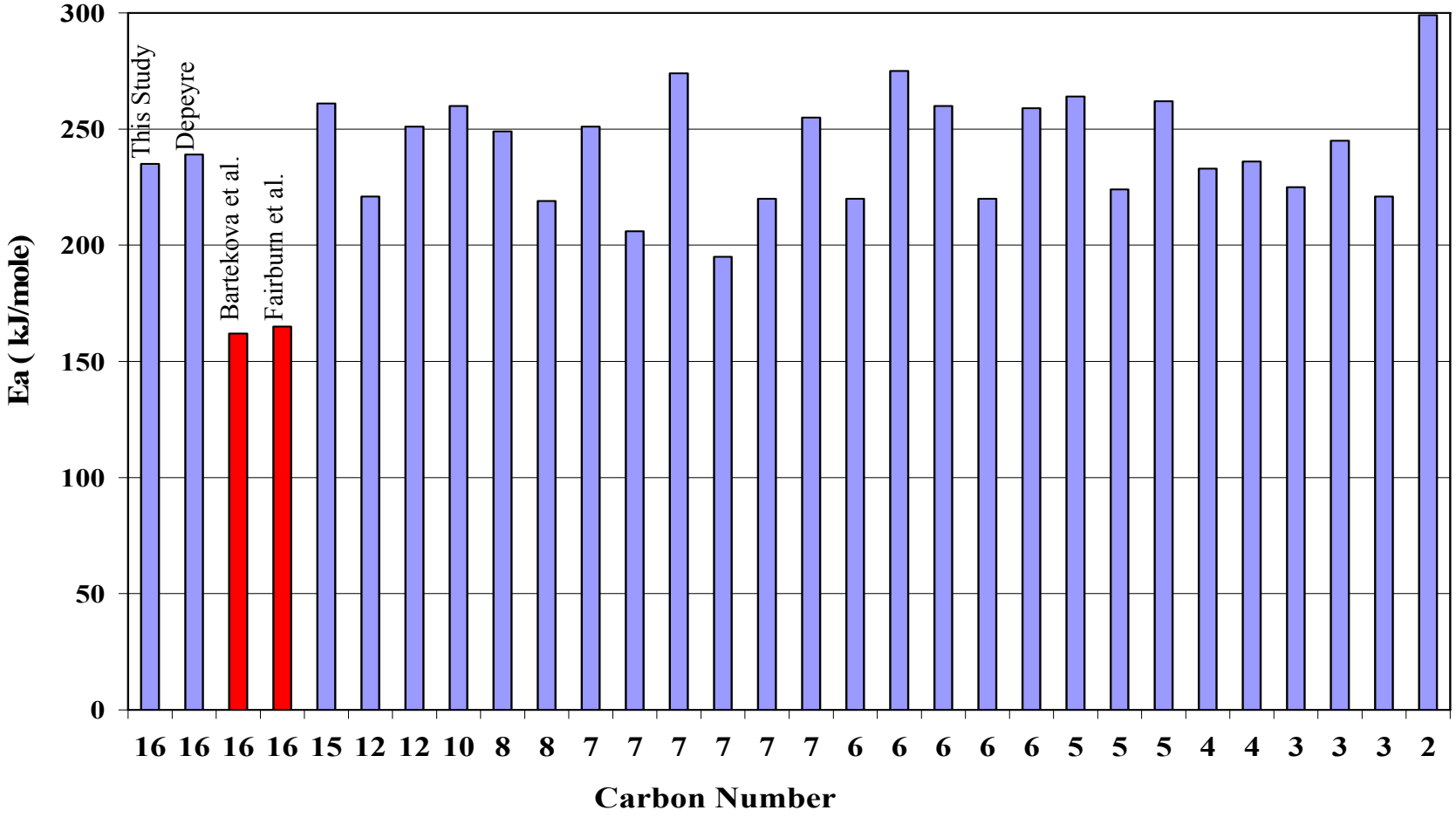

Figure 4.19 Comparison of the activation energy of thermal cracking of n-alkanes reported by 14 different researchers 700 °C and atmospheric pressure

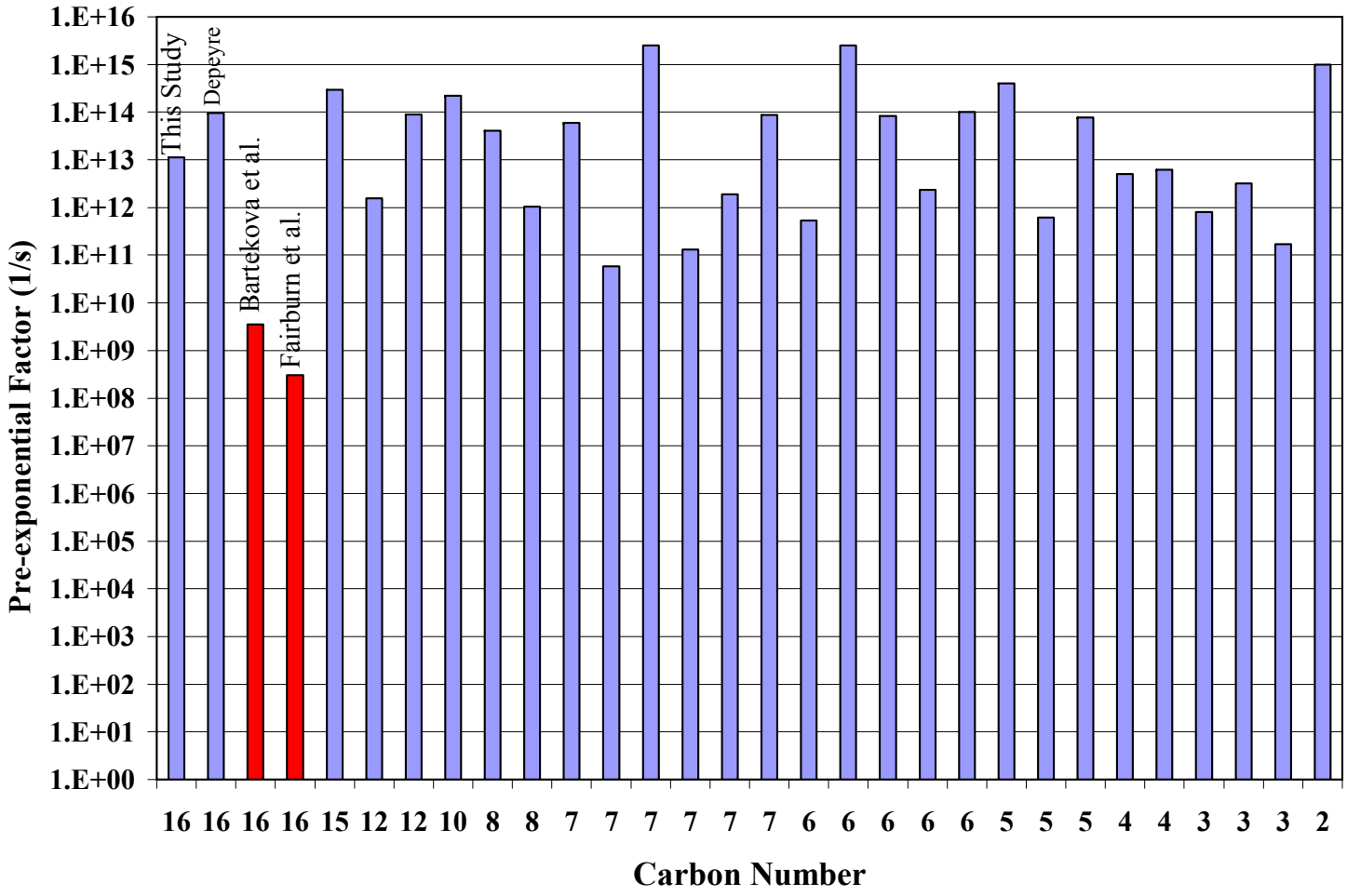

Figure 4.20 Comparison of the activation energy of thermal cracking of n-alkanes reported by 14 different researchers at 700 °C and atmospheric pressure

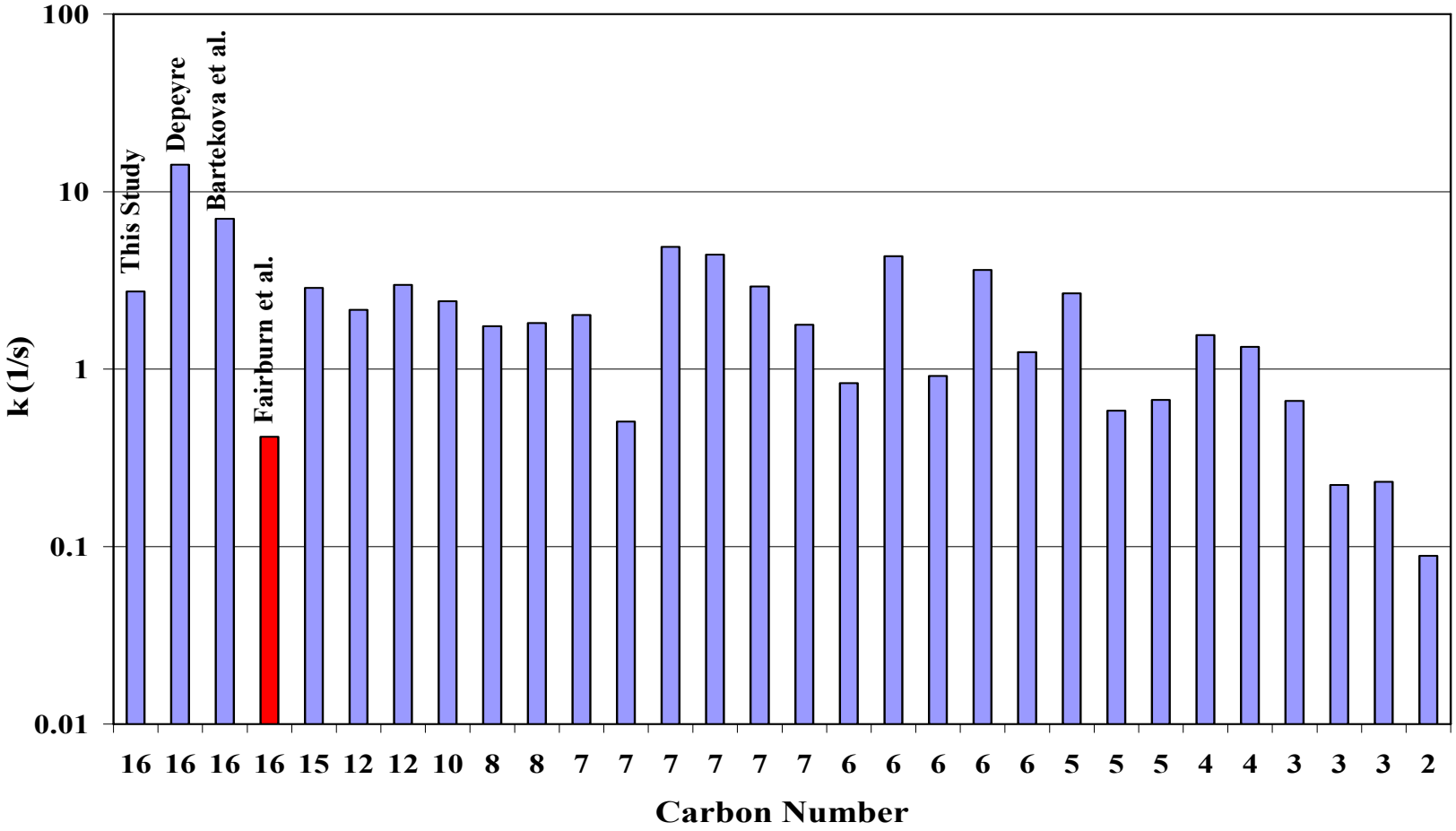

Figure 4.21 Comparison of rate constant of thermal cracking of n-alkanes reported by 14 different researchers at 700 °C and atmospheric pressure

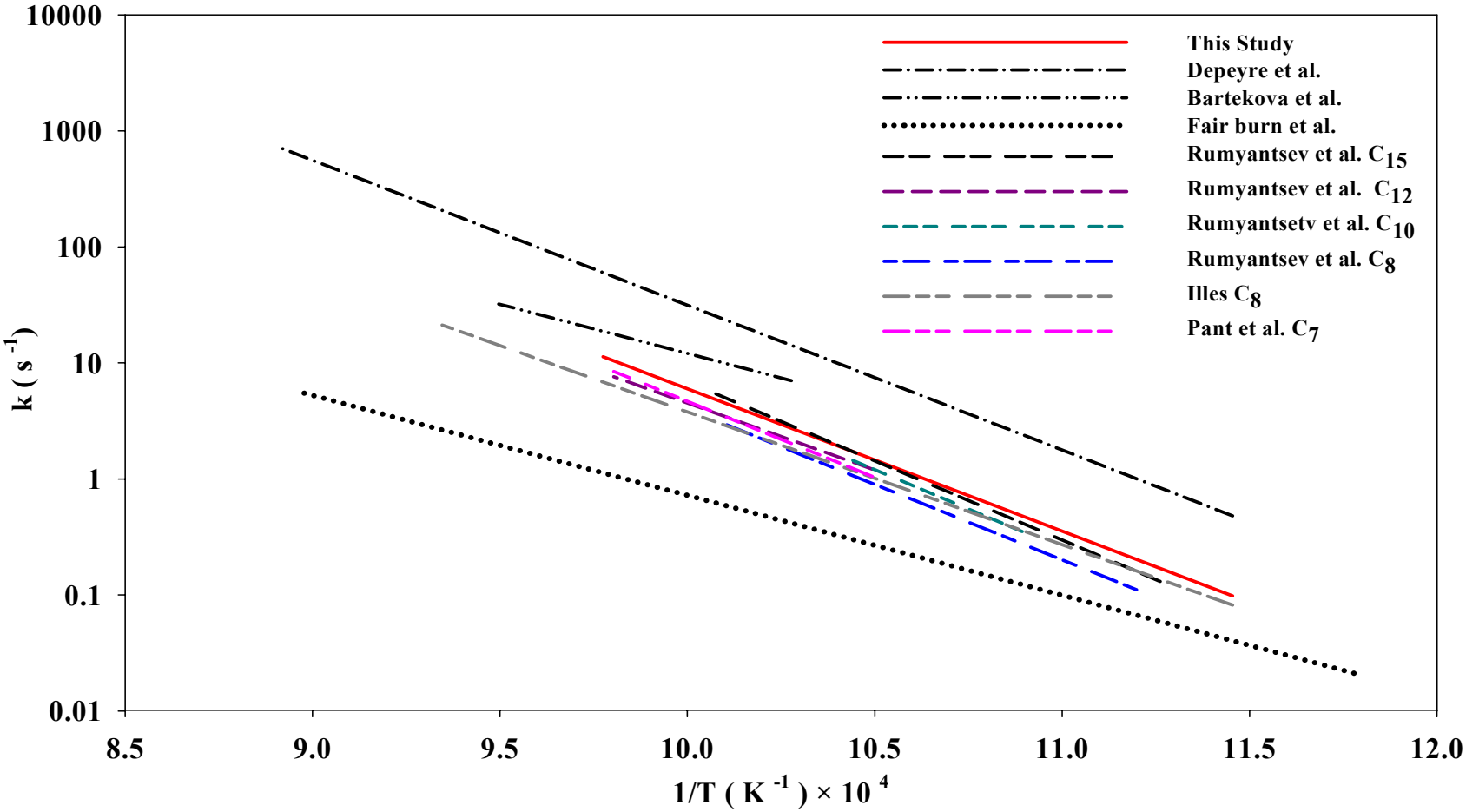

Figure 4.22 Comparison of the prediction of the rate constant versus temperature for n-hexadecane with lower n-alkanes from different researchers

4.3 Conclusions

In this research, the technology of microstructured mixer was introduced and demonstrated as a practical means of achieving an isothermal condition. This reactor was tested with n-hexadecane. Among the studies on thermal cracking of *n*-hexadecane at temperatures above 600°C, the results of this study for the activation energy, pre-exponential factor, and the predicted rate constants of the reaction, were found to be the most consistent with the majority of the reports in the literature for thermal cracking of n-alkanes.

Chapter 5

Thermal Cracking of Aerosol Droplets of Athabasca Vacuum Residue

This chapter presents the methodology and results for a continuous - flow aerosol reactor. This technology was developed to study thermal cracking of heavy oils, which contain fractions that remain in the liquid phase at the reaction temperature. The design philosophy of the aerosol reactor is given in Chapter 3. In summary, the merits of the introduction of feed into the reactor as aerosol of very small droplets or particles are as follows:

1. Prevention of formation of solid-liquid agglomerates
2. Minimization of the interference of transport phenomena with the intrinsic kinetic study (heat transfer and diffusive mass transfer)
3. Maximization of vaporization of the feed in the reactor

Application of industrial-size atomizers in kinetic studies at laboratory scales is not feasible. Additionally, these atomizers generate particles which are much larger than the required size in this research (maximum of 2 μm). The nature of the feed does not permit use of an aerosol generator external to the reactor. The developed technique requires that atomization takes place inside the reaction tube. This requirement rules out the use of a microstructured mixer, with its ability to give isothermal operation (as described in Chapter 4), because the feed must be subjected to high temperatures immediately to evaporate vacuum residue and minimize coalescence of droplets. As a result of the limitations on the introduction of an atomized vacuum residue solution, the only possible reactor was a non-isothermal straight tubular reactor without internal obstructions. This reactor design was used to carry out all the experiments with vacuum residue. The rate of thermal cracking of Athabasca vacuum residue in toluene was measured at the temperature range of 700 to 800°C and atmospheric pressure.

5.1 Materials and method

The following are the essential chemicals, which were used in the experiments.

- Athabasca vacuum residue provided by Syncrude Canada Ltd. Table 5.12 gives the properties of the prepared feed. The measured TGA residue is significantly lower than the reported MCR of 27.8 for Athabasca vacuum residue [64]. The value of TGA residue is expected to be lower because of the removal of about 3 wt% of toluene insoluble materials from Athabasca vacuum residue during feed preparation. In addition, the design of a standard MCR analyzer is different from TGA, and even if the same temperature program is applied in using both apparatuses, different results are expected.

Table 5.12 Properties of the prepared feed

MW (g/mol)	554
TGA residue (wt %)	18
524°C+ (wt %)	86.7
Aromatic C / total C (%)	34
H/C (molar ratio)	1.4
N/C (molar ratio)	7.5×10^{-3}
S/C (molar ratio)	6.0×10^{-2}

- Toluene certified ACS, purity higher than 99.5 % from Fisher Scientific, Canada
- Dichloromethane certified ACS, purity higher than 99.5 %, Fisher Scientific, Canada
- Helium with purity of 99.995 % , O_2 < 5 ppm and H_2O < 5 ppm provided by Praxair, Edmonton

The apparatus was consisted of the following essential sections, which are illustrated in Figure 5. 1:

- Reaction tube
- Nebulizer
- Furnace
- Manifold
- Data acquisition system
- Feed atomization
- Cryogenic condensers
- Gas chromatographs

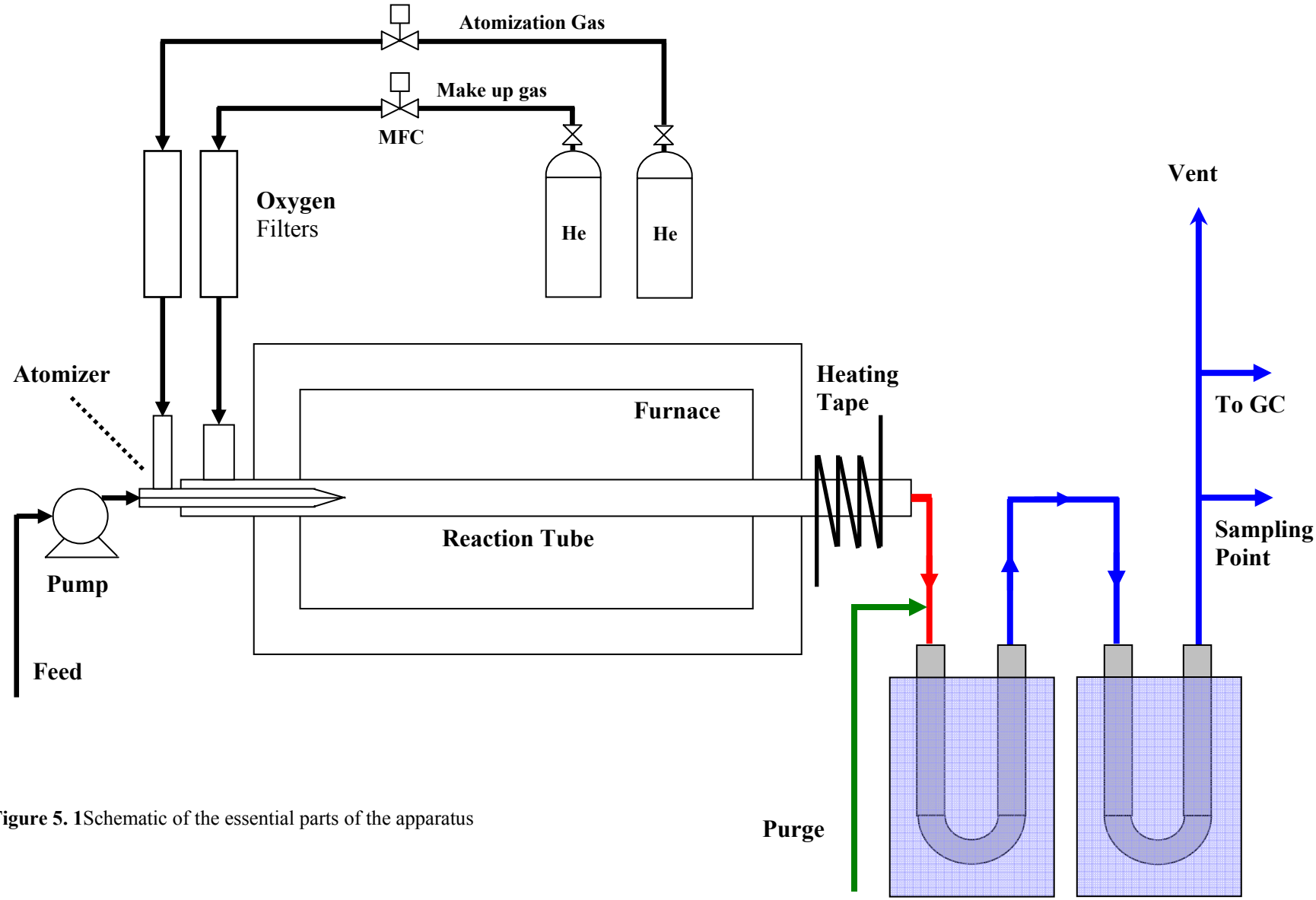

Figure 5. 1 Schematic of the essential parts of the apparatus

5.1.1 Reaction tube

The reaction tube was a straight seamless 316 stainless tube with outside diameter of 0.5 inch (1.3 mm) and average wall thickness of 0.049 in (1.2 mm). The length of the reaction tube within the furnace was 91.4 cm (36 in). The reaction tube was fixed at the upstream end. The reaction tube expanded at high temperature and slid outside the furnace through the down stream port of the furnace. The expansion of the furnace body and insulation was insignificant. Therefore, the length of the tube, which was exposed to the heating zones, was the same as the total length of the heating zones, or 91.4 cm (36 in). The atomization was achieved by use of a direct injection high efficiency nebulizer(DIHEN) [65].The tip of the nebulizer was inserted 15 mm inside the reaction tube, which was measured from the inner wall of the furnace at the up stream end. . The thermal expansion of these components was insignificant. Thus, the distance from the inlet end of the furnace to the tip of the nebulizer was constant. The active length of the reaction tube was from the tip of the nebulizer to the inner wall of the furnace at the downstream port of the furnace. The reaction tube extended out of the furnace from both the upstream and the down stream. At the upstream end, make-up gas was introduced through an ultra-vacuum tee fitting. The make-up gas was helium with the same quality as the atomization gas. A pressure transducer (Model PX726A 0-50 psi Omega Company, Laval, Quebec) was installed at the upstream of the reaction tube at the make-up gas line which measured the pressure of the reaction tube. The extension of the reaction tube at the down stream end was wrapped with a heating tape, which kept the temperature of the tube at 250-300ºC, to avoid condensation of the liquid products before they entered the inlet tubing of the condenser.

5.1.2 Furnace

The reaction tube was placed inside a tubular furnace with three heating zones. The same furnace was used to study thermal cracking of n-hexadecane, and it was described in Chapter 4. However, the purpose of using this furnace in these experiments was different compared with the application in Chapter 4. In all of

the thermal cracking experiments in this chapter, this furnace function was to first heat up the fluid, and when the fluid reached the reaction temperature, it was used to keep the fluid in reaction temperature. Thus, all the experiments were operated at non-isothermal condition over an entry length at the reactor inlet.

5.1.3 Manifold and the data acquisition system and control cabinet

The manifold consisted of the mass flow controllers (MFC), oxygen filters, particle filters, and the required tubing to facilitate conducting the carrier gases into the reactor. The same manifold, which was used for the experiments in Chapter 4, was used with minor modification for all the experiments in this chapter. The same data acquisition system and control cabinet were used for the experiments of thermal cracking of vacuum residue.

5.1.4 Preparation of Feed and Feed Solution

Athabasca vacuum residue was used as the feed. Toluene was use to reduce the viscosity of feed in order to make it possible to pump it into the atomizer. The feed should not contain any toluene-insoluble particles. Such particles were very likely to clog the very fine capillary tube inside the nebulizer. Athabasca vacuum residue was dissolved in toluene in a 1:40 ratio then it was mixed in an ultrasonic bath for 40 minutes. The solution was vacuum filtered. The filter paper was Millipore Durapore PVDF (polyvinylidene fluoride) with average pore size of 0.22 micron, which was purchased from Fisher Scientific Canada. The solvent was removed from the filtrate by evaporating under vacuum at 40°C using a rotary evaporator. The solid free vacuum residue was dried in an oven at 80°C. By this procedure the removed insoluble materials in toluene was 2.9 wt% of the Athabasca vacuum residue. The filtered Athabasca vacuum residue, which was prepared according to the above-mentioned procedure, is called feed in this chapter. Sufficient amount of feed was prepared once and the same feed was used in all of the experiments. A 5 wt % solution of the feed in toluene was made by mixing in an ultrasound bath at room temperature for 40 minutes. The evaporation of solvent during the mixing was found insignificant. This solution is referred to

as the feed solution in this chapter. About 30 to 40 mL of feed solution was transferred to a graduated cylinder, which served as the feed solution container at each experiment.

5.1.5 Introduction of the feed

The introduction of feed into the reactor can be designed based on the boiling point range of the feed. The feed can be injected directly or through a pre-heater if its boiling point range is sufficiently low to let complete vaporization occur at a temperature below the reaction temperature. Direct injection or use of a pre-heater is not feasible for a feed with fractions which remain in liquid phase at reaction temperature. In order to minimize the effect of heat and mass transfer resistance as discussed in Chapter 3, the feed was introduced into the reactor in the form of an aerosol of very small particles.

The feed solution was prepared just before injection and the left over was not kept in a freezer to be used for another experiment, to avoid plugging of the nebulizer. The weight of the container of the feed solution was measured after filling up the injection pump tubing and the liquid line of the nebulizer. The liquid line of the nebulizer was transparent (1/16 inch Teflon tube) to let the researcher observe the movement of the feed solution through the lines and inside the nebulizer. The weight of the container of the feed solution was measured at the end of the experiment. Thus, the total weight of the injected feed solution and the flow rate of injection was calculated. The feed was injected by a Masterflex peristaltic pump. This was the same pump which was used to study thermal cracking of *n*-hexadecane and its specifications were given in Chapter 4. It was important to maintain a constant flow rate of the feed during the operation for the following reasons:

- The concentration of feed should be known at the inlet of the reaction tube. Knowing the concentration might not be a requirement for the kinetic study of a first order reaction but the value is required to evaluate the

effect of heat of vaporization and reaction on the temperature profile. It was desirable to set this concentration sufficiently low that such effects could be neglected and had the most insignificant effect on the fluid temperature profile.

- When the concentration of feed at the inlet of the reaction tube was constant, the concentration of the gas products in the vent stream also became constant. The gas chromatograph could not analyze the samples immediately and it took at least 5 minutes to analyze C_1 to C_3 hydrocarbons. Therefore, the number of samples of the vent gases (gases that escaped the cryogenic condenser) was limited. A constant concentration of gases in the vent stream thus significantly minimized the error due to limitation of the number of samples. However, comparing with the long operation time of 1 to 2 hours the number of the samples were sufficient to let integration of data to calculate the total gas products, which escaped to the vent.
- The size of the feed droplets or particles, which was generated by the atomizer, depended on the flow rate of the liquid stream [66]. A consistent flow rate of feed solution during each operation maintained the same size distribution for the feed particles through the end of the operation. The kinetics of the reaction can depend on the size distribution of the feed particles. Thus, a constant flow rate of feed solution to the atomizer maintains the same kinetics during each reaction and ensures the repeatability of the experiments.

In all methods of atomization which were tested, vacuum residue had to be dissolved in an aromatic solvent to sufficiently lower its viscosity for atomization. The possibility of interaction of solvents with vacuum residue in the thermal cracking reactions is reviewed in Chapter 2. The reactor size was too large to be placed under a typical laboratory fume hood. Benzene was a better candidate because of its stability at high temperatures compared with toluene (Chapter 2), but the toxicity of toluene is much less than benzene, therefore toluene was used

instead of benzene. The possible inhibitive effect of toluene will be discussed in Chapter 7 after comparing the results of this study with predictions of the previous researchers.

5.1.6 Cryogenic Condenser

The same condenser which was used for the experiments in Chapter 4 was used for all the experiments of thermal cracking of vacuum residue. A 1/8 inch OD thermocouple was installed inside the U-tube at the first stage that demonstrated the temperature of gas at the outlet branch of the first stage of the condenser at the area which was submerged inside the liquid nitrogen and outside the area that the solvent and liquefied gases might build up. The U-tubes were placed inside two buckets, which were made of insulation material and were filled with liquid nitrogen during the operation. The level of the liquid nitrogen was maintained manually during the operation. The boiling point of liquid nitrogen is -196ºC. The temperature of the helium passing the first stage of the condenser at the measurement point reached to -170ºC.

5.1.7 Recovery and analysis of the products

The products of the thermal cracking were in gas, liquid and solid forms. The recovery and analysis of the gas products followed exactly the same procedure from Chapter 4 for thermal cracking of n-hexadecane.

After the collection of the gas products were completed, the collection of the liquid products was started. Dichloromethane was used as a solvent to wash the liquid and coke products out of the cryogenic condenser and the associated tubes. In order to separate coke from the liquid products , the collected liquids were vacuum filtered by filter papers with average pore size of 0.22 μm (Millipore Durapore PVDF membrane filter, hydrophobic, supplied by Fisher Scientific, Canada). After collection of the solids, the filter paper, which contained the coke solids, was placed in an oven at 80ºC and was left for about 12 hours to evaporate the toluene. The net weight of the filter paper itself did not change. This was verified by repeating the procedure with a blank filter paper. The difference

between the weight of the blank filter paper and the filter paper plus the solids was therefore the net weight of the collected solid products. The toluene insoluble materials were removed from the feed prior to the reaction therefore the solids were all coke and thus the yield of coke products could be calculated. Coke also deposited on the walls of the reactor. The reaction tube was inspected at the end of each experiment with an endoscope (Model FOI-150-TT, supplied by Titan Tool Supply Inc. NY, USA). The coke deposits inside the reactor were collected by brushing. This material was washed onto a filter, collected, and weighed separately from the coke from the condensers.

After filtration, the liquid products were in solvent solution, containing toluene from the feed and dichloromethane. Use of an atmospheric distillation unit for removal of the solvents was unsatisfactory. Toluene could not be effectively separated. Application of higher temperature at atmospheric pressure could cause further coking and evaporation of liquid products together with the solvents. This could be verified visually by change in the color of the collected solvents at the receiver of the distillation unit from clear to yellow. The evaporation of the liquid products could also be verified by another visual observation; upon vaporization of the liquid products, a white fog was formed above the black colored liquids. This fog slowly moved toward the condenser. When the fog condensed and mixed with the collected solvents in the receiver (initially clear liquids), it turned the color of the solvents to yellow. Vacuum pressure could theoretically accelerate evaporation of the liquid products, but under 80 °C no change of color of the collected solvents was observed in the receiver of the evaporator. Thus, the liquid products were transferred to a rotary evaporator to separate the solvents . The pressure of the rotary evaporator was set at about 13 kPa abs (vacuum pressure 26 inch of mercury). The temperature of the heating bath was started at 40°C and when all the dichloromethane was evaporated was gradually raised to 80°C. The rotary evaporator were equipped with a cryogenic condenser with liquid nitrogen which could collect the portion of dichloromethane and possible light liquid products which could escape the water condenser of the unit. Separation of

toluene from the liquid products of thermal cracking was more difficult. The vacuum pressure helped to separate toluene from the heavy liquid products of thermal cracking. The temperature was always kept below 80°C to avoid vaporization of the lighter fractions of liquid products under vacuum. The pressure and temperature for such separation was found by experimentation.

The gas and liquid samples were analyzed by the same two HP 5890 II units as described in Chapter 4. A GC - MS was used to detect specific light liquid products. After removal of all the solvents from the collected liquid products, the samples were left under a fume hood and the weight checked frequently to see if there was any change of weight due to any solvent which was retained in the heavy products and could evaporate in time. The weight of these samples indicated the weight of unconverted vacuum residue and liquid products, which was used in mass balance. After separation of dichloromethane and toluene, the remainder which consisted of unconverted vacuum residue and liquid products was solved in CS_2 (carbon disulfide ACS certified, purity > 99.9, supplied by Fischer Scientific Canada) and transferred to vials of suitable size (clear glass threaded vials , 21 × 70 mm, supplied by Fisher Scientific Canada) and placed under a fume hood. After CS_2 was evaporated, the vials were sent for simulated distillation analysis to Syncrude Canada Ltd. The applied method by this company was proprietary. The liquefied gas products were collected with the exact same procedure which was used in Chapter 4 and the same instrument and method were used for gas chromatography analysis of the concentration of the gas components. The gas chromatograph was equipped with a flame ionization detector, which could not measure the concentration of hydrogen and hydrogen sulfide in the products.

5.1.8 Thermal Gravimetric Analysis

The instrument which was used was Perkin Elmer Pyris 1 TGA. Nitrogen applied at a pressure of 10 psig and flow rate of 40 mL/min on the balance and 20 mL/min on the sheath. The sample heated from 25 °C to 500 °C at 15 °C/min and

hold for 15 minutes at 500°C. The weight was read when the temperature cooled off back to 25°C. This temperature program procedure was adopted from ASTM 4530 for measurement of MCR content.

5.1.9 Development of the atomization technique

On the industrial scale, vacuum residue is atomized by use of two-phase fluid atomizers, with steam as the atomization fluid. Miniaturization of the industrial method for atomization of vacuum residue, which is used in fluid coking, is not practical in a laboratory scale. Even if it were considered technically possible, the average diameter of the feed particles, which could be generated by this method, is 50 to 80 μm which would not be suitable for this research. This large size of feed particles would result in formation of solid-liquid agglomerates (Chapter 2). A variety of technologies for aerosol generation were tested in the laboratory. The criteria to select a target value for the size of aerosol particles was as follows:

1. Generation of the finest particles which are practically possible to ensure minimization of mass transfer
2. Minimization of heat transfer resistance so that the particles can follow the temperature of the carrier gas
3. The particles should be small enough in order to follow the streamlines and do not deposit inside the reactor or on the related components.

As explained in Chapter 3, feed particles with an average diameter of 2 μm or less is desirable for this research. Initially two types of aerosol generators, submerged jet and ultrasonic, were used to atomize the feed. The extensive coalescence of the feed droplets and deposition on the walls of the outlet tubing of the devices did not provide a useful mass of feed aerosol in a 2 hour test of operation. The failure of aerosol generation outside the reactor led us to investigate the *in situ* atomization of feed at high temperature inside the reactor. This environment leads to the sudden evaporation of the solvent and the light fractions upon generation of the feed droplets, which could enhance the disintegration of the droplets. Acon et

al. [65] reported on using a direct injection high efficiency nebulizer (DIHEN) interface for microbore high-performance liquid chromatography – inductively coupled plasma mass spectrometry. According to the manufacturer, this technology can generate fine particles with Sauter mean diameter as small as 1.2 to 1.5 μm.

The following models of atomizers were used for the thermal cracking experiments. DIHEN-170-A0.3 and DIHEN-Qtz-170-A0.3 (supplied by Meinhard Glass Products, Colorado) made from glass and quartz respectively. Both atomizers had the same specifications with the exception of the material from which they were made. The atomizers should operate at temperatures below the annealing point of their material. The annealing point of glass and quartz are 560 and 1215°C, respectively. The quartz nebulizer could be used for reaction at the higher limit of the reaction temperature range. The operating pressure of the atomizer was 1.17 MPa (170 psig) and the recommended flow rate for the liquid is less than 0.3 mL/min. The nebulizer was connected to the reaction tube using ultra high vacuum fittings provided by Swagelok Company. The tip of the nebulizer was inserted 15 mm inside the reaction tube (measured from the inner wall of the furnace).

Prior to use the very fine long - barrel DIHEN atomizer , a regular atomizer , Model TR-50-A0.5 (supplied by Meinhard Glass Products, Colorado), was used for preliminary tests. Figure 5. 2 shows the regular atomizer with a short barrel compared with the glass DIHEN atomizer. The regular type was made from glass and according to the manufacturer could generate particles with average diameter of 10 to 15 μm from water at room temperature, liquid flow rate of 1.1 mL/min and atomization gas pressure at 170 kPa (25 psi). Because of its short barrel, the tip of this atomizer could not be placed inside the active part of the reaction tube where it was exposed to the heating zone of the furnace. Indeed, the tip of this nebulizer was located about 15 cm (6 inches) outside the heating zone of the furnace. Because an external source of aerosol generator had the potential of

application with the technology of micro-mixer, this preliminary test was valuable. Deposition of feed was expected, but examining the extent of the deposition, size of the coke particles and if any material could pass the reaction tube at the operating condition were the other goals of this test.

Figure 5. 2 TR-50-A0.5 (short barrel) vs. DIHEN-170-A0.3 (long barrel) supplied by Meinhard Glass Products

The operating condition of the two experiments with TR-50-A0.5 is given in Table 5.13. The normal operating pressure and flow rate of liquid for this atomizer was 345 kPa gauge (50 psig) and 0.5 mL/min. The applied flow rates of the liquid feed were lower than the design flow rate . This was at the first place to minimize the concentration of feed in the carrier gas, which flowed inside the reactor, and to improve the performance of the atomizer to generate the finest possible particles. For concentric pneumatic nebulizers the mean droplet size can be predicted by Nukiyama-Tanasawa equation [66]:

$$D_{3,2} = \left(\frac{585}{V}\right)\left(\frac{\sigma}{\rho}\right)^{0.5} + 597\left[\frac{\eta}{(\sigma\rho)^{0.5}}\right]^{0.45}\left(10^3\frac{Q_l}{Q_g}\right)^{1.5} \quad (5.1)$$

In which :

$D_{3,2}$ is Sauter mean diameter (μm)

V is the difference between the velocity of the gas and liquid that flows and the tip of the nebulizer (m/s)

Q_l volumetric flow rate of liquid (cm^3 /s)

Q_g volumetric flow rates of gas (cm^3/s)

ρ density of the liquid (g/mL)

η viscosity of the liquid (dyn.s/cm^2)

σ surface tension of the liquid (dyn/cm)

This equation indicates that application of lower liquid flow rate and higher gas flow rate, rather than the normal operating condition can help to generate finer particles.

Table 5.13 Operating condition for preliminary experiments with regular nebulizer TR-50-A0.5

	Experiment 1	Experiment 2
Furnace T (°C)	600	700
Atomization Gas	N_2	He
Flow rate of atomization gas (SLM)	1	3.5
Concentration of VR in feed solution (wt%)	10	10
Flow rate of liquid (mL/min)	0.2	0.2
Atomization pressure (kPa)	430	330
Choke flow (SLM)	1.5	3.5

Experiment 1 showed extensive deposition of coke inside the reaction tube. A bed of coke was formed all along the reaction tube but only at the bottom (Figure 5.3.A).

Figure 5.4 shows the extensive deposition of feed inside the fitting, which held the atomizer. As this figure does show the deposition of feed extended to the upstream of the tip of the nebulizer. This result could be an indication of eddy currents in that region. In Experiment 2, the atomization gas was changed to helium. This change caused a higher flow rate of atomization gas, 3.5 times higher, passed through the nebulizer. Figure 5.3.B shows that the coke particles randomly distributed inside the reaction tube the deposition was not directed by the direction of the gravitational field. This was an indication of reduction in coalescence and deposition of the feed particles inside the reactor.

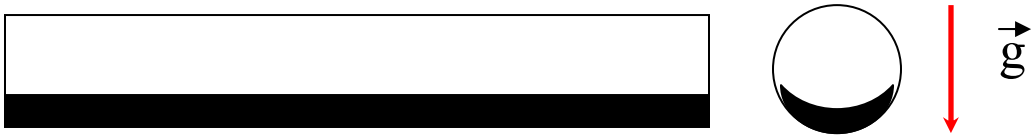

(5.3A)

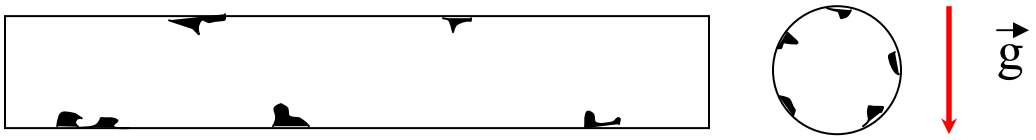

(5.3B)

Figure 5.3 Deposition of coke inside the reaction tube g is the gravitational vector

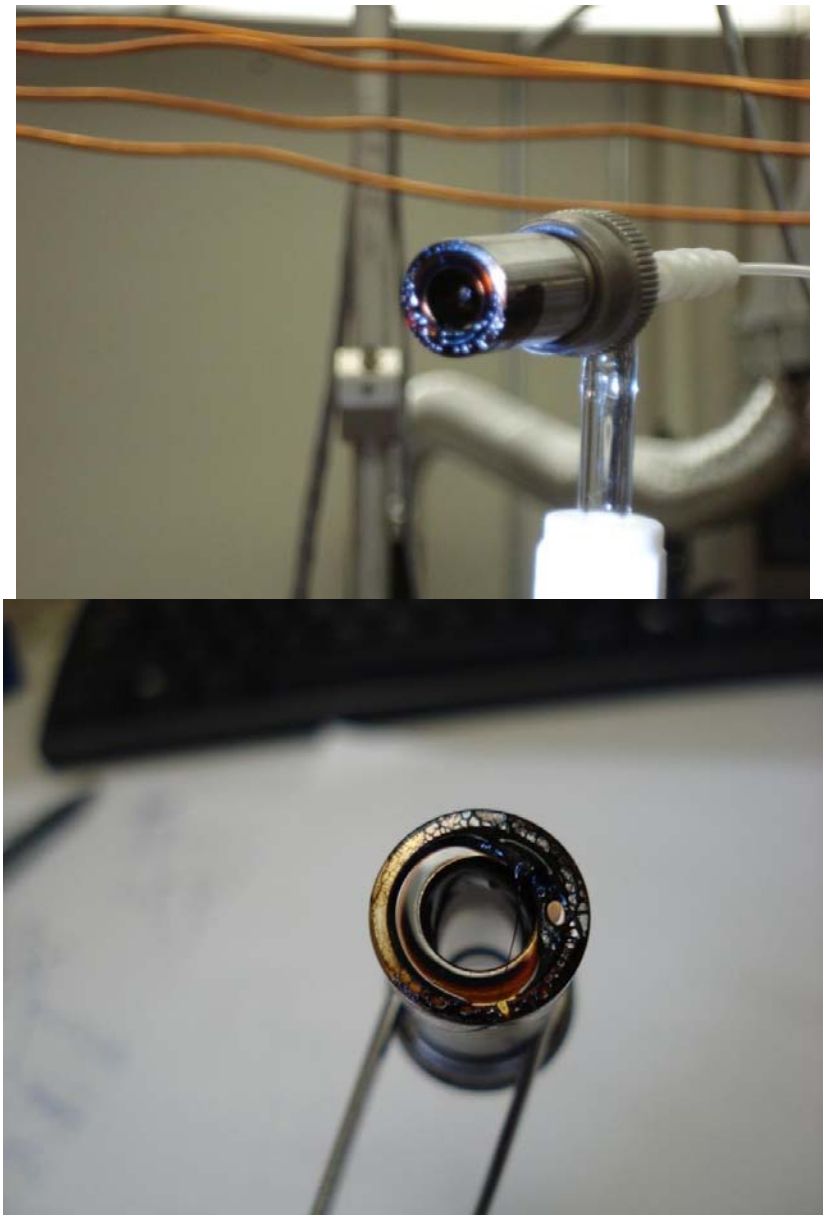

Figure 5.4 Extensive deposition of feed inside the nebulizer fitting and upstream of the tip of the nebulizer at experiment 1 with the short-barrel regular nebulizer.

In Experiment 2, 56 wt % of the total coke was collected by washing the reaction tube and its extension outside the furnace by simply passing through a solvent (dichloromethane). This coke included the mass of the coke which had passed the reactor but deposited in the extension of the reaction tube downstream of the furnace. 22 wt% of the total coke was collected by scrubbing the reaction tube and 22 wt% was collected from the cryogenic condenser.

The samples of the collected coke from the experiment 1 were analyzed by scanning electron microscope (SEM) of the Department of Earth and Atmospheric Sciences at the University of Alberta. Figure 5.5 shows an SEM micrograph of a blank filter paper, which was used for the separation of coke and sampling for scanning electron microscopy. Figure 5.6 shows a micrograph of the filtered coke from the cryogenic condenser. All the coke particles are a perfect spherical shape. The average diameter of the coke particles from the condenser was 600 nm. This average was calculated according to the following formula:

$$d_{ave} = \sqrt[3]{\frac{\sum_{i=1}^{N} d_{p_i}^{\ 3}}{N}} \tag{5.2}$$

In which d_{ave} is the average diameter of the coke particle

d_{pi} is the diameter of the coke particle

ρ is the density

m_i is the mass of the individual coke particles

N is total number of the counted particles

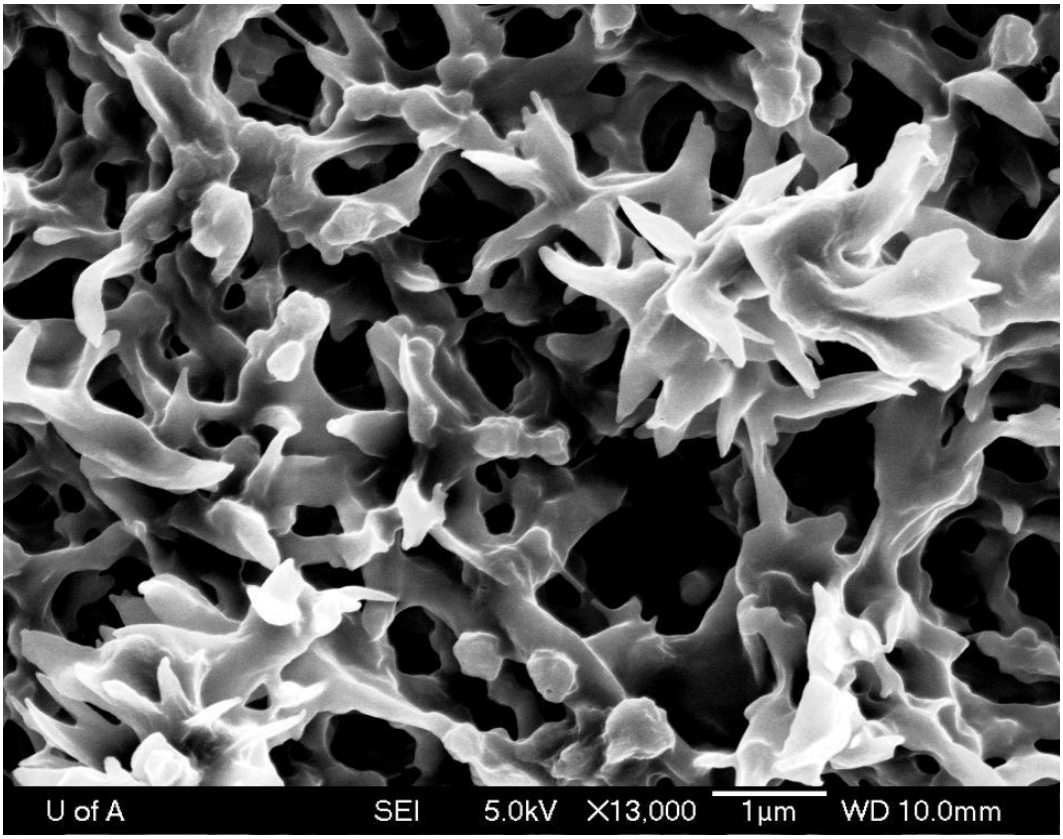

Figure 5.5 Blank filter paper average pore size of 0.22µm. This figure can be used as reference in interpretation of the SEM micrographs to distinguish between the texture of the filter paper and the coke particles.

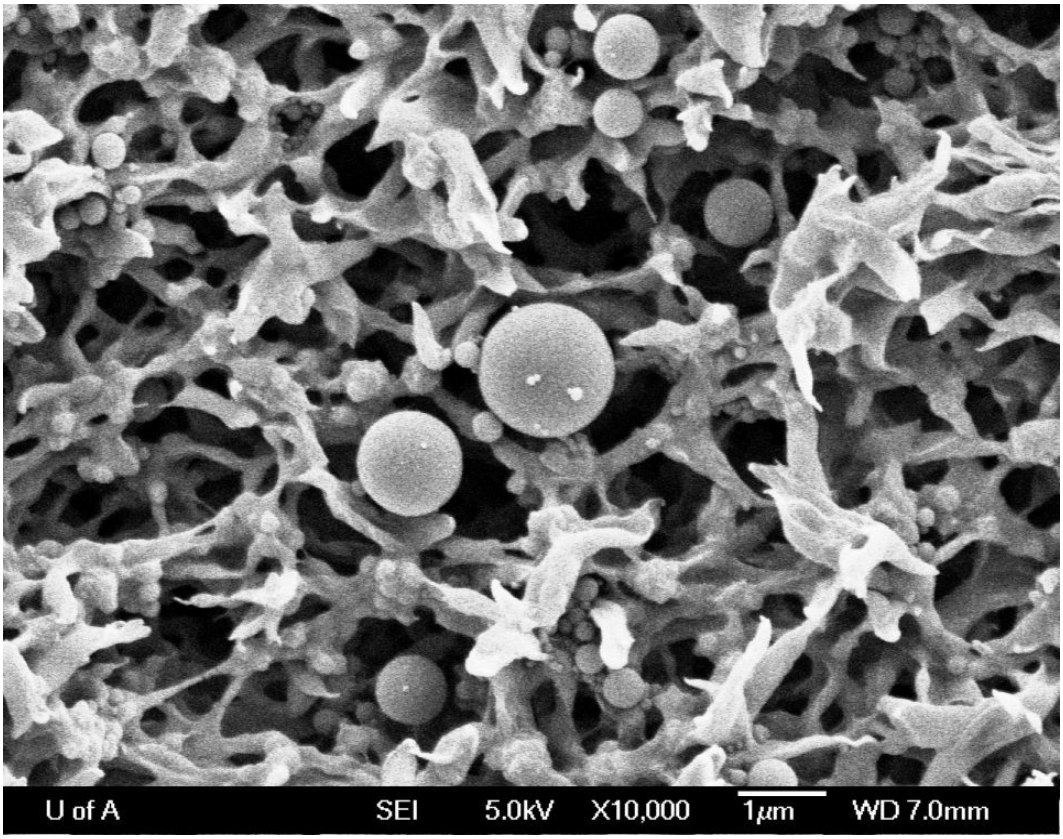

Figure 5.6 Experiment 1 with the regular atomizer TR-50-A0.5. The coke products collected from the cryogenic condenser with d_{ave} = 600 nm

The images in Figure 5.7 to Figure 5.12 show micrographs of some of the samples which were collected from the coke deposits inside the reaction tube in experiment 1. Almost all the coke was in form of chips and plates. Few coke microspheres were found in the coke samples from the deposits inside the reactor, and the few that were observed were much larger than the particles in the downstream condenser. No agglomerates of solid coke particles were observed. The rod-shape materials in these micrographs are fibers of glass wool which came to contact with the coke particles at the time of sampling after the reaction operation, and were not present at the time of reaction and did not affect the results of SEM.

Figure 5.7 Experiment 1 with the regular atomizer TR-50-A0.5. The coke deposits collected from inside the reactors. The rod shape materials are glass wool which entered at the time of sampling.

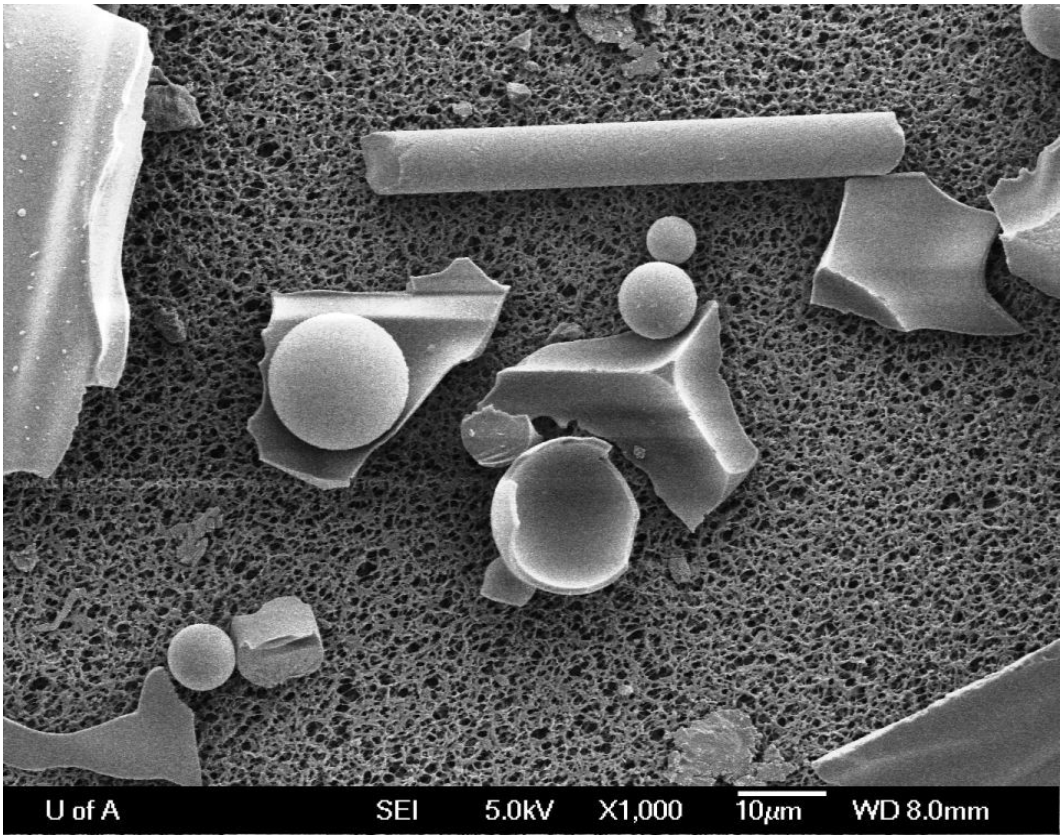

Figure 5.8 Experiment 1 with the regular atomizer TR-50-A0.5. The coke deposits collected from inside the reactors. The rod shape materials are glass wool which entered at the time of sampling.

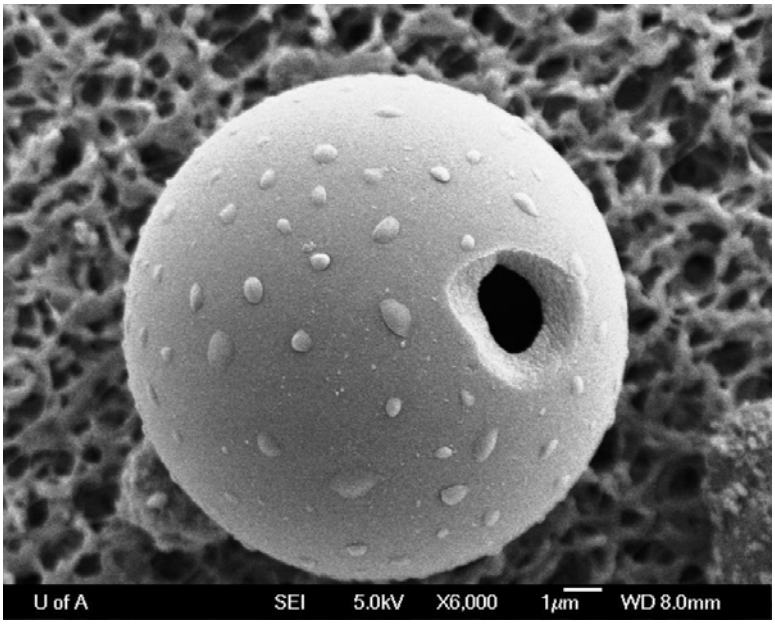

Figure 5.9 Experiment 1 with the regular atomizer TR-50-A0.5. A coke sphere found in the coke deposits collected from inside the reactors.

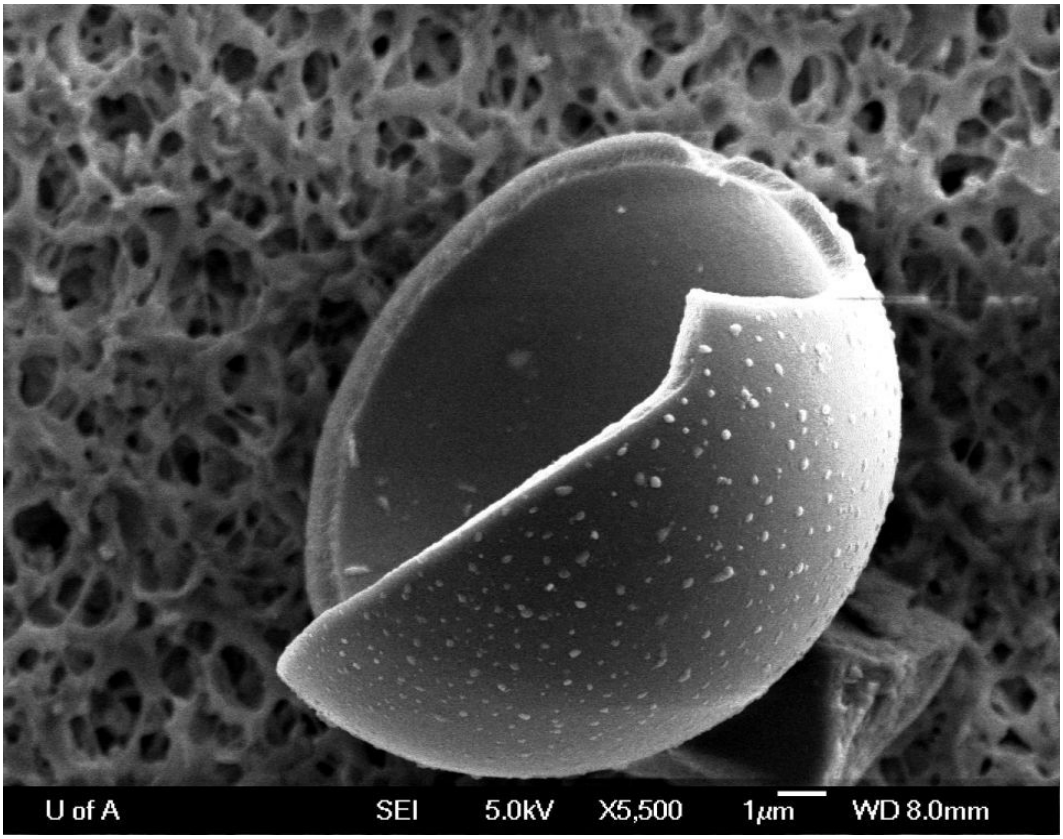

Figure 5.10 Experiment 1 with the regular atomizer TR-50-A0.5. A broken coke sphere found in the coke deposits collected from inside the reactors.

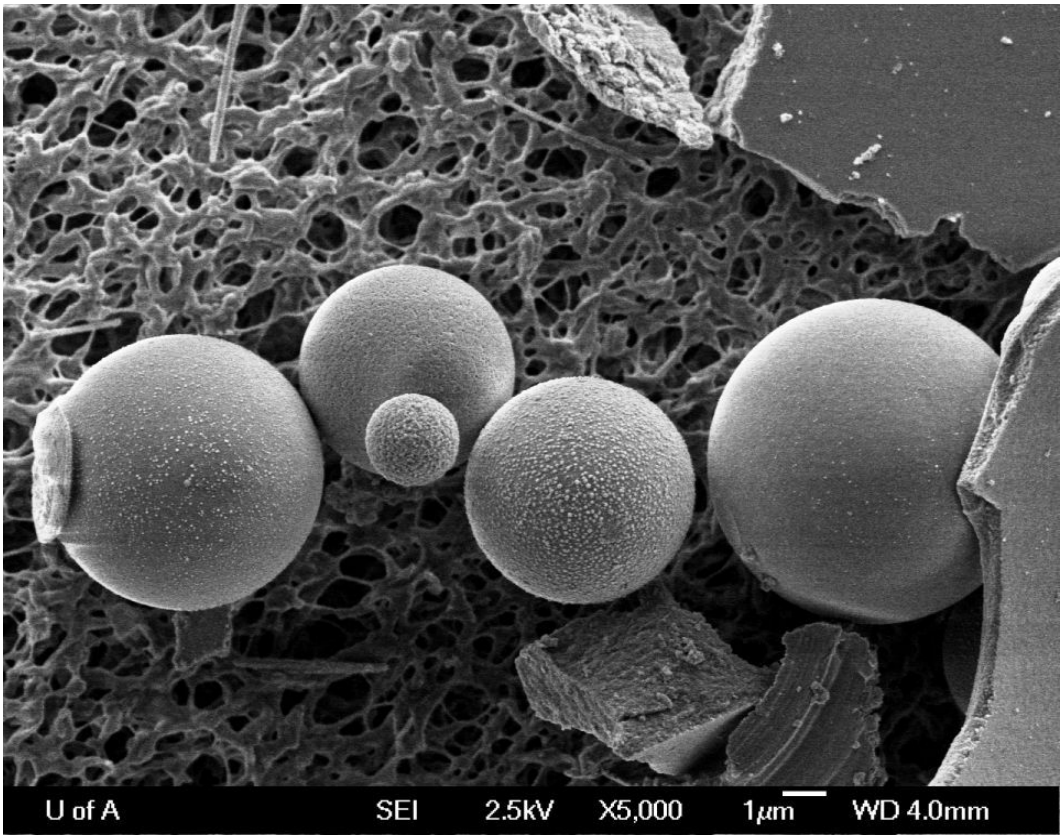

Figure 5.11 Experiment 1 with the regular atomizer TR-50-A0.5. The coke spheres found in the coke deposits collected from inside the reactors. The figure shows the variety of the quality of the texture of the surface of the coke spheres.

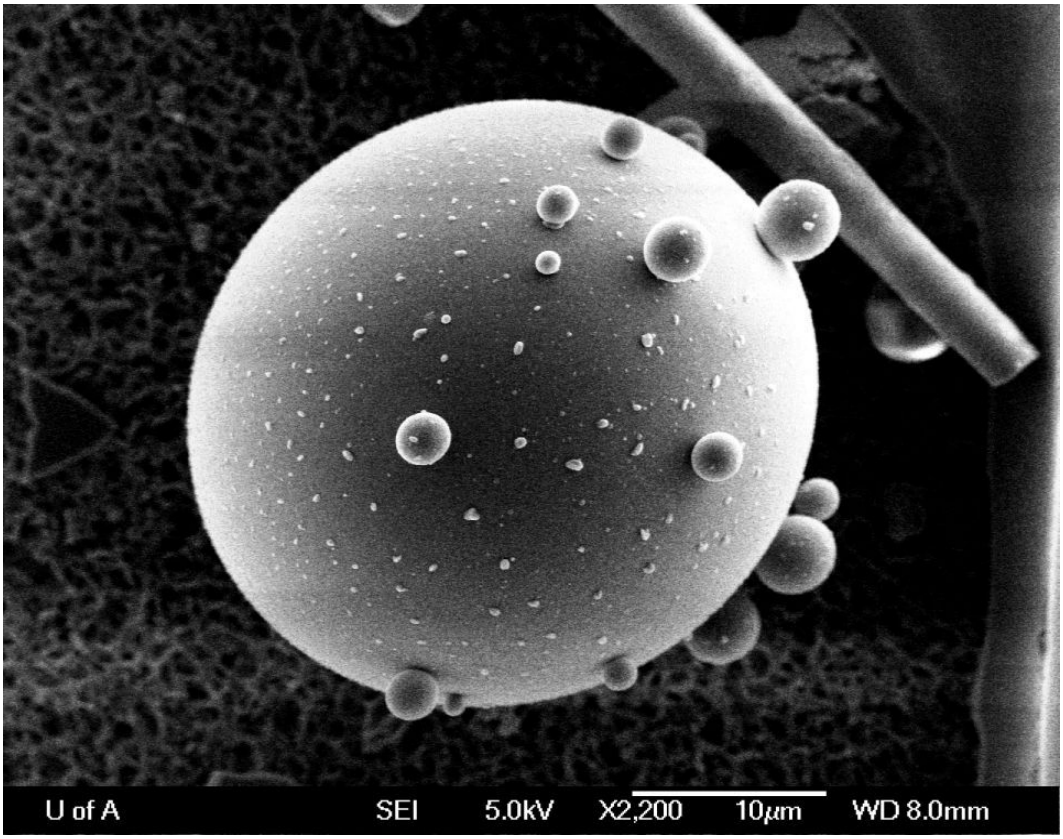

Figure 5.12 Experiment 1 with the regular atomizer TR-50-A0.5. The largest coke sphere found in the samples from the coke deposits collected from inside the reactors.

The limited number of spheres in the coke deposits in the reactor were circa 10-20 μm in diameter, over 10X larger than the coke particles that passed the reactor. According the manufacturer, the regular nebulizer would yield an aerosol of water with most of the droplets ranging from 15 to 20μm at room temperature. The SEM micrographs show that the coke particles sampled from the coke deposits from inside the reaction tube are in the same range. Figure 5.12 represents the largest coke sphere which was imaged by SEM. A number of these larger spheres were broken, indicating that the larger spheres are hollow with a thin crust, comparable to carbon cenospheres formed during incomplete combustion of heavy fuels [67]. All the broken micro-sphere indicated that the inside of the spheres was hollow with a uniform thickness of the crust.

My objective in operating the reactor was to minimize the deposition of liquid feed inside the reactor tube. Experiment 1 and Experiment 2 with the regular

nebulizer demonstrated the necessity of insertion of the tip of the nebulizer inside the actively heated zone of the reaction tube in order to obtain good results. The reduction in deposition of coke in Experiment 2 suggests that introduction of a make-up stream of inert gas could further minimize the deposition of coke inside the reaction tube. Based on the experience with all the atomization devices, it was decided to lower the concentration of feed in toluene to 5 wt % for actual thermal cracking experiments with the DIHEN nebulizer. Independent of the atomization technique which were used, I observed that higher concentrations of feed intensified the coalescence of the aerosol particles.

In the thermal cracking experiments with DIHEN nebulizers, make-up gas was introduced to minimize the deposition of the aerosol of feed on the wall of the reaction tube. The inspection of the reaction tube with a fiber optic device (endoscope) demonstrated that when make-up gas was not applied, a significant amount of feed deposited on the wall of the reaction tube near the tip of the atomizer. Some larger particles were randomly attached to the wall of the reaction tube around the middle of the reactor and the last 1/3 of the reactor looked clean of any deposits. The coke deposits were found starting at about 2.5 cm (1 inch) upstream of the tip of the atomizer, and extended about 7.5 cm (3 inch) downstream of the tip of the atomizer. Some coke deposits were collected from the body of the nebulizer. The fact that the deposition occurred upstream of the tip of the nebulizer, on both the wall of the reaction tube and the body of the nozzle, indicated the existence of vortices to give recirculation. Introduction of the make-up gas reduced the deposition of the feed on the wall of the reaction tube; with make-up gas flow rates below 3 SLM, the collected coke deposits exceeded 7 wt% in some experiments. The TGA residue of the feed is below 20 wt %. Therefore, in order to ensure that at least 95 wt% of the feed would pass the reactor, the coke deposit should be less that 1 wt % of the feed. The make-up gas can help to minimize deposition and eddy currents when its velocity is similar to the velocity of the spray streamlines. If it is faster or slower, it can exacerbate the situation by causing more vortices. A make-up flow rate of 12 SLM helium was

found to reduce the coke deposits inside the reaction tube to less than 1 wt% of the feed with both glass and quartz DIHEN nebulizers while helium was also applied as the atomization gas (see Section 5.3.4). Because of this critical constraint, mean residence time of the gas in the reactor was not an operational parameter which could be varied in these experiments; rather it was dictated by total of the flow rate of atomization and make-up gas required to suppress coke deposition.

5.2 Operating condition for thermal cracking of Athabasca vacuum residue

The choice of the operating conditions for the experiments were limited by the required total flow rate of gas inside the reaction tube to avoid coalescence and deposition of feed on the wall of the reaction tube. The flow rate of the feed solution was limited by the specification of the nebulizer. The concentration of the feed in the feed solution was limited by a critical value that was found by experimentation. Above this concentration the aerosol of the feed solution demonstrated an intense tendency to coalescence and below this value the solution was so dilute that made the operation time very long (above 2 hours) and made the mass balance impractical. Table 5.14 shows the operating conditions.

Table 5.14 Operating conditions for the experiments. The outlet pressure refers to the outlet of the cryogenic condenser.

Experiment Name	Furnace Temperature (°C)	Inlet pressure (kPa)	Outlet pressure (kPa)
700-1	700	105.6	102.9
700-2	700	110.2	102.2
750-1	750	112.2	109.8
750-2	750	112.6	110.4
800-1	800	113.3	110.9
800-2	800	107.0	102.7

Table 5.15 gives initial concentration of feed solution, feed, vacuum residue fraction and toluene at the inlet of the reaction tube where the thermal cracking reaction started. Table 5.16 shows the molar ratio of toluene to the feed in different experiments at the same place inside the reaction tube. Table 5.17 gives the flow rates of helium, feed, toluene, and total of fluid components in the inlet of the reaction tube. Table 5.17 gives the mean residence time of the fluid for each experiment. The heat transfer model of the non-isothermal reactor, which is explained in Appendix D., was used to calculate the temperature profile for calculation of these values.

Table 5.15 Initial amount of feed solution, feed, vacuum residue fraction and toluene at the inlet of the reaction tube where the thermal cracking reaction started

Experiment	Concentration of feed in the solution (wt %)	Concentration of feed at the inlet (wt %)	Concentration of VR at the inlet (wt %)	Concentration of toluene at the inlet (wt %)
700-1	5.00	0.32	0.28	6.15
700-2	4.56	0.36	0.31	7.50
750-1	4.99	0.38	0.33	7.30
750-2	5.01	0.38	0.33	7.11
800-1	4.80	0.38	0.33	7.59
800-2	4.79	0.35	0.31	7.05

Table 5.16 Molar ratio of toluene to the feed in different experiments

Experiment	Concentration of feed at the inlet (mole %)	Concentration of toluene at the inlet (mole %)	Molar ratio of toluene/feed
700-1	2.5E-03	0.28	114
700-2	2.8E-03	0.35	126
750-1	3.0E-03	0.34	114
750-2	2.9E-03	0.33	114
800-1	3.0E-03	0.36	119
800-2	2.8E-03	0.33	120

Table 5.17 Flow rate of helium, feed, toluene, and total of fluid components in the inlet of the reaction tube

Experiment	Flow rate of He (mole/min)	Flow rate of feed (mole/min)	Flow rate of toluene (mole/min)	Total flow rate at the inlet (mole/min)
700-1	0.661	1.65E-05	1.89E-03	0.663
700-2	0.598	1.68E-05	2.11E-03	0.600
750-1	0.641	1.92E-05	2.20E-03	0.644
750-2	0.648	1.90E-05	2.16E-03	0.650
800-1	0.613	1.84E-05	2.19E-03	0.615
800-2	0.615	1.70E-05	2.03E-03	0.617

Table 5.18 Mean residence time

Experiment name	Mean residence time
700-1	105
700-2	115
750-1	107
750-2	108
800-1	107
800-2	100

5.2.1 Temperature profiles

The temperature of the body of the reaction tube for each experiment was measured with the thermocouples which were attached along the reaction tube. The outside diameter of the thermocouples was 1/16 inch (1.6 mm) and all of them were of the same model. They were also of the same model which was used in experiments in Chapter 4. They were attached and secured to the tube surface by using nickel - chromium wires as clamps. Thus, the thermocouples could be opened at the end of each experiment and the reaction tube could be removed to

probe inside and be brushed out of the possible coke deposits. Thermocouples with smaller diameter were desirable, but their usage at high temperature where frequent reopening were a requirement, was not practical. Application of finer thermocouples was desirable to measure temperature. This required custom-made compression fittings. The disadvantage of such an installation was that the thermocouples were fixed and could not be removed after exposure to temperatures above 600°C. The necessity of frequent removal of the reaction tube with all the attached thermocouples from the furnace in order to probe for deposits and to wash and brush out the reaction tube was considered. Such a fixed installation increased the risk of breaking of the thermocouples. In addition, in such installation with custom-made compression fittings and adaptors, if one thermocouple had broken, the entire reactor should have been replaced. Welding was not a solution. Welding could deform the tube from inside and make obstacle in the way of flow of feed and coke particles. Previously, the extreme tendency of these particles to coalesce and deposit was experienced. In addition, after welding the thermocouples required recalibration due to possible effect of mixture with the welding material or any other adverse effect. This was not possible with considering the length of the reactor and the number of the attached thermocouples. In case of a broken thermocouple, if a permanent connection like welding or compression fittings were used, the whole reactor and the other thermocouples needed to be disposed.

If compression fittings were used, there were more mass of metal at the connection spot compared with the rest of the reaction tube where no thermocouples were attached. The higher local mass of metal around the tip of the thermocouple could cause local hot spots and a higher temperature could be measured. The thermocouples were ungrounded, that means the actual tip of the thermocouple does not attach the tip of the exterior sheath, therefore the direct attachment of the tip of the sheath to the surface of tube was not an advantage compared with attachment with clamps. However, it was important that the clamp cover the tip of the thermocouples to ensure that the heat transfer to the

thermocouple was by conduction from the reactor wall and not by radiation from the heating element. The temperature of the heating elements of the furnace was estimated to be 50 °C or higher than the furnace temperature by the manufacturer. However, as the effective reaction temperature was close to the furnace temperature, the effect of thermal radiation on the reading of the thermocouples could not be significant due the small temperature gradient between the body of the reaction tube and furnace temperature.

The size of the thermocouples and method of attachment could be considered as sources of error in measuring the temperature. .While there were alternative options, they were either not practical with regard to the requirement of the operation or they introduced other comparable sources for measurement errors.
The axial temperature profile of the fluid along the reaction tube was calculated. The temperature at any distance along the axial axis is the average temperature of the fluid at that cross-section of the tube. The heat transfer model which used for this calculation is explained in the Appendix D. Figure 5.13 shows the temperature profile of the wall of the reaction tube which was measured by the thermocouples for the case of experiment 700-2. In this experiment, the temperature of the furnace was set at 700°C. The wall temperature is compared with the average fluid temperature which was calculated. The x-axis represents the distance of the thermocouples from the inner wall of the furnace at upstream divided by the length of the reaction tube. The wall temperature profile and the fluid temperature profile for all other experiments look very similar therefore they are not shown here.

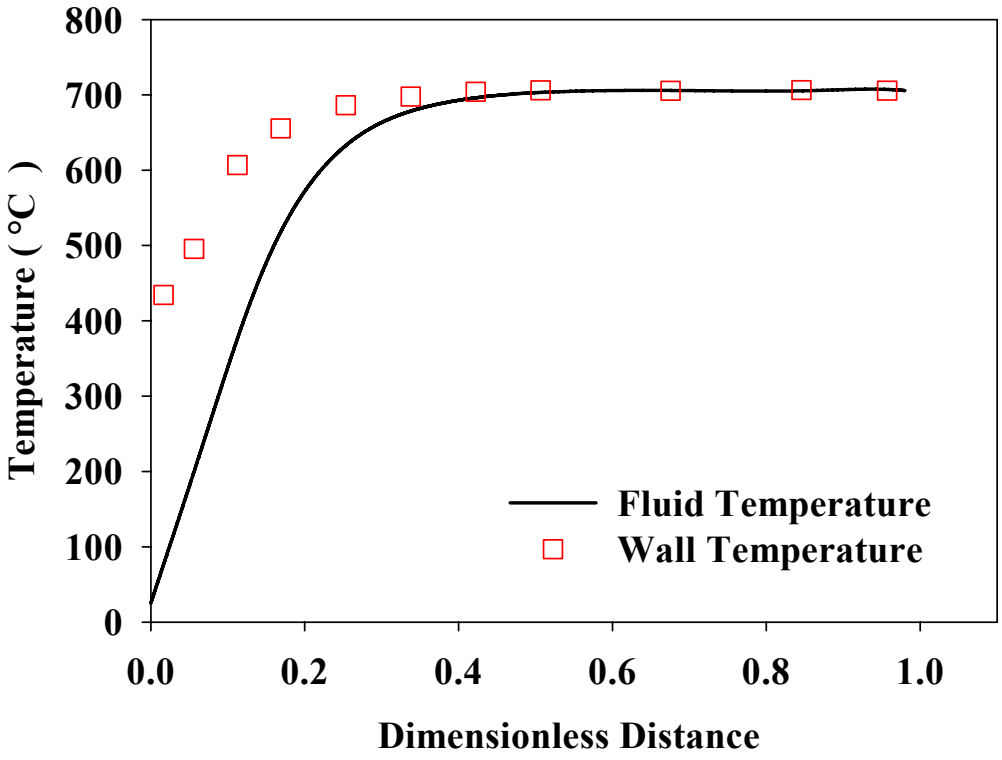

Figure 5.13 The measured temperature profile of the wall of the reaction tube and the calculated temperature profile of the fluid for the case of experiment 700-2 in which the furnace temperature was set at 700 °C

Figure 5.14 to Figure 5.16 show the fluid temperature profile inside the reaction tube. In experiment 700-2, the quartz nebulizer was used which used a lower flow rate of atomization gas at the operating pressure (1170 kPa gauge). This led to lower flow rate of fluid in the reactor in experiment 700-2 compared with experiment 700-1 in which the glass nebulizer was used. Naturally, the residence time in experiment 700-2 was longer than in experiment 700-1. This difference can explain the difference in the temperature profile between these two experiments which both were carried out at the furnace temperature of 700 °C. The experiments 750-1 and 750-2 were intended to be a measure for repeatability. Therefore, it was attempted to apply similar operating condition to both cases. Figure 5.15 shows that the measured fluid temperature profiles for these two experiments are very close.

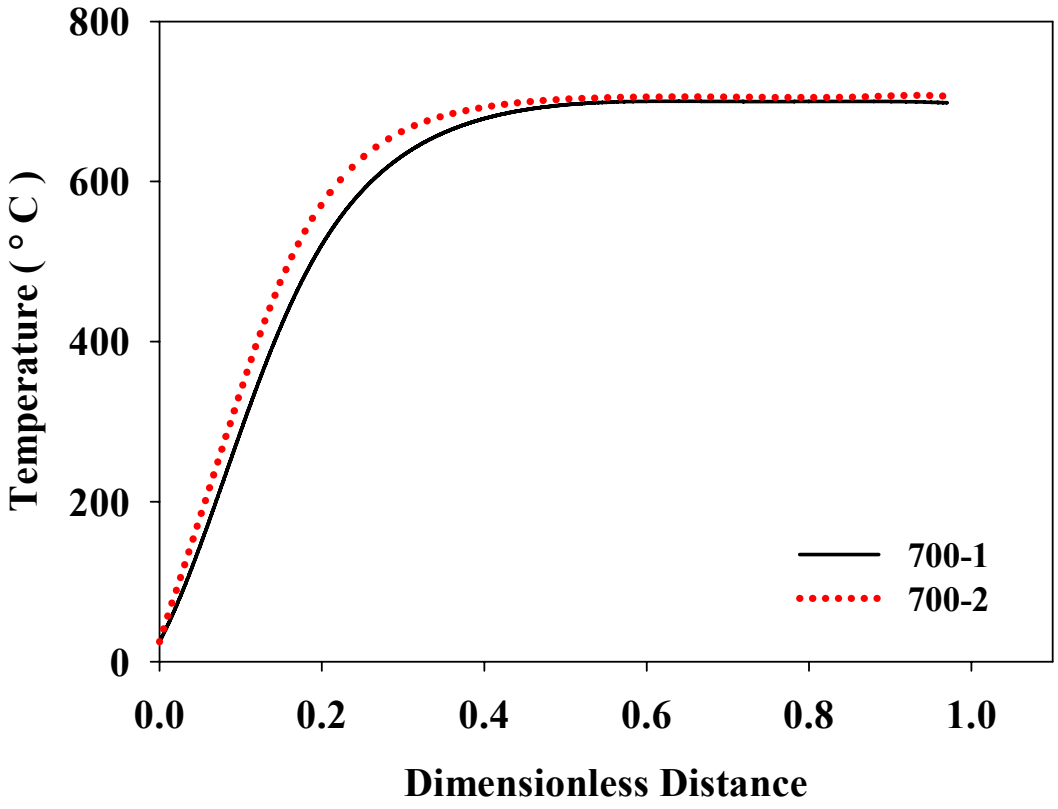

Figure 5.14 Comparison of the fluid temperature profile along the reactor for the case of experiments 700-1 and 700-2

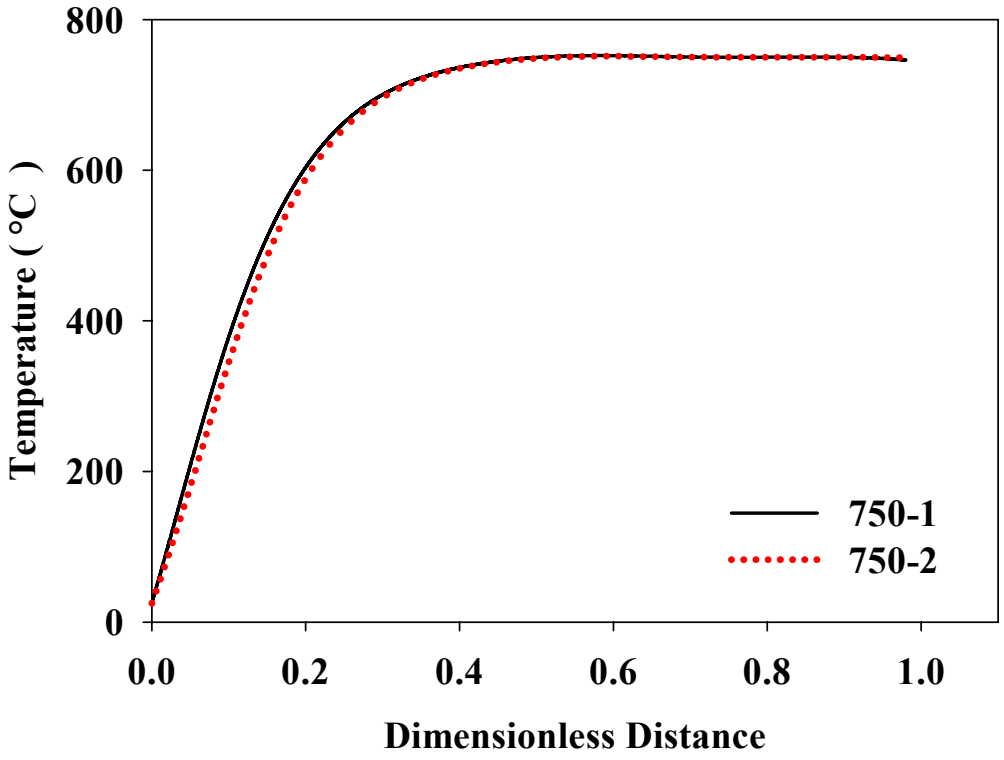

Figure 5.15 Comparison of the fluid temperature profile along the reactor for the case of experiments 750-1 and 750-2

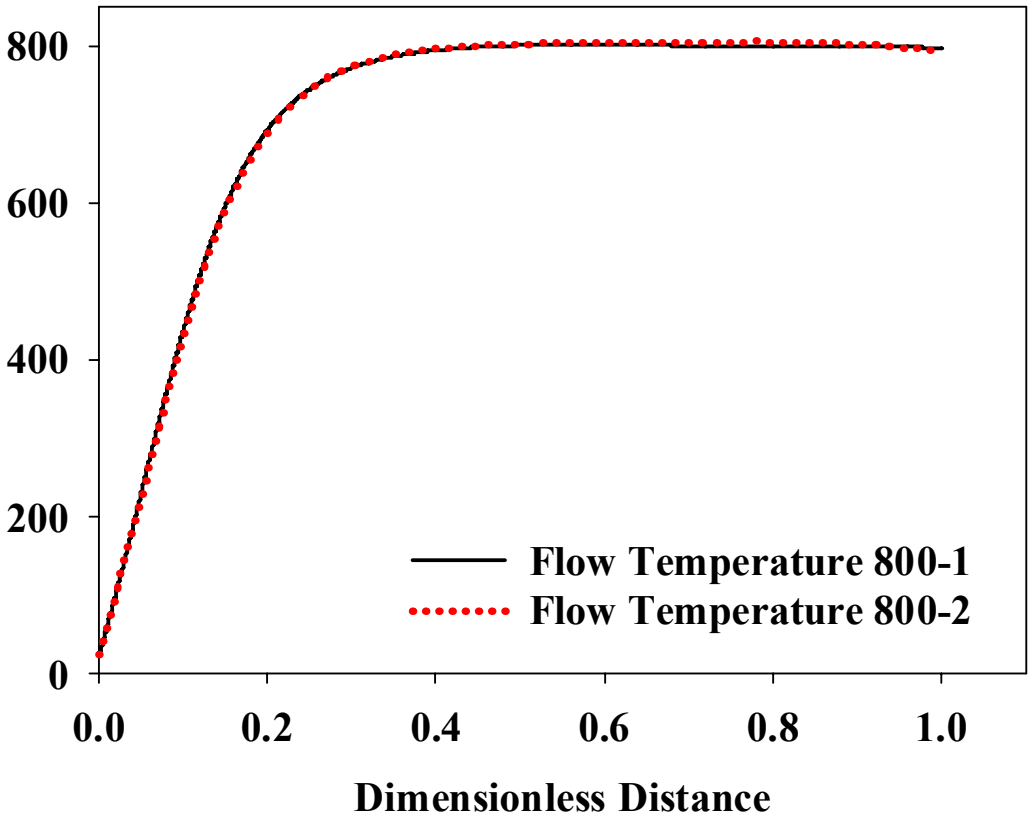

Figure 5.16 Comparison of the fluid temperature profile along the reactor for the case of experiments 800-1 and 800-2

5.2.2 Flow regime and residence time

The residence time that the reactant spent to reach any point along the reactor is called the cumulative residence time, which was calculated by adding up the residence times of the fluid at each segment of the reactor at a temperature that was estimated using the heat transfer model in Appendix D.The velocity of the fluid, density, cumulative mean residence time, and Reynolds number which are reported in this section were calculated by the heat transfer model for the non-isothermal reactor (Appendix D). Figure 5.17 to Figure 5.19 show the velocity of the fluid in the reaction tube for each experiment. As was mentioned earlier, experiment 700-1 and 700-2 were not replicates. The higher velocity of the fluid in experiment 700-1 compared with experiment 700-2 is consistent with the

higher flow rate of helium which applied in the case of experiment 700-1. The experiments 750-1 and 750-2 were replicates and Figure 5.18 shows clearly that the velocity profiles of the fluid in both experiments are similar. Experiments 800-1 and 800-2 cannot be considered as replicates, as a consequence of the difference in the reactor pressure. This difference is not very significant but it caused a significant difference in the velocity of the fluid in the reactor. Figure 5.16 shows that the temperature profiles are the same for both experiments at furnace temperature of 800°C, nevertheless the effect of the difference in the reactor pressure on the density of the fluid caused the difference in the fluid velocity. The density of the fluid in experiments 800-1 and 800-2 are demonstrated in Figure 5.20. The lower velocity and higher density of the fluid in experiment 800-1 compared with experiment 800-2 is consistent with the fact that the reactor pressure in experiment 800-1 was higher than the reactor pressure in case 800-2 (Figure 5.19 and Figure 5.20).

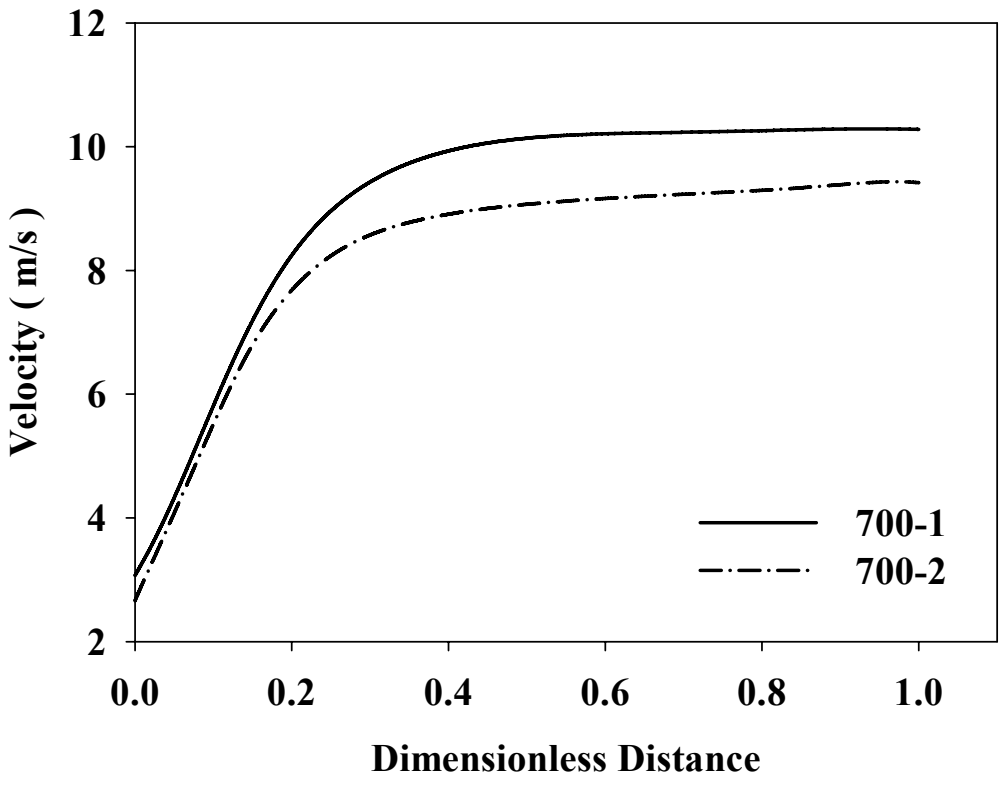

Figure 5.17 Velocity profile for experiments 700-1 and 700-2

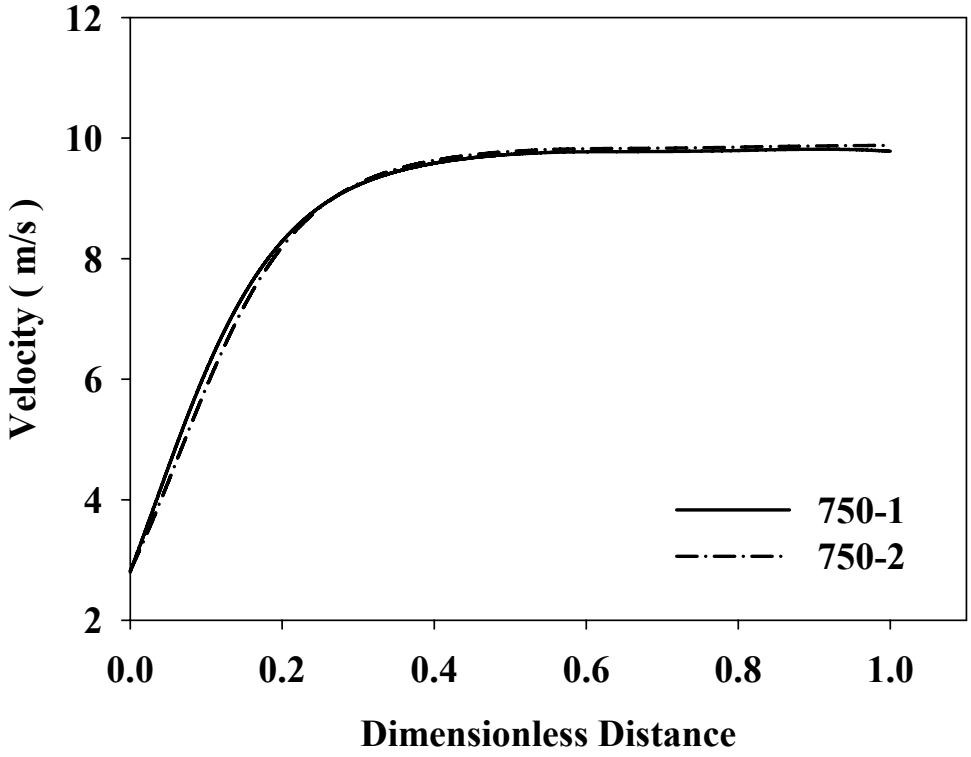

Figure 5.18 Velocity profile for experiments 750-1 and 750-2

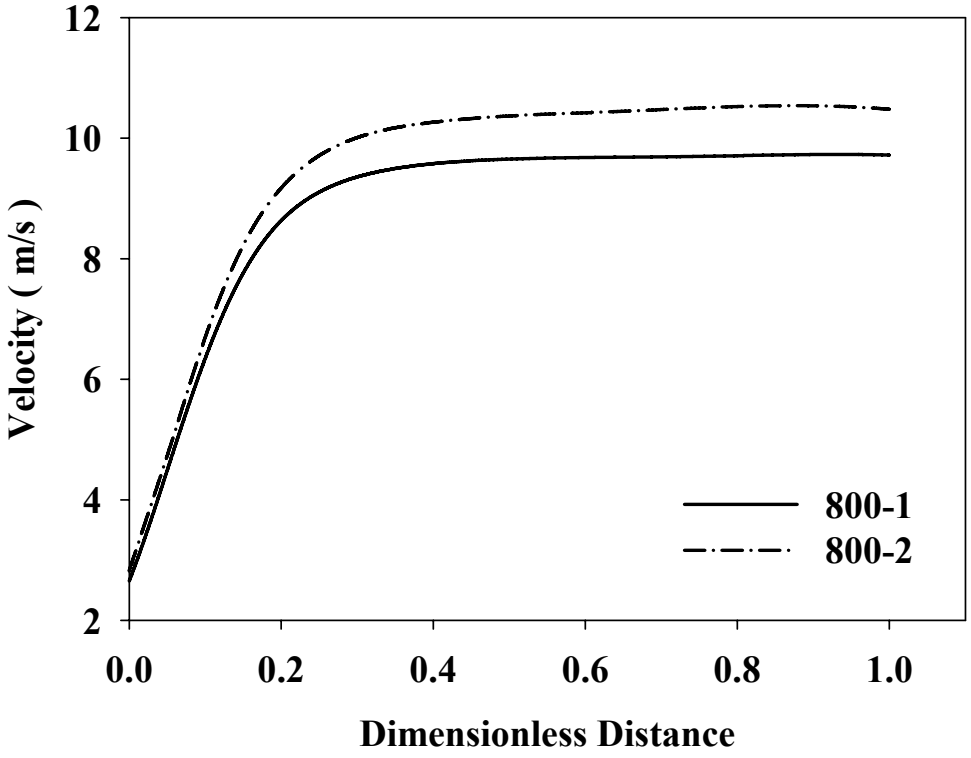

Figure 5.19 Velocity profile for experiments 800-1 and 800-2

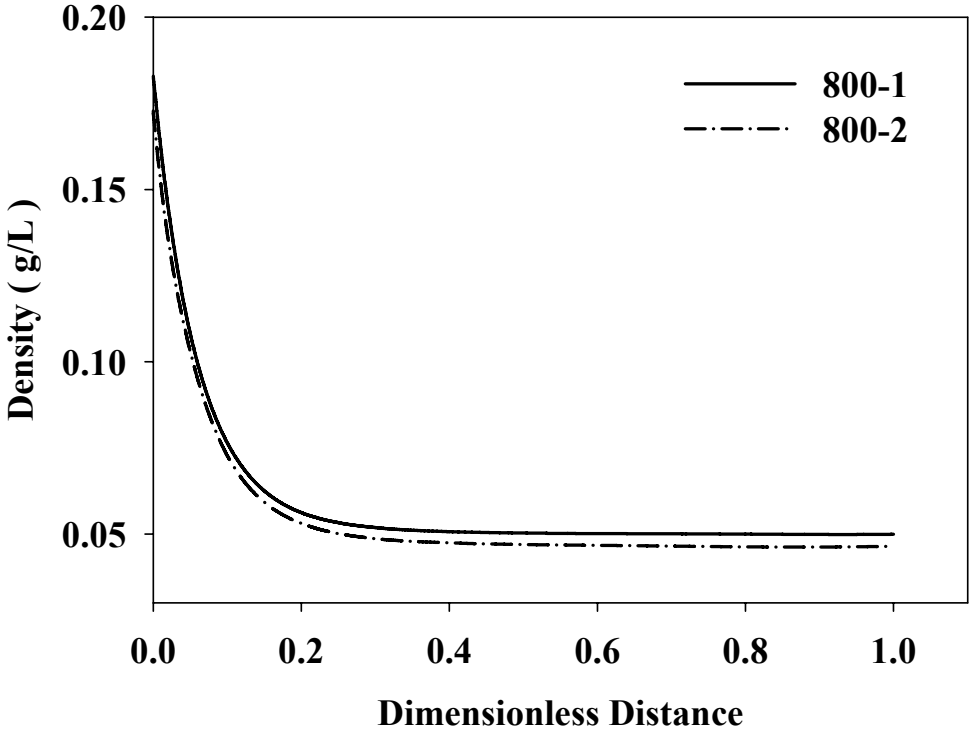

Figure 5.20 Density of the flow in experiments 800-1 and 800-2

Table 5.18 gives the total residence time of the fluid in the non-isothermal reactor, which is calculated using a temperature profile from the heat transfer model of the reactor (Appendix D). Figure 5.21 to Figure 5.23 show the cumulative mean residence time along the reactor. Higher flow rate of fluid in experiment 700-1 caused a lower fluid mean residence time compared with experiment 700-2. The mean residence time of experiment 750-1 and 750-2 are similar. Consistent with the aforementioned discussion about the effect of reactor pressure and lower density of fluid in the case of experiment 800-2, the mean residence time of fluid along the reactor in this case is significantly lower.

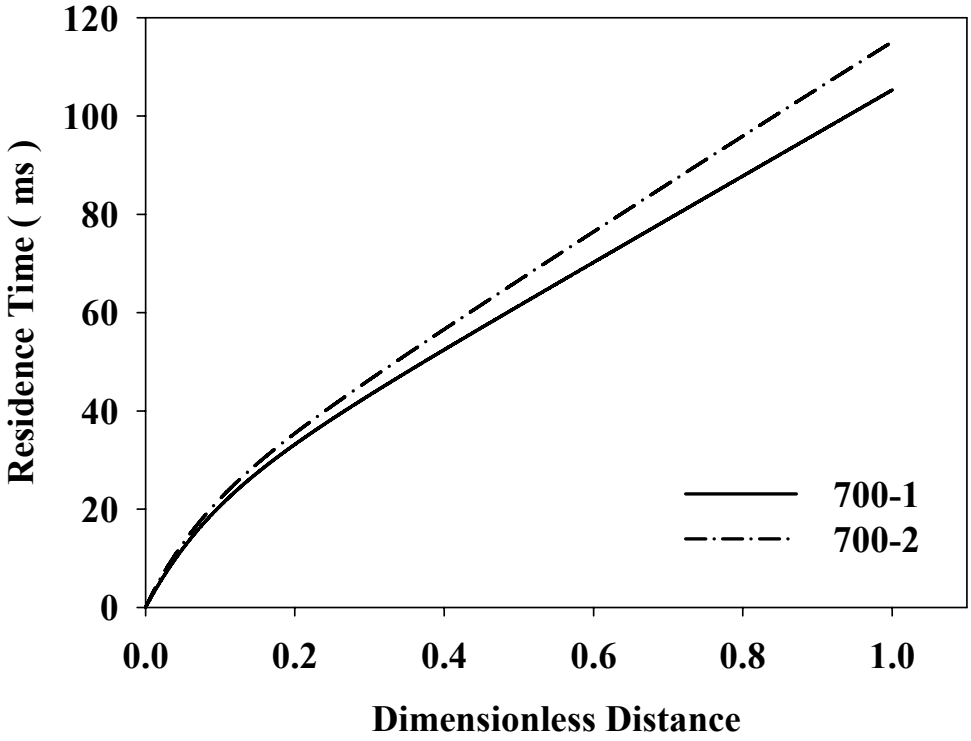

Figure 5.21 Cumulative residence time for experiments 700-1 and 700-2

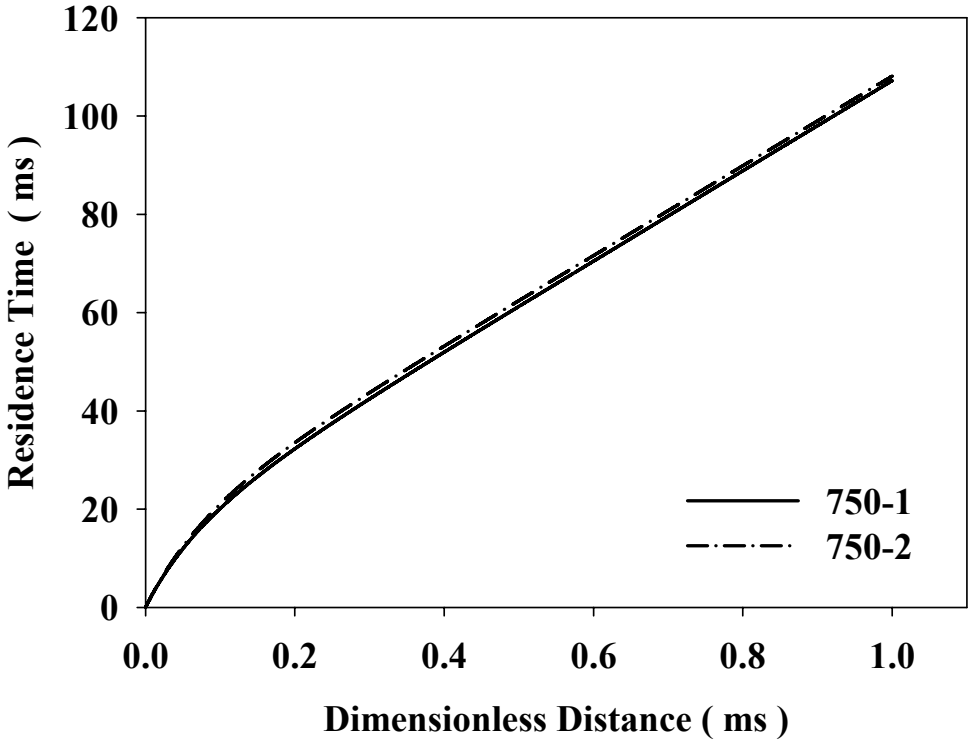

Figure 5.22 Cumulative residence time for experiments 750-1 and 750-2

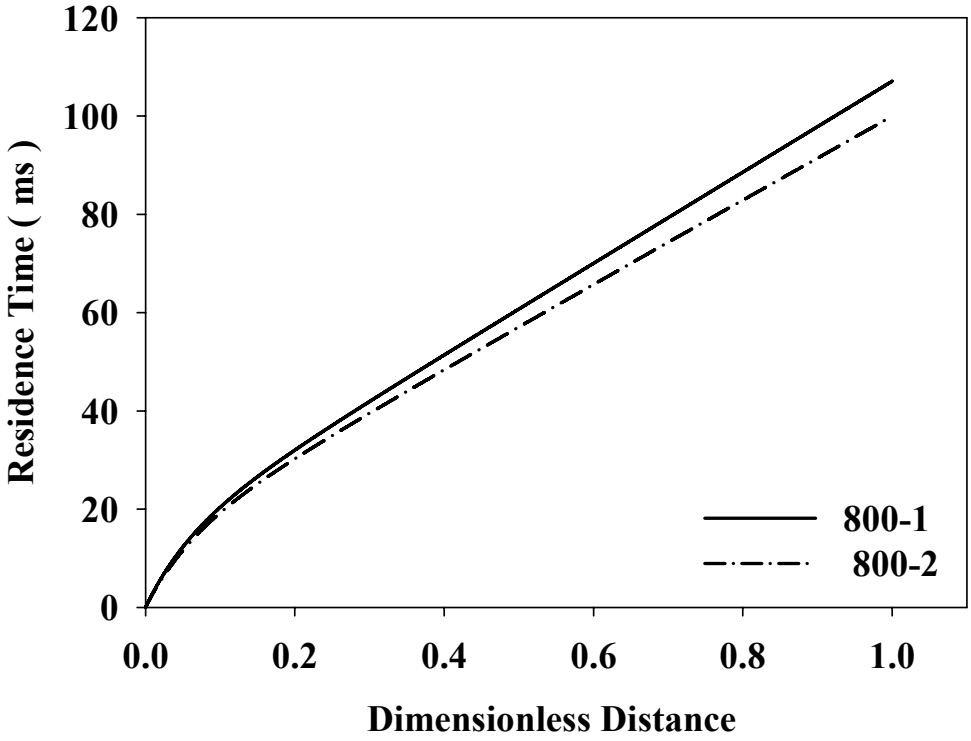

Figure 5.23 Cumulative residence time for experiments 800-1 and 800-2

Figure 5.24 to Figure 5.26 show the Reynolds number of the fluid flow along the reaction tube. In all the experiments, the Reynolds numbers are always below 280 which indicates a laminar flow regime. This is a desirable flow regime because of high tendency of the aerosol particles of the feed to coalesce, to form larger particles, and eventually to deposit on the wall of the tube. The higher Reynolds number in Experiment 700-1 compared with Experiment 700-2 is due to the higher fluid velocity for Experiment 700-1. The experiments 750-1 and 750-2 are replicates and consequently as it is expected the Reynolds numbers are similar for both cases along the reactor. Figure 5.26 shows similar Reynolds number profile along the reactor for both Experiments 800-1 and 800-2. This can be explained by the fact that, in Experiment 800-1 the density of the fluid is higher as the consequence of higher operating pressure. The higher density causes lower velocity. The fluid temperature profiles are the same for both case hence the

viscosity of the fluid should be similar. Therefore, the velocity and density can balance each other and give the same Reynolds number.

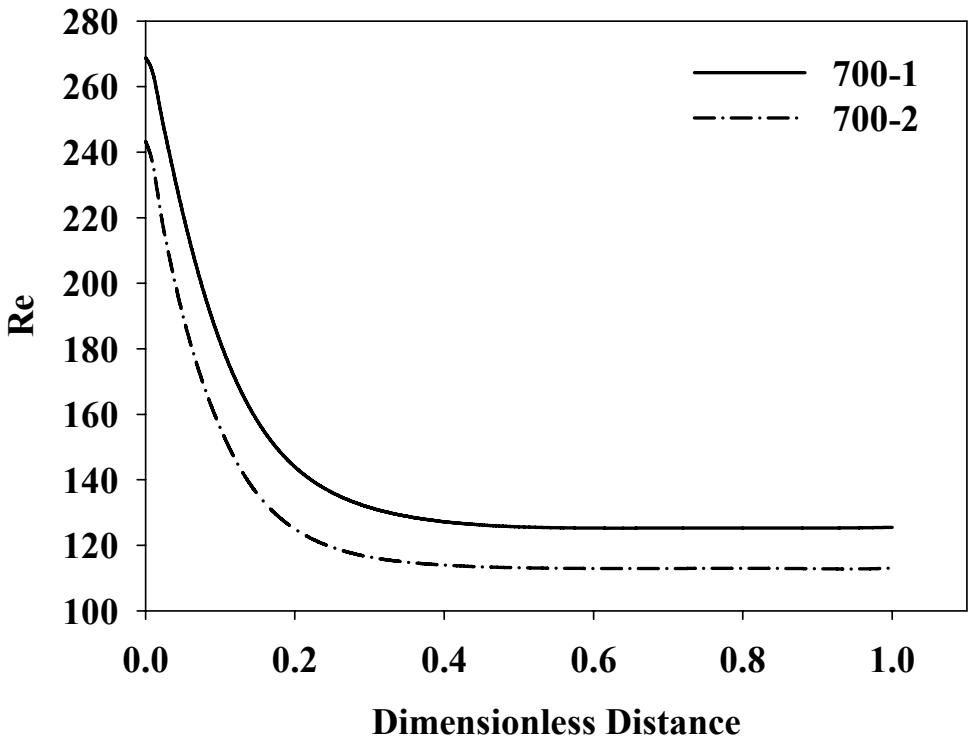

Figure 5.24 Reynolds Number along the reactor for experiments 700-1 and 700-2

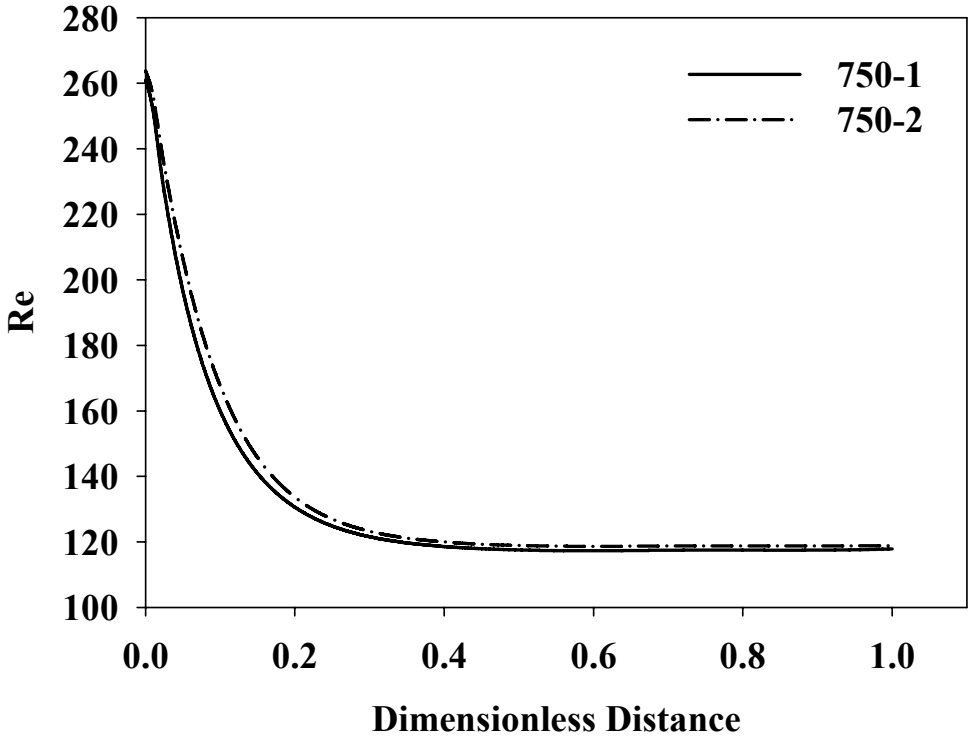

Figure 5.25 Reynolds number along the reactor for the experiments 750-1 and 750-2

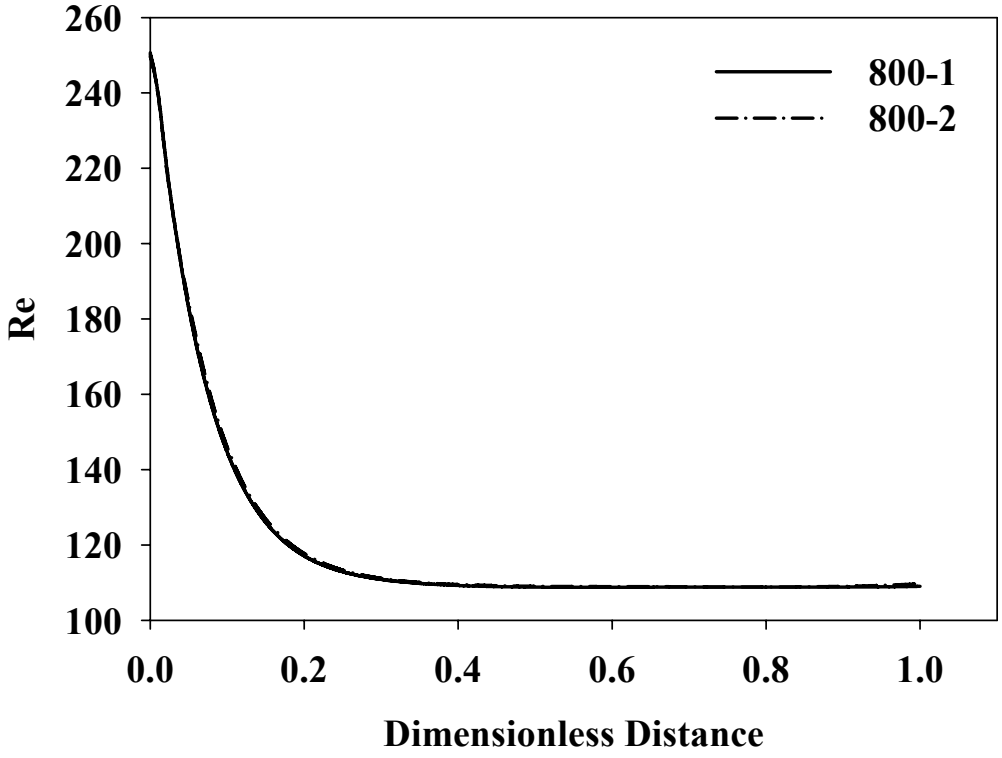

Figure 5.26 Reynolds number for the experiments 800-1 and 800-2

5.3 Experimental results of thermal cracking of Athabasca vacuum residue

Products of the thermal cracking were gas, liquids and coke. The portion of the gas which captured by the cryogenic condenser in the operation time is referred to as the liquefied gases. The gas components, which could escape the cryogenic condenser and exited the system, were called vent gases. Vent gases consisted only of helium and methane. The liquefied gases consisted of components up to C_8 (approx. BP 120°C) including a portion of toluene, which was the feed solvent. The liquid products consisting of the unconverted vacuum residue (BP above 524 °C) and liquid products (BP above 177°C) which separated from the solvents in a rotary evaporator and did not evaporate with the solvents. As explained in section 5.1.7 , lighter liquids which could evaporate with solvents, with boiling point less than 177°C, were not detected unless collected with the liquefied gas products .

5.3.1 Definition of conversion, yields and selectivity

Vacuum residue is defined as the fraction with boiling point above 524°C. The feed consisted of a significant portion with boiling point below this temperature (13.3 wt %). Both of these fractions could undergo thermal cracking in the reactor. Equation (5.3) is defined to follow the conversion of 524°C + fraction, that is the conversion of vacuum residue.

$$\text{Conversion} = \frac{\text{mass of VR fraction in feed} - \text{mass of VR in products}}{\text{mass of VR fraction in feed}} \qquad (5.3)$$

The products were generated by thermal cracking of both vacuum residue and the lighter fraction, therefore the yields of products are defined based on the weight of the feed:

$$\text{Yield} = \frac{\text{mass of product - mass of product in feed}}{\text{mass of feed}} \qquad (5.4)$$

Alternatively, the selectivity can be defined as the following:

$$\text{Selectivity} = \frac{\text{mass of the component of product}}{\text{mass of converted feed}} \qquad (5.5)$$

The following relationship holds between the sum of the yields of the products and conversion of vacuum residue:

$$\text{Conversion} = \frac{Y_G + Y_L + Y_C}{C_{VR0}} \qquad (5.6)$$

In which Y_G, Y_L, and Y_C are yields of gas, liquids (boiling point below 524ºC), and coke respectively. C_{VR0} is the initial fraction of vacuum residue in the feed, which is equal to 0.867. The importance of the equation (5.6) is that it shows the conversion of vacuum residue is dependent on the sum of the yield values and this should be considered in the definition of the objective function in the non-linear regression analysis of the data.

5.3.2 Simulation Distillation Analysis

Simulated distillation analysis is used to measure the fraction of vacuum residue in the feed and in the liquid products. In this method a range of n-paraffins are used to mark the boiling point versus retention time of the components, which elude through the GC column. Heavy oils and their products are not all paraffinic and consist of a significant aromatic fraction, the aromatic structure can be the dominant structure at higher boiling point range. In addition, due to rather high temperature and retention time of the heavy products in the column, the components may undergo further cracking reactions inside the GC column. According to ASTM a bias cannot be determined or calculated for the result of simulated distillation analysis. The boiling point distribution is defined based on a test method. In addition, a rigorous, theoretical definition of the boiling point range distribution of petroleum fractions is not possible due to the complexity of the mixture as well as the unquantifiable interactions among the components. Use of physical processes such as conventional distillation processes to define a boiling point distribution results in a method-dependent definition. This does not constitute a true value from which bias can be calculated [68 to 72]. However, simulated distillation analysis can be precise (repeatable) and reproducible and it has been used for. kinetic study of heavy oils according to the literature (Chapter 2). Table 5.19 shows that the fraction of vacuum residue in the collected liquid products decreases monotonically with increases in conversion, as expected by definition. High yields of middle distillate fractions were measured at higher conversions. The calculated conversions in Experiments 750-1 and 750-2, which were replicate experiments, are very close.

Table 5.19 Boiling point range of feed and liquid products and conversion

	VR	700-1	700-2	750-1	750-2	800-1	800-2
Naphtha < 177°C (%)	0.1	0.3	0.1	0.1	0.1	0.1	0.1
Middle Distillate 177 – 343 °C (%)	0.6	14.8	15.2	22.0	25.7	25.6	37.8
Gas oil 343-524°C (%)	12.7	31.8	27.2	33.8	37.6	58.3	28.4
Residue 524 °C + (%)	86.7	53.0	57.5	44.3	33.3	16.1	33.8
Conversion %	0	46.59	50.29	65.65	66.62	89.13	78.27

5.3.3 Mass balance

Table 5.20 shows that the overall mass balance is in a desirable range of 100 ± 5%. The mass balance of toluene is satisfactory in most cases. The first row of the table compares the feed on a solvent-free basis to the total mass of products (coke from the reactor and the condenser, liquid products (excluding toluene) and gases). The second row indicates the mass balance on toluene alone. Table 5.20 also shows the percentage of the initial toluene solvent that was found in the collected liquefied gas products as it was measured directly by GC. The gas chromatograph was equipped with FID, which cannot detect hydrogen and hydrogen sulfide. However, the mass of these products should not be high enough to affect the mass balance. Table 5.20 shows that the mass balance is satisfactory even without considering the mass of these two products.

Table 5.20 Mass balance

Experiment	700-1	700-2	750-1	750-2	800-1	800-2
Mass Recovery excluding solvent (%)	104.0	95.4	95.1	99.6	101.8	96.7
Mass Recovery of toluene (%)	97.0	ND	94.8	101.8	75.2	ND
Percentage of toluene evaporated with liquefied gases (%)	3.2	4.8	3.3	1.8	11.7	4.4

Two errors in material balance can arise from the use of toluene solvent in the reactor experiments. First, retention of toluene in liquid products could cause an overestimate of product yield. Adding to this possible error would be any reaction products formed from the toluene, such as benzene and ethylbenzene. The second, offsetting error would result from the loss of light liquid products when the toluene is evaporated. These two errors could balance each other. The liquid products of thermal cracking were separated from the solvents first by rotary evaporator under vacuum. In the collected solvents, only presence of benzene and ethylbenzene were verified by direct GC analysis. These components were the products of thermal cracking of toluene in the presence of vacuum residue at the time of reaction (The detailed discussion based on the quantitative results is given Chapter 7). . The absence of the peaks of light liquid products of thermal cracking in the gas chromatogram of the separated solvents could be due to high dilution of this species in dichloromethane. The initial concentration of the feed in toluene was only 5 wt%, which was a dilute solution. After conversion, the concentration of products in toluene would be even less. This dilute solution, at the end of reaction was collected by washing the cryogenic condenser and the related tubing and hoses with 1.5 to 1.7 liter of dichloromethane. At such volume of solution, if

vacuum residue had not converted at all, its concentration would have been about 0.02 to 0.04 wt%. Therefore, the concentration of the very light liquid products, which could evaporate with dichloromethane in the rotary evaporator, should be extremely dilute (a small fraction of the maximum 0.04 wt %).

The GC was calibrated for quantitative analysis for concentrations as low as 0.1 wt% with acceptable repeatability and accuracy. The peak of a component with a concentration of 0.005 wt% could still be recognized without much interference with the noise of the background line. Therefore, it was attempted to collect samples, which were rich in toluene and contained minimum dichloromethane. This sampling was possible by switching to a different receiver when evaporation of dichloromethane was ended and it was required to increase the temperature of the bath. Injection of the separated toluene did not indicate any light liquid products in the sample. From these experiments, I conclude that if such liquid components could escape with the evaporated toluene, then their concentrations in the collected toluene should be less than 0.005 wt%. Thus, the effect of such evaporation of lighter liquid products could not cause a significant error in the mass balance.

5.3.4 Deposition of coke within the reactor

Figure 5.27 shows the percentage of the feed which was collected as coke deposits from the wall of the reaction tube at the end of each experiment. It is clear that application of the make-up gas was quite successful in limiting the amount of the coke deposits to below 1 wt% percentage of the feed. This figure also demonstrates that at the highest furnace temperature, which applied, that is at 800°C when the rate of conversion was the fastest, the coke deposits were minimized. In all cases with make-up gas, the coke deposition occurred at the upstream of the reactor close to the tip of the DIHEN nebulizer and the rest of the reaction tube was found clean from any coke deposits. It should be noted here that the in situ atomization of the feed, that is atomization inside the flowing reactor, was a successful solution to the problem of the atomization of the feed. Even

without make-up gas, a considerable portion of feed could pass the reaction tube. In this chapter, all kinetic data are for operation with make-up gas, which minimized the coke deposition to less than 1 wt% of feed.

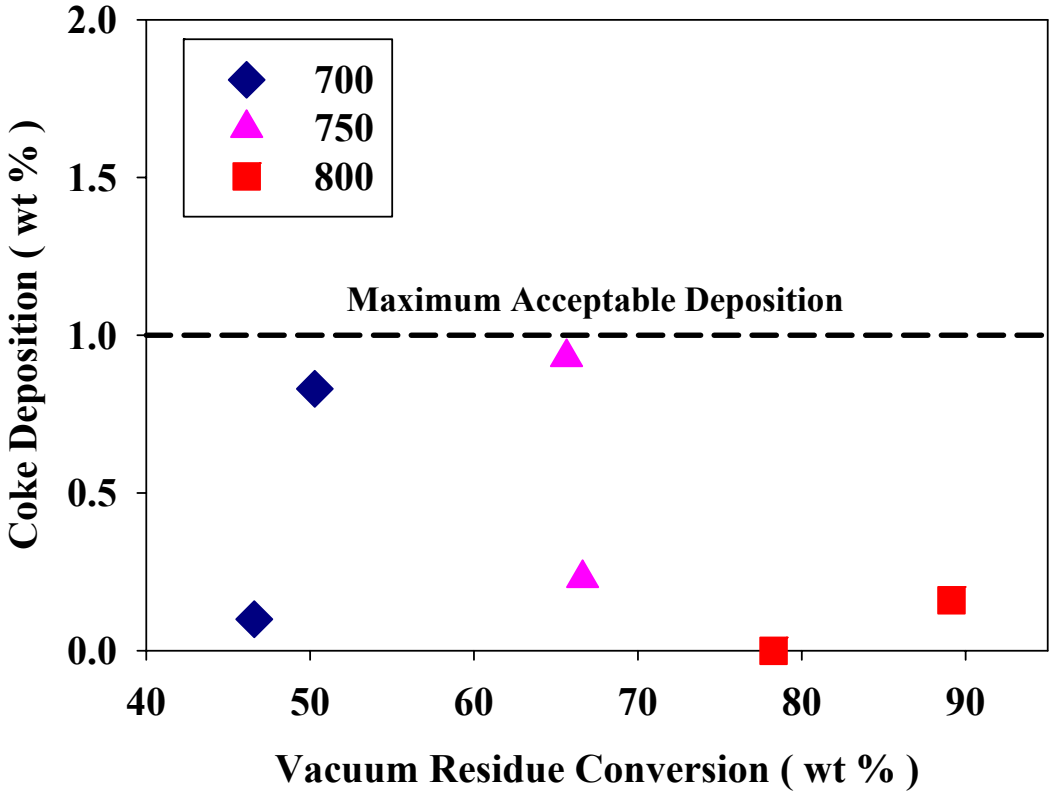

Figure 5.27 Percentage of feed that deposits in the reaction tube versus the vacuum residue conversion. The coke deposit in all the experiments are less than 1 wt % of the feed. This result indicates that more than 95 wt % of the feed passes the reaction tube considering that the TGA residue of the feed is below 20 wt%.

5.3.5 Yield of coke as aerosol

Figure 5.28 shows the yield of coke aerosol particles, which were separated from the condensed liquid products, versus conversion of the vacuum residue. The mean value of the yield of coke is 6.3 wt % and standard deviation is 1.9 wt %. The data on the yield of coke do not show a statistically significant trend or a significant variation with conversion of vacuum residue (or temperature). The residence time of the reaction does not vary from experiment to experiment

significantly higher conversions are achieved in fact by applying higher reaction temperature.

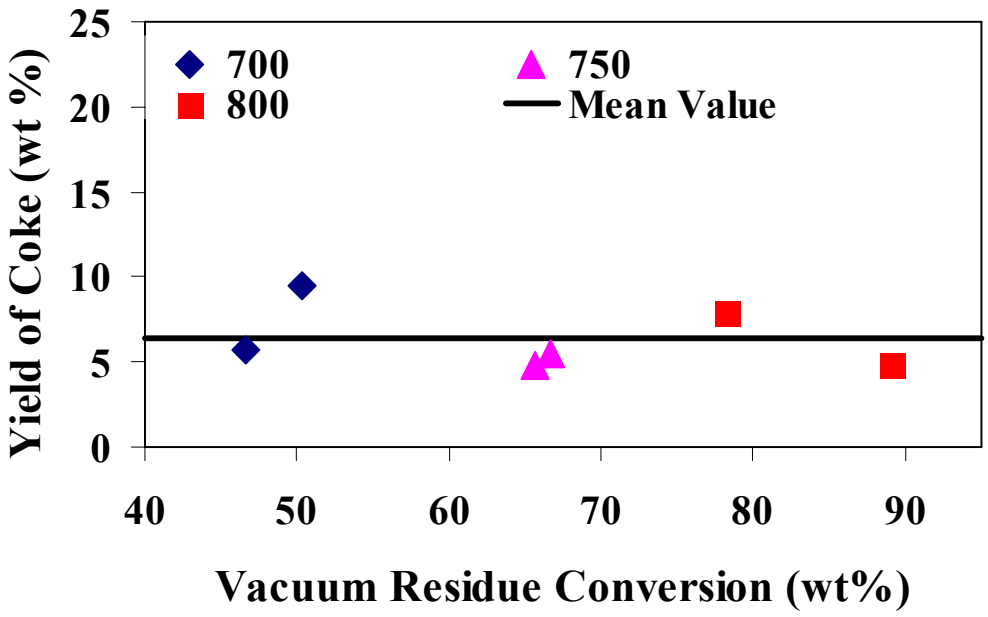

Figure 5.28 Yield of coke versus conversion of vacuum residue. Mean value for the yield of coke is 6.3 wt %.

Figure 5.29 and Figure 5.30 show the SEM micrographs of coke which was separated from the liquid products for experiment 750-1.The micrographs for other experiments look quite similar but are not shown here. The coke particles are perfect spheres. Agglomerates of spheres were not detected. The in situ atomization of feed does not allow the use of any measuring device to verify the size of the feed particles by direct measurement, because the flash vaporization of solvent out of the feed droplets and the immediate start of coking reactions have contributions to the success of this method. However, the average initial size of the feed particles can be approximated indirectly by use of the mean value for the yield of coking and the fact that the value of the yield of coke is not sensitive to temperature. If a feed particle is assumed to shrink as it converts to the coke particle, and the average yield of coke, 6.3 wt%, is applied for all the experiments,

then the effective size of feed particle can be estimated as it is given by Table 5.21.

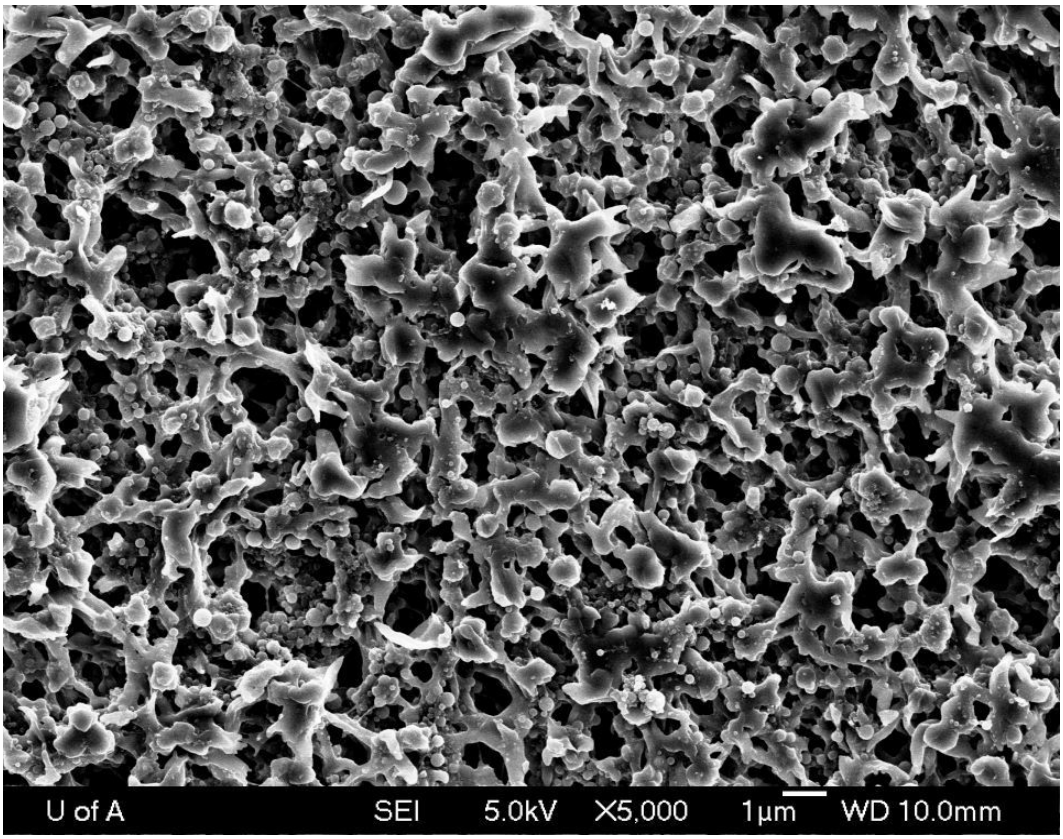

Figure 5.29 Experiment 750-1Coke products 750 average 150 nm

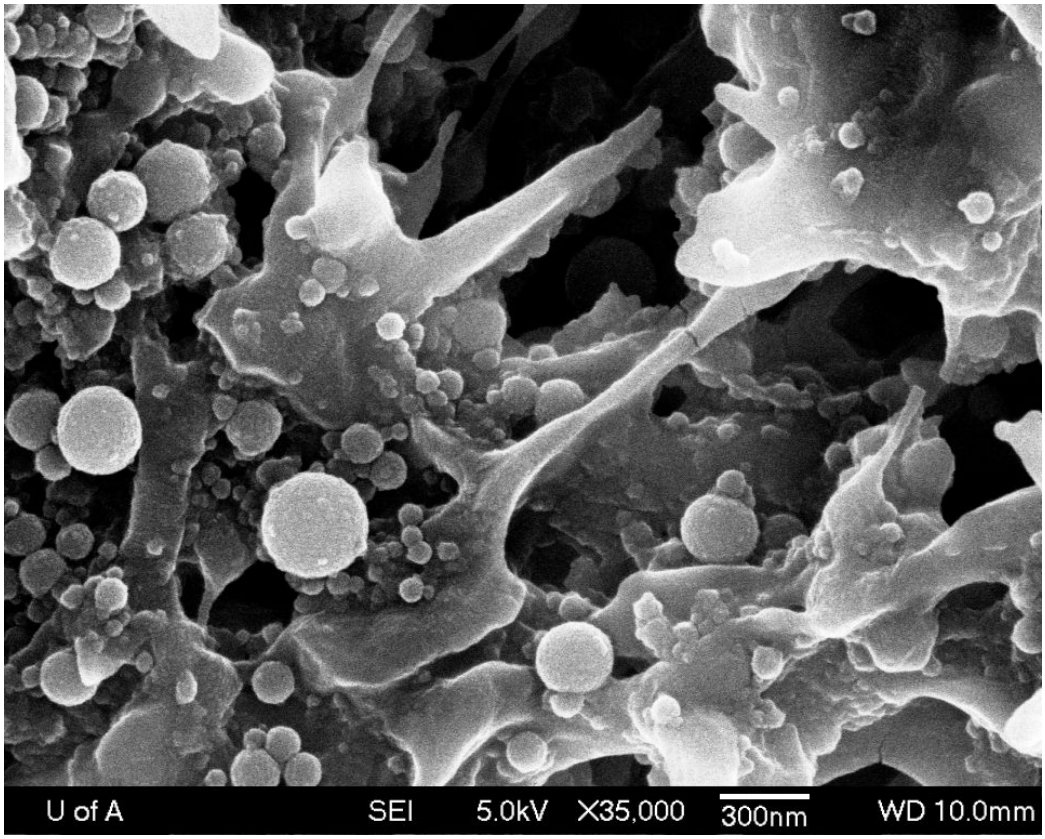

Figure 5.30 Experiment 750-1 Coke from products at 750°C Average particle diameter 100 nm

Table 5.21 Effective Size of the feed particle calculated based on average coke yield of 6.3 wt%

SEM Micrograph	Magnification	Number of Counted Spheres	d_{ave} Coke (nm)	d_{ave} feed (nm)
700-1	5000	81	170	475
750-1	5000	89	150	420
750-1	7500	65	130	370
750-1	35000	280	100	280
800-1	5000	175	190	550

5.3.6 Yield of gas products

Figure 5.31 shows the yield of gas products versus conversion of the vacuum residue. Gas products are the collected products, which are in gas phase at room temperature. The yield of gas increases linearly with conversion. The determination factor for goodness of fit, R^2, is 0.98. The error bar in Figure 5.31 indicates the standard deviation due to the uncertainty of the simulated distillation analysis for the vacuum residue conversion in experiment 800-2. This standard deviation is equal to 1.3 %. This value for experiment 750-1 is 0.6 %. These values calculated based on the repeated measurement of the vacuum residue fraction by simulated distillation analysis and by calculating the propagation of error using the following formula [73]:

$$V_w = \left(\frac{\partial w}{\partial x}\right)^2 V_x + \left(\frac{\partial w}{\partial x}\right)^2 V_x + \left(\frac{\partial w}{\partial x}\right)^2 V_x \qquad (5.7)$$

In which w is a value, and is calculated as a function of the independent variables of *x*, *y*, and *z*:

$$w = f(x, y, z) \qquad (5.8)$$

V is the variance of each variable.The contribution in the uncertainty of the yield values from measurements by gas chromatography of the gas samples is the smallest, compared with other source for uncertainties; in experiment 700-1 the standard deviation of the yield of gas is 0.05 % that is calculated based on four repeated measurements of total gas components and by equation (5.7).

5.3.7 Yield of Liquid Products

The data of Figure 5.32 demonstrate the yield of liquid products versus the conversion of the vacuum residue. The liquid products are all the material which were collected at the room temperature minus the coke and the unconverted vacuum residue. The coke was separated from the liquid products but the converted vacuum residue stayed with liquid products and the result of the simulated distillation analysis were used to calculate the yield of liquid products, that is the liquid products which had boiling point less than 524°C. Figure 5.32 shows an increasing trend for the yield of liquid products versus conversion of the vacuum residue. The fact that the yields of coke products are insensitive to conversion and that the yield of gas represents a linear relationship, suggests that such a linear relationship should be observable between the yield of liquid products and the conversion of the vacuum residue. The R^2 for the data in Figure 5.32 is only 0.41. Figure 5.33 shows the yield of all the collected liquids including the unconverted vacuum residue against conversion of the vacuum residue. The R^2 in this case is 0.83, which demonstrates a very significant improvement toward a linear relationship by including the vacuum residue fraction. If the yield of coke is added to the yield of liquids then R^2 increases to 0.91.

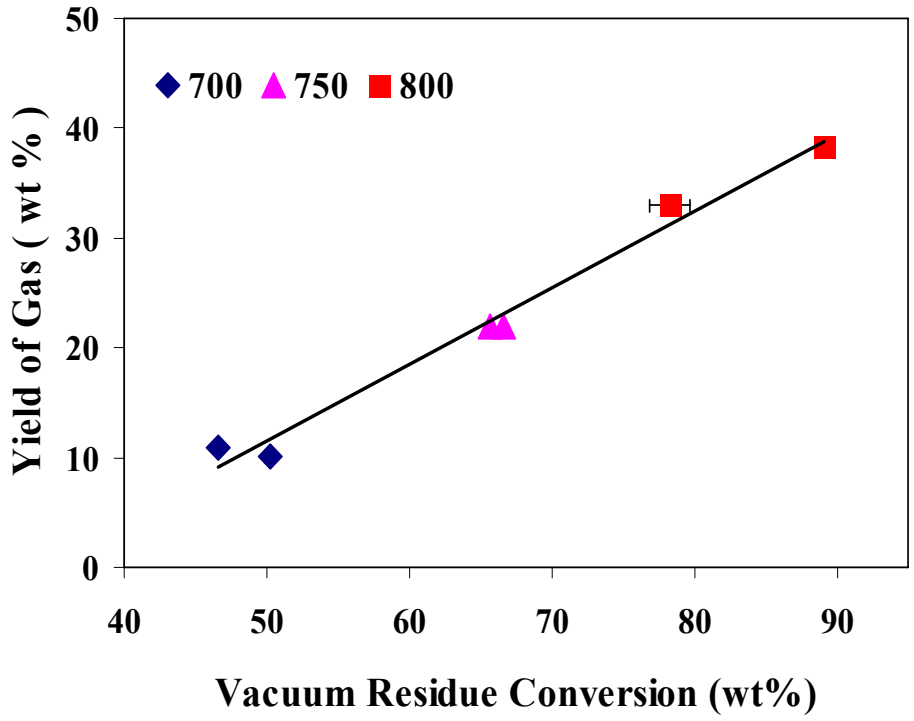

Figure 5.31 Yield of total gas products versus conversion of vacuum residue. The error bar indicates the standard deviation that the uncertainty of simulated distillation analysis imposes on the calculated conversion of the vacuum residue.

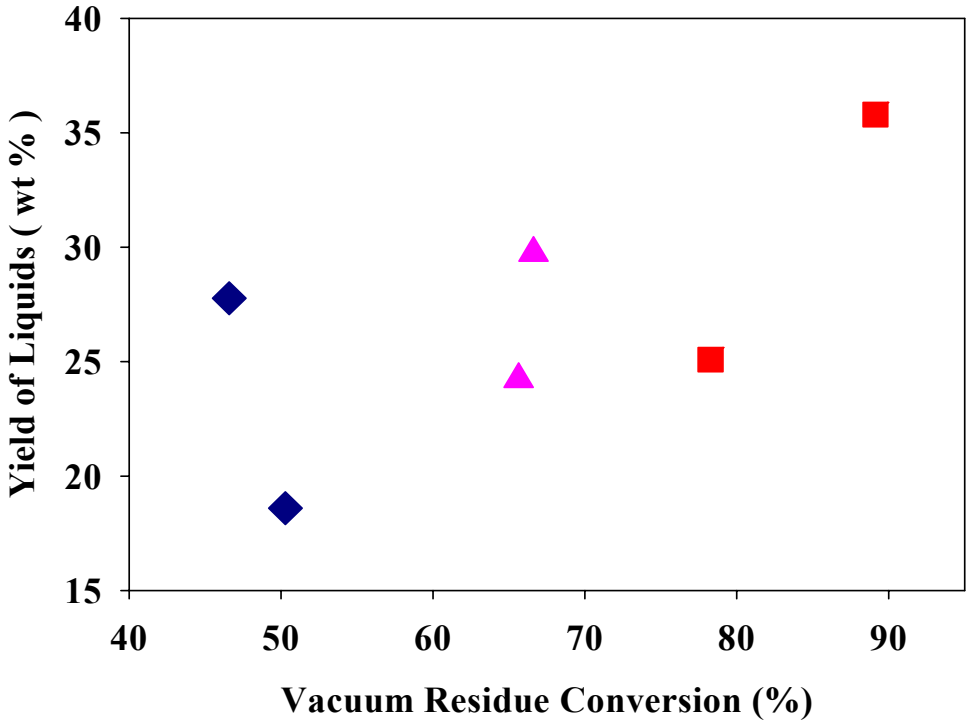

Figure 5.32 Yield of liquid products versus conversion of vacuum residue. The legends are defined the same as Figure 5.31.

Two factors can account for the data in Figure 5.32. First, the liquids are reaction intermediates, so that at higher conversion the formation of the liquid products is balanced by their conversion. Second, this fraction is subject to the most uncertainty due to evaporative losses, which are not significant for the vacuum residue, coke, or gas products.

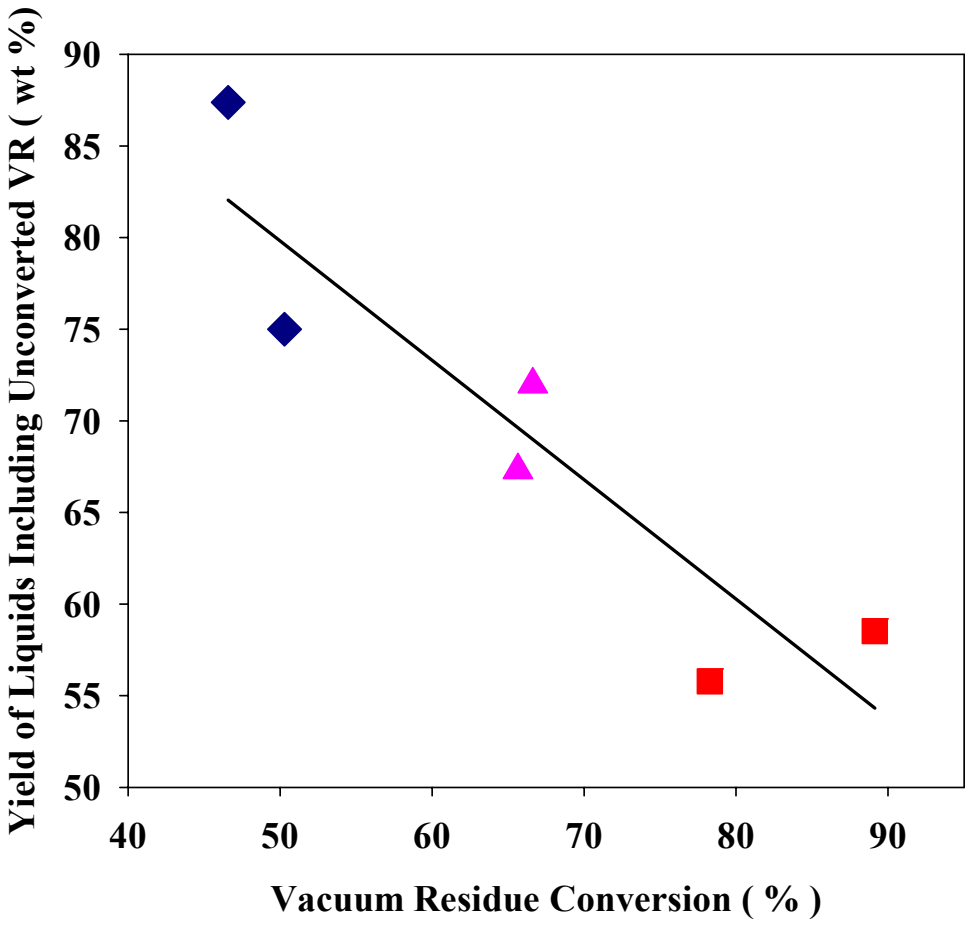

Figure 5.33 Yield of all the collected liquids including unconverted vacuum residue versus conversion of vacuum residue. The legends are defined the same as Figure 5.31.

Figure 5.34 to Figure 5.36 show the yield of major alkane products in the gas products. Yield of methane shows a close linear relationship with conversion of vacuum residue with R^2 of 0.92. Yield of ethane indicates a slow monotonic increase with conversion. Yield of propane was insensitive to an increase in conversion, based on statistical analysis of the slope of the data.

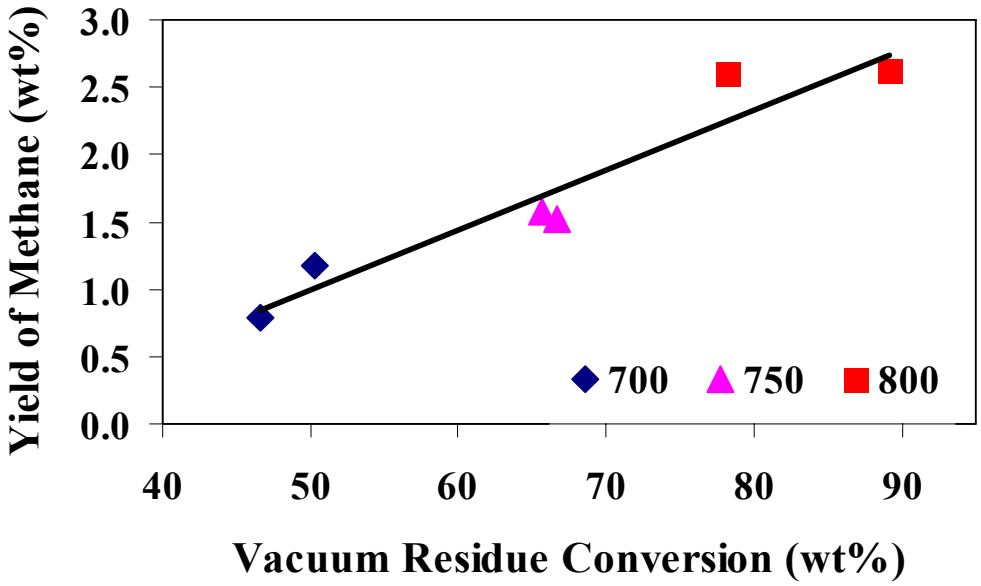

Figure 5.34 Yield of methane versus measured conversion

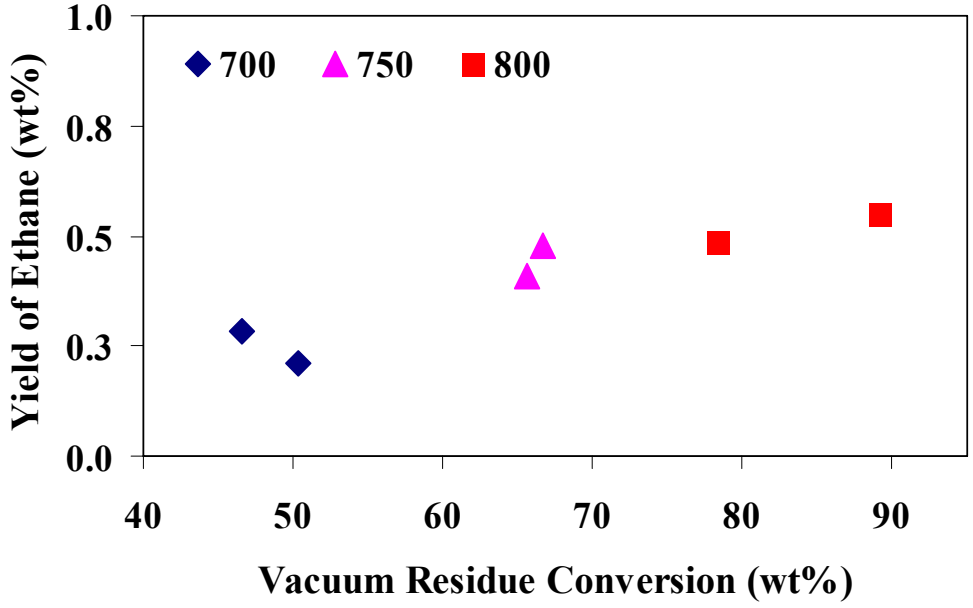

Figure 5.35 Yield of ethane versus measured conversion

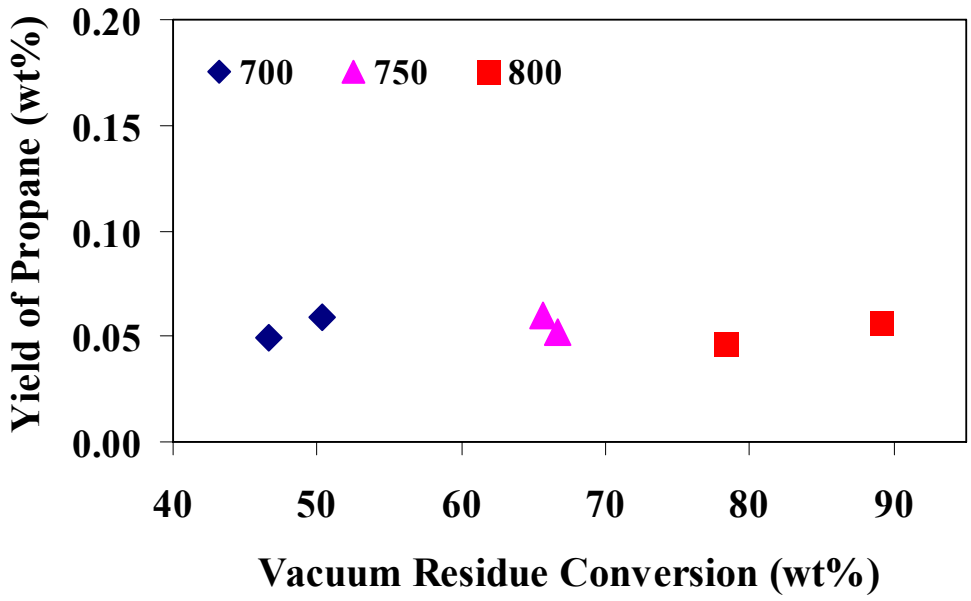

Figure 5.36 Yield of Propane versus measured conversion

The sensitivity of change of the yield with conversion systematically decreases from C_1 to C_3 in the alkanes. In contrast, the data of Figure 5.37 and Figure 5.38 show that yields of ethene and propene increase with conversion. The yield of propene increases linearly with conversion. The determination factor, R^2, for the goodness of fit is 0.97 in this case. Ethene is the major gas products and propene is in the second place. It can also be seen in Figure 5.34 to Figure 5.38 that the yield values for experiment 750-1 and 750-2, which are the replicate experiments, are very close. This result verifies the operation of the reactor for repeatability of the experiments. Figure 5.39 compares sum of C_2 and C_3 for alkenes and alkanes. It is clear that the alkenes are the dominant gas products. This figure also shows the increasing trend of total yield of C_2 and C_3 alkenes with conversion of vacuum residue while the total yield of C_2 and C_3 alkanes are fairly insensitive to the conversion and thus the temperature.

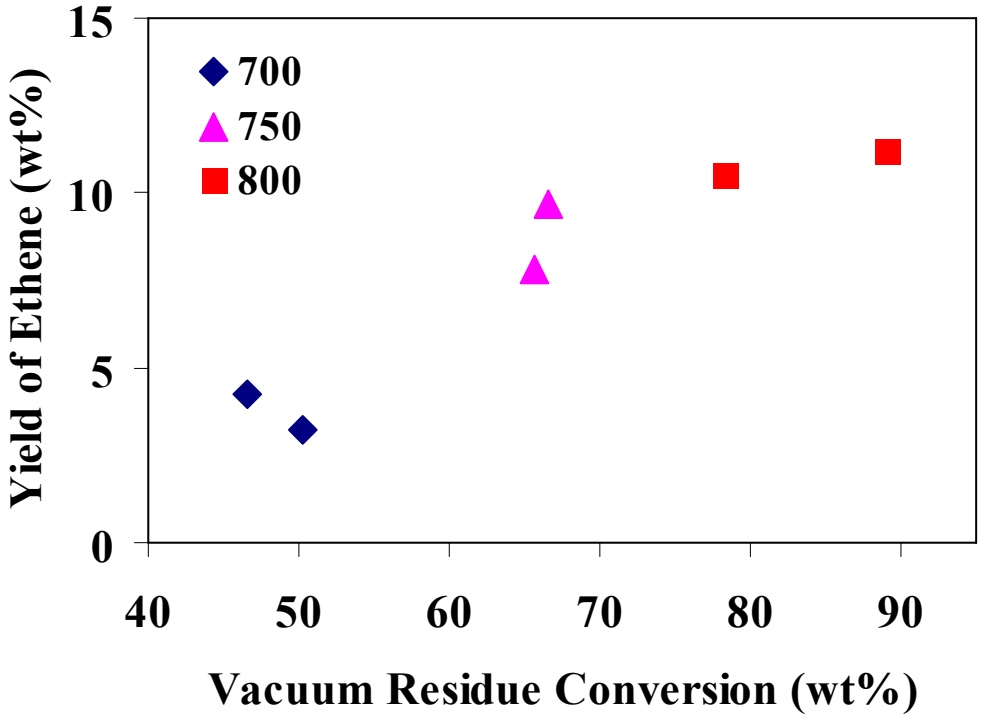

Figure 5.37 Yield of Ethene versus measured conversion

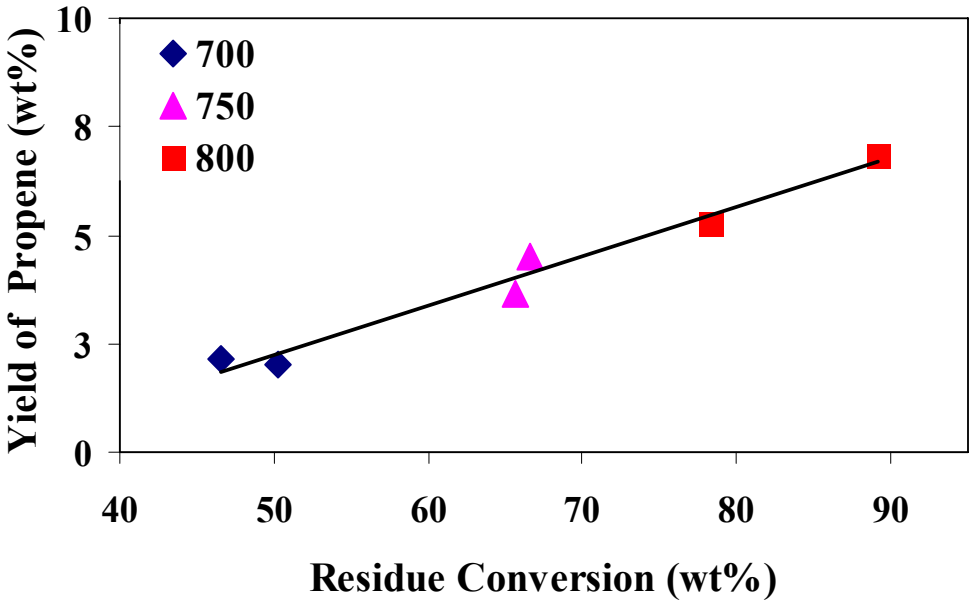

Figure 5.38 Yield of propene versus conversion of vacuum residue

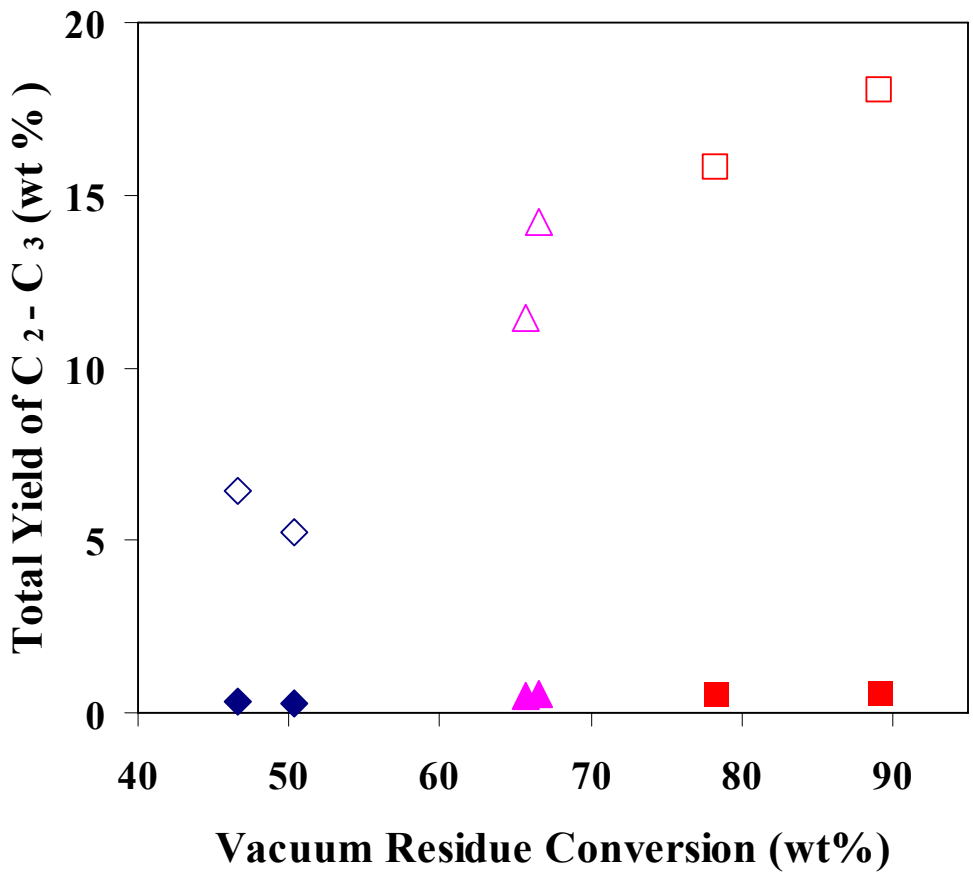

Figure 5.39 Total Yield of C_2 and C_3 alkanes and alkenes versus measured conversion of vacuum residue. The legends are defined the same as Figure 5.38, the solid legends refers to alkanes while the hollow ones refer to alkenes

5.3.8 Selectivity of gas products

Figure 5.40 shows that the selectivity of methane increases with conversion although the slope is not steep. Selectivity of ethane appears to pass through a maximum. The selectivity of propane decreases with conversion and thus with the reaction temperature. The conversion on the x- axis is proportional to the reaction temperature. Figure 5.41 demonstrates that selectivity of ethene rises first and then falls as conversion increases. The selectivity of propene increases

monotonically with increase of conversion and thus reaction temperature within the temperature range of the study.

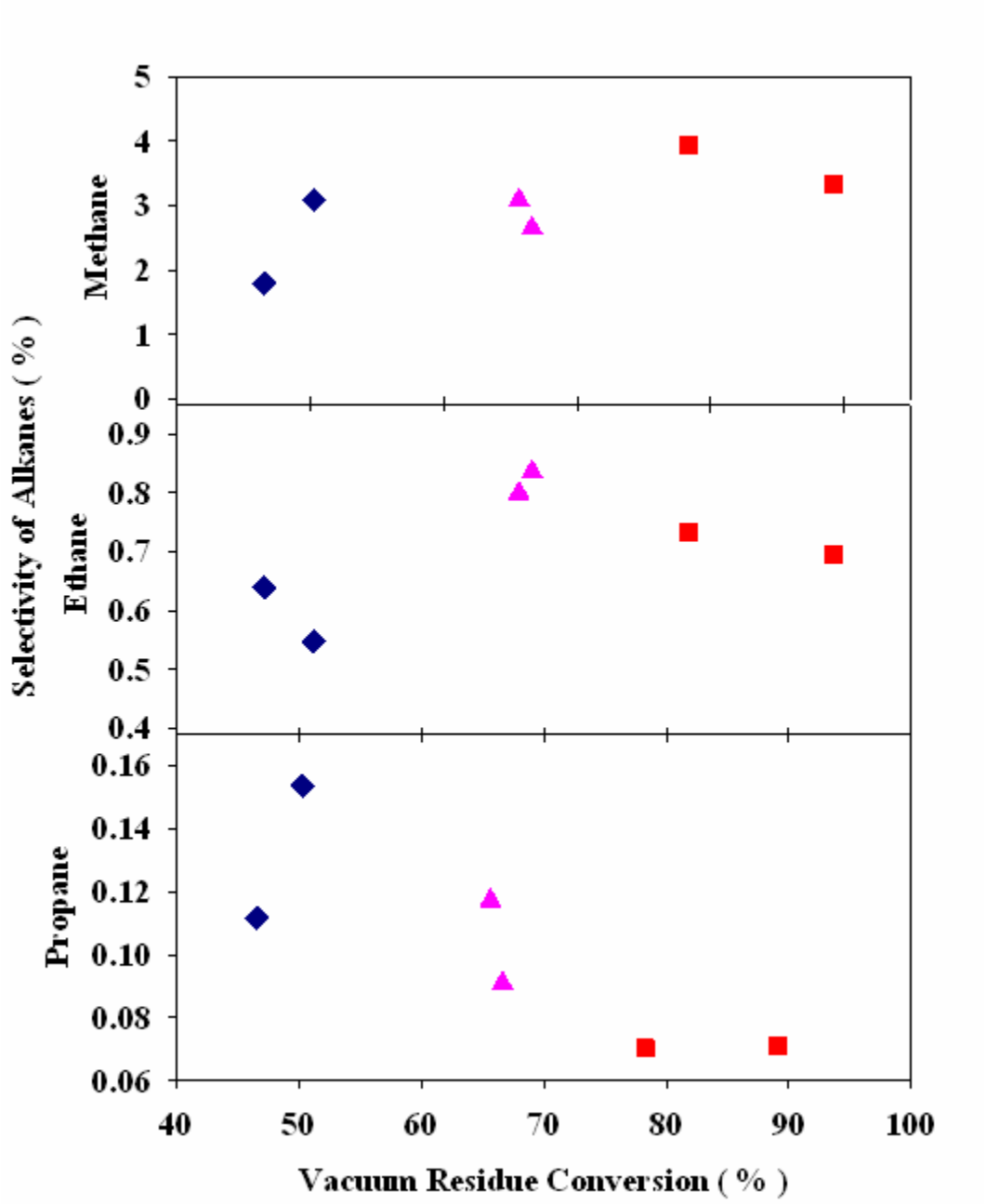

Figure 5.40 Selectivity versus conversion of vacuum residue on mass basis. The symbols have the same definitions as in Figure 5.38.

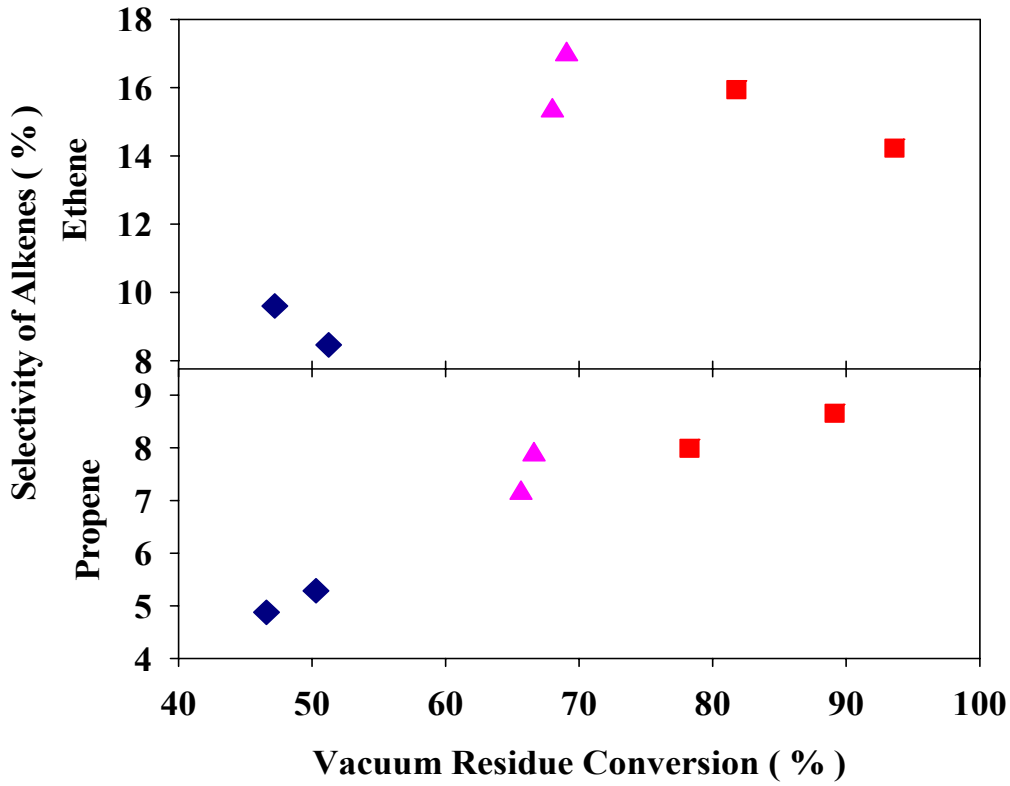

Figure 5.41 Selectivity of alkenes on mass basis. The symbols have the same definition as in Figure 5.38

5.3.9 TGA of the collected liquids

The amount of the collected liquids (including unconverted vacuum residue) was not sufficient for MCR analysis. In order to approximate the microcarbon residue of the heavy liquid products, thermal gravity analysis was used. The instrument which was used was not the same as defined in this ASTM, therefore, the results can be considered as an approximation of MCR and are not expected to be the same. Figure 5. 42 shows the loss of weight of the initial sample with time. The conversion of the samples are in the following order: 700-1< 700-2< 800-2. The differences in the weight loss of the product samples are mainly between 200 to 400°C, which is in range with boiling point temperature of light and heavy gas oil fractions. The pattern of the weight loss in this figure is consistent with the order of the conversion, in that product from 800-2 contains more volatile liquids compared with 700-2, and 700-2 contains more volatile components compared

with 700-1 which is the lowest in the level of conversion. In addition, all of the three samples are compared with the feed. Figure 5.44 shows the weigh loss for the same experiments plotted against the temperature.

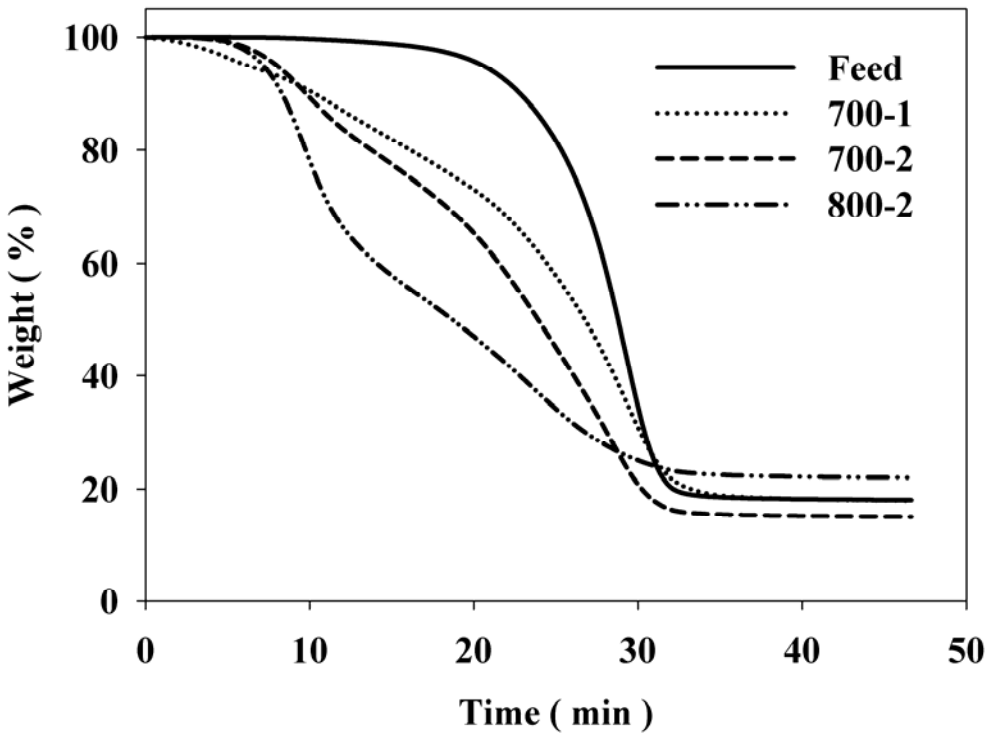

Figure 5. 42 TGA analysis of the heavy liquid products. Y axis shows the weight of the sample as the percentage of the initial weight.

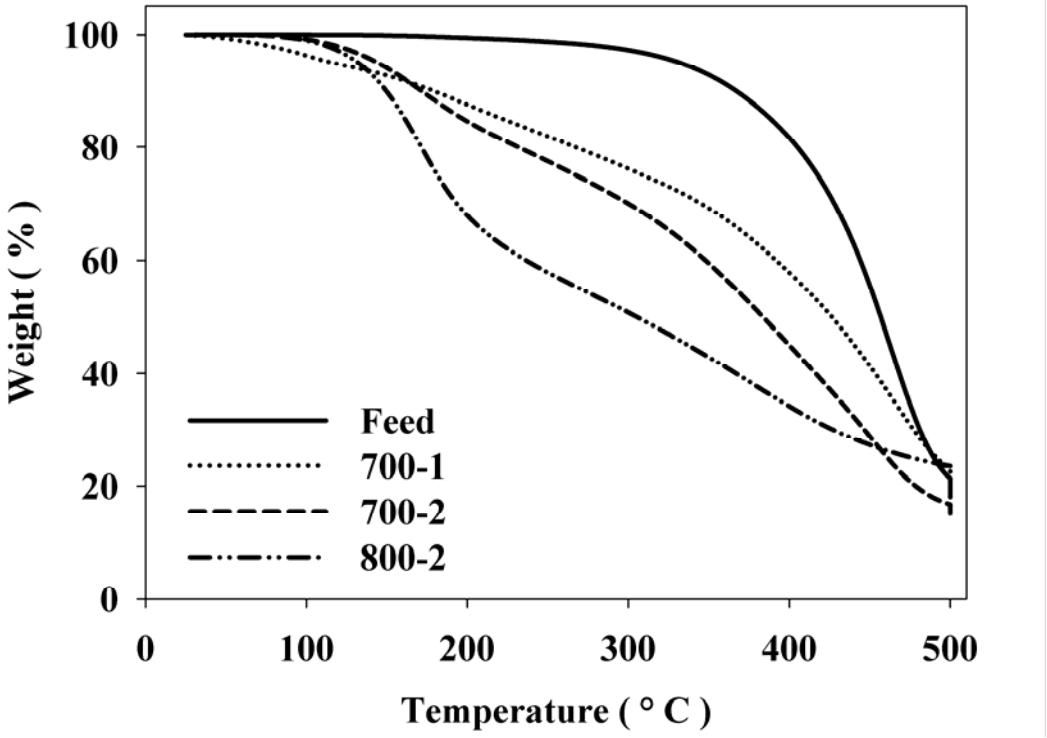

Figure 5. 43 TGA analysis of the heavy liquid products. Y axis shows the weight of the sample as the percentage of the initial weight.

Figure 5.44 shows the TGA residue of the heavy liquid products of experiment 700-1, 700-2 and 800-2 compared with TGA residue of the feed. It is noticeable that the highest measured TGA residue is at the highest conversion. That is 22 wt% for liquid products, including the unconverted vacuum residue, for experiment 800-2 in contrast with 18 wt % for the feed. Note that experiments 700-1 and 700-2 are not truly replicate experiments.

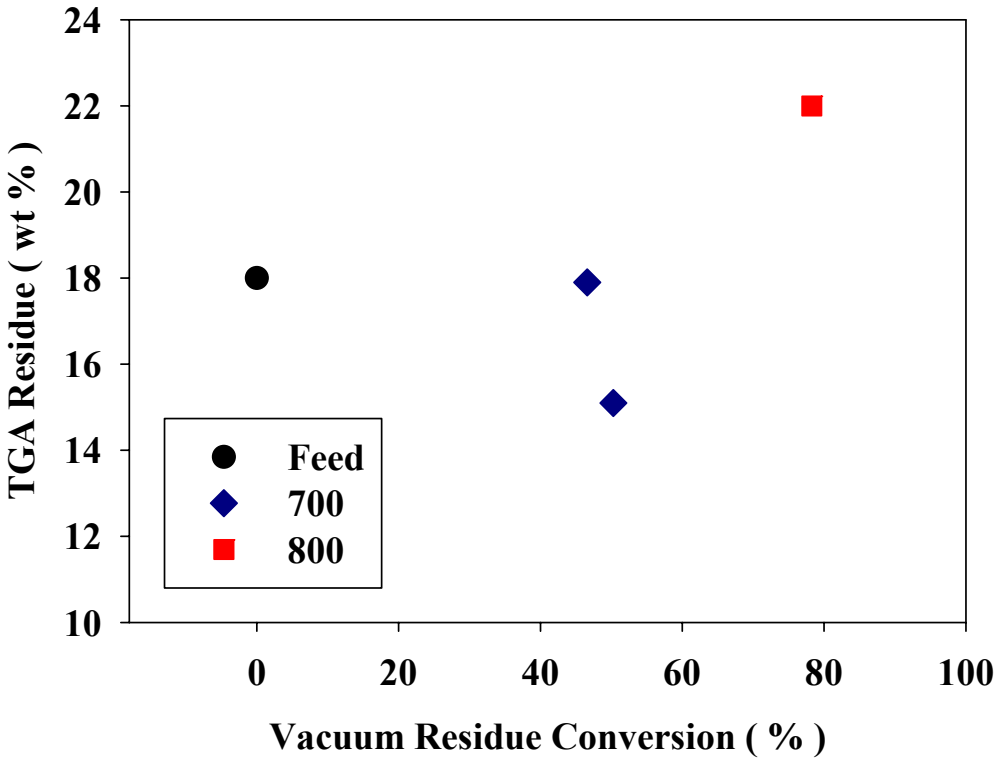

Figure 5.44 TGA residue

5.3.10 Elemental analysis of the liquids

The collected liquids, which include the unconverted vacuum residue, were tested for the amount of H, C, N, and S elements. The results of elemental analysis shows a lack of sensitivity in change of weight percent of C, N, and S with conversion of vacuum residue, while change in hydrogen content is significant (Figure 5.45 and Figure 5.46). The data of Figure 5.47 demonstrate that the molar ratio of H/C decreases with increase in conversion.

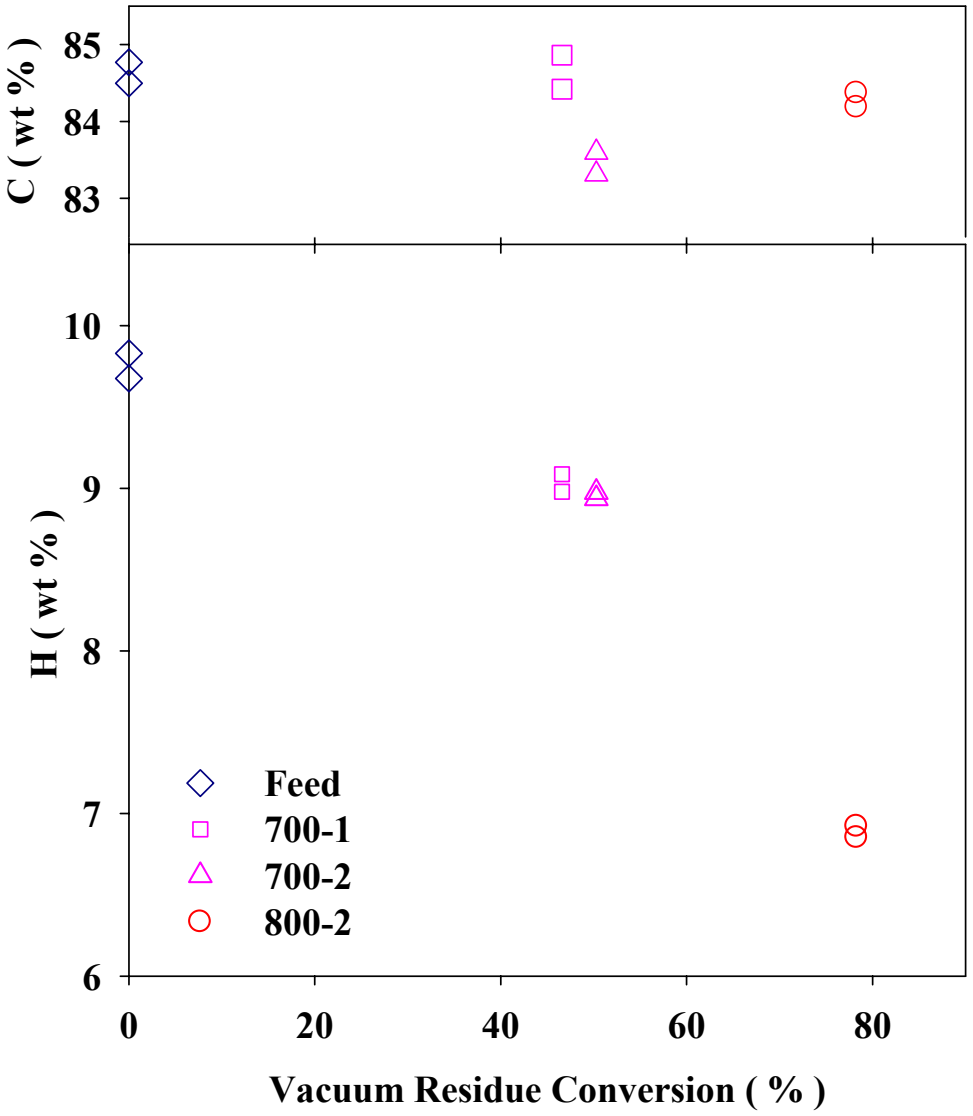

Figure 5.45 Results of the elemental analysis for H and C in liquid products including the unconverted VR. Each sample has been run twice

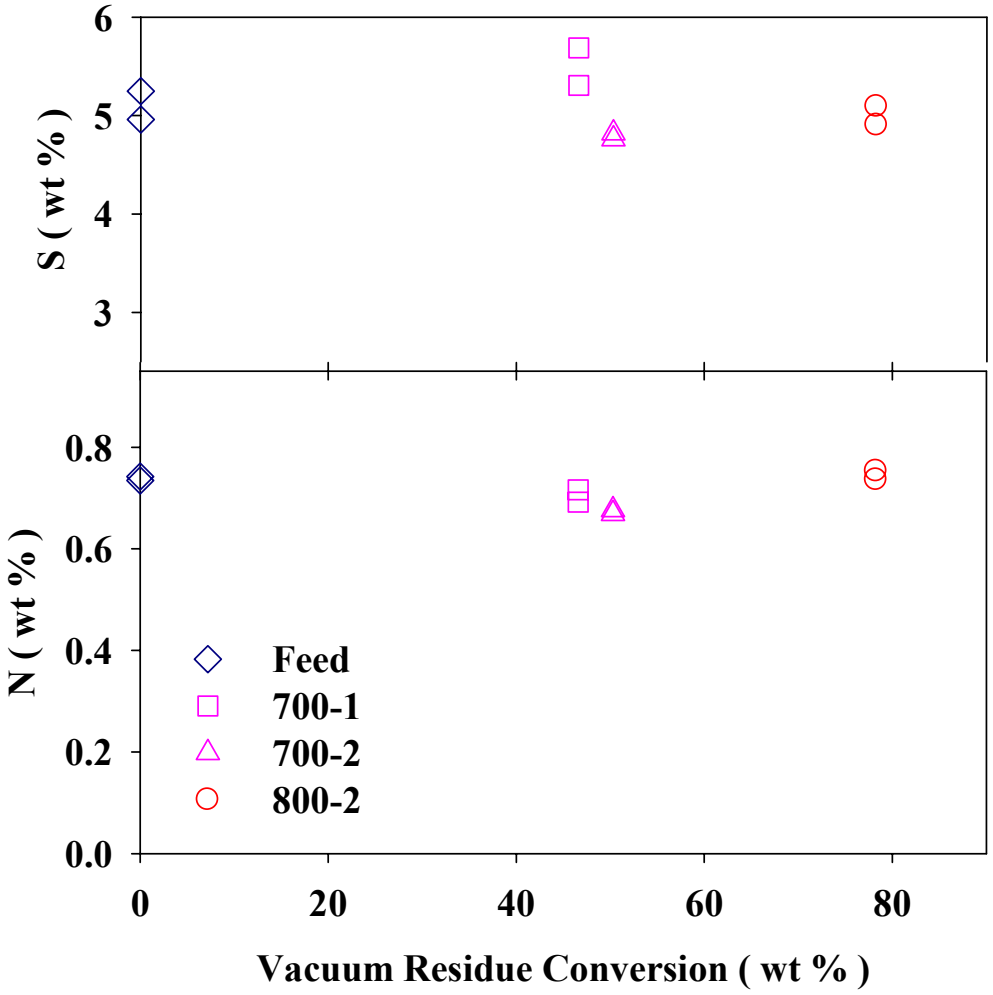

Figure 5.46 Result of elemental analysis of liquid products including unconverted VR. Each sample has been run twice

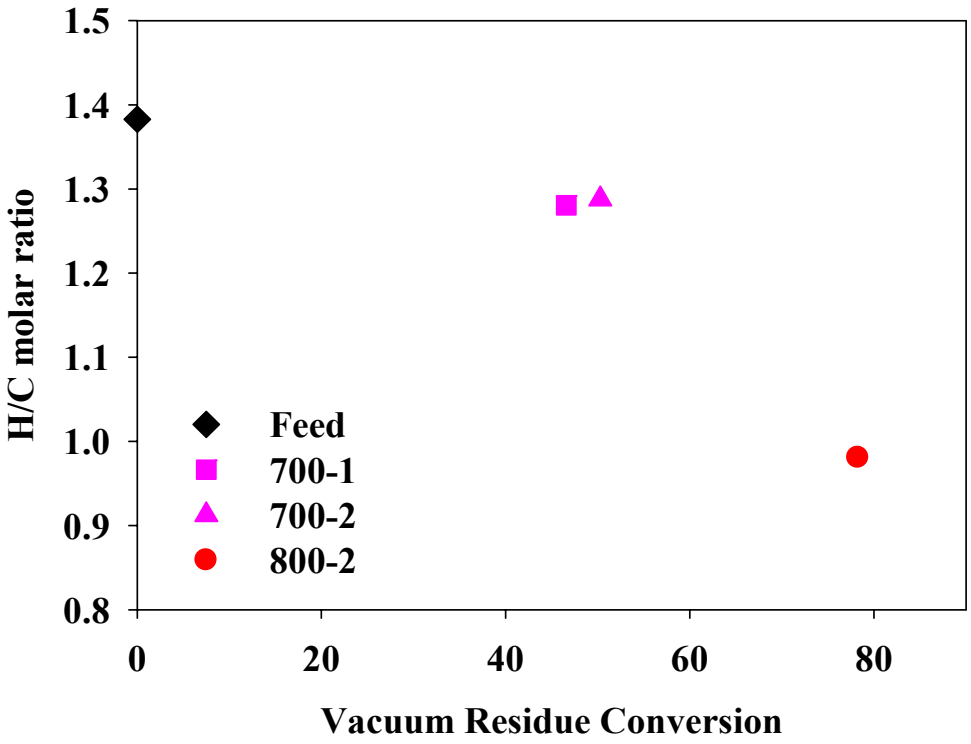

Figure 5.47 H/C ratio analysis of heavy liquid products

5.3.11 Nuclear Magnetic Resonance Spectroscopic Analysis

In order to measure the ratio of aromatic carbon to aliphatic carbon for the collected liquids ^{13}C NMR spectroscopy analysis is used. Attached proton test, ATP, used to measure ratio of CH to C quaternary for aromatic carbons and CH_2 and CH_3 for aliphatic carbons [74]. Figure 5.48 shows that the percentage of aromatic carbon increases monotonically with conversion. The results of simulated distillation analysis, which are given in Table 5.19 indicates that the residue content of the collected liquids decreases with conversion. The hydrogen content of the collected liquids also decreases monotonically with increase in conversion (Figure 5.45). The result of simulated distillation analysis (Table 5.19) suggests that the collected liquids have more volatile fractions compared with the feed. This is consistent with the results of TGA analysis (section 5.3.9). These trends reflect the idea that the collected liquid products can be fractions with

lower molecular weight than the residue fraction but are higher in aromatics. Figure 5.49 shows the significant contribution of CH carbon in increase of aromatic carbon with conversion. The plot of quaternary carbon versus conversion has a much smaller slope which may be due to aromatic ring structures not undergoing thermal cracking reactions. As the aliphatic attachments to the aromatic structure crack the naphthenic rings are dehydrogenated more of CH aromatic carbon appears. Figure 5.50 indicates that the fall of aliphatic carbon is mostly due to CH_2 carbon compared with CH_3. The removal of CH_2 carbon is easier than CH_3. The thermal cracking of pure toluene under the operating condition which applied to the experiment 700-1, 750-1 and 800-1 demonstrated that CH_3 bond with benzene ring cannot be broken easily under non-catalytic thermal cracking to produce methane (Chapter 7). In Figure 5.53, the mass ratio of the aromatic carbon of liquid products (including unconverted vacuum residue) to the aromatic carbon of the feed were plotted against the conversion. This plot suggests a slow increase in the aromatic carbon with conversion.

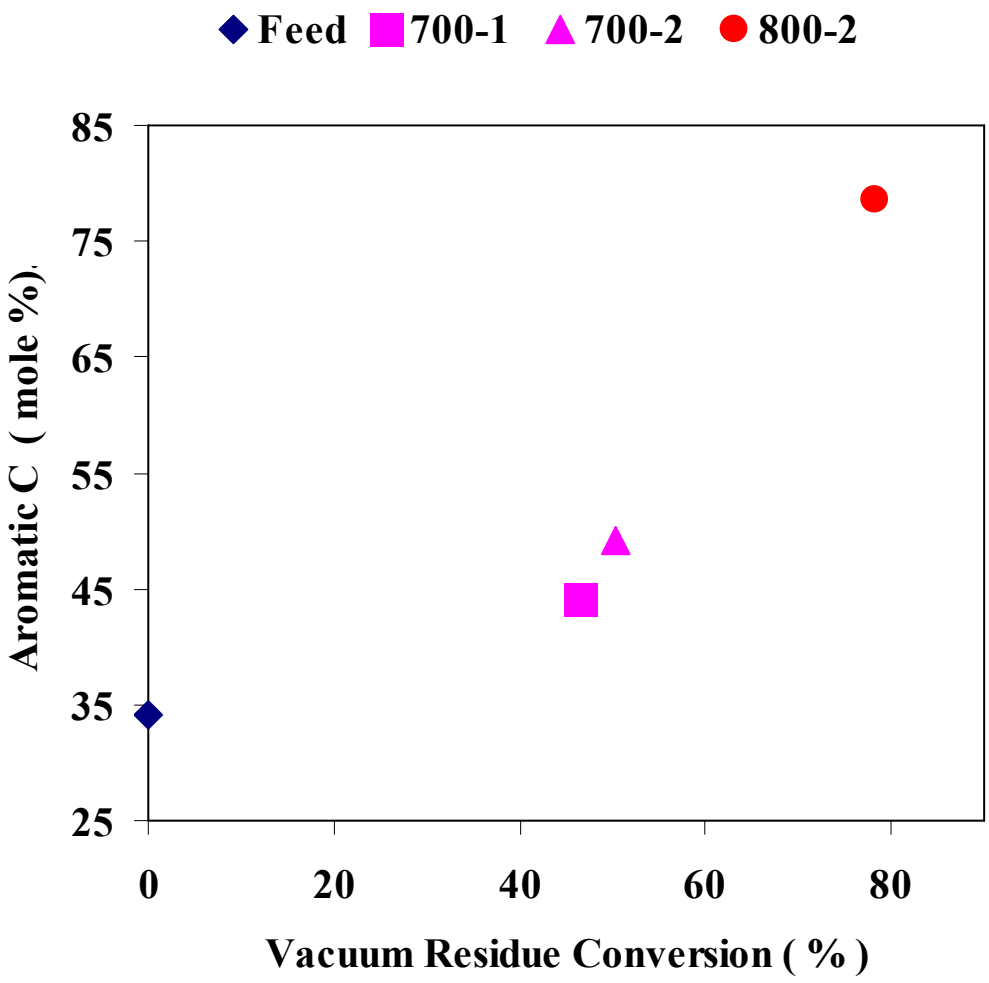

Figure 5.48 Total aromatic carbon from NMR ^{13}C analysis of liquid products including unconverted VR

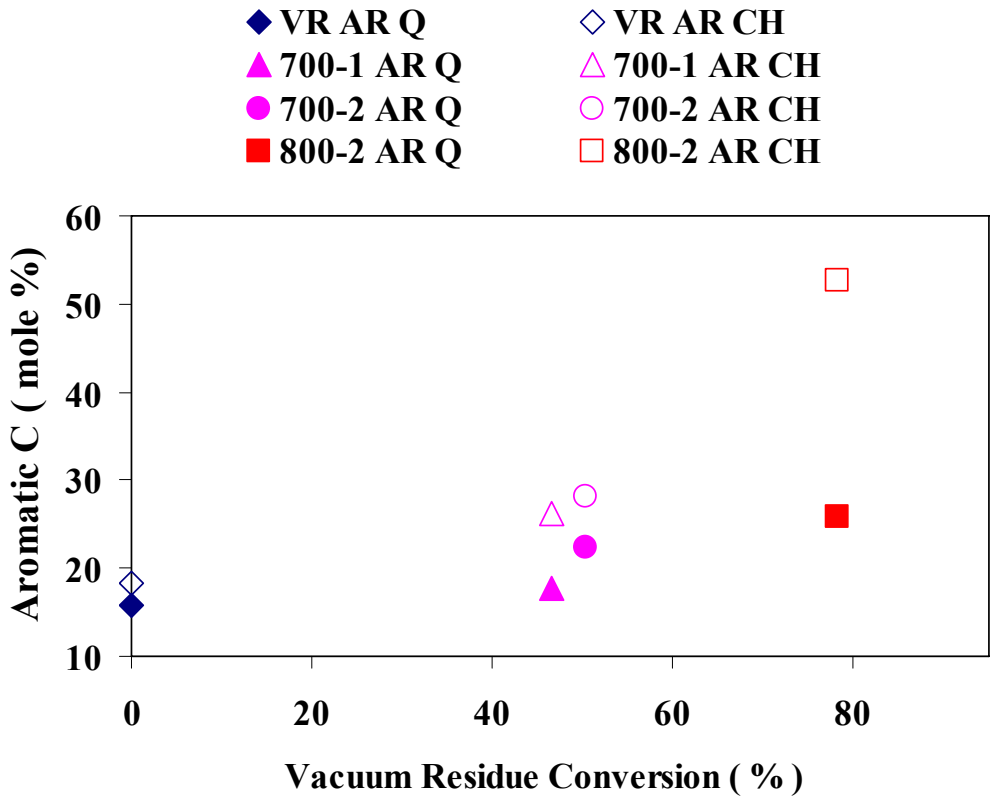

Figure 5.49 Quaternary aromatic carbon (AR Q) and aromatic CH (AR CH) from ^{13}C NMR analysis of liquid products including unconverted VR

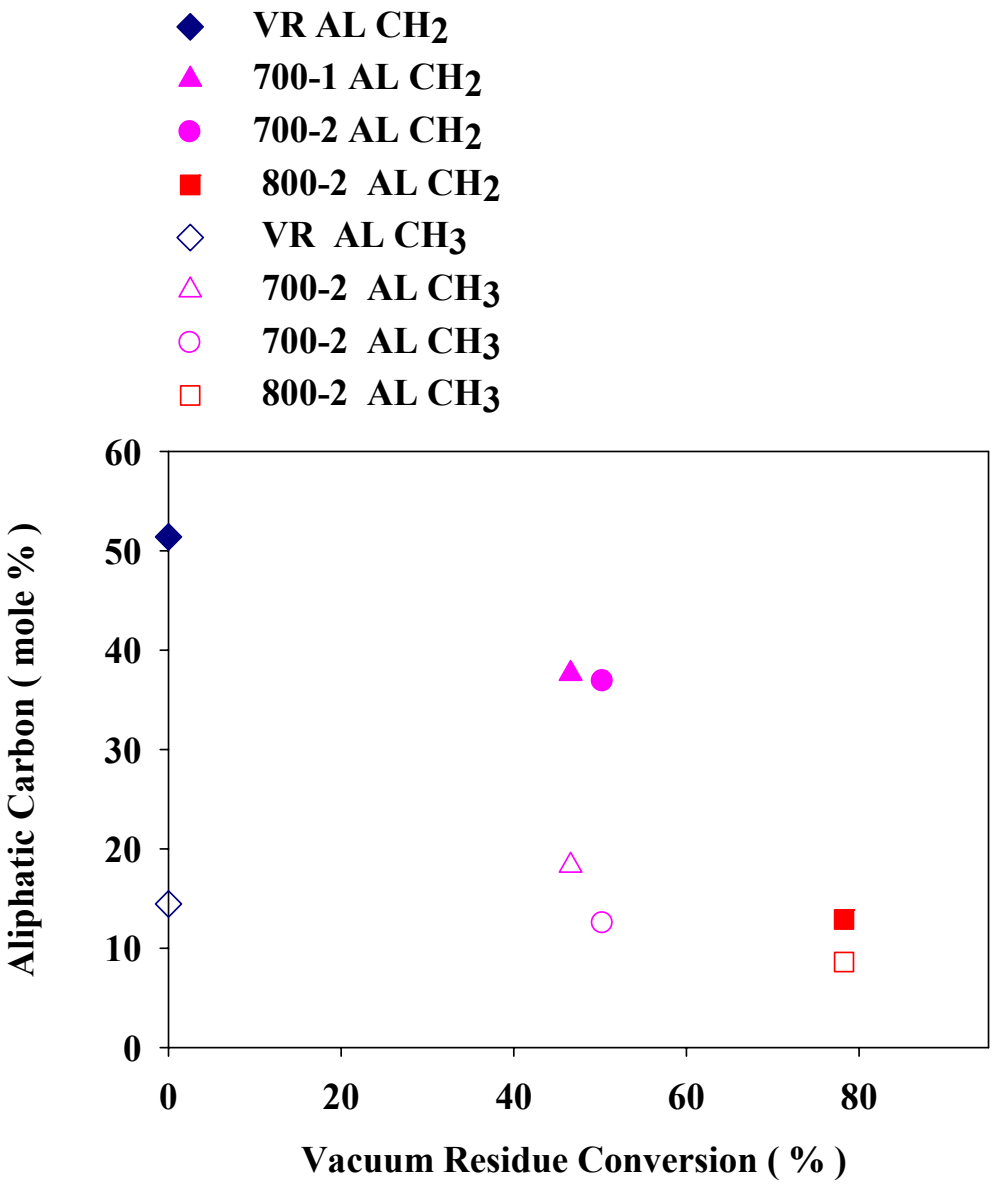

Figure 5.50 Aliphatic CH_2 (AL CH_2) and aliphatic CH_3 (AL CH_3) from ^{13}C-NMR analysis of liquid products including unconverted VR

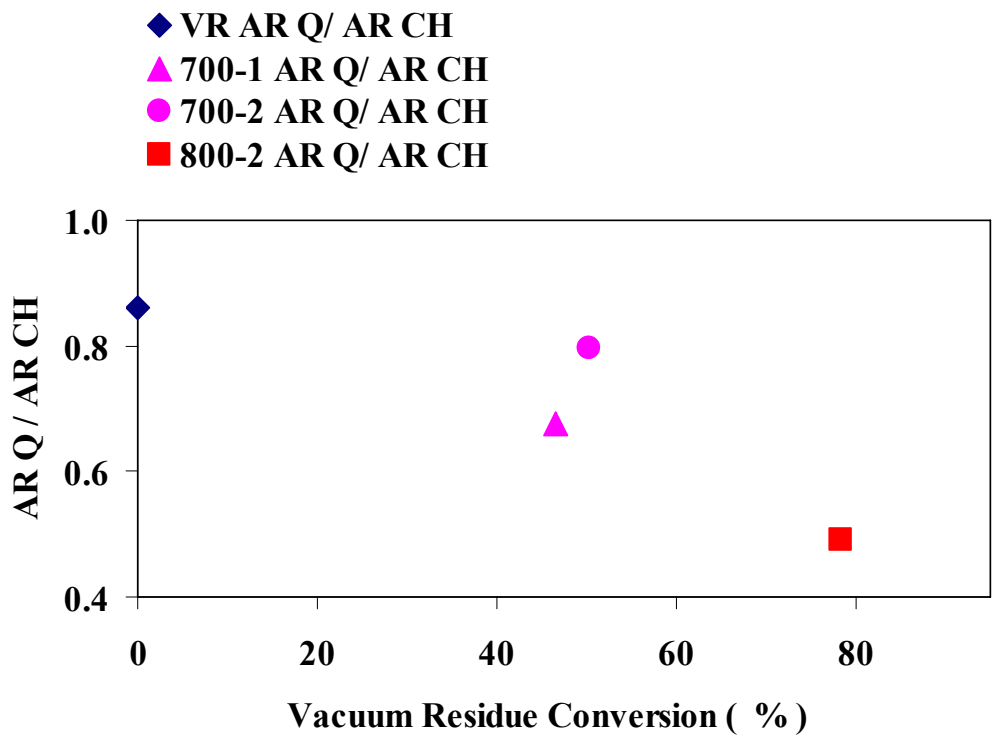

Figure 5.51 Molar ratio of aromatic quaternary carbon to aromatic CH from ^{13}C-NMR spectroscopy analysis of liquid products including unconverted VR

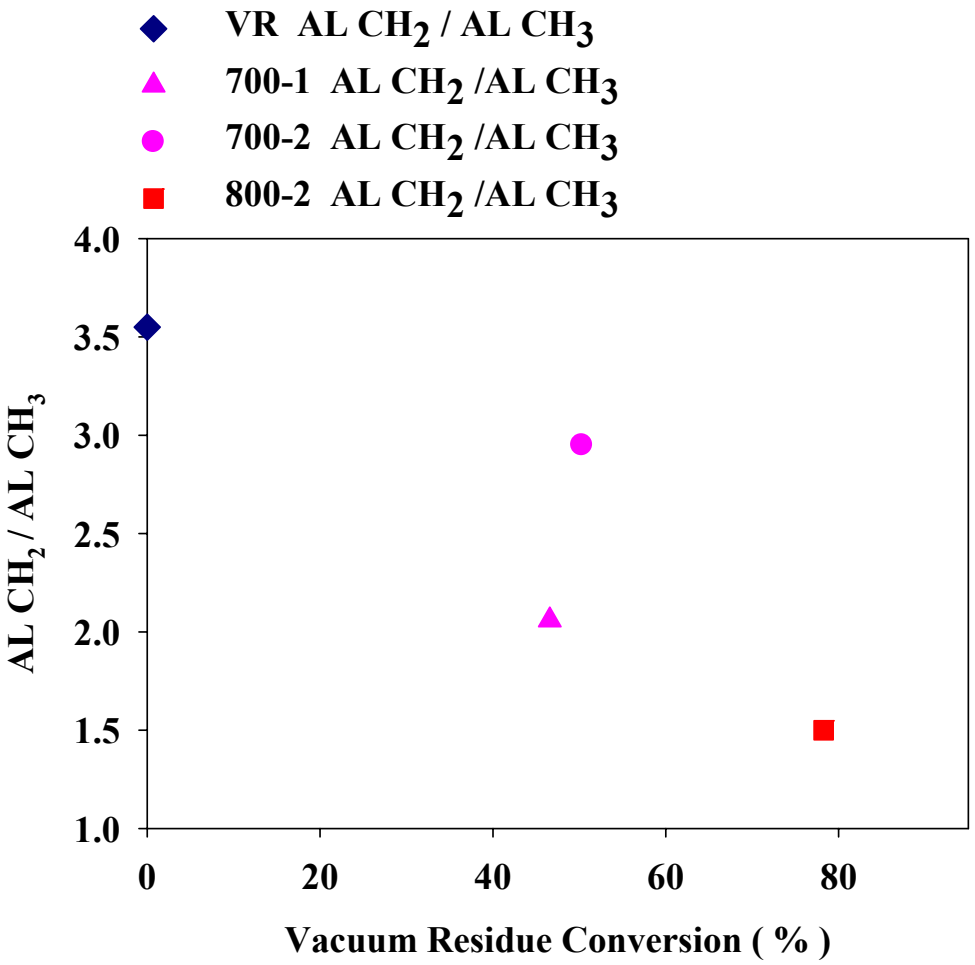

Figure 5.52 Molar ratio of aliphatic CH_2 (AL CH_2) and aliphatic CH_3 (AL CH_3) from ^{13}C-NMR spectroscopy results for heavy liquid products of VR cracking

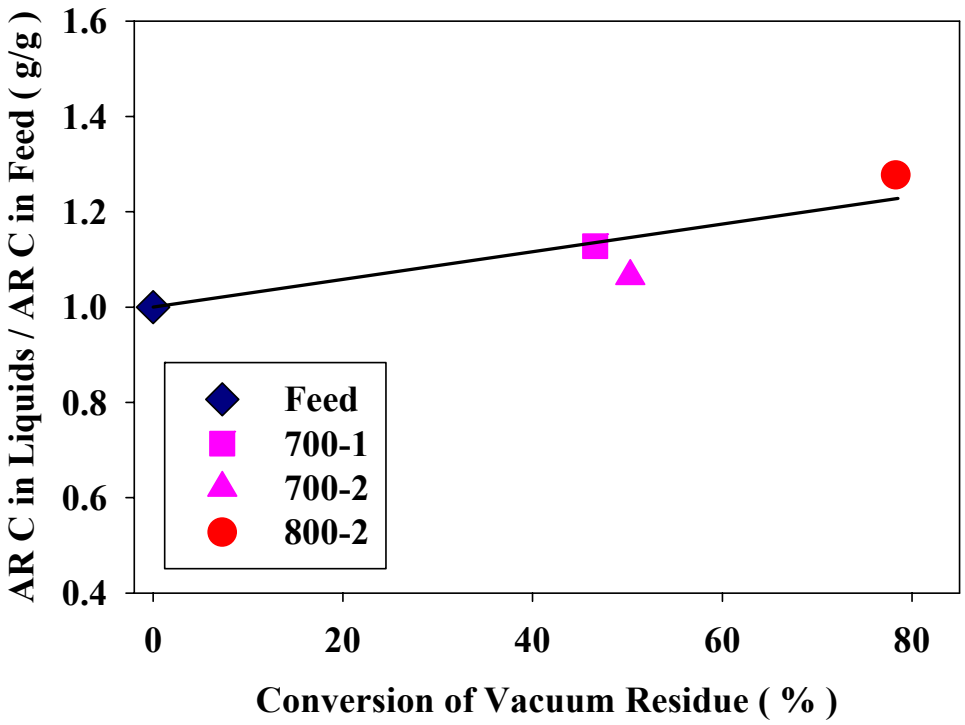

Figure 5.53 Ratio of the aromatic carbon in the collected liquid products to the aromatic carbon in the feed.

5.4 Discussion of results and comparison to literature data

In this chapter, I examine the results from the thermal cracking experiments, compare them to literature data, and describe additional experiments intended to define kinetic interactions during the high-temperature vapor-phase cracking.

5.4.1 Yield of coke and insensitivity of yield temperature

In comparison to conventional coking processes, the results from these experiments show a much lower yield of coke and a significantly increased yield of light olefins. The vacuum residue feed in these experiments contains 20 wt% microcarbon residue (MCR), therefore, the yield of coke from a delayed coker and a fluid coker would be 35 and 23 wt % respectively [8]. The average yield of coke in these experiments is 6.3 wt %, which is significantly lower than the MCR content. Consistent with previous studies on the coking of thin films of liquid, the

yield of coke was insensitive to temperature [75]. The distinct difference in this case was a coke yield that was insensitive to conversion.

I expected that all the coking would occur in the liquid phase, where the rate of addition reactions is much faster than in the vapor phase. This hypothesis can be verified experimentally by looking at the SEM micrographs of coke products (Figure 5.29 and Figure 5.30). All the collected coke particles from the condenser downstream of the reactor are in the form of spheres with average diameter from 100 to 190 nm. This dimension of coke particle implies an average diameter of the feed droplets, based on the average yield of the coke yield of 6.3 wt%, ranging from 280 to 550 nm. The largest coke particles, which could be seen in the SEM samples, were smaller than 500 nm and few in number. As a result of achieving submicron feed particles, the rate of evaporation of the liquid feed to the vapor phase was significantly enhanced and accelerated by the high ratio of the evaporation surface to volume of the liquid. The atomization occurred inside the reaction tube, therefore upon generation of the feed particles, toluene immediately could flash out of the liquid solution. Given the known performance of the spray nozzle with water, giving droplets in average size of 1.2 to 1.5 μm, the measured sizes of the coke particles, and the spherical shape of all the coke particles collected with the product, I suggest that the rapid evaporation of toluene was accompanied by breakup or explosion of the feed droplets. These smaller droplets then reacted and evaporated, giving smaller spherical particles of coke with mean size of 100-190 nm. By atomization to fine droplets, the liquids can evaporate readily even below their boiling point temperature. The minimum applied furnace temperature was 700°C. The fluid temperature reaches the furnace temperature after a short time, on the order of magnitude of 50 ms. On this basis, I would expect rapid evaporation of material even with boiling point above 700^{o}C. At such high temperatures and small particles of feed, the conditions are optimal for maximizing reaction in the vapor phase and minimizing liquid phase reactions. The formation of extrinsic coke may result in sensitivity to conversion. Since such sensitivity was not detected, therefore, such coke was likely not generated. Figure

5.54 compares the result of this study with the data which were collected by Gray et al. [16] by using an inductively heated furnace (Curie reactor). The yield of coke descends monotonically with the reduction of the liquid film thickness following a near-linear trend. This result suggests consistency between the observed coke yield and the observed dimension of the coke particles in the reactor products. This trend also suggests that the yield of coke at high conversion is more sensitive to the liquid film thickness rather than to the reaction temperature. These data suggest that the reduction of the path length for release of components from the liquid droplets resulted in vaporization of most of the thermally crackable feed fractions, and only the fractions which are left behind in the liquid phase form intrinsic coke.

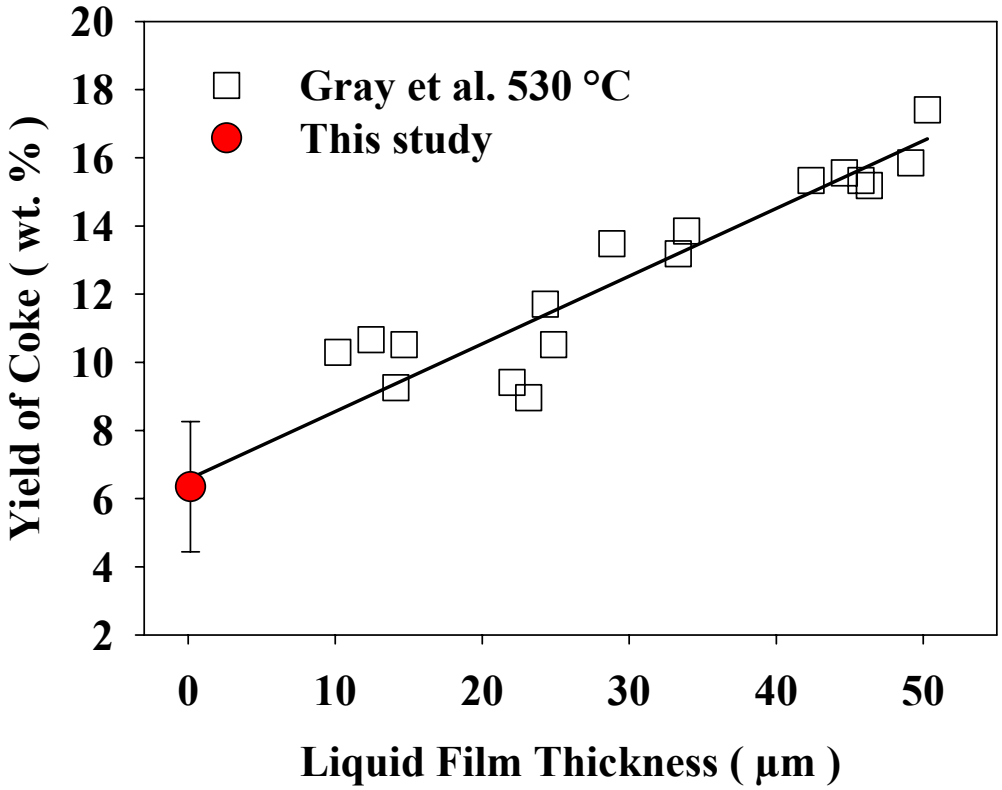

Figure 5.54 Comparing the yield of coke measured by Gray et al. [16] versus liquid film thickness with the results of this study. The error bar shows the standard deviation of the measured yield of coke.

5.4.2 Comparison of olefin yields

Yields of olefins in gas products were significant. Typical total yields of light ends from coking processes are in the range of 5 to 7% [8]. In this study, the total yield of C_2 and C_3 olefins alone ranged from 5 to 18 wt % , which respectively were 19 to 30 times higher than the alkanes with the same carbon number. C_2 and C_3 alkenes together formed 47 to 65 wt % of the total gas products. This result is consistent with prevalent thermal cracking in vapor phase, which favors production of olefins [10]. Under dilute vapor-phase conditions, the β-scission reactions are favored over either addition or hydrogen transfer reactions. Thus, olefins are formed preferentially compared with alkanes.

The only attempt to study thermal cracking of heavy oils at high temperatures above 600°C was reported in PhD thesis of Tan [34], but no associated published work was found in the literature based on his results. Figure 5.55 and Figure 5. 56 compare the yield of ethene and conversion as a function of temperature based on the reported data by Tan for Cold Lake heavy oil with the data from this study. The reported data by Tan were collected at a higher residence time and higher temperature, yet both the yields of ethene and conversion were systematically lower than in the present study. These results are consistent with the effective transfer of feed components into the vapor phase by atomizing the feed efficiently.

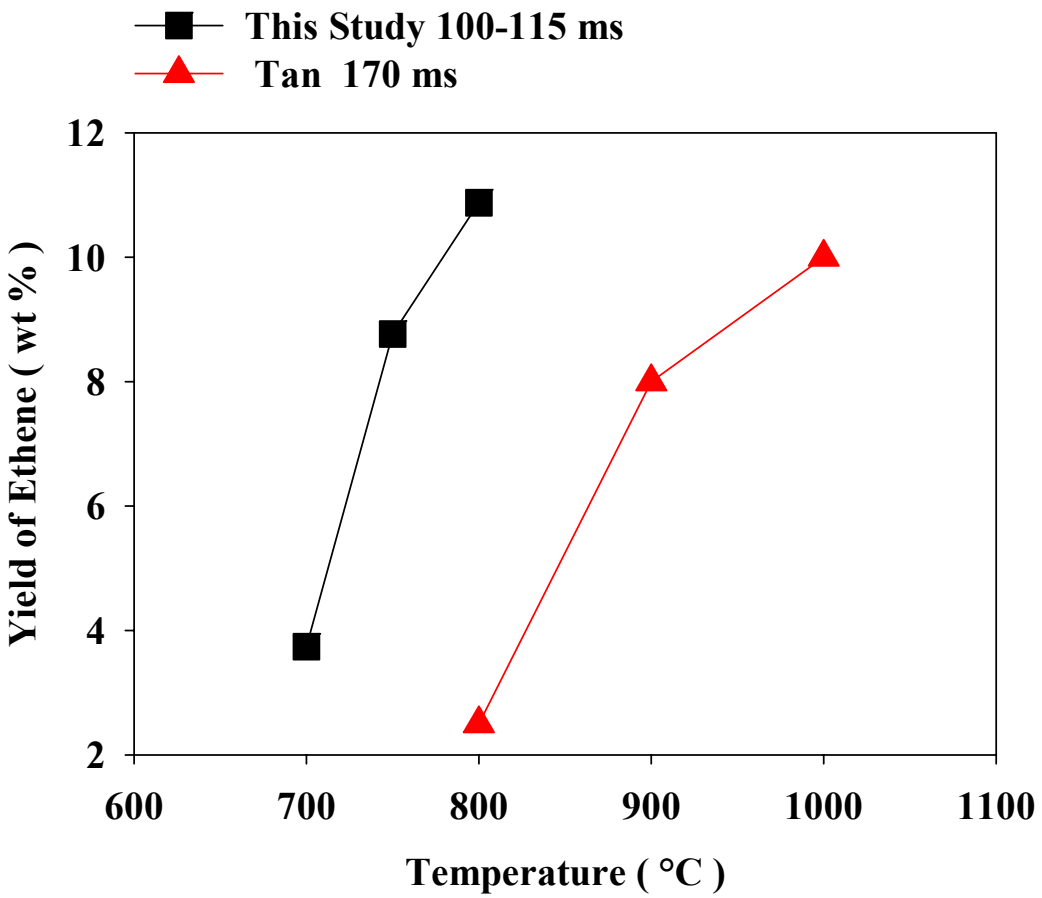

Figure 5.55 Comparison of the measured yield of ethene in thermal cracking of Athabasca VR from this study with the results of thermal cracking of Cold Lake's heavy oil by Tan [34].

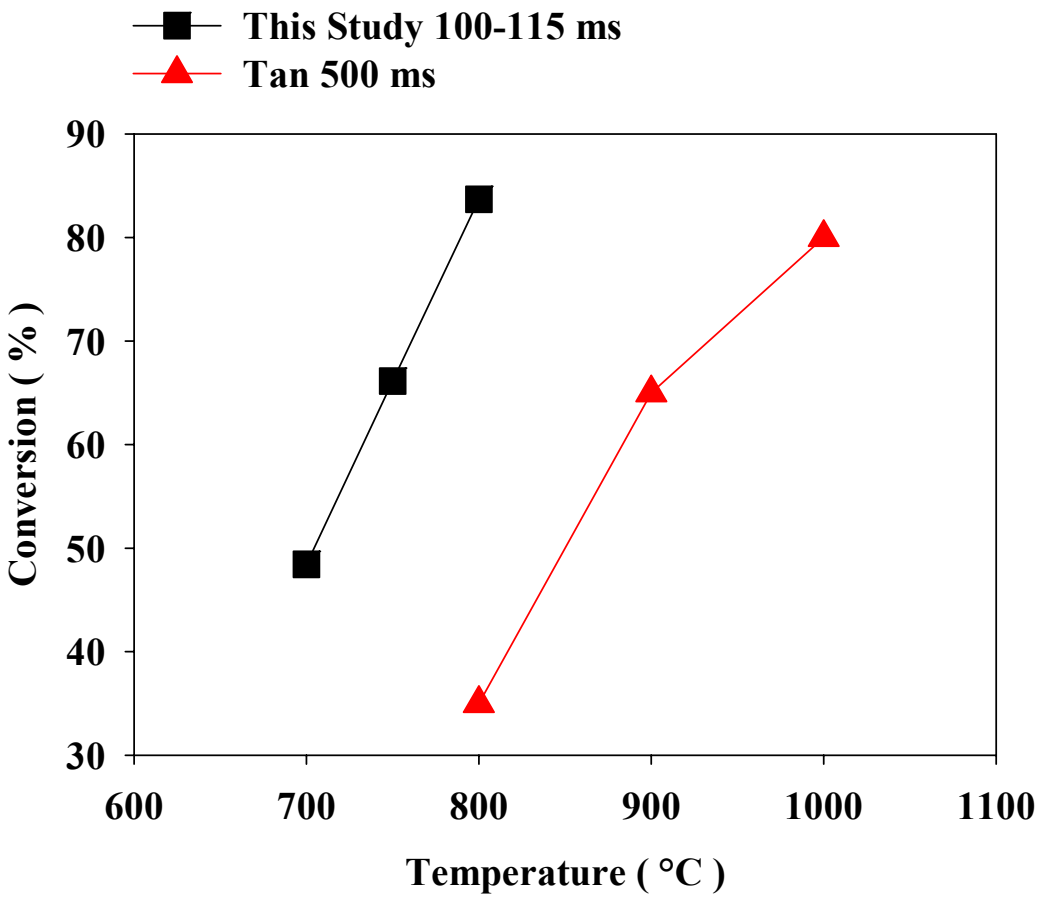

Figure 5. 56 Comparison of the measured conversions in thermal cracking of Athabasca VR from this study and the results of thermal cracking of Cold Lake's heavy oil by Tan [34]

5.5 Conclusions of the experiments of thermal cracking of Athabasca vacuum residue

An aerosol reactor was designed and constructed. The reactor was used to study the rate of thermal cracking of Athabasca vacuum residue in toluene. The generation of fine particles of feed was enabled by in situ atomization, which took advantage of the high temperature at the atomization spot and make-up gas which eliminate formation of vortices by adjustment the velocity and direction of the streamlines. Thus, coke particles with average diameter of less than 190 nm were generated. Considering the average yield of coke the average particle size of feed was estimated to be less than 550 nm.

The higher yield of alkenes compared with alkanes is consistent with the dominance of thermal cracking reactions in vapor phase. This result is also consistent with generation of fine particles of feed, which could intensify evaporation of the heavy fraction despite their high boiling temperatures. The very high surface to volume ratio of submicron feed particles would enhance vaporization. The insensitivity of yield of coke to conversion and reaction temperature and absence of liquid-solid agglomerates in SEM micrographs of the collected samples, suggests the possibility that all the liquids with a chemical structure, which could go under thermal cracking reaction ,evaporates and leave only the fractions behind which cannot undergo non-catalytic thermal cracking reaction and form intrinsic coke. Consistent with reduction of ratio of hydrogen to carbon atoms in the collected liquids, the aromaticity rises dramatically with increase in conversion. A significant change in the ratio of carbon to nitrogen and sulphur atoms was not detected compared with these ratios for the feed. In Chapter 7, it will be shown that at the most severe thermal cracking case the conversion of the feed in the non-isothermal section of the temperature profile along the reactor was below 10 wt%, therefore the choice of the non-isothermal reactor was suitable for this study.

Chapter 6
Kinetic Modeling of Vacuum Residue Conversion

This chapter presents an analysis of the lumped kinetics of the conversion of vacuum residue into coke and lower-boiling components. In order to calculate the kinetic parameters, a first order reaction was assumed for thermal cracking of vacuum residue to gas, liquid and coke products. This assumption is supported by the literature as reviewed in Chapter 2. The Arrhenius model was used to determine the temperature sensitivity of the rate constants of the reaction. Because the tubular reactor has a significant heating zone upon entry of the feed, a non-isothermal model was solved iteratively to find the kinetic parameters (activation energy and pre-exponential factor for each reaction) which can minimize an objective function. The temperature profiles were presented previously in Figure 5.13 and Figure 5.15.

The concentration of feed and products are very dilute in the carrier gas, therefore heat of vaporization and reaction of vacuum residue does not affect the temperature profile. Therefore, the temperature profile can be assumed to independent of the reaction. Once the temperature profile is calculated it can be used without any requirement for reevaluation by change of kinetic parameters. The equation of the design for a tubular reactor can be written as follows [59]:

$$r_j = \frac{dF_j}{dV} \tag{6.1}$$

in which F_j and r_j are the mass flow rate and reaction rate of component j respectively and V is the reactor volume. The rate of the *ith* reaction of component j, r_{ij}, is described by the following equation:

$$r_{ij} = k_{ij} C_j^{\,n} \tag{6.2}$$

in which k_{ij} is the rate constant of the *ith* reaction of component j , C_j is mass concentration of the component j , and n is the order of the reaction. The

Arrhenius equation was used to relate the rate constant to the reaction temperature. The design Equation (6.1) was discretized and integrated with a variable step Runge-Kutta method (using the ordinary differential equation solver MATLAB ode45), to find the conversion or yields of products based on the initial guess for the Arrhenius kinetic parameters. A constrained optimization procedure (MATLAB fmincon) was used to minimize the objective function, equation (6.3), to find the kinetic parameters which give the best fit of the assumed model to the experimental data. The objective function is defined as the following:

$$\Phi = \sum_{j=1}^{q} \sum_{i=1}^{n} \frac{\left(Y_{i,m}^{j} - Y_{i,p}^{j}\right)^2}{\sigma_j^{\,2}} \tag{6.3}$$

in which Φ is the objective function, Y is the yield of product j, i is the number of the experiments , m refers to the measured values from experiments, p refers to the predicted value by the model, σ_j is the standard deviation of the measurement of the yield of component j, n is the total number of the experiments, and q is the total number of the components. When the minimum value of Φ is found, the kinetic parameters at that point are the values which gives the best fit of the assumed model to the data.

In case when only one reaction is considered, that is cracking of vacuum residue to the products, q =1, and Y is the conversion. In a model in which vacuum residue is assumed to crack to gas , liquid, and coke in three separate reactions, then q = 3, and Y_j is used for the yield of gas, liquid, and coke products. In σ_j should be in fact the standard deviation of Y_j values based on repeated measurements, however, because of limitation in number of the repeated experiments, these values were estimated rather than setting them equal to 1.0 [76] . In order to properly estimate standard deviation of Y_j, the standard deviation of GC analysis, simulated distillation analysis, and simple weighing were calculated based on the repeated measurements with the related instruments. Then, by use of the definition of the yield and conversion, and use of equation

(5.7) (propagation of errors) the standard deviation for yield and conversion values were calculated. Table 6.1 gives the calculated standard deviation for yields of gas, liquid, coke, and conversion which are used in equation (6.3).

Table 6.1 Standard deviation of yields and conversion

	Standard Deviation (%)
Yield of Gas	2.62
Yield of Liquids	3.26
Yield of Coke	0.93
Conversion	1.98

6.1 Lumped kinetic models

Considering the complex mixture of components in vacuum residue, lumped kinetic models can serve the best for modeling. The simplest model can be described as the following:

$$VR \xrightarrow{k} \text{Products} \qquad (6.4)$$

This model is referred to as Model 1 in this chapter. The products in equation (6.4) include total gas, liquid and coke products. By using the non-isothermal reactor model, the parameter of Arrhenius equation was calculated. Table 6.2 shows the results of the solution of the model for the kinetic parameters of model 1. The value for the objective function, Φ, is calculated by Equation (6.3). The residuals are the difference between the predictions of the model for conversion and the measured values in this case.

Table 6.2 The calculated parameter for Arrhenius equation and their 95% confidence interval . The objective function in this case is equal to the sum of the square of the residuals for conversion

E (kJ/mol)	Log A (s^{-1})	$\Phi \times 10^3$
85.8±9.7	5.58± 0.5	1.51

Other lumped kinetic models can be suggested by considering vacuum residue to crack in separate reactions to gas, liquid and coke products. The rate constant for cracking of vacuum residue to gas products can be considered the same for cracking of liquids to gas since the bonds, which can undergo thermal cracking reaction, are expected to be of the same nature in both fractions. Furthermore, this assumption helps to reduce the number of the parameters of the model compared with the number of available experimental data. Five models of this kind are given below.

Model 2:

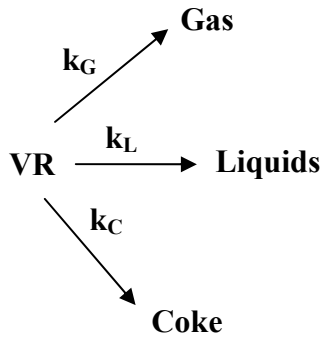

Model 3:

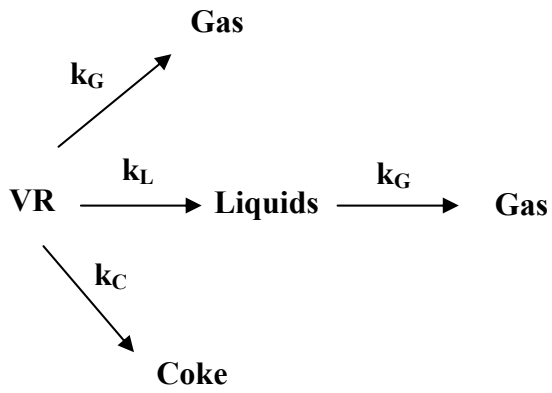

Model 4:

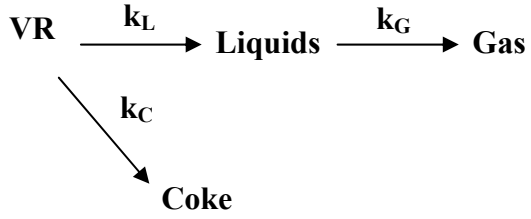

Model 5:

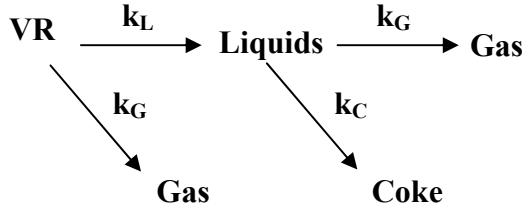

Model 6 :

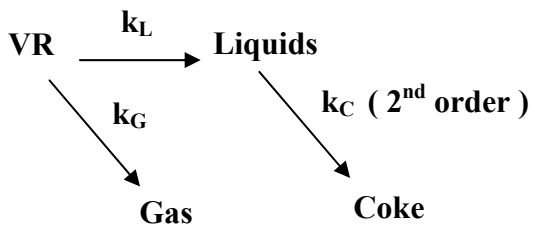

In Model 2 vacuum residue simply cracks to gas, liquid, and forms coke products. In Model 3 vacuum residue cracks to liquids and forms coke, but does not crack directly to gas products. Only liquids crack to gas products. It seems more realistic that vacuum residue cracks directly to gas products as well as liquid products, however, Model 3 is considered to evaluate if the fit of the model to the data is sensitive to such a modification. Model 2 does not show that liquids can also crack to gas products. In Model 4, direct cracking of vacuum residue to gas products and cracking of the liquids to gas products are both considered. Liquid products can undergo addition reactions and eventually form coke. Model 5 is in fact a test model, to see what could be the results if liquid products are considered as responsible for formation of coke rather than the vacuum residue fraction. The addition reactions are bimolecular reactions, so in Model 6, a bimolecular reaction is considered to describe formation of coke.

The data of Table 6.3 show the result of solution of the reactor model to find the kinetic parameters for Model 2 to Model 6. The objective function, Φ , is the weighted sum of the squares of the yields. The minimum values for the objective function for each model, are given in this table. SSR for the gas, liquids, coke, and conversion are also given separately. SSR for conversion is given for the purpose of comparison of these model with Model 1.

Table 6.3 SSR and objective function for kinetic Model 1 to 6

Model No.	**Φ×10^3**	**SSR Gas ×10^3**	**SSR Liquids ×10^3**	**SSR Coke ×10^3**	**SSR Conversion ×10^3**
1	1.51	na	na	na	5.911
2	3.588	2.244	14.918	1.623	7.782
3	3.698	2.592	15.831	1.601	7.791
4	3.678	2.395	15.904	1.602	7.845
5	4.238	2.576	17.381	1.946	9.976
6	5.240	2.928	21.804	2.414	18.706

By comparison of the minimum values of the objective function Model 5 and 6 should be removed from the list of acceptable models. Model 2 , 3, and 4 are not very different when the minimums of the objective functions and SSR values are compared , nevertheless, Model 2 is mathematically a better fit to the data with the exception for the yield of coke that Model 3 and 4 predict slightly closer values. If the minimum of the objective function for Model 1 is compared with SSR of conversions for Model 2 to 6 ; it can be concluded that the predictions of Model 1 is a better fit to the measured conversion values. The residual values for each model can be analyzed separately to see if they are distributed randomly or there is a bias or a pattern in the distribution. A bias or a recognizable pattern in distribution of the errors can reflect a systematic shortcoming of the mathematical model in ability for being fit to the data. Figure 6.1 to Figure 6.5 show the residuals of the conversion and yield values for Model 1 and Model 2. The residuals are given in fractions (instead of percentage). The residuals look randomly distributed versus measured conversion.

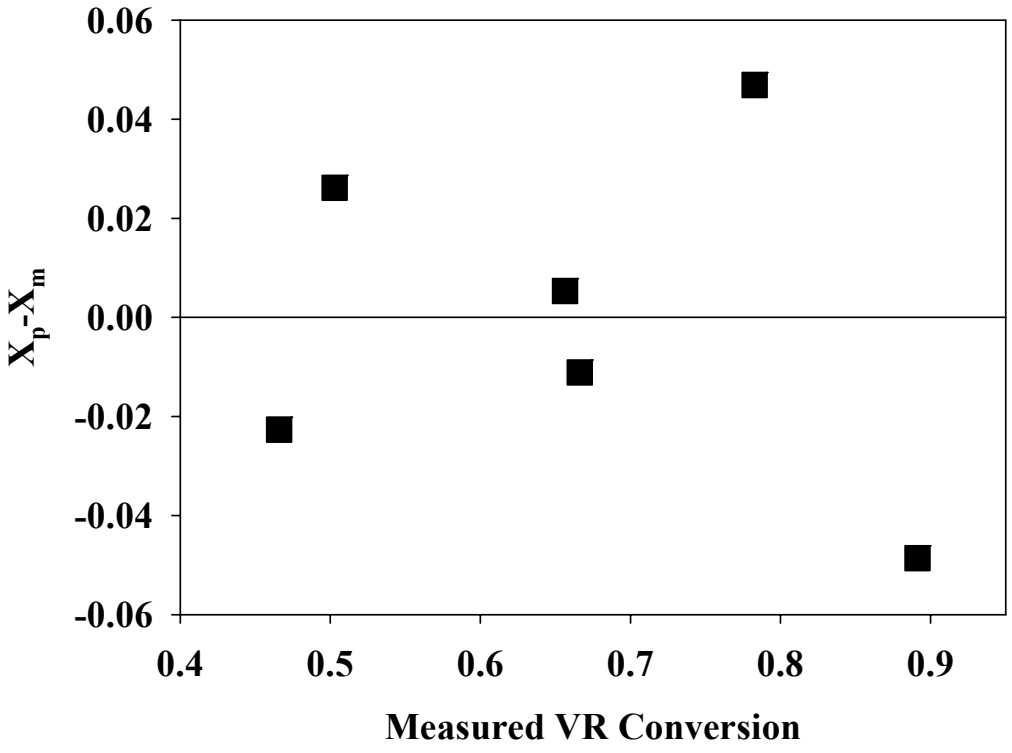

Figure 6.1 Residuals of conversions for Model 1 versus measured values for vacuum residue conversion. Conversion is given in fraction

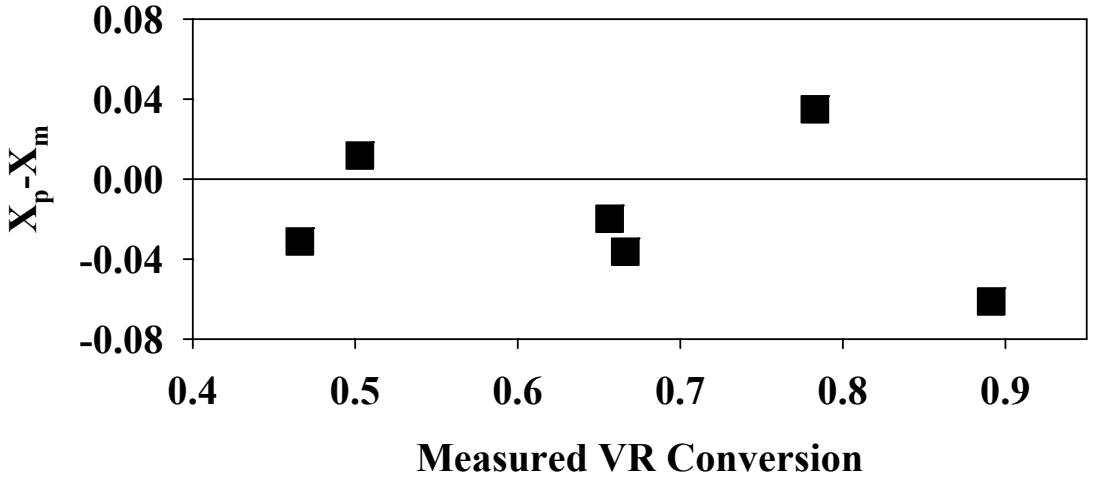

Figure 6.2 Residuals of conversions for Model 2 versus measured values for vacuum residue conversion. Conversion is given in fraction

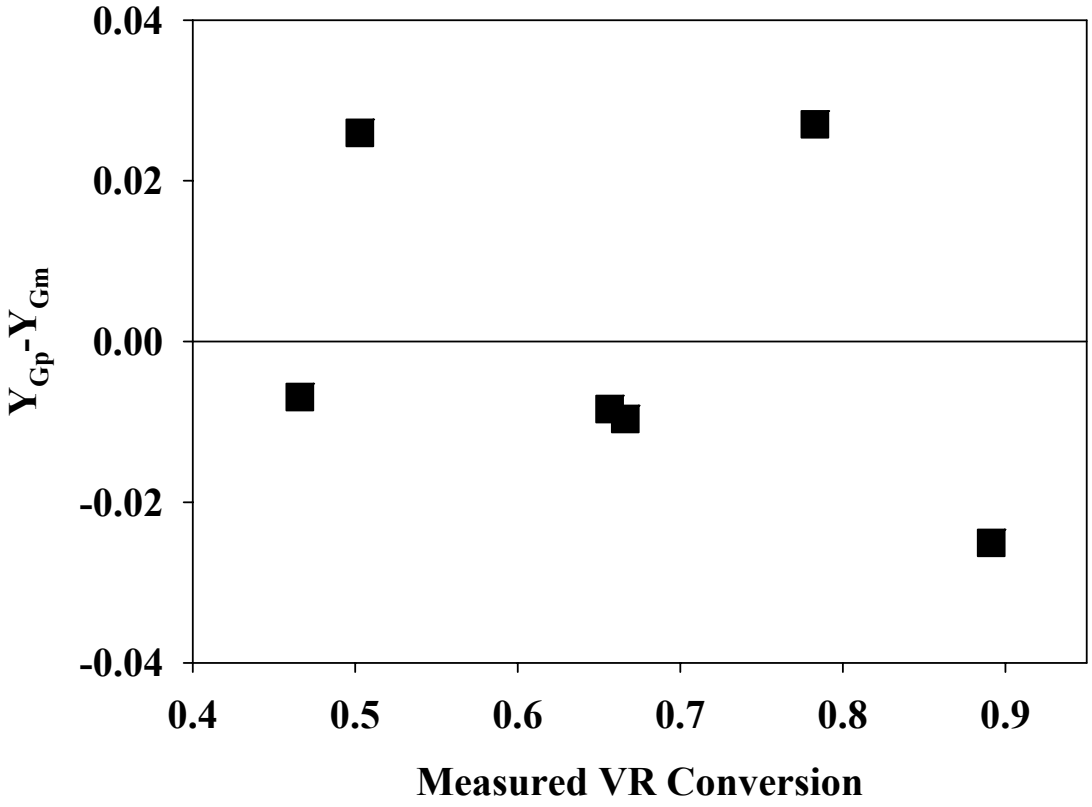

Figure 6.3 Residuals of gas yields versus measured vacuum residue conversion for Model 2, the yield values and conversions are given as fractions.

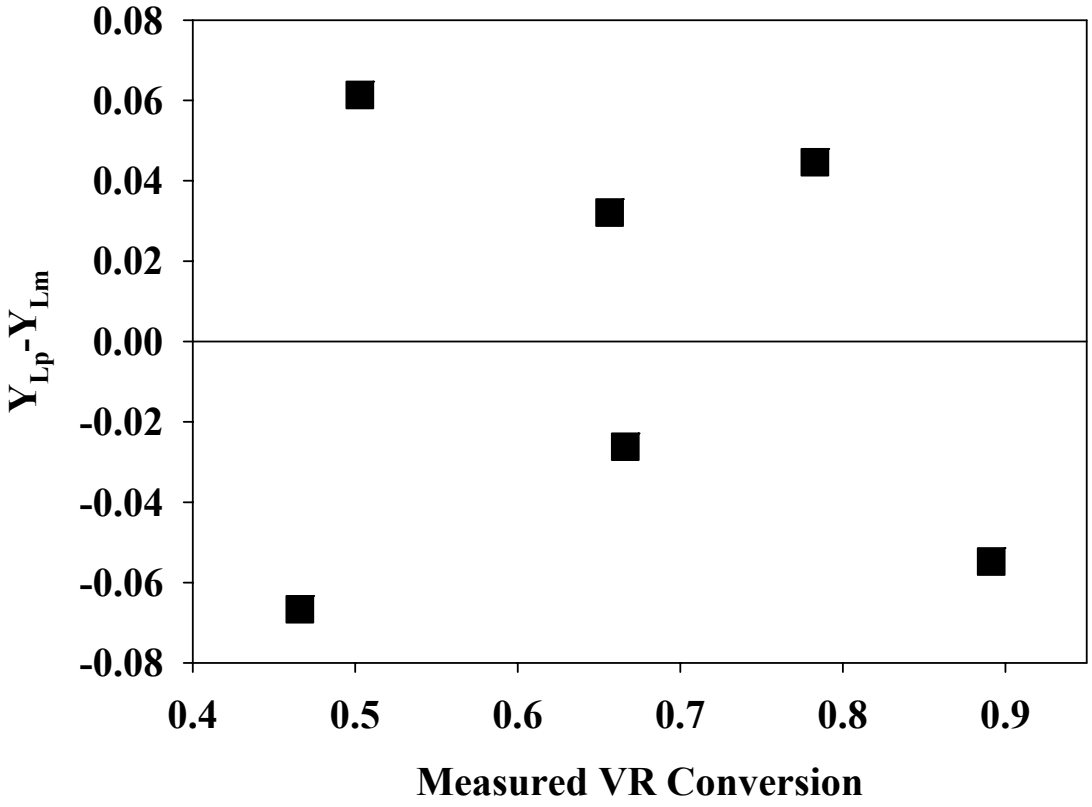

Figure 6.4 Residuals of liquid yields versus measured vacuum residue conversion for Model 2, the yield values and conversions are given as fractions.

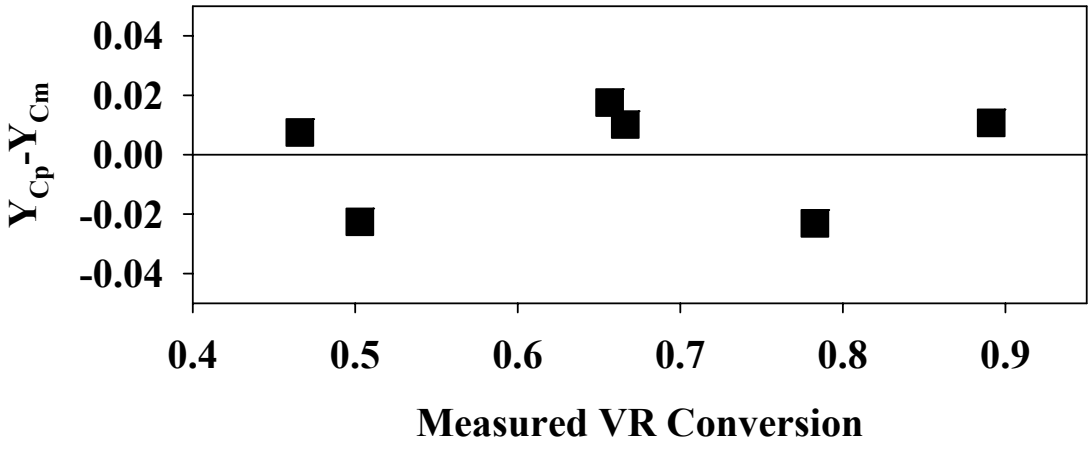

Figure 6.5 Residuals of coke yields versus measured vacuum residue conversion for Model 2, the yield values and conversions are given as fractions

Thus, Model 1 is the best model for conversion values and Model 2 is the best model which predicts the yield of the individual products. As indicated in the above residual plots, the scatter of the data are random as a function of the residue conversion. Table 6.4 gives the kinetic parameters for Model 2. The 95% confidence levels of the kinetic parameters are calculated by Monte Carlo method as suggested by Alper and Gelb [77].

Table 6.4 The kinetic parameters for Model 2

Ea Gas (kJ/mol)	137.7±31.6
Ea Liq (kJ/mol)	58.4±31.4
Ea Coke(kJ/mol)	16.9±11.9
Log A Gas(s^{-1})	7.83±1.6
Log A Liq (s^{-1})	3.82±1.6
Log A Coke (s^{-1})	0.986±0.68

Figure 6.6 and Figure 6.7 compare the measured conversion and the predicted conversion by Model 1 and 2 separately. Model 1 shows a better fit to the data especially for the middle range of conversion.

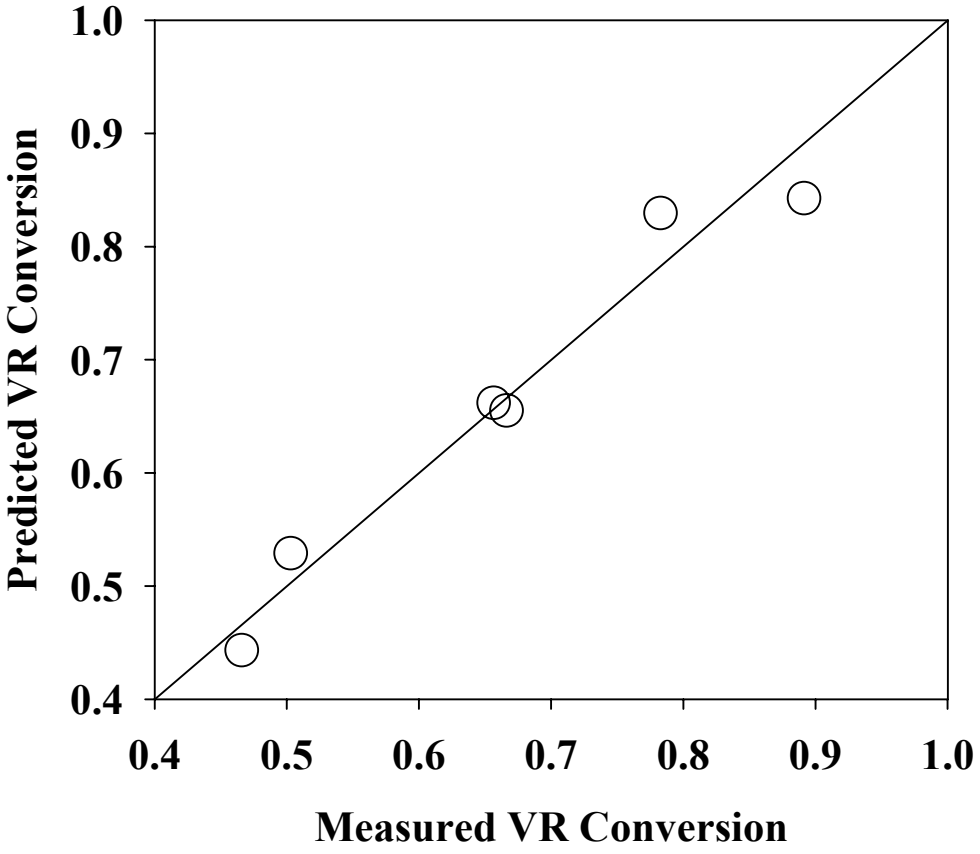

Figure 6.6 Comparison of the predicted VR conversion by Model 1 with measured VR conversion.

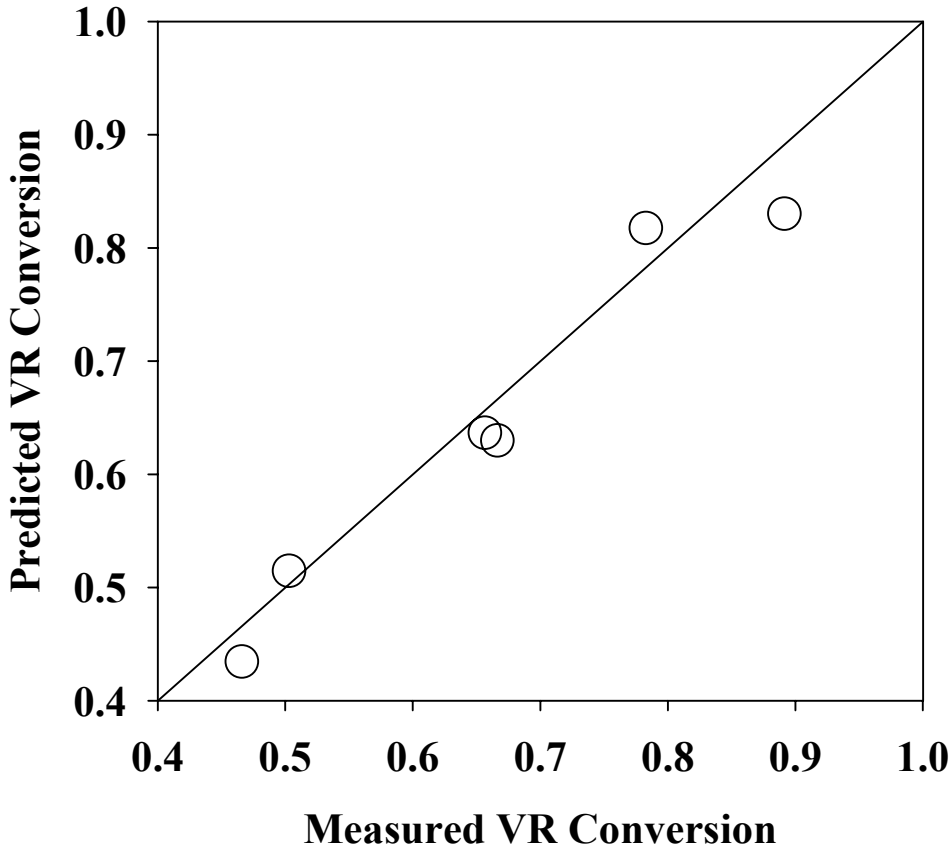

Figure 6.7 Comparison of the predicted VR conversion by Model 2 with measured VR conversion values.

6.2 Comparing the kinetics results with previous studies

There is no published work in the literature about kinetics of thermal cracking of vacuum residue or bitumen at temperatures above 600°C. Table 6.5 gives a summary of the available data for residue conversion. The study of Gray et al. [36] on kinetics of thermal cracking and devolatilization of Athabasca residue is limited to a maximum temperature of 530°C. Both Model 1 and 2 give values for activation energy which are lower than the calculated values by Gray et al.. Figure 6.8 compares the rate of thermal cracking of light residue (524 to 650°C) and heavy residue (650°C+), which is calculated according to the reported kinetic

Table 6.5 Comparison of the activation energy with the available data

	Feed	E (kJ/mol)	A (s^{-1})	Temperature range of the study (°C)
Olmstead and Freund [44]	Cold Lake 706°C+ Residuum	213	1.6×10^{13}	400- 530
Olmstead and Freund [44]	Arabian heavy 696°C+ Residuum	215	1.6×10^{13}	400-530
Gray et al [36]	Heavy residue 650 °C +	218	1.2×10^{13}	457 to 530
Gray et al. [36]	Light residue 524 to 650 °C	218	2.7	457 to 530
Radmanesh et al. [75]	Heavy residue 650 °C	230	10^{14}	457-530
Radmanesh et al. [75]	Light Residue 524 to 650 °C	188	10^{11}	457-530
Tan [34]	Peace river and cold lake heavy oils	58 to 107	92×10^{8} to 1.4×10^{8}	800- 1000
This study	Athabasca VR	85.8	3.8×10^{5}	700-800
This study	n-hexadecane	235	1.1×10^{13}	600 - 750

parameters by Gray et al., with the results of this study for the rate of thermal cracking of Athabasca vacuum residue (based on kinetic Model 1). Gray et al. assumed the same activation energy for thermal cracking of heavy residue and light residue in their model with different values for the pre-exponential factor. The two studies are compared in temperature range of 600 to 800°C. This means that the results of this study was extrapolated to 100°C below the minimum temperature in which the experiments were carried out, that is 700°C. The results of Gray et al. were also extrapolated up to 270°C above the maximum temperature of their experiments (that is 530°C). Such extensive extrapolation, out of the temperature range of the experimental study, does not ensure a valid conclusion. However, in absence of any other reliable published data, this comparison can be justified. Figure 6.8 shows that the rate of thermal cracking, which is predicted by the result of this study is significantly higher than the rate that Gray et al. predicts for light residue in the temperature range of 600 to 800°C.

However, the results of the two studies are closer for heavy residue. For temperatures below 640°C this study predicts higher rate of thermal cracking and for temperatures above 640°C the predicted rate by Gray et al. is higher. At 800°C the rate constant which is predicted by Gray et al. model is about one order of magnitude larger. The most reliable region for this comparison is 600 to 630°C, where the extrapolation for both this study and Gray et al. remains below 100°C. In this area, the prediction of this work is either equal or higher with less than of one order of magnitude difference.

Radmanesh et al. [75] developed a more detailed kinetic model based on the original work and data of Gray et al. [36]. In this model, different activation energies were considered for heavy and light residue. Figure 6.9 demonstrates that below 640°C this study predicts higher rates for thermal cracking of heavy residues (650°C+) compared with the Radmanesh et al. predictions. However, Radmanesh et al. model predicts higher rate of thermal cracking for temperatures above 650°C. The prediction of the model of Radmanesh et al. for rate constant at 800°C is more than one order of magnitude higher than the rate constant that this study predicts. For light residue, this study and Radmanesh et al. predict the same rate at around 710 °C. At lower temperatures, this study predicts higher rate constant, and at higher temperatures, it predicts lower rate constants. For the case of light residue, this difference at 800°C is less than one order of magnitude. Both Figure 6.8 and Figure 6.9 indicate that the slope of the plot, that is the activation energy, is significantly lower in this study. This suggests that the results of this study indicate a lower rate of thermal cracking compared with the predictions of both Gray et al. and Radmanesh et al..The rate of thermal cracking of n-hexadecane from this study is also compared with the rate of thermal cracking of vacuum residue in Figure 6.9 The results of thermal cracking of n-hexadecane is extrapolated only 50°C above the maximum temperature of the study (750°C).

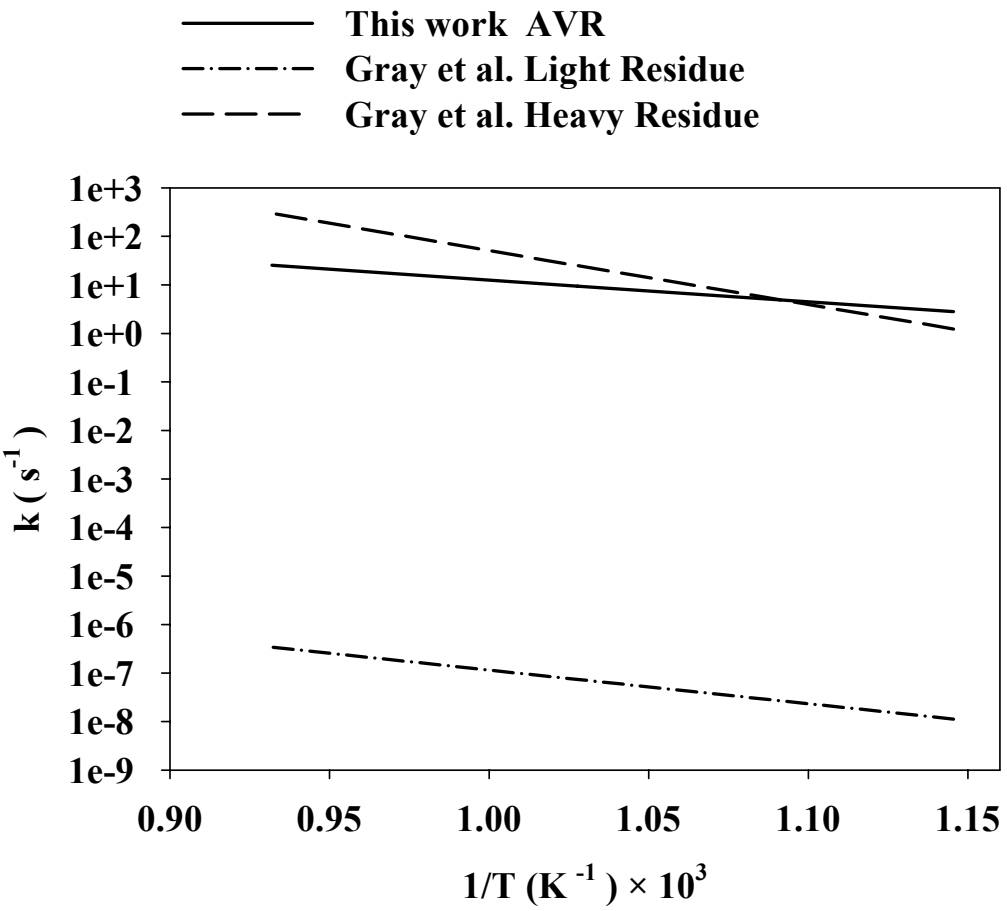

Figure 6.8 Comparison of this study with Gray et al. [36]

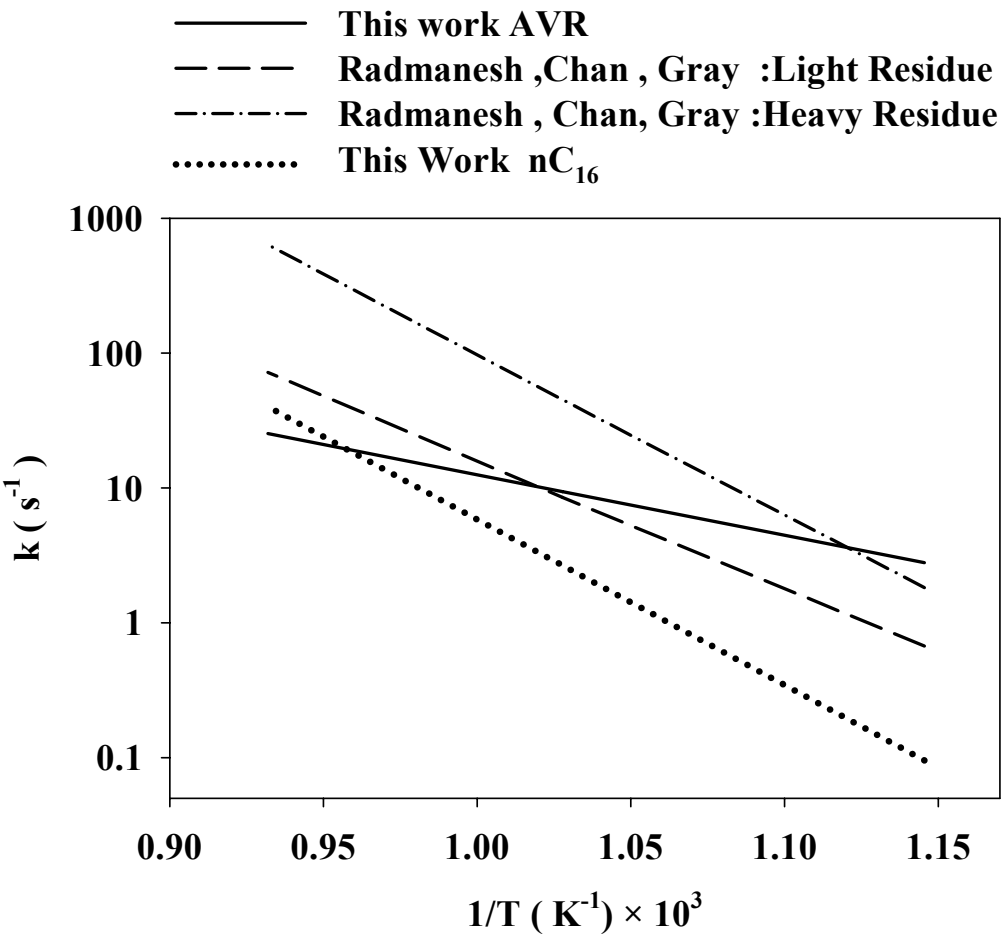

Figure 6.9 Comparison of this study with Radmanesh et al. [75]

The only attempt to study the kinetics of thermal cracking of heavy oils at high temperatures above 600°C was reported in PhD thesis of Tan [34], but no associated published work was found in the literature based on his results. Figure 6.10 compares the rate constants of thermal cracking according to the kinetic parameters, which are reported by Tan, with the predictions of this study in temperature range of 700 to 1000 °C. Figure 6.10 shows that the range of the rate of thermal cracking that Tan predicts is significantly higher than the predicted rate by this study. This is inconsistent with the trend, which Figure 5.55 and Figure 5. 56 demonstrate as Tan reported lower yield of ethane and lower conversions for thermal cracking experiments which carried out at higher temperature and higher residence time (Chapter 5). Table 6.5 shows that the range of activation energy

that Tan reported for thermal cracking of heavy oils of Cold Lake and Peace River is much lower than the activation energy which is reported by Gray et al. [36]. Tan used his apparatus to measure rate of thermal cracking of *n*-hexadecane at the temperature range of 800 to 1000°C and reported activation energy of 85.4 kJ/mole and pre-exponential factor of 2.91×10^4 (s^{-1}). This activation energy is far lower than the calculated values for these parameters in this study, and the results of most of previous researchers.

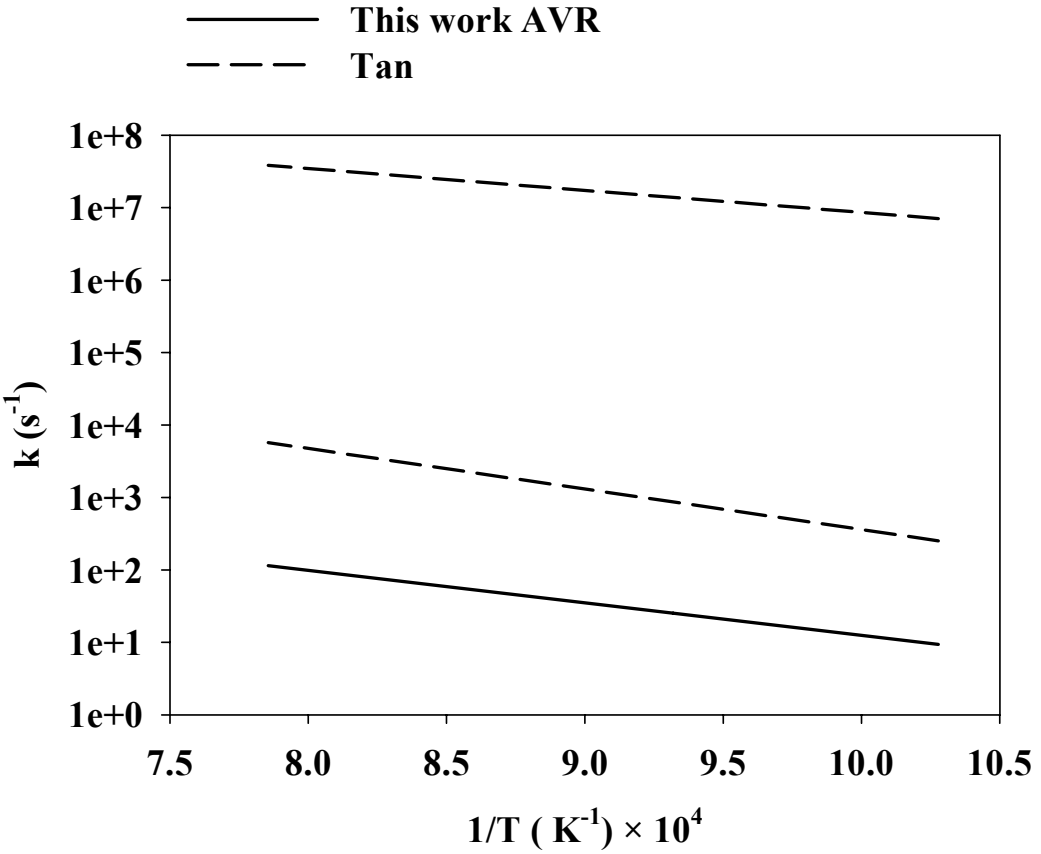

Figure 6.10 Comparison of the results of Tan [34] for rate constants of thermal cracking with this study

Figure 6.9 shows that at above 770°C, the rate of thermal cracking of n-hexadecane exceeds the rate of thermal cracking of vacuum residue. The activation energy which was calculated for thermal cracking of vacuum residue is significantly lower than the activation which is calculated for thermal cracking of n-hexadecane. Before any conclusion is made based on these comparisons, recall

that the activation energy of *n*-hexadecane was calculated based on the data which are collected at lower conversion in comparison with the case of vacuum residue. In addition, as the reaction proceeds, at higher conversions the nature of the bonds does not significantly change for the case of thermal cracking of n-hexadecane since the products are 1-alkenes. In contrast, the nature of the bonds will change for the case thermal cracking of vacuum residue as the conversion increases; as the aliphatic portion of vacuum residue cracks away, the remainder consists of more poly aromatics that would not go under thermal cracking reaction.

6.3 Sensitivity analysis of the kinetic model

The activation energy which is calculated in this study is lower than the activation energy which is calculated for thermal cracking of *n*-hexadecane, for breakage of alkyl C-C bonds, and the value which reported by Gray et al.[36]. This raises the question whether lack of accuracy in temperature and pressure measurement could cause such a bias in the value of the activation energy for thermal cracking of vacuum residue. This question can be investigated by analyzing the sensitivity of the activation energy and the pre-exponential factor of the Arrhenius equation to a certain assumed bias in temperature and pressure measurement. The same approach can be adopted to study the sensitivity of these kinetic parameters to a bias in measurement of conversion of the feed. Kinetic Model 1 and the non-isothermal reactor model was used to calculate the variation of the kinetic parameters due to imposition of such biases in temperature, pressure, and conversion.

The accuracy of the thermocouples is ± 1.1°C or 0.4% of the measured temperature whichever is greater according to the manufacturer. Therefore, for a measurement at furnace temperature of 800°C the accuracy of the measured temperature is within ± 3.2°C. Other sources of error can broaden this range of accuracy. The attachment of the thermocouples to the tube and possible non-uniformity of temperature along the furnace can cause the thermocouple read a different value from the real temperature. The latter does not seem to be a significant issue because of good quality of the reaction furnace, which is selected

for this research work. The sensitivity of activation energy to temperature measurement was analyzed by use of kinetic Model 1 and the non-isothermal reactor model. The original activation energy, 85.8 kJ/mole changes ±2 and ±4 kJ/mole for ±5% and ±10% error in accuracy of the temperature measurement respectively. At positive temperature bias, higher values for activation energy were calculated. The pre-exponential values vary from 3.51×10^5 to 4.19×10^5 s^{-1} for ±5% error in temperature measurement and from 3.26×10^5 to 4.66×10^5 for ±10% error in temperature measurement. The lower value of pre-exponent factor is calculated for positive bias in temperature measurement. The original pre-exponential factor is 3.81×10^5 s^{-1}. The uncertainty of experimental data causes this value to range from 1.2×10^5 s^{-1} to 1.2×10^6 s^{-1}. This is a wider range of uncertainty compared with the uncertainty caused by the bias in temperature measurement. The uncertainty in calculation of activation energy, which is caused by the uncertainty of data, as reported in Table 6.2, is ±9.7 kJ/mole. A 10% bias in measurement of temperature is unlikely, but such an inaccurate temperature measurement would cause less than half of the uncertainty that caused by uncertainty of the experimental data.

The uncertainty of the pressure transducers which used to measure the reactor pressure (Model PX726A 0-50 psi Omega Company, Laval, Quebec) had a high accuracy of ±0.15 %. The error from the pressure measurement device itself was so small, but mild change of reactor pressure due to the build of liquefied gases, frozen solvent, and coke particles inside the cryogenic trap could be a source of error. This error can reduce the accuracy of the residence time calculation, and hence affects the value of the activation energy. The sensitivity analysis by use of kinetic Model 1 and the reactor model shows that ±10% bias in pressure measurement did not change the calculated activation energy of 85.8 kJ/mole which was calculated for an assumed bias free data set. The pre-exponential factor, however changes from 3.63×10^5 to 4.02×10^5 s^{-1} for ±5 % bias and from 3.47×10^5 to 4.24×10^5 for ±10% bias in pressure compared with the original value of 3.81×10^5 s^{-1} which is calculated for a bias free system. The lower values of the

pre-exponential factor are related to the positive bias in pressure. At higher reaction pressures, the mean residence time is smaller and given the fact that the activation energy was found to be insensitive to bias in pressure, a higher value of pre-exponential factor is required to compensate for the rate of thermal cracking to achieve the measured conversion values in the model.

Thus, the activation energy was found to be insensitive to ± 10 % bias in temperature and pressure measurement. It can be concluded that the low value which is calculated for the activation energy is not due to such inaccuracy in temperature and pressure measurements. The variation of the pre-exponential factor due to ± 10 % bias is smaller than the uncertainty of this quantity which is caused by the uncertainty of the experimental data. Therefore, the fact that the measured rate of the thermal in this study is lower than the prediction of Gray et al. [36] cannot be due to such biases in temperature and pressure measurement.

A ±10 % bias in measurement of conversion ranges the activation energy from 76.2 to 100.2 kJ/mole with the higher value for the positive bias. Pre-exponential factor ranges from 9.94×10^{4} to 2.59×10^{6} with the higher value for the positive bias. Comparing with the uncertainty of the kinetic parameters which are given by Table 6.2, it can be concluded that the activation energy is not sensitive to the significant bias of ±10 % in conversion to an extent that can explain the difference with the prediction of Gray et al. [36] for this quantity.

6.4 Conversion in non-isothermal section of reactor

Two basic questions can be asked at this point:

1- How much error in calculation of the kinetic parameters would arise if the reactor were assumed to be isothermal?
2- How much of the feed is converted in the non-isothermal part of the reactor?

If the reactor is assumed to be an isothermal reactor and the mean residence time is evaluated accordingly, then the activation and pre-exponential factor can be calculated easily by a linear regression of the values for natural logarithms of rate constants versus inverse of temperature if kinetic Model 1 is used. The calculated activation energy and the pre-exponential factor from such regression are 93.3 kJ/mol and 7.13×10^5 respectively. The R^2 for this regression is 0.96. The activation energy for the non-isothermal reactor ranges from 76.1 to 95.5 kJ/mole and the pre-exponential factor from 1.2×10^5 to 1.2×10^6. Thus, the estimate by isothermal assumption is in the range of the results of a more sophisticated calculation based on the temperature profile for a non-isothermal reactor.

The second question can be answered by plotting the temperature profile of the fluid in the non-isothermal reactor against the conversion. Figure 6.11 demonstrates the dimensionless temperature profile and conversion of the feed along the reactor. The lower and higher extremes of the severity of reaction was selected for this demonstration that is furnace temperatures of 700 and 800°C (experiment 700-1 and 800-1). This figure shows that when the fluid reaches 95 % of the reaction temperature, then the conversions of vacuum residue is 6.4 % to 9.5 % at furnace temperature of 700 and 800°C, respectively. At the most severe case, less than 10% of the feed converted in the non-isothermal section of the temperature profile and at lower furnace temperatures the conversion is even lower. That means that application of a non-isothermal model was a proper choice, and the non-isothermal model cannot cause a significant error in calculation of the kinetic parameters.

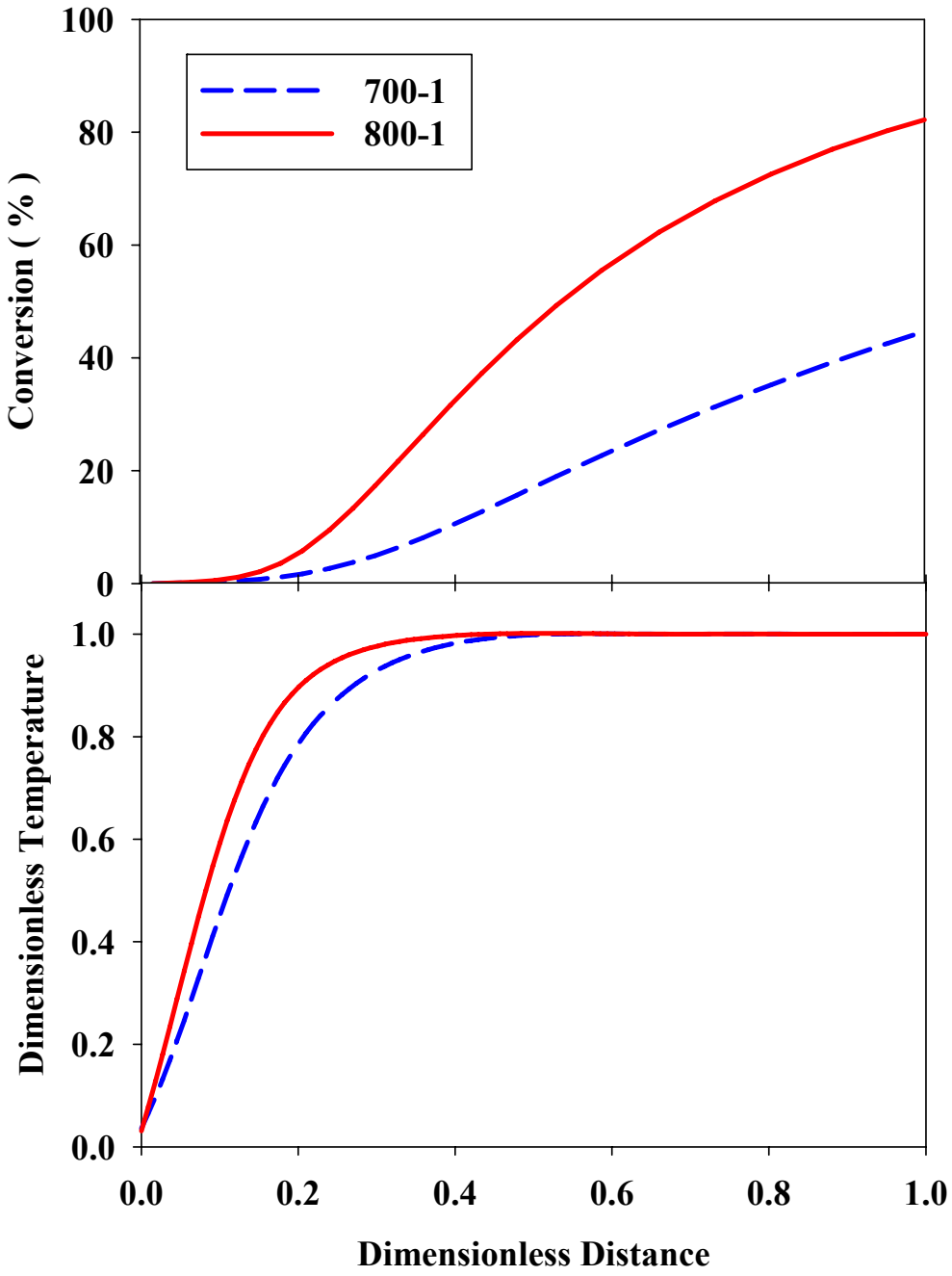

Figure 6.11 For experiment 700-1 and 800-1 when the fluid reach 95 % of the reaction temperatures the conversion of VR is 6.4 % to 9.5 % respectively

6.5 Effect of the assumed order of reaction on the calculated value of the activation energy

The assumption of an over all first order reaction for thermal cracking of *n*-alkanes and heavy oils is supported in general by the literature as reviewed in Chapter 2. The reaction order in kinetic models in this study was assumed to be one. The exception was kinetic Model 6, in which a bimolecular reaction was considered to form coke. If in the kinetic Model 1, order of the reaction varies from 1 to 3, the calculated activation energy increases. Simultaneously, the calculated minimum value for the objective function increases. That means the fitness of the model to the data deteriorates by increasing the order of the reaction. Table 6.7 gives the values for activation energy and pre-exponential factor, and the minimums of the objective function for the reaction order of 1 to 3. This trend might suggest that the order of reaction of thermal cracking of vacuum is increased by some interactions, which cannot be described by the given lumped kinetic models, as they do not consider these interactions. Two possibilities for such interactions are interaction of thermal cracking free radical chain reactions with toluene (the feed solvent) and dehydrogenation of the naphthenic rings in vacuum residue. The first factor might contribute to an apparent increase the order of the reaction, and the second factor can change the rate of the reaction by changing of the nature of the bonds from aliphatic in the initial feed to aromatic in partly reacted vacuum residue, and thereby decrease the rate of thermal cracking at higher conversion levels.

Table 6.7 Effect of higher order of the thermal cracking reaction

order	E (kJ/mol)	A (s^{-1})	**Φ**× 1000
1	85.836	3.81E+05	1.51
1.5	109.88	6.75E+05	1.69
2	135.88	1.54E+06	2.16
2.5	164.14	4.73E+06	2.61
3	194.7	1.95E+07	2.96

The kinetic data for conversion of vacuum residue show an unexpectedly low rate of reaction, based on extrapolation of available data for similar feeds. In particular, the activation energy is too low for a process dominated by breakage of carbon-carbon bonds. This observation is not sensitive to errors in temperature, pressure or conversion measurements, or to the choice of the overall reaction order. The most likely explanation is kinetic interaction between the vacuum residue and the toluene, which is discussed in Chapter 7

Chapter 7

Effect of Toluene Solvent on Kinetics of Thermal Cracking of Vacuum Residue

The analysis of the reaction kinetics of vacuum residue in Chapter 6 suggested that the reactions of the vacuum residue components were unexpectedly low. Here I examine the possible inhibition due to the presence of toluene, and present experimental data to test this hypothesis.

7.1 Effect of solvent

Khorasheh and Gray [14] studied thermal cracking of *n*-hexadecane in aromatic solvents at temperature range of 398 to 451°C and 13.9 MPa. They found that in the case of thermal cracking of *n*-hexadecane in benzene, the apparent first-order rate constants changed with the initial concentration of *n*-hexadecane in benzene, which indicates that the overall reaction order with respect to *n*-hexadecane was greater than 1. Khoraheh and Gray analyzed the literature data and concluded that the overall reaction order of thermal cracking with respect to the parent alkane can be less than 1, approximately equal to or greater than 1 depending on the reaction conditions of temperature and pressure.

The overall order of the reaction with respect to the concentration of *n*-alkanes depends on the order of the initiation reaction and on the type of radical combinations in the chain termination reactions [14]. For a first-order initiation reaction, the overall reaction order can vary between 0.5 to 1.5, depending on the concentration of β and μ radicals (Chapter 2). The concentrations of these radicals depend on the relative magnitude of two propagation steps of hydrogen abstraction and β-scission. At low temperature and high concentration (at high pressure), the parent radicals μ are the dominant radicals and the overall reaction order is 0.5. At high temperature and low alkane concentration when β radicals are dominant, the overall reaction order tends to 1.5 [14]. The interaction of solvent with the free radical chain of reactions can also change the overall order

of the reaction. Khorasheh and Gray concluded that "for a complex free-radical mechanism for thermal cracking of n-hexadecane in benzene, especially with solvent interactions, a simple power-law rate expression is not adequate to represent the observed kinetics over the range of conditions employed" in their studies. They emphasized on the interaction of benzene with the thermal cracking reactions of *n*-hexadecane; they stated "The presence of biphenyl as a major reaction product suggested that benzene cannot be considered as an inert diluent in thermal cracking of alkanes at relatively mild temperatures (400-450°C)". Indeed, the data that they presented demonstrate that as the initial concentration of the *n*-hexadecane in benzene increases, the rate constant increases from values which are first below the rate constants measured for pure *n*-hexadecane cracking to rate constant which are distinguishably higher than the rate constants for the case of pure *n*-hexadecane. If these reported higher rate constants are not affected by uncertainty of data, this trend suggests that as the concentration of *n*-hexadecane in benzene increases, benzene which initially has an inhibitive effect, gives an accelerating effect on the rate of thermal cracking at higher concentrations. Herbinet et al. [50], who studied thermal cracking of norbornane in benzene, accepted that the interaction with benzene did exist, but they found that at their operating condition ($600 < T < 700$°C and 106 kPa) the effect is negligible.

Khorasheh and Gray [14] also studied thermal cracking of *n*-hexadecane in toluene and ethylbenzene at the same operating conditions, which they applied to the experiments with benzene. They found that the apparent first order rate constants for cracking in the presence of toluene and ethylbenzene were less than when benzene was used or when pure *n*-hexadecane was used. They explained the slower rate of thermal cracking in toluene and benzene by suggesting that abstraction of benzylic hydrogen from the solvents would slow the chain reaction. The mechanism, which they suggested for inhibition of the rate, was reviewed in Chapter 2. The dominance of benzylic radicals was suggested to account for the significant product selectivities for alkylbenzenes formed by addition to α-olefins.

A simple kinetic model which includes the interaction of toluene with vacuum residue in a free radical chain reaction is given in Appendix E. It can be shown that the rate of thermal cracking of vacuum residue follows the form of the following equation:

$$-\frac{d[P]}{d\tau} = \frac{a_1}{[T]^2}[P]^2 + \frac{a_2}{[T]}[P]^{5/2} + a_3[P]^{3/2} \qquad (7.1)$$

in which P is the concentration of the parent reactant (vacuum residue), T is toluene, the constants a_i are functions of the rate constants for the elementary reaction steps, and τ is the mean residence time. By comparing Equation (7.1) with the first reaction order rate equation, the effect of toluene on the overall rate equation based on the concentration of vacuum residue can be summarized as the following:

1. A single overall- reaction order cannot be assigned to the reaction, but the apparent order of reaction tends to be higher than 1.5, and up to 2.5. This is consistent with the trend given in Table 6.7. A higher order of reaction gives a higher activation energy which is closer to the expected value; however, Table 6.7 also shows deterioration of the fit as the order of the reaction increases. This is also mathematically reasonable as Equation (7.1) suggests a complex function of concentration rather than the single power law relationship:

   $$r = k\,C^n \qquad (7.2)$$

2. Equation (7.1) shows that the rate of the reaction depends on the concentration of toluene, therefore the value of the apparent activation energy which is calculated for the first order reaction should be affected as the concentration of toluene was not considered. It can also be explained that based on the rate constants and concentration of toluene in

Equation (7.1) the value for the apparent over all activation energy which is calculated based on Equation (7.2) at n = 1, can be higher or lower than the expected activation energy (activation energy of higher n-alkanes). Equation (7.1) also shows that at higher concentration of toluene, the activation energy is less dependent of the concentration of the reactant. The concentration of toluene at which such effect can be observable is based on the rate constants of the elementary radical reactions. In this research however, the concentration of toluene was kept low in the carrier gas for technical reasons mostly related to the requirements of the atomization technique and the aerosols reactor, which were explained in earlier sections.

7.2 By products of toluene thermal reactions

The study of Khorasheh and Gray [14] and Lannuzel et al. [48] which was reviewed in Chapter 2, suggest that when toluene is used as the solvent for thermal cracking of *n*-hexadecane and *n*-octane, ethylbenzene should be observed as a by product of the inhibition mechanism. Pure toluene does not convert under thermal cracking easily. The yield of methane was measured by thermal cracking of pure toluene, at operating conditions similar to the experiments 700-1, 750-1 and 800-1. The results were compared with the yield of methane from thermal cracking of vacuum residue in toluene in those experiments. The data of Figure 7.1 demonstrate this comparison. The yield of methane from pure thermal cracking of *n*-hexadecane was negligible.

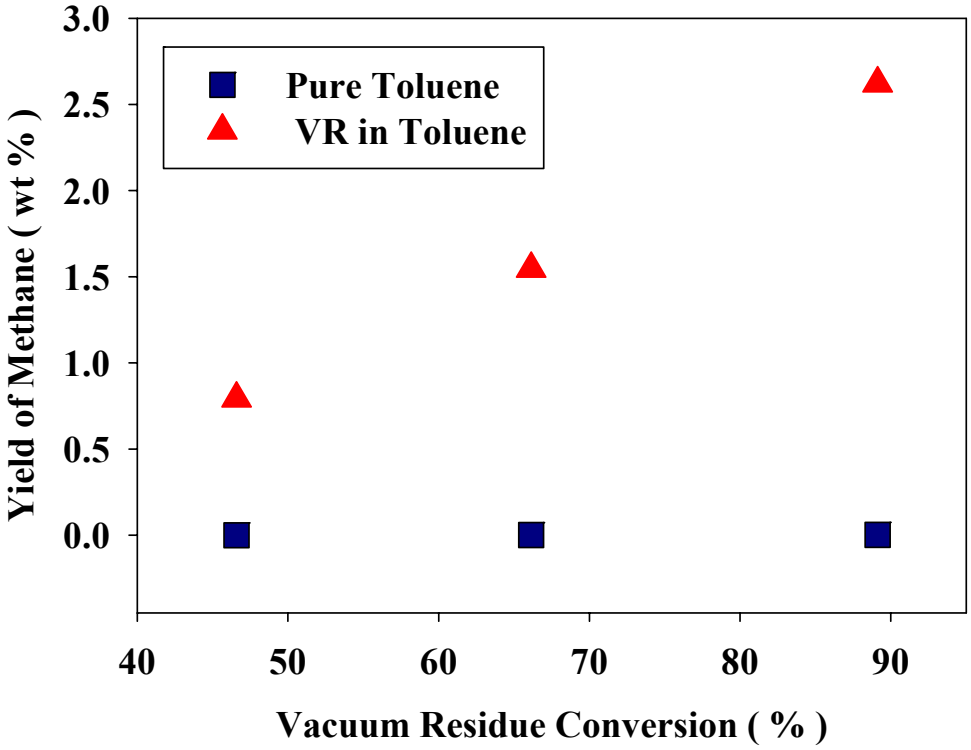

Figure 7.1 Comparing the yield of methane obtained by thermal cracking of pure toluene and in cracking of VR solved in toluene. The pure toluene was cracked at the same operating condition that VR was cracked and the result are plotted vs. the corresponding conversion from the experiment with VR .

The data of Figure 7.2 present the yields of benzene and ethylbenzene from thermal cracking of vacuum residue in experiments 700-1, 750-1, 750-2 and 800-1. Table 7.1 compares the yields of benzene and ethylbenzene when they are calculated based on toluene or feed(prepared Athabasca Vacuum Residue). If these components were derived from vacuum residue then they would be the significant product of thermal cracking. At a furnace temperature of 800°C, the yield of these products based on the initial weight of the feed are so high that they can be considered as the dominant product of the thermal cracking of vacuum residue, which cannot be true. These benzene and ethylbenzene yields are products of thermal cracking of toluene and by-products of interaction of this solvent with vacuum residue in the thermal cracking reaction.

Table 7. 1 Comparison of the yield of benzene and ethylbenzene, which are calculated on different basis

Experiment	Furnace T (°C)	Yield of benzene based on toluene (wt%)	Yield of benzene based on feed (wt %)	Yield of ethylbenzene based on toluene (wt %)	Yield of ethylbenzene based on feed (wt %)
700-1	700	0.11	2.04	0.15	2.90
750-1	750	0.28	5.30	0.44	8.35
750-2	750	0.30	5.71	0.47	8.98
800-1	800	1.04	20.57	0.68	13.50

The concentration of vacuum residue feed in toluene was only about 5 wt%, and much lower on a molar basis. The yields of benzene and ethylbenzene increase with conversion. However, the values of these yields were not high enough to affect the material balance on toluene. The yield of benzene and ethylbenzene, which were measured in experiment 750-1 and 750-2, are very close and represent the repeatability of the experiments at the similar operating condition. The major impurities of toluene were xylene and ethylbenzene, these impurities were recognized and corrected in calculating the yield of ethylbenzene which was produced by thermal cracking of toluene (or by interaction toluene with thermal cracking reactions). Indeed, the concentration of the impurities of the toluene were insignificant in the GC sample because they were highly diluted with dichloromethane at the time of measurement and the measureable concentration of ethylbenzene was due to the products of thermal cracking of toluene. The yield of benzene and ethylbenzene are defined by the amount of these component divided by the initial amount of toluene.

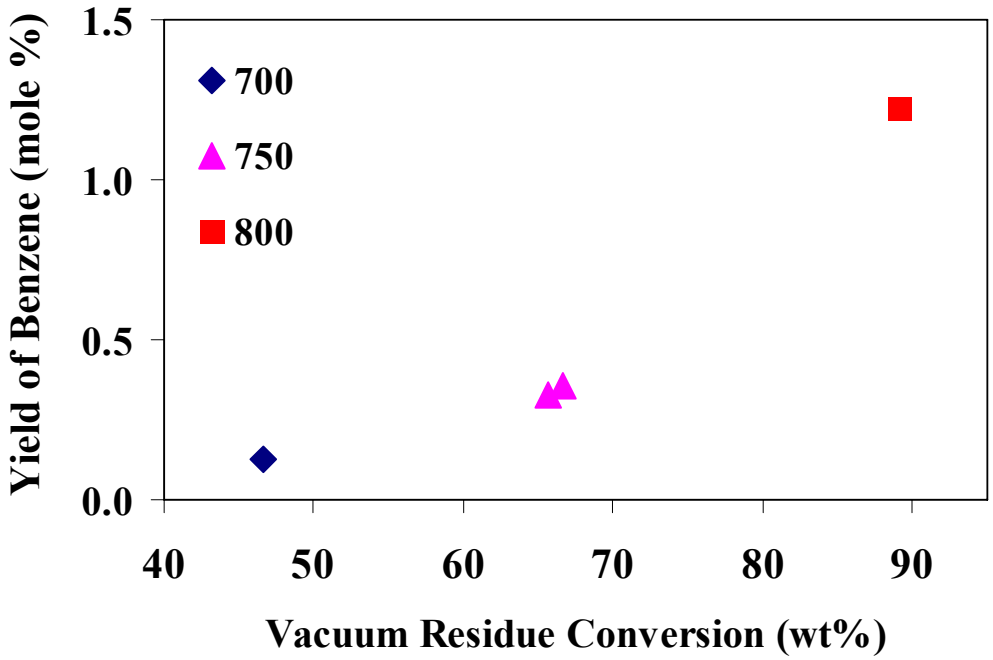

Figure 7.2 Conversion of toluene to benzene

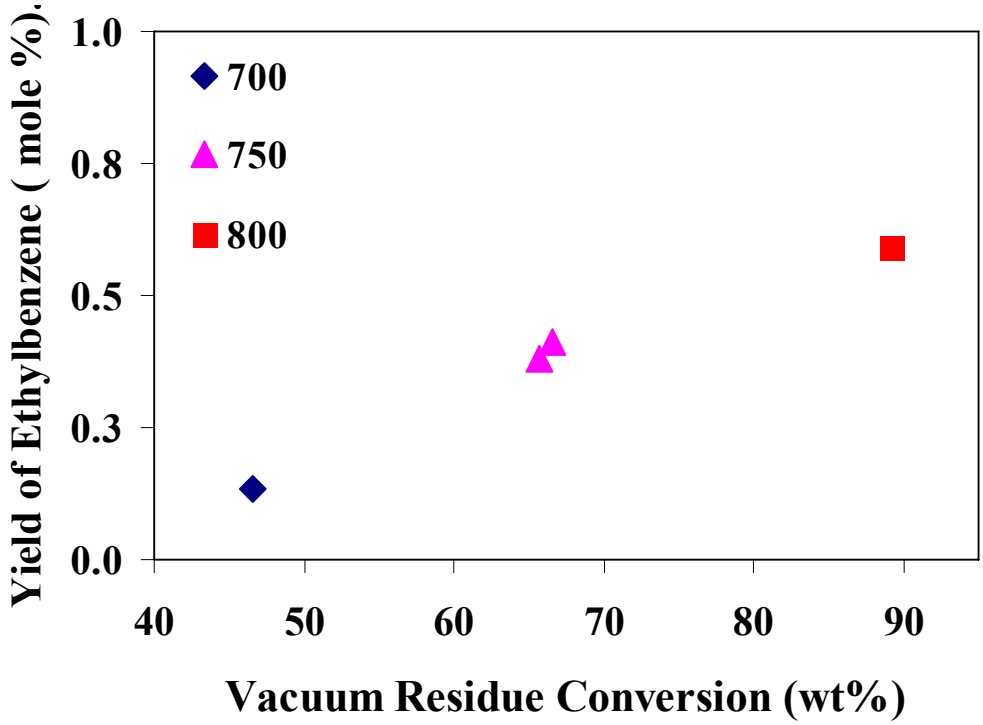

Figure 7.3 Conversion of toluene to Ethylbenzene

Benzene and ethylbenzene are the only measurable products of thermal cracking of toluene. Therefore, it was assumed that the conversion of toluene was equal to the sum of the yields of benzene and ethylbenzene. Figure 7.4 compares the conversion of toluene in experiment 700-1, 750-1 and 800-1 compared to conversion of pure toluene at the same operating condition. The conversion of pure toluene was calculated by use of the kinetic data from NIST Chemical Kinetics Database [32] and use of the non-isothermal reactor model which is explained in Appendix D. Figure 7.5 shows the ratio of conversion of the toluene when it is used as a solvent of vacuum residue in the above mentioned three experiments and when it is pure. It is obvious that conversion of toluene is significantly higher when it is mixed with vacuum residue. Therefore, it can be concluded that there are interactions between toluene and vacuum residue that accelerate the conversion of toluene. It is probable that these interactions may in turn decelerate or inhibit the conversion of vacuum residue.

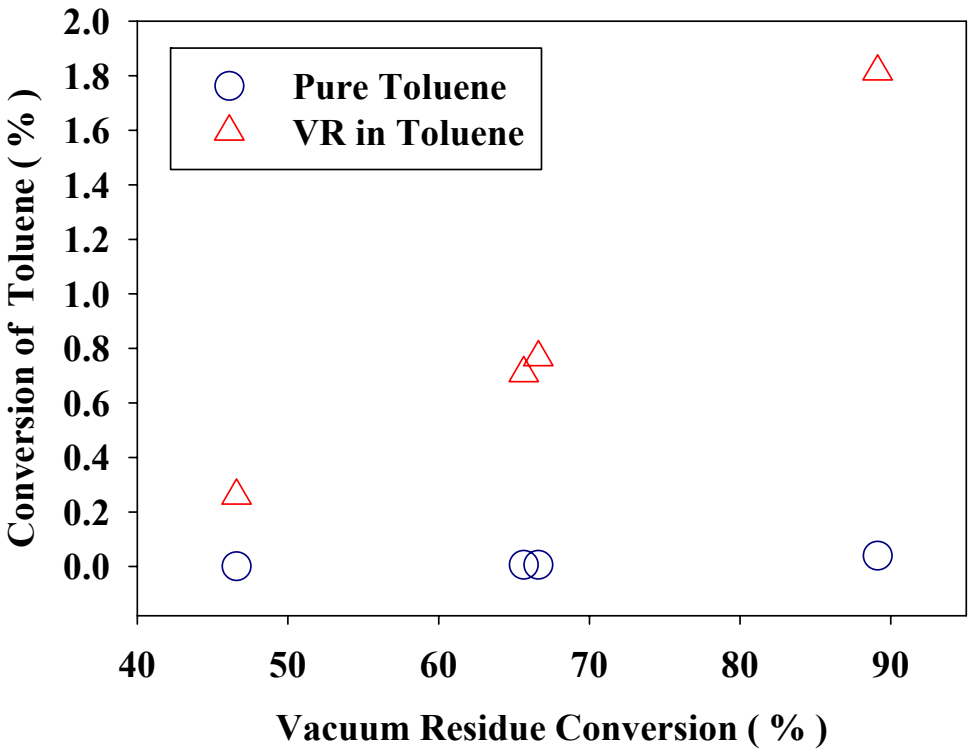

Figure 7.4 Conversion of toluene from cracking of VR by measurement compared with conversion of pure toluene from simulation at the same operating condition.

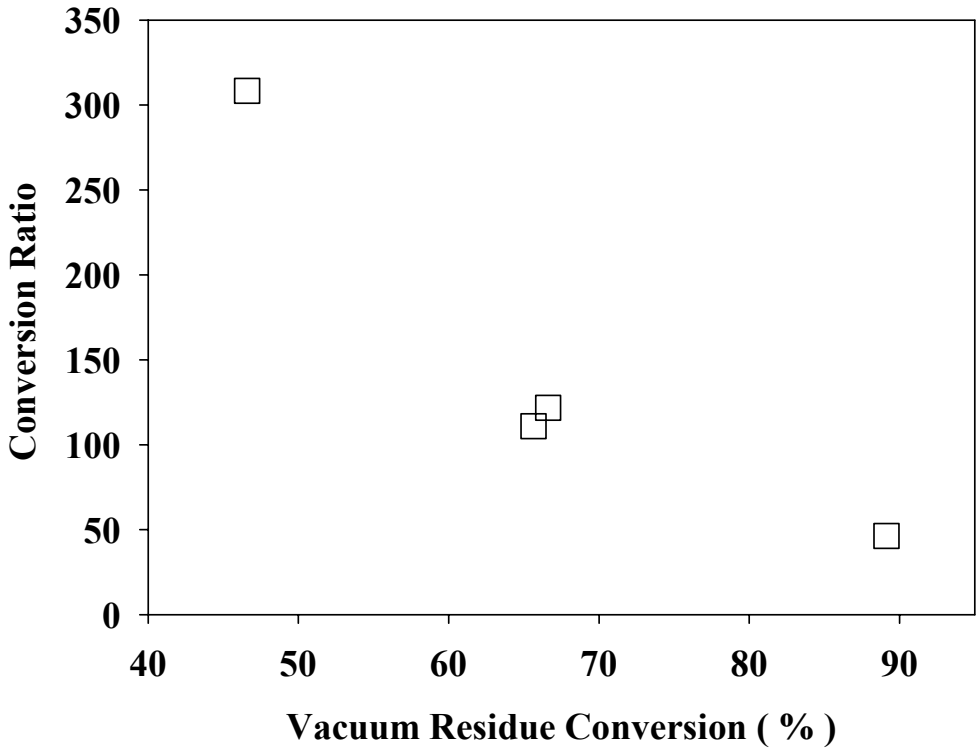

Figure 7.5 Ratio of conversion of toluene in presence of VR compared with thermal cracking of pure toluene at the same operating conditions

According to kinetic model of Lannuzel et al. [48] the following reactions can be responsible for production of benzene:

Unimolecular initiation reaction (thermal cracking of pure toluene):

$$\text{toluene} \leftrightarrow C_6H_5^{\cdot} + CH_3^{\cdot} \quad (7.3)$$

Ipso addition (thermal cracking of pure toluene)

$$\text{toluene} + H^{\cdot} \rightarrow C_6H_6 + CH_3^{\cdot} \quad (7.4)$$

Metathesis on a benzylic H Atom (thermal cracking of pure toluene)

$$\text{toluene} + C_6H_5^{\cdot} \rightarrow \text{benzyl}^{\cdot} + C_6H_6 \quad (7.5)$$

Reaction on alkenes (cross reaction toluene and n-octane)

$$n\text{-}C_8 + C_6H_5^{\cdot} \rightarrow \mu_8^{\cdot} + C_6H_6 \quad (7.6)$$

In can be assumed that *n*-octane in equation (7.6) represents aliphatic part of the vacuum residue The rise of concentration of $\mu_8^{\cdot}$ can increase production of $\beta^{\cdot}$

radicals through reaction (2.37) and (2.41), but through reaction (2.43) it can reduces the concentration of YH and increases the concentration of μH and Y˙. Therefore, without calculation for a specific operating condition ,it cannot be concluded that phenyl radicals has a direct accelerating or inhibitive role if I consider equation (2.53) for the case of low pressure / high temperature thermal cracking. Nevertheless, cross reaction (7.6), between n-octane, which represents aliphatic part of of VR, with toluene according to the kinetic model of Lannuzel et al. can be consider the cause of the extra measured yield of benzene compared with the case of pure thermal cracking of toluene.

Production of ethylbenzene in both cases of pure thermal cracking of toluene and thermal cracking of the mixture of toluene and *n*-alkane (vacuum residue in this case) is through the same reaction of

$$\text{benzyl}^{\cdot} + CH_3^{\cdot} \rightarrow C_6H_5CH_3 \qquad (7.7)$$

Methyl radical is generated through initiation and radical decomposition reactions in pure thermal cracking of n-alkanes. In a mixture of toluene and n-octane (*n*-alkane or in this case vacuum residue), the fact that the concentration of methyl radicals is higher than the case of thermal cracking of pure toluene, is consistent with higher yield of reaction. Components like propylbenzene and butylbenzene were not observed among the products of thermal cracking of vacuum residue in toluene. This result may be explained that at high temperature thermal cracking, radicals higher than methyl are favored to yield alkenes rather than react with benzyl radical to form alkylbenzyl molecules. Nevertheless, a significant yield of ethylbenzene compared to the case of pure toluene pyrolysis is an indication of interaction of toluene with vacuum residue which is consistent with the model of Lannuzel et al. for the case of *n*-octane cracking.

7.3 Investigation of the kinetic effect of toluene

The interaction of toluene with vacuum residue during thermal cracking could be investigated by injection of a feed solution of high concentration of vacuum

residue in toluene. This experiment was not possible because the atomization technique was limited to feed solution which were highly diluted with toluene (5 wt% VR or less in toluene). Therefore, it was decided to use n-hexadecane instead of vacuum residue to investigate whether toluene could show any inhibitive effect at such diluted concentration inside the reactor at the conditions of this study. Although, *n*-hexadecane is not a representative of the structure of vacuum residue, it can partly represent the aliphatic bonds in the structure of feed. The initial concentration of the toluene in helium in the reaction tube varied from 0.28 to 0.36 mole % in different experiments. The initial concentration of the vacuum residue in helium at the inlet of the reaction tube varied from 2.5×10^{-3} to 3.0×10^{-3} mole %. The molar ratio of feed to toluene varied from 114 to 126 in different experiment with vacuum residue. The middle furnace temperature, that is 750°C, was selected and the same operating conditions of the experiment 750-1 were applied, one time with pure n-hexadecane and one time with n-hexadecane which were diluted with toluene to the same ratio molar ratio of vacuum residue to toluene in 750-1 experiment.

In order to replicate the operation and product recovery of experiment 750-1, the same cryogenic condenser was used. Because the large volume of this condenser, the related tubes, and hoses, large amount of dichloromethane (1.5 to 1.7 liter) were used to wash out the products completely. Because of high dilution of *n*-hexadecane in dichloromethane, measurement of the concentration of this component and therefore its conversion was subject to a significant uncertainty of measurement. In order to eliminate any obvious source of uncertainty from the method of measurement, it was decided to only measure the yield of gas components and the total yield of gas. GC analysis of the gas sample is the most precise measurement among all the analytic measurements in this study. The experiments were repeated three times with pure *n*-hexadecane and three times with diluted *n*-hexadecane with toluene. With the exception of methane, toluene caused a significant reduction in yield of gas components and the yield of total gas. The conversion were not calculated directly, however, the yield of total gas is

representative of a significant portion of the conversion and a significant decrease in the yield of total gas products reflects a significant reduction in conversion of *n*-hexadecane. It is unlikely that for a vapor phase cracking at high temperature and low pressure, even in presence of toluene, the reduction of the yield of total gas can be compensated by increase in yield of liquid products due addition reactions or a shift of selectivity to generate heavier α-olefins which are liquid at room temperature. Figure 7.6 and Figure 7.7 demonstrate these results for yields of total gas and ethene between these two sets of the experiments.

A t-test was performed to see that the average value of the yield values in each two group could be distinguished as significantly different when 95% uncertainty level of the data were considered. The results of the t-test are given in detail in Appendix F. According to the result of this test, it could not be concluded that there is a significant difference between the yields of methane for two set of the experiments. However, for all of the other components and the yield of total gas there was a significant difference between the yield values of the two set of the experiments. Thus, a possible explanation for low rate of thermal cracking reaction in this research is inhibition of the rate by bimolecular reactions with toluene, likely via benzyl radicals.

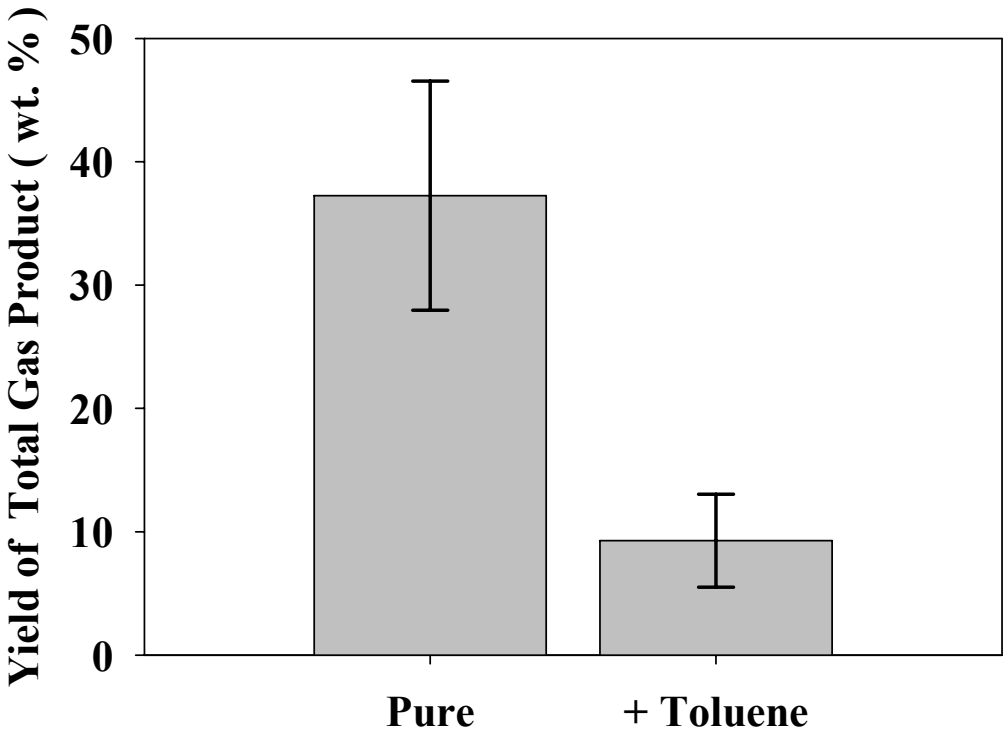

Figure 7.6 Yield of total gas in thermal cracking of pure *n*-hexadecane and its solution with toluene. The operating condition and the molar ratio of toluene to n-hexadecane is the same as experiment 750-1. The error bars indicate the standard deviation of the yield values.

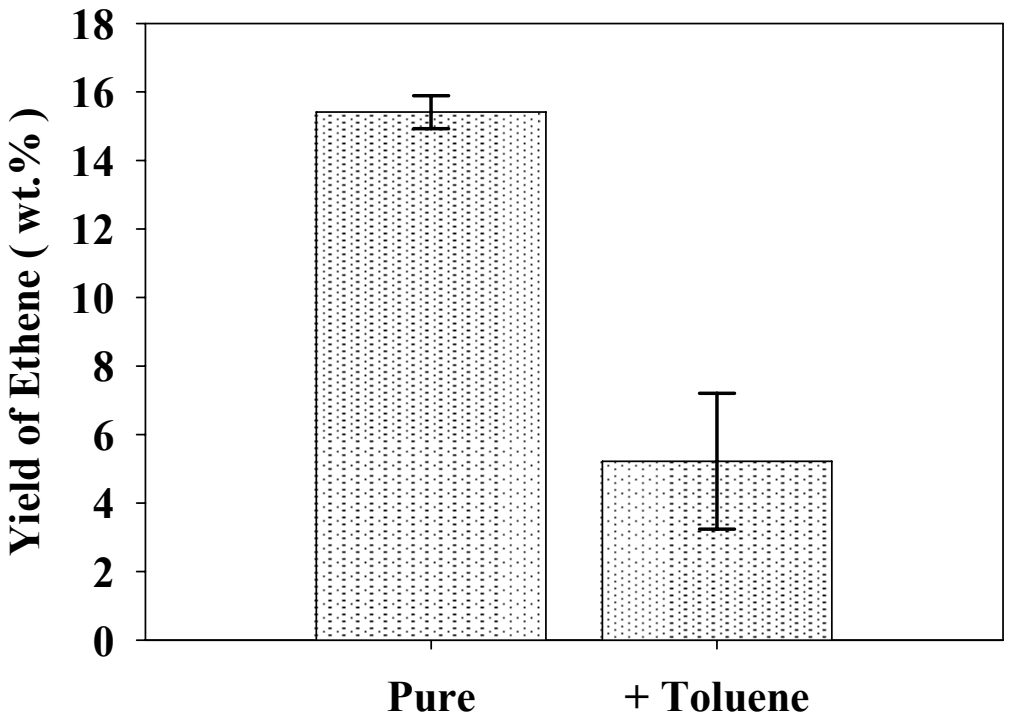

Figure 7.7 Yield of ethene in thermal cracking of pure *n*-hexadecane and its solution with toluene. The operating condition and the molar ratio of toluene to n-hexadecane is the same as experiment 750-1. The error bars indicate the standard deviation of the yield values.

For the case of thermal cracking of the mixture of *n*-hexadecane and toluene, the average yield of total gas is 9.3 %. For vapor phase thermal cracking it is very unlikely that the yield of the liquids were so high that the conversion of *n*-hexadecane exceeded 30 %. In Chapter 2, the study of Lannuzel et al. [48] on thermal cracking of the mixture of n-octane and toluene, and the mechanisms that they suggested for the inhibition of the rate of thermal cracking were reviewed. In all the experiments on thermal cracking of vacuum residue, the conversion exceeds 40%. According to the mechanism that Lannuzel et al. reported for the case of mixture *n*-octane with toluene, above conversion of 30 %, the inhibition of the rate should be insignificant. However, the inhibition of the rate of thermal cracking was significant for the case on n-hexadecane mixture with toluene at the applied operating condition. It should be noted that *n*-alkanes are not a

representative of the chemical structure of vacuum residue. Based on the result of these experiments, it can be assumed that toluene contributed to slow down the rate of thermal cracking of vacuum residue in this study, nevertheless it cannot be concluded that the intensity of such inhibition be the same as for the case of *n*-hexadecane .

The conversion of the pure *n*-hexadecane in this experiment can be calculated by use of kinetic parameters which were derived in Chapter 4 by the non-isothermal reactor model for experiment 750-1. This calculation gives a conversion of 50%, which is consistent with the measured yield of produced gas by thermal cracking of pure *n*-hexadecane in this experiment and consistent with the ratio of the yield of gas to conversion which is given in Chapter 4. For the case of thermal cracking of n-hexadecane mixture with toluene, the conversion can be approximated by assuming that toluene does not change the selectivity of the distribution of gas and liquid products. Toluene may inhibit the rate of thermal cracking , but it is unlikely to make a dramatic change in the distribution of gas and liquid products at a high of 750°C when thermal cracking occurs in the vapor phase. The conversion of the mixture for the average yield of gas of 9.3 % is approximated 20.8%. The inhibition factor, which is defined by equation (2.35), for this conversion is 2.4. If I consider the uncertainty of the measurement of the yield of gas in the replicate experiment, the standard deviation of the approximated values for inhibition factor can be calculated as 0.79. The approximation of the yield of liquids or conversion from the yield of gas based on the data from pure n-hexadecane , and the assumption that toluene does not affect distribution of the gas and liquid products are the major source of uncertainty in these approximations. Figure 7.8compares the results of this study with the mixture of n-hexadecane and toluene at furnace temperature of 750°C and operating condition of the experiment 750-1 with the study of Lannuzel et al. [48]. The significant inhibition of toluene at higher conversions, which is inconsistent with the results of Lannuzel et al., can be due to the higher reaction temperature which was applied in this study. Besides the difference in pressure, the data of Lannuzel

et al. indicates an increase in inhibition factor with temperature. Increasing the temperature from 500 to 750 °C in the Lannuzel et al. work , they would achieve a trend which could be fit to the inhibition factor which were calculated in this study.

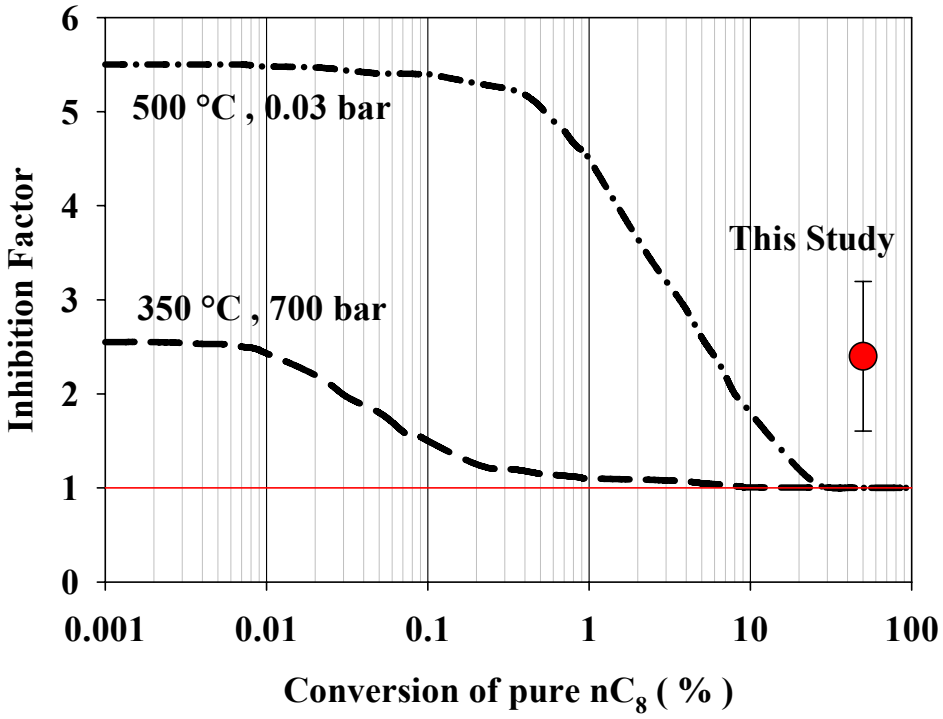

Figure 7.8 Comparison of the approximated inhibition factor in this work with mixture of *n*-hexadecane and toluene with the results of Lannuzel et al [48] . The error bars represent the standard deviation of inhibition factor calculated for the repeated experiments.

The inhibition factor can be approximated by calculation of the ratio of the conversion which is predicted by Model 1 from this study and the conversion that the Radmanesh et al. [75] model predicts. It should be noted that the reactor design and operation conditions of these two studies were quite different. Such an approximation can help only if it demonstrates a very significant trend. The conversion ratios for the heavy residue were calculated at residence time of 4 ms and for the light residue at 30 ms. These values of residence times were selected to let both models give conversion values below 100 % and above zero. Heavy

residue is defined as the fraction with boiling point of 650°C+ and light residue by the fraction with boiling point range of 524 to 650°C. In Figure 7.9 the results were compared with the inhibition factor which is approximated based on the data from the experiments with mixture of toluene and n-hexadecane. The inhibition of the rate by toluene for the case of n-hexadecane is significantly closer to the inhibition of the rate of thermal cracking of light residue. The inhibition of the rate of thermal cracking for the heavy residue is

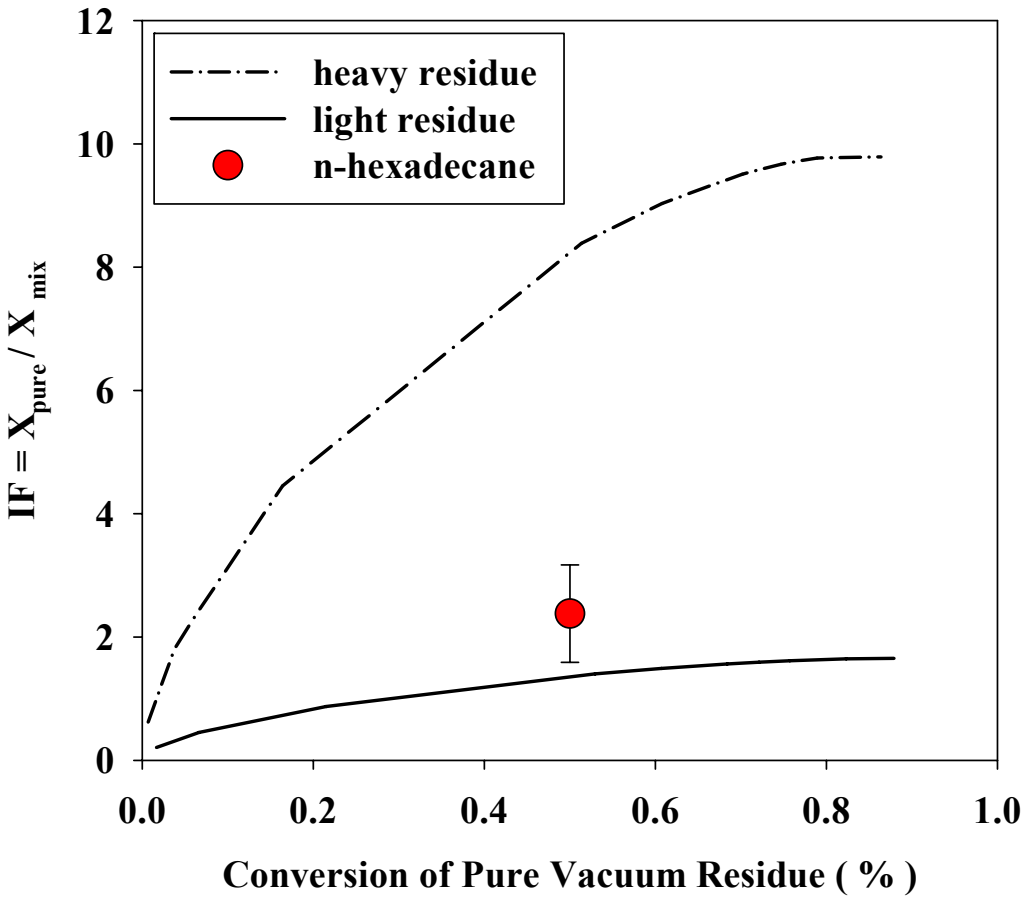

Figure 7.9 Comparison of the inhibition factors (IF) , that is ratio of conversion of pure vacuum residue (Xpure) to conversion of mixture of vacuum residue (Xmix). The ratios were calculated by the use of kinetic parameters from the work of Radmanesh , Chan ,and Gray [75] and kinetic Model 1 from this study. The ratios for the heavy residue was calculated at residence time of 4 ms and for the light residue at 30 ms . The solid circle shows the value of the inhibition factor (IF) which were calculated for mixture of n-hexadecane and toluene. Heavy residue is defined as the fraction with boiling point of 650°C+ and light residue by the fraction with boiling point range of 524 to 650°C.

much higher than the inhibition factor for the mixture of n-hexadecane and toluene. The light residue naturally has more aliphatics than the heavy residue. While the aliphatic bonds can undergo thermal cracking reactions, the aromatic structure cannot undergo non-catalytic cracking reactions. Therefore, it is expected that the inhibition of the rate which is approximated for n-hexadecane is close to that predicted for light residue. The significantly higher rate of inhibition which is estimated for the heavy residue portion suggests that other factors beside the effect of solvent can be involved.

7.4 Low values of the activation energy and rate of thermal cracking

A lumped kinetic model does not represent all the elementary free radical reactions. In this case, I expect that toluene solvent interacts with other radicals in the thermal cracking reaction. The activation energies which were calculated cannot be representative of the activation energy of a certain chemical bond. In Section 7.1, it was shown that a simple kinetic model which consider the interaction of solvent can justify the conclusion that toluene can affect both overall order and activation energy of the reaction. Figure 7.9 demonstrates that the inhibition of the rate for the heavy residue (650°C +) is estimated to be much higher compared with the light residue (524 to 650°C). The inhibition factor, which is approximatly based on the experiments with mixture of *n*-hexadecane and toluene, indicates a much lower level of inhibition compared with the inhibition factor for the heavy residue fraction. This figure is an approximation; however, it suggests an interesting trend. The heavier the fraction is, the higher the inhibition factor will be. In addition, the higher the conversion, the higher will be the inhibition factor. As the thermal cracking of vacuum residue proceeds, the aliphatic portions which can undergo non-catalytic thermal cracking is consumed and leaves the heavy PAH which does not undergo thermal cracking reaction. This suggests that at higher conversion a different rate and apparent activation energy can be expected. Additionally, it should not be expected that the value of the apparent activation energy in thermal cracking of vacuum residue, especially

at higher conversions, to be comparable with the activation energy of the *n*-alkanes.

For a first order reaction, the rate of reaction (not the rate constant) depends on the concentration of the feed. If a portion of the aliphatic part of the feed turns to products which increase the amount of high boiling point fraction, and therefore compensate reduction of the boiling point by production of more aromatics, then the rate of thermal cracking would be measured at a lower rate than expected. The conversion is calculated by measuring the change of the boiling point of the liquid products. Dehydrogenation of naphthenic groups can occur under non-catalytic thermal cracking conditions. For example, tridecylcyclohexane under thermal cracking gives toluene as a significant product [78]. Partially hydrogenated aromatics in vacuum residue can be dehydrogenated in reactions with olefins [8]. Zhao et al. who studied thermal cracking of asphaltenes described the role of cyclization of alkyl chains and dehydrogenation of naphthenic rings as the steps toward formation of coke [79]. The work of Zhorov and Volokhova [49] about the effect of PAH contents of gas oil and kerosene on the yield of products was reviewed in Chapter 2. They experimentally verified the effect of PAH contents of gas oil and kerosene in decreasing the yield of products, which they referred to as a self-inhibition action. Zou et al. [17], who studied thermal cracking of atmospheric gas oil in the temperature range of 790 to 935°C and atmospheric pressure, reported that thermal cracking of atmospheric gas oil shows a self-inhibition of rate especially at higher conversion. They did not use a solvent with their feed in their experiments. They suggested the following empirical equation to consider the effect of conversion on the rate constant:

$$k_F = \frac{k_0}{1+\alpha X} \tag{7.8}$$

in which :

$$k_0 = A \exp\left(-\frac{E}{RT}\right) \tag{7.9}$$

$$\alpha = 3.50 \times 10^5 \exp\left(-\frac{10367}{T}\right) \tag{7.10}$$

by this definition they calculated the overall activation energy and pre-exponential factor for thermal cracking of feed into the products as 213.4 kJ/mol and 4.52 × 10^{11} (s^{-1}) respectively.

Su et al. [80] studied thermal cracking of light gas oil in the temperature range of 670 to 760°C and atmospheric pressure. They reported a self-inhibition effect of the products on the rate of thermal cracking of light gas oil and suggested the same equations as (7.8) and (7.9) with different values for the parameters which are given in Equation(7:11)

$$\alpha = 6.39 \times 10^8 \exp\left(-\frac{18529}{T}\right) \tag{7.11}$$

They calculated the overall activation energy and pre-exponential factor for thermal cracking of feed into the products as 287.0 kJ/mol and 8.59 × 10^{15} s^{-1} respectively. For the range of temperature and residence time (conversion) which these researchers applied in their experiments, the activation energy which they could calculate, based on the Arrhenius relationship between rate constant and temperature, were as follows. For the study of Zou et al., the activation energy should be in the range of 70 to 110 kJ/mole and the pre-exponential factor varies from 1.7 × 10^4 , 3.5 × 10^5 s^{-1}, repectively. For the study of Su et al.the activation energy of about 87 kJ/mole and the pre-exponential factor of 2.4 × 10^5 s^{-1} was estimated. These values of activation energy and pre-exponential factor are in range with the activation energy and pre-exponential factor of Model 1, 85.8 kJ/mol and 3.8 × 10^5 s^{-1} and kinetic parameters of Model 2 which are given in Table 6.4.

Review of the NMR and elemental analysis results in the earlier sections in this chapter show that the aromaticity of the liquid products were significantly higher than the feed and the liquid products were deprived of their hydrogen content. These all suggests that the lower measured rate of thermal cracking in this research may not be entirely due to the interaction of toluene. There could be a significant series of reactions which compete with simple thermal cracking of aliphatic bonds. Cyclization and dehydrogenation reactions could be considered as such reactions which compete with thermal cracking in consumption of the aliphatic portion, yet do not contribute to a reduction of boiling point of the products.

7. 5 Conclusion

The rate of thermal cracking and the activation energy of Athabasca vacuum residue in this study were both below the value which is predicted by Gray et al. [36] and below the values which were calculated for *n*-hexadecane in Chapter 4. This result could be because of the interaction of toluene with the free radical chain reactions of thermal cracking of vacuum residue. Thermal cracking of a mixture of *n*-hexadecane with toluene in similar concentrations and operating condition for the case of thermal cracking of vacuum residue, showed a significant reduction of the yield of gas products compared with the case of thermal cracking of pure n-hexadecane. Vacuum residue could not be used for this test because of the limitations of the atomization techniques. The approximate inhibition factor could not be generalized from the case of *n*-hexadecane – toluene mixture to the case of vacuum residue cracking. However, this experiment suggested that toluene should have a significant impact on the rate of thermal cracking of vacuum residue.

The literature suggests other mechanism for lower measured rate of thermal cracking like self-inhibition of the rate due to the effect of the aromatic contents of the feed and olefin products. The change in the nature of the structure and chemical bonds of vacuum residue at higher conversion could also be a reason. It

is possible that cyclization and dehydrogenation reactions of aliphatic bonds compete with thermal cracking of this part of the feed, that is the only portion which can go under non-catalytic thermal cracking. Thus, it could not be concluded that the low rate of thermal cracking and the low value for the calculated activation energy is entirely due to inhibition by toluene before the internal effect of the structure and the products on the rate of thermal cracking are understood.

Chapter 8
Conclusions and recommendations

There are two challenges in kinetic studies of heavy oils at high temperatures, which were discussed in the literature. At high temperature, the rate of thermal cracking is fast; therefore, the reactants should be brought to the reaction temperature in a short time to avoid significant conversion taking place below the reaction temperature. The other problem is the complexity of a heterogeneous reactive gas, liquid and solid system to study. In fluidized-bed reactors, formation of solid-liquid agglomerates increases the diffusion path of the volatile products which accentuate their involvement with addition reactions which can eventually result in a rise in the yield of coke. In order to study the intrinsic kinetic of such systems the effect of heat and mass transfer resistance should be taken into account. In this research, these two problems were addressed.

In order to minimize the rise time of the reactant to the reaction temperature, the technology of micro-structured mixers was investigated. A stream of cold helium, which carried the feed, was mixed with a stream of hot helium to bring the mixture, which continuously flowed inside a tubular reactor to the reaction temperature within a few milliseconds. The short temperature rise time made this reactor close to an ideal isothermal reactor. The maximum deviation from the average fluid temperature along the reactor was only 4.5°C. This reactor was used to study rate of thermal cracking of *n*-hexadecane in the range of 600 to 750°C and atmospheric pressure. The activation energy and the pre-exponential factor of Arrhenius equation for the overall first order reaction was calculated as 235 kJ/mole and 1.13×10^{13} s^{-1}, respectively. The results of the study were consistent with most of the reports in the literature for thermal cracking of *n*-alkanes.

An aerosol reactor was developed to minimize the effect of heat and mass transfer, which interfered the kinetic study of the thermal cracking of heavy oils. The atomization technique took advantage of the high temperature and flow of the

additional make-up gas inside the reactor, therefore a non-isothermal tubular flow reactor was selected to match the atomization technique. Much of the effort of this research was focused on developing the atomization technique. It was not possible to atomize the vacuum residue outside of the reactor, and then introduce an aerosol of feed droplets with a verified size distribution into the reactor. After considerable efforts, it was found that the high tendency of the fine droplets of the vacuum residue (which were dissolved in toluene) to coalesce was responsible, and this effect was independent of the technique of atomization.

The rate of thermal cracking of Athabasca vacuum residue, which was dissolved in toluene, was studied at 700 to 800°C at atmospheric pressure and mean residence time of 100 to 115 ms, by this reactor. The average yield of coke was 6.3 wt%, and the measured yield of coke was found to be insensitive to the conversion of the vacuum residue. The average size of the coke particles was smaller than 190 nm. Based on the average diameter of the coke particles and the yield of coke, the generated feed particles were submicron droplets.

Using aerosolized feed generated within the reactor, the yield of coke is reduced to a minimum, which was predicted by previous researchers as the intrinsic coke yield. Introduction of feed as submicron droplets at a very dilute concentration in helium enhanced the vaporization of liquid fractions at temperatures much below their boiling point temperature. The minimization of fractions in the liquid phase at the reaction temperature in turn caused minimization of the yield of coke. Given the prevalence of the thermal cracking reaction in the vapor phase, the results showed high yields of olefins. The total yield of ethene and propene alone ranged from 5 to 18 wt% which were respectively 19 to 30 times higher than the total of ethane and propane. Ethene and propene together formed 47 to 65 wt% of the total gas products. These results are consistent with prevalent thermal cracking in vapor phase and indicate the enhanced vaporization of feed through generation of submicron droplets of vacuum residue.

The rate of thermal cracking of the vacuum residue in toluene was found to be slower than the rate which extrapolation of the work of previous researchers predicted. In addition, the calculated value of the apparent over all activation energy was much lower than the value of the activation energy which was predicted by the previous researchers and the activation energy of *n*-alkanes for cracking of C-C bonds. The atomization technique did not enable change in the concentration of the vacuum residue in toluene, therefore the effect of toluene on *n*-hexadecane at the same operating condition and different concentration was studied. The experiments showed that toluene reduced by four times the yield of the total gas products, compared with thermal cracking of pure *n*-hexadecane at furnace temperature of 750°C. The suppression of the rate of thermal cracking and the calculated low activation energy were consistent with the interaction of toluene with the free radical chain reactions to form benzyl radicals. However, other competitive reactions like cyclization and dehydrogenation could have a role in slowing down the rate. The rate of thermal cracking is measured based on the reduction of the vacuum residue portion, which were defined based on the boiling point range. Cyclization of the linear aliphatics followed by dehydrogenation could add to the high boiling point fraction, while consuming the fractions which could undergo non-catalytic thermal cracking.

As explained in Chapter 7, the researchers who studied the rate of thermal cracking of gas oil without use of any aromatic solvents, had to devise empirical equations to avoid a low value for the apparent activation energy or an unexplained low overall rate of thermal cracking. These researchers claimed a self-inhibition effect in thermal cracking of gas oil, especially at higher conversions. This idea that the overall apparent activation energy of thermal cracking of vacuum residue should be the same as that of higher n-alkane should be re-examined. The same applies to the idea that the heavier the oil is the faster should be the rate of thermal cracking. Replacing toluene with benzene could help with this re-examination. However, an easier task is to measure the overall rate of thermal cracking of heavy gas oil based on a first order reaction and a power law

relationship between the rate constant and the concentration, and to see if the calculated apparent activation energy would be the same as n-alkanes.

Based on the results of this research, the following can be recommended for further study on thermal cracking of heavy oils:

1. In this study it was shown that generation of submicron feed droplets can reduce the yield of coke to approach the intrinsic coke value. The efforts in developing the atomization technique indicated the high tendency of these fine feed particles to coalesce and form larger droplets. In industrial fluidized bed reactors, in addition, solid-liquid agglomerates are formed which direct more liquid products to yield coke. Therefore, a useful line of study could be improving the atomization techniques to first generate smaller droplets of the feed, and then to maintain the fluid flow in a manner to minimize the coalescence of the feed particle. In such condition, smaller coke particles should form which in turn could result in formation of fewer solid –liquid agglomerates.

2. Use of benzene is expected to eliminate the inhibitive effect of toluene on the rate of thermal cracking, but it does not guarantee to measure an apparent activation energy the same as *n*-alkanes or the values which are calculated by previous researcher for thermal cracking of vacuum residue at lower range of temperatures. It should also be remembered that although benzene is regarded as an stable solvent at high temperature (below 700°C) it is not considered entirely as an chemically inert solvent according to the literature. Replacing of toluene with benzene requires extensive safety revisions. Therefore, the best first step in continuing this research is to study high temperature thermal cracking of gas oil without addition of any solvent and to compare the apparent activation energy of gas oil with n-alkanes and the thermal cracking studies on vacuum residue at lower range of temperature.

References

[1] Energy Resources Conservation Board, Alberta's Energy Reserves 2007 and Supply/Demand Outlook 2008-2017, 2008, ECRB ST98-2008 (Cross reference from Gray, M. R. , Fundamentals of Oil Sands Upgrading , 2011)

[2] M. Radler, Global reserves, oil production show small increases for 2005, Oil & Gas Journal, 2005, December 19, 20-22

[3] Rice, F.O. and Herzfeld, K.F. The thermal decomposition of organic compounds from the standpoint of free radicals,VI. The mechanism of some chanin reactions, Journal of the American Chemical Society, 1934, 56, 284-289

[4] Kossiakoff, A. and Rice,O.R. Thermal decomposition of hydrocarbons, resonance stabilization and isomerization of free radicals, Journal of the American Chemical Society ,1943,65, 590-595

[5] Gray, M. R. , McCaffrey, W.C., Role of chain reactions and olefin formation in cracking, hydroconversion, and coking of petroleum and bitumen fractions, Energy and Fuels, 2002,16,756-766

[6] Dente, M. E. and Ranzi, E. M., (Editors : Albright, L. F., Crynes, B.L. and Corcoran , W. H.), Mathematical modeling of hydrocarbon pyrolysis , Chapter 7, Pyrolysis: Theory and industrial practice, 1983, Academic Press,

[7] Gonzalez Delgado, P.R., Mechanisms of aerosol formation in bitumen cracking, 2004, MSc Thesis, University of Alberta

[8] Gray, M.R., Upgrading petroleum residues and heavy oils, Marcel Decker: New York, 1994

[9] Khorasheh F. and Gray M. R., High-pressure thermal cracking of n-hexadecane, Industrial Engineering Chemistry and Research, 1993, 32,1853-1863

[10] Wu, G., Katsumura, Y., Matsuura, C. and Ishigure, K., Comparison of liquid –phase and gas-phase pure thermal cracking of n-hexadecane, Industrial Engineering Chemistry Research , 1996,35,4747-4754

[11] Goncalves M.A, Ribeiro D. A., Teixeira A. R. F. and Teixeira M.A.G.,Influence of asphaltenes on coke formation during the thermal cracking of different Brazilian distillation residues, Fuel, 2007, 86 ,619-623

[12] Wiehe, I. A., A phase – separation kinetic model for coke formation, Industrial Engineering Chemistry Research, 1993, 32, 2447-2454

[13] Alshareef A. H., Scherer A., Tan X., Azyat K., Stryker J. M., Tykwinski R.R., and Gray M.R., Formation of Archipelago structures during thermal cracking implicates a chemical mechanism for the formation of petroleum asphaltenes, Energy and Fuels, 2011, 25, 2130-2136

[14] Khorasheh, F. and Gray, M. R., High pressure thermal cracking of n-hexadecane in aromatic solvents, Industrial Engineering Chemistry Research, 1993, 32, 1864-1876

[15] Lu, M. and Mulholland, J. A., Aromatic hydrocarbon growth from indene, Chemosphere ,2001, 42, 625-633

[16] Gray, M.R., Le, T., McCaffrey, W.C., Berruti, F. , Soundararajan, S., Chan, E., Huq,I. and Thorne C. , Coupling of mass transfer and reaction in coking of thin films of an Athabasca vacuum residue, Industrial and Engineering Chemistry Research, 2001, 40,3317-3324

[17] Zou, R., Lou, Q., Mo, S. and Feng, S., Study on a kinetic model of atmospheric gas oil pyrolysis and coke deposition, Industrial Engineering Chemistry Research, 1993, 32, 843-847

[18] Le Page, J. F., Chatila, S.G. and Davidson, M., Resid and heavy oil processing, 1992, Éditions Technip

[19] Rana, M. S., Samano,V. ,Ancheyta and Diaz,J.A.I. , A review of recent advances on process technologies for upgrading of heavy oils and residua, Fuel, 2007, 86, 1216-1231

[20] Joshi,J. B., Pandit, A.B., Kataria, K.L., Kulkarni, R. P. , Sawarkar, A.N. , Tandon, D., Ram, Y. Kumar, M. M. , Industrial Engineering Chemistry Research, 2008, 47, 8960-8988

[21] Vogiatzis, A. L., Briens,C. L. and Bergougnou, M.A. ,Selected applications of ultra-rapid fluidized (URF) reactors, Ultrapyrolysis of heavy oils and ultra-rapid catalytic cracking, AIChE Symposium Series, Fluidization and fluid particle systems: fundamental and applications, 1989, 85,270, 69-76

[22] Laidler, K.J. and Wojciechowski, B.W., Kinetics of thermal decomposition of propylene,and of propylene-inhibited hydrocarbon decompositions, Proceedings of the Royal Society of London, 1960, A259, 257

[23] Laidler, K.J., Sagert, N.H. and Wojciechowski, B.W., Kinetics and mechanism of the thermal decomposition of propane, I. The uninhibited reaction, Proceedings of the Royal Society of London, 1962, A270,242

[24] Kershenbaum, L.S. and Martin, J.J, Kinetic of the nonisothermal pyrolysis of propane, A.I.C.h.E. Journal, 1967, January, 148

[25] Depeyre, D., Flicoteaux, C. and Chardaire, C., pure n-hexadecane thermal stream cracking, Industrial and Engineering Chemistry Process Design and Development, 1985, 24, 1251-1258

[26] Bajus M. , Vesely V. , Leclercq, P. A. and Rijks J. A., Steam cracking of hydrocarbons. 1. Pyrolysis of heptane, Industrial Chemical Production Research and Development, 1979, 18, 1, 30-37

[27] Bartekova, E. and Bajus, M., Pyrolysis of hexadecane, Collection of Czechoslovak Chemical Communications, 1997, 62, 1057-1069

[28] Billaud, F. , Ajot, H. and Freund, E. Unite Micropilote Pour L'Etude De Charges De Vapocraquage, Example D'Un Melange De Normales Paraffines : Micropilot Plant for the study of Steam-cracking Feedstock.Example of a Mixture of Noraml Parafins, Revue De L'Institute Francais Du Petrole, 1983, 38,6, November-December, 763-781

[29] Rastogi, A., Svrcek, W.Y. and Behie, L. A., Novel microreactor with quench system for kinetic study of propane pyrolysis, AIChE Journal, 1988, 34, 9, 1417-1422

[30] Rastogi, A., Svrcek, W.Y. and Behie, L. A., The importance of temperature rise time in pyrolysis kinetic studies, The Candian Journal of Chemical Engineering, 1988,66, April, 303-306

[31] Fairburn, J. A., Behie, L.A. and Svrcek W. Y., Ultrapyrolysis of n-hexadecane in a novel micro-reactor, Fuel,1990, 69, December, 1537-1545

[32] NIST chemical kinetic database, http://kinetics.nist.gov/kinetics/index.jsp, visited in April 2012

[33] Heilman, H. H. ,High temperature thermal cracking of petroleum fractions, World Petroleum, 1947, 18 (12), 86-88

[34] Tan, Z. , Measurement of the reaction kinetics for the ultrapyrolysis of Alberta Heavy Oils, PhD Thesis, Department of Chemical and Petroleum Engineering, University of Calgary, 1993

[35] Billaud, F.; Berthelin, M. and Freund, E. ,Thermal cracking of vacuum distillates, Journal of Analytical and Applied Pyrolysis, 1986, 10, 139-151

[36] Gray, M.R., McCaffrey, W.C., Huq, I. and Le, T., Kinetics of cracking and devolatilization during coking of Athabasca residues, Industrial and Engineering Chemistry Research, 2004, 43,5438-5445

[37] Fanter, D.L., Levy, R. L. and Wolf, C. J., Laser pyrolysis of polymers, Analytic Chemistry, 1972, 44,1,January ,43-48

[38] Levy, R. L., Fanter, D. L. and Wolf, C. J., Temperature rise time and true pyrolysis temperature in pulse mode pyrolysis gas chromatography, 1972, Analytic Chemistry, 44,1,January, 38-42

[39] Westerhout, R.W.J., Kuipers, J.A.M. and Van Swaajj, W.P.M.,Development, modeling and evaluation of a laminar entrained flow reactor for the determination of the pyrolysis kinetics of polymers,Chemical Engineering Science, 1996, 51,10,2221-2230

[40] Chen, J.C. Niksa, S., A radiant flow reactor for high-temperature reactivity studies of pulverized solids, Review of Scientific Instruments, 1992, 63 (3), 2073-2083

[41] Chen, J.C. and Niksa, S., Coal devolatilization during rapid tranisient heating. 1. Primary devolatilization, Energy and Fuels,1992, 6,254-264

[42] Chen, J.C. ,Castagnoli,C.and Niksa, S. ,Coal devolatilization during rapid transient heating. 2. Secondary pyrolysis, Energy and Fuel, 1992, 6,264-271

[43] Zhao H., Cao Y., Sit,S.P.,Lineberry Q. and Pan W., Thermal characteristics of bitumen pyrolysis, Journal of Thermal Analysis and Calorimetry, 2011, 1-7

[44] Olmstead W.N. and Freund,H. , Thermal conversion kinetics of Petroleum Residua, AIChE, 1998 Spring national meeting, New Orlean , LA

[45] Gray, M. R., Fundamental of bitumen coking processes analogous to granulations: A critical review, The Canadian Journal of Chemical Engineering, 2002, 80, June 393-401

[46] Ali M., Courtney M., Boddez L. and Gray M., Coke yiled and heat transfer in reaction of liquid solid agglomerates of Athabasca vacuum residue, The Canadian Journal of Chemical Engineering, 2010,88,48-54

[47] Khorasheh F. and Gray M.R., High pressure thermal cracking of n-hexadecane in aromatic solvents, Industrial Engineering Chemistry Research, 1993, 32, 1864-1876

[48] Lannuzel F., Bounaceur R., Michels R., Sacchi G. and Marquaire P., Reassessment of the kinetic influence of toluene on n-alkane pyrolysis, Energy and Fuels, 2010, 24, 3817-3830

[49] Zhorov Y.M. and Volokhova, G. S., Influence of aromatic hydrocarbons on pyrolysis of various feedstocks, Chemistry of Fuels and Oils (English translation), 1980, 16, 8,507-509

[50] Herbinent O., Sirjean B., Battin-Leclerce F., Fournet R. and Marquaire P., Thermal decomposition of Norbornane (bicycle [2.2.1] heptane dissolved in benzene: Experimental study and mechanism investigation, Energy and Fuels, 2007, 21, 1406-1414

[51] Nagaishi H., Ikeda K., and Kitano K., Chan E. W., Gray M. R., Observation of heavy oil vaporization under rapid heating, Energy and Fuels, 1998, 12 ,6, 1174–1180

[52] Pfeifer P., Bohn L., Görke O., Haas-Santo K., Schygulla U., Schubert K., Microstructured mixers for gas-phase processes –manufacture, characterization and applications, Chemical Engineering Technology, 2005,28,4,439-445

[53] Haas-Santo K., Pfeifer, P., Schubert, K., Zech, T., Hönicke, D., Experimental evaluation of gas mixing with a static microstructure mixer, Chemical Engineering Science, 2005, 60 2955 – 2962

[54] Bird, R. B., Stewart, W. E. and Lightfoot E. N., Transport Phenomena, 1960, John Wiley and Sons

[55] Incropera,P.,I. and Dewitt,D. P. , Fundamentals of heat and mass transfer, 1990,third edition, John Wiley and Sons

[56] NIST Chemistry WebBook visited in 2007 to 2012
http://webbook.nist.gov/chemistry/

[57] Finlay, W., H., The mechanics of inhaled pharmaceutical aerosols, an introduction, 2001, Academic Press

[58] Omega.ca, http://www.omega.ca/, visited in April 2012

[59] Scott Fogler, H., Elements of Chemical Engineering, Second Edition, 1992, Prentice- Hall, Chapter 13

[60] Levenspiel, O., Chemical Reaction Engineering, Third Edition, 1999, John Wiley and Sons, Chapter 15

[61] Seyer, F. A.; Gyte, C. W. In *AOSTRA* Technical handbook on oil sands, bitumens, and,heavy oils; Hepler, L. C., Hsi, C., Eds.; AOSTRA: Edmonton, AB, 1989, p 155. (Cross reference from Gray, M. R. , Fundamentals of Oil Sands Upgrading , 2011)

[62] Peries, J. P.; Renard, P.; Des Courieres, T.; Rossarie, J. In 4th UNITAR/UNDP Conf. Heavy Crude Tar Sands Edmonton, AB, 1988, p Paper No. 95. (Cross referece from Gray, M. R., Fundamentals of Oil Sands Upgrading, 2011)

[63] Strausz, O.P.; Lown, E. M. The Chemistry of Alberta Oil Sands, Bitumens, and Heavy Oils; AERI: Calgary, AB., 2003. (Cross referece from Gray, M.R. , Fundamentals of Oil Sands Upgrading , 2011)

[64] Rahmani, S., McCaffrey, W. C. and Gray, M. R., Kinetics of solvent interactions with asphaltenes during coke formation, Energy Fuels 2002, 16, 148-154.

[65] Acon B. W., McLean J. A. and Montaser A., A direct injection high efficiency nebulizer interface for microbore high-performance liquid chromatography-inductively coupled plasma mass spectrometry, Journal of Analytical Atomic Spectrometry , 2001, 16,852-857

[66] Canals A. , Hernadis V. and Browner R. F., Experimental evaluation of the Nukiyama-Tanasawa equation for pneumatic nebulisers used in plasma atomic emission spectrometry, Journal of Analytical Atomic Spectrometry , 1990, 5, 61-66

[67] Hopke, Philip K., Receptor modeling in enviromental chemistry, Wiley-Interscience, pp. 43-44, 1985

[68] ASTM D2887

[69] ASTM D5307

[70] ASTM D6352

[71] ASTM D7169

[72] ASTM D7213

[73] D.G.Peters, G.M. Hieftje, and J.M Hayes, Chemical separation and measurement, Theory and practice of analytical chemistry, 1974, Saunders .

[74] P. Danial-Fortain, T. Gauthier, I.Merdrignac, and H. Budzinski, Reactivity study of Athabasca vacuum residue in hydroconversion condisitions, Catalysis Today, 2010, 150,255-263

[75] Radmanseh, R., Chan, E. and Gray, M.R., Modeling of mass transfer and thermal cracking during the coking of Athabasca residues, Chemical Engineering Science, 2008, 63, 1683-1691

[76] Constandinides, A. and Mostoufin, N., Numerical methods for chemical engineers with MATLAB applications, 1999, Prentice Hall

[77] J.S.Alper and R. I. Gelb, Standard errors and confidence intervals in nonlinear regression: comparison of monte carlo and parametric statistics, Journal of Physical Chemistry, 1990, 94,4747-4751

[78] Savage, P. E.; Klein, M. T., Asphaltene reaction pathways. 4. Pyrolysis of tridecylcyclohexane and 2 ethyltetralin, Ind. Eng. Chem. Res., 1988**,** 27, 1348-1355.

[79] Zhao, Y., Wei, F., and Yu Y., Effect of reaction time and temperature on carbonization in asphaltene pyrolysis, Journal or Petroleum Science and Engineering, 2010,74,20-25.

[80] J. Su, J. Yang, and H. Wang, Kinetic investigation of pyrolysis for Daqing light gas oil, Petroleum Sciece and Technology, 1997,15(9 & 10),823-837.

[81] C. F. Lange, F. Durst and Breuer, Momentum and heat transfer from cylinders in laminar cross flow at $10^{-4} \leq Re \leq 200$, International Journal of Heat and Mass Transfer ,41, 1998, 3409-3430

[82] W. M. Kays, and M.E. Crawford, Convective heat and mass transfer, Second Edition, MCGrawHill, 1980.

[83] Fox, R. W. and McDonald, A.T., Introduction to fluid mechanics, 1994, fourth edition, John Wiley

Appendix A
Temperature History of a Feed Particle

Atomization of feed to give very fine particles decreases the mass transfer resistance in the liquid phase against diffusion of the products of thermal cracking into the vapor phase. In addition, generation of such fine particles can help to reduce the time which it takes to heat up the particles to the reaction temperature. The heat-up time of the feed particles should be significantly smaller than the half-life of the reaction, so that the conversion of the feed particles is negligible before they reach the reaction temperature. In order to design the reactor for the kinetic study, it is important to know the temperature history of the reactant inside the reactor.

In this design, the concentration of feed in the carrier gas is small and the cooling effect of the bulk of feed particles on the carrier gas can be neglected. The size of the particles is very small compared to the size of the reaction tube, so the particles can be considered to be in an enclosed cavity when the effect of thermal radiation is considered. The fluid is optically thin, so scattering of the radiation by the particles is not considered. Thus, the problem can be simplified to motion of a single particle on the central axis along the tube in one dimension. A lumped heat transfer model is assumed for the single particle. No heat of reaction and vaporization is considered, and it is assumed that the particle size does not change along the reactor. The temperature of the particle versus time is calculated by solving the following differential equation:

$$m_p C_p \frac{dT_p}{dt} = A_p h (T_f - T_p) + A_p \sigma (T_w^4 - T_p^4) \qquad (A.1)$$

In which:

m_p mass of the particle

C_p specific heat of the particle at constant pressure

A_p surface area of the particle

h heat transfer coefficient

T_f fluid temperature

T_p temperature of the particle

T_w reaction tube wall temperature

σ Stefan - Boltzmann constant

t mean residence time

Because the heat of vaporization and reaction are neglected, the time which is calculated for the feed particle to reach the reaction temperature will be smaller than it should be in reality. The particle can be cooled off by vaporization or through the slightly endothermic thermal cracking reactions. From the other side, vaporization of the feed particle would reduce its size; consequently, the particle could be heated up more quickly because it becomes smaller.

It is instructive to study the pure effect of the size of the particle on the time of heat-up. Figure A.1 shows the required time for a particle of bitumen with a specified diameter to reach the reaction temperature when the particle moves in a tubular reactor where the carrier gas and the wall temperature are both set at 800ºC. Density of the particle is assumed to be 1110 kg/m^3 and the heat capacity of the particle at reaction temperature is calculated by relationship which is provided in reference [61, 62, 63].

The transport properties for helium are calculated according to reference [54] and Nusselt number assumed to be equal to 2 for a spherical particle at low Reynolds number [55]. The carrier gas is helium. Figure A.1 shows that for a particle to

reach 95% of the reaction temperature in the order of magnitude of 10 ms , the size of the feed particle should be in order of magnitude of 10 μm or less.

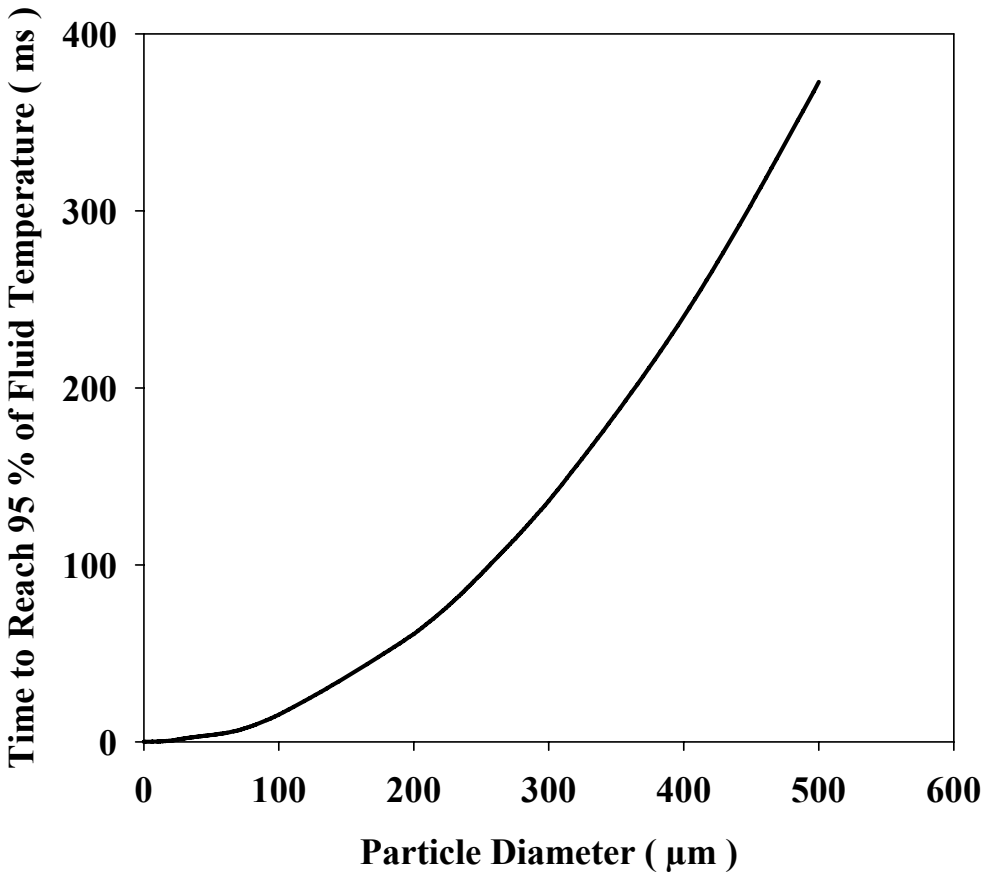

Figure A.1 Particle in Isothermal Reactor, Fluid and the wall at 800 °C

For the case of a non-isothermal reactor for thermal cracking of vacuum residue, both the feed particles and the carrier gas must be heated-up. In order to find the temperature history of a single particle in the non-isothermal reactor, equation (A.1) can be used again. The temperature profile of the tube wall has been measured and the temperature of the fluid can be calculated by the heat transfer model for the non-isothermal reactor tube (Appendix D).

Figure A.2 shows the result for the particle temperature history in the non-isothermal tubular continuous flow reactor and operating condition of the experiment 800-1. A minimum particle diameter of 20 μm is required so that the particle follows the fluid temperature based on the simplifying assumptions given above. These simplifying assumptions can bias the result toward shorter time to increase the temperature for the particle. For a particle which enters an isothermal reactor, if the particle is at 24°C and the fluid flowing in the reactor is at 800°C, given the total of heat of reaction and vaporization is 650 kJ/kg, for a 50% conversion the order of the magnitude of the delay which is caused by supplying the heat of reaction is given by the following formula :

$$Delay\ time = \frac{heat\ of\ reaction \times mass\ of\ the\ particle}{heat\ flux} \qquad (A.2)$$

For a particle with diameter size of 20 μm this delay time is 4.6×10^{-8} μs. In the case of the non-isothermal reactor ,in the non-isothermal section of the temperature profile when the temperature of the fluid is initially the same as the temperature of the particle, that is fluid is at 24 °C and the wall is at 800°C, the delay time is calculated as 2×10^{-5} μs ,and the heat flux is provided through thermal radiation. When particle is approaching the fluid temperature in the isothermal section of the reactor, the particle temperature is close to the furnace temperature, for example 790°C, and fluid and the wall are at the reaction temperature, 800°C, then using the equation (A.2), the delay time is calculated as 3.6×10^{-6} μs. These results are expectable because the mass of the particle is very small, that is 4.6×10^{-12} kg. The heat which is required to convert 50 % of this mass is 1.5×10^{-6} J. Thus, it can be concluded that the heat of reaction and vaporization does not affect the temperature rise time, which is calculated by equation (A.1). Therefore, a particle with diameter size of 20 μm will follow the temperature of the fluid.

Another outcome of this case study is the conclusion that thermal radiation cannot heat up the temperature of the particle above the fluid temperature because of the

rapid exchange of heat between the gas and the liquid droplet. Repeating the calculation for the particles with diameter size of less than 20 μm indicates that fluid temperature is a maximum limit for the temperature of the particles at any place along the reactor. The average size of feed particle diameters that the industrial atomizers can generate varies between 50 to 80 μm. At such size range, the particle temperature can be different from the carrier gas temperature in a short residence time reactor.

The data of Figure A.2 also show another limitation of the application of non-isothermal reactor in kinetic study of thermal cracking at elevated temperatures. If the feed particle is small enough, it follows the temperature of the carrier gas but no matter how small the feed particle is, it does take a certain time for the carrier gas to reach the reaction temperature. The heat-up time of the carrier gas in a non-isothermal reactor is independent of the size of the feed particles when the concentration of the feed in the reactor is very low. If the heat-up time of the carrier gas compared to the half-life of the reaction is not acceptable, then an isothermal operation can be the better choice, yet this option imposes other technical difficulties. The particles cannot be heat up faster than the carrier gas to reach the reaction temperature.

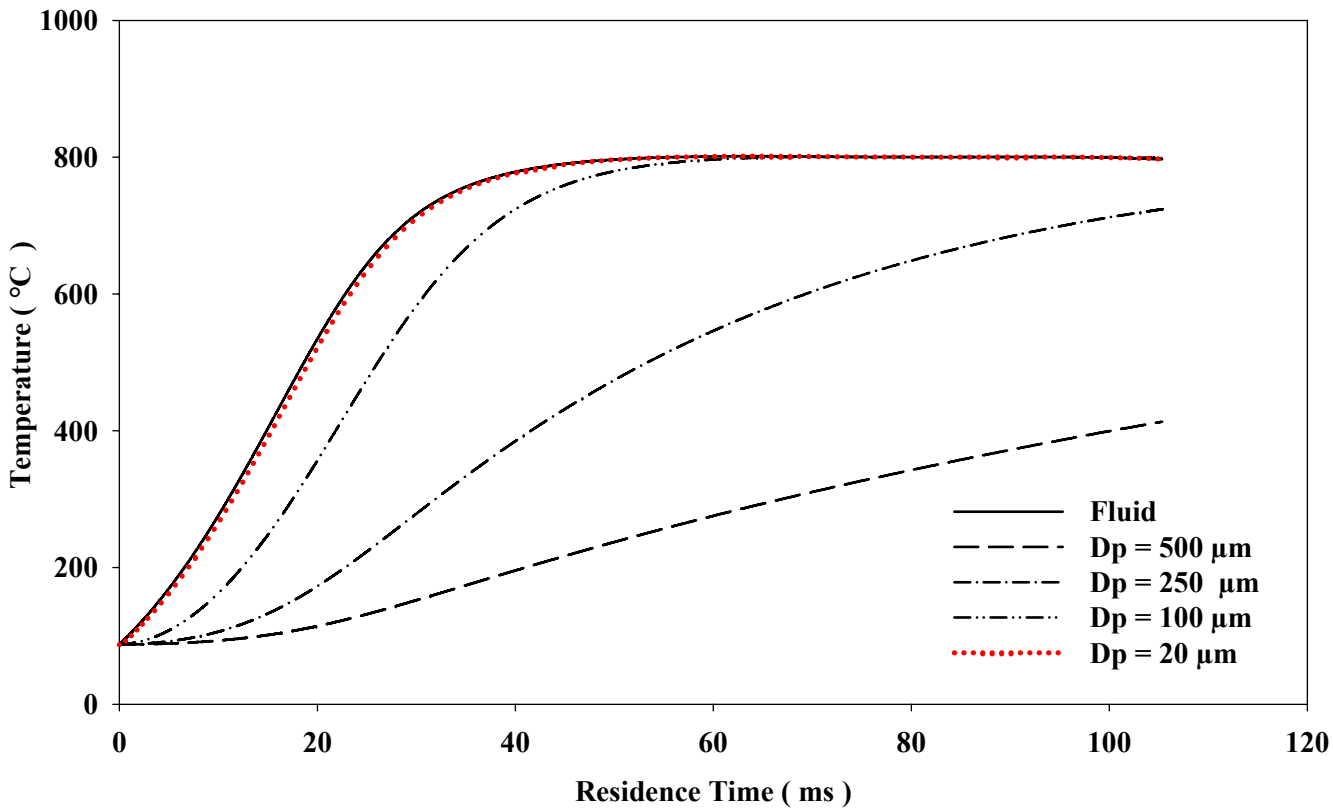

Figure A.2 Temperature history of a feed particle in the non-isothermal reactor at operating conditions of the experiments 800-1

Appendix B

Sedimentation of the Feed Particles inside the Apparatus

In selection of the atomization technique, the required size of the feed droplets or particles should be known. The size of the feed particle in this research is selected based on the requirement to minimize the heat and mass transfer within the liquid phase. In practice I cannot generate infinitely small particles; therefore, the maximum size of particle above which deposition of particles would occur should be examined. The feed particles can coalesce prior to their introduction to the reactor or as they are moving inside the reactor. Increasing of the size of the particles naturally heightens the tendency for deposition. However, in the following study, just a single particle is assumed which does not interact with other particles. In this appendix, three cases are studied which consider the real geometry of the apparatus and the same range of operating conditions which were applied in the experiments on thermal cracking of vacuum residue. The deposition in the aerosol reactor in this research can occur through the following mechanisms [57]:

1. Gravitational settling
2. Diffusion
3. Inertial impaction

For each case study, the maximum size of the particle which can cause deposition through each of these mechanisms are examined.

B.1 Stokes Number

The Stokes number can be interpreted as the non-dimensional time required for the particle's velocity relative to the fluid to drop to 37% of its initial value when injected into the fluid. If a stationary particle is introduced into a fluid flowing with velocity U_0, then the distance between the fluid element which it started out of it to the point when it reaches the fluid velocity is called the starting distance.

The Stokes number can also be interpreted as the ratio of the starting distance to the characteristic length, D, in the fluid [57]. The Stokes number defines as

$$St = \frac{\tau U_0}{D} \tag{B.1}$$

In which *St,* is Stokes number, U_0 is the fluid velocity, and τ is particle relaxation time which is defined by

$$\tau = \frac{\rho_{particle} d^2 C_c}{18 \mu} \tag{B.2}$$

In which *d* is diameter of the particle, μ is the viscosity of the surrounding fluid, λ is mean free path , and C_c is Cunningham slip correction factor:

$$C_c = 1 + 2.52 \frac{\lambda}{d} \tag{B.3}$$

The particle relaxation time is the dimensional time required for the particle's velocity relative to the fluid to decay to 37% of its initial value, and the Stokes number it simply a dimensionless particle relaxation time [57].

B.2 Settling velocity

The settling velocity of a particle can be calculated by the following formula providing that Reynolds number is much less than one.

$$V_{settling} = \frac{C_c \rho_{particle} g d^2}{18 \mu} \qquad \text{Re} << 1 \tag{B.4}$$

B.3 Brownian diffusion

For very small particles, collisions with randomly moving molecules of the carrier gas will cause the particle to undergo a nondeterministic random movement, which is called the Brownian motion. Einstein formulated the equation for the

displacement of the particle in time t (t >> the time between the molecular collision) as the following:

$$x_d = \left(2D_d\, t\right)^{1/2} \tag{B.5}$$

$$D_d = \frac{k\,T\,C_c}{3\pi\,\mu\,d} \tag{B.6}$$

in which D_d is the particle diffusion, k = 1.38 × 10 $^{-23}$ J K^{-1} is the Boltzmann's constant, T is temperature in Kelvin, C_c is the Cunningham slip factor from equation (B.3). Equation (B.6) shows that as the diameter of the particle decreased, the diffusion factor, D_d, increases and the diffusion becomes important for the very small particles. In order to evaluate the importance of diffusion, the ratio of the displacement of the particle of the particle due to diffusion to the distance that the particle travels due to gravitational settling can be calculated by the following equation [57]:

$$\frac{x_d}{x_s} = \frac{1}{\rho_{particle}\, g}\sqrt{\frac{216\mu\,k\,T}{\pi\,t\,d^5\,C_c}} \tag{B.7}$$

Diffusion can be considered negligible if $x_d/x_s < 0.1$ [57].

B.4 Inertial impaction

Besides diffusion and gravitational settling, a third mechanism that can cause that the particles move relative to the carrier gas and deposit on the walls is inertia. If the fluid travels around a bend, if the particle is heavy enough, it may not be able to execute the bend and will deposit on the wall. Deposition of the particles in this way is called inertial impaction [57].In order to determine whether a particle will deposit by impaction its trajectory should be determined. It can be shown that if St << 1, a particle that encounters a rapid change in the direction of the streamlines will follow the streamlines (neglecting the gravitational settling), and if Stokes ≈ 1 or larger, it will not follow the sudden changes in the direction of the streamlines [57].

B.5 Case Study I : Sedimentation inside the reaction tube

In this case study, motion of a single feed particle inside the reaction tube is considered. The specifications of the reaction tube are described in Chapter 5. The reactor is considered isothermal at temperature of 600°C and with flow rate of 16 sL/min helium. In the thermal cracking of vacuum residue the temperature of the furnace is set from 600 to 800°C. However, the fluid undergoes a temperature profile before it reaches the middle of the reactor. The experiments show that the deposition is mostly in the non-isothermal zone where the temperature of the fluid is below 700°C. Therefore, for this case study a fluid temperature of 600°C is selected. Figure B.1 shows the Stokes number of the particles of different diameters as they flow inside the reaction tube. When the particle diameter is below 7 μm, then the Stokes number is less than 0.1, ensuring that the particle follows the streamlines if the particle encounters a sharp bend of the streamline or a vortex. Figure B.2 shows the ratio of the displacement of the particle through the gravitational settling to the displacement by following the streamlines of the carrier gas. This figure shows that for the particle inside the reaction tube, this ratio stays below 0.1 for all of the range of the diameters which are studied (up to 50 μm), therefore the deposition through settling cannot be an issue under the operating condition of the study. Figure B.3 demonstrates the ratio of the displacement of the particle through diffusion to the displacement by following the streamlines of the carrier gas for a particle moving down the axis of the reaction tube. The results show that in the range of study the distance that the particle travels due to diffusion is insignificant compared with the distance that the particle travels by following the streamlines of the carrier gas. Figure B.4 demonstrates the ratio of the displacement of the particle due to diffusion to the gravitational settling. For particles with diameter smaller than 2 μm, the motion due to diffusion becomes significant compared to the gravitational settling, nevertheless the motions due both of these mechanisms are insignificant compared with the motion following the streamlines of the carriers gas.

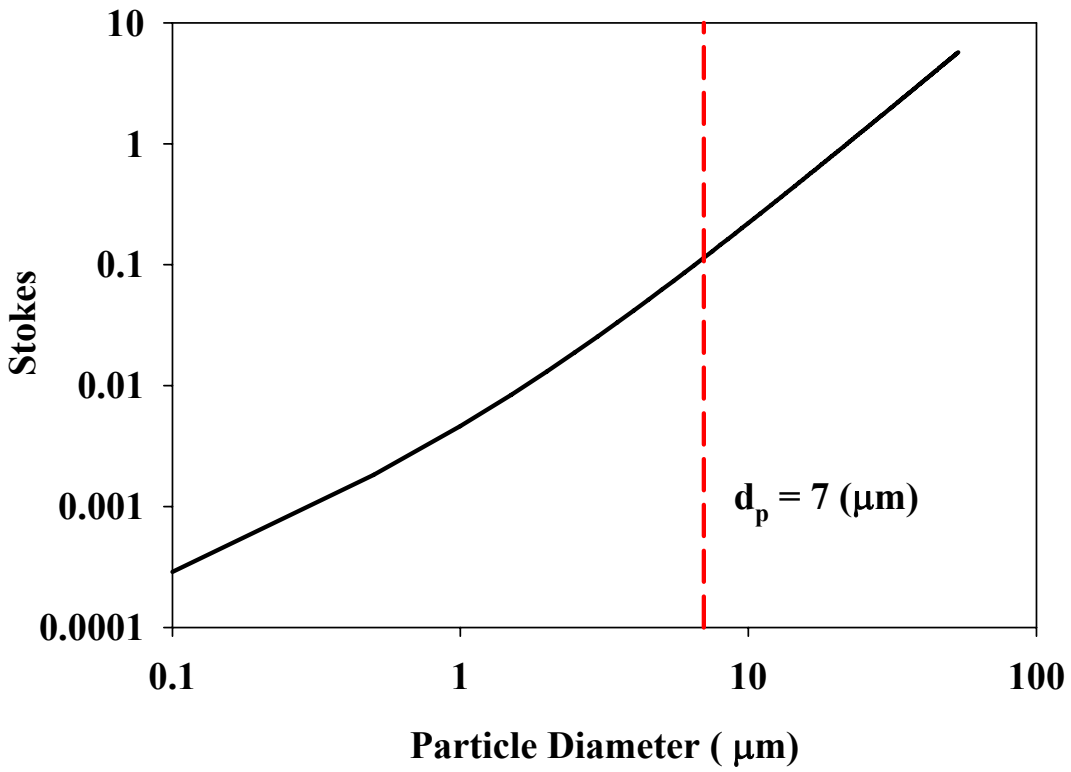

Figure B.1 Stokes number of a particle moving inside the reaction tube

B.6 Case study II : The motion of the particle at the entrance to the array of the micro channels

If the aerosol of the feed is introduced into the reactor through the micro-structured mixer, the most important question is the maximum size of the feed particle that ensures the minimum risk for deposition on the walls. Figure B.6 illustrates the motion of the feed particle through an array of the micro-channels. In this case study the real size of the micro-channels for a two dimensional geometry is considered (200 μm the height of the channel and 170 μm the fin between the channels). The flow at the inlet port of the mixer is 3 sL/min. The study considers the entry of a single micro-channel, over a distance of 5 mm , and the velocity of the streamlines of the flow at this distance are assumed to be the same as the velocity inside the channel, 7.6 m/s, and the flow is at room temperature, 24°C. Figure B.7 shows that when the diameter of the particles is

below 6 μm the Stokes number is below 0.1 and the particle is expected to execute the sharp curves following the streamlines that bend into the channel. Figure B.7 shows that transport of the feed particles through diffusion, compared with the transport of the particle by following the streamline of the carrier gas, is insignificant in the entire range of the study. The study also shows that the effect of the gravitational settling is insignificant. For the close distance at the entrance to the micro-channel, that is 5 mm, this is an obvious and expected result.

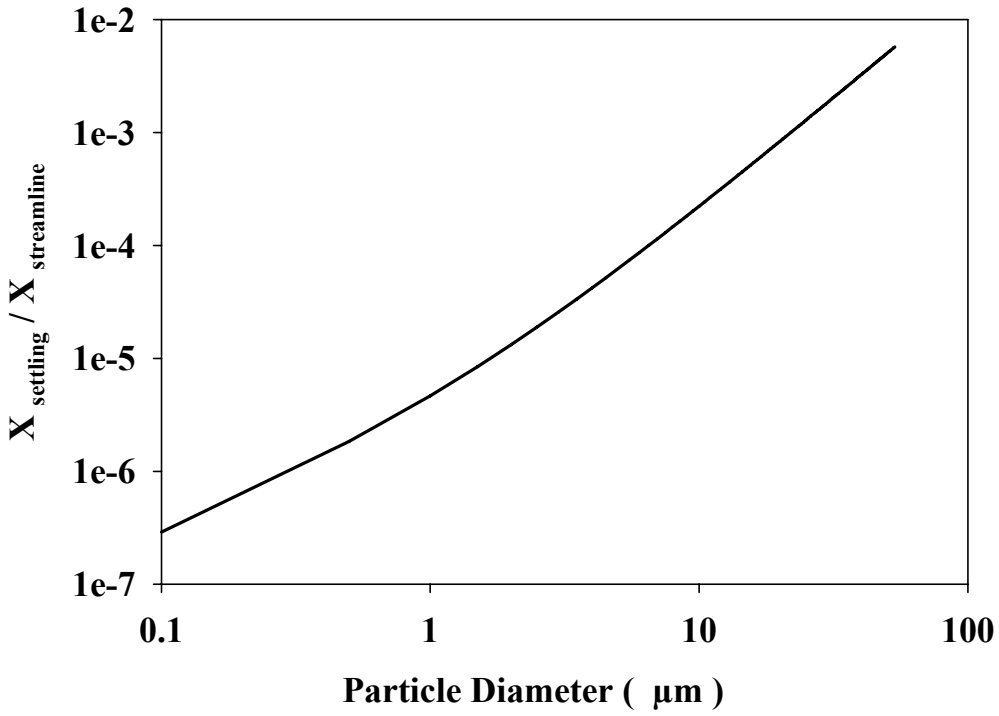

Figure B.2 Ratio of the displacement of the particle by gravitational settling to the displacement by following the streamline of the carrier gas.

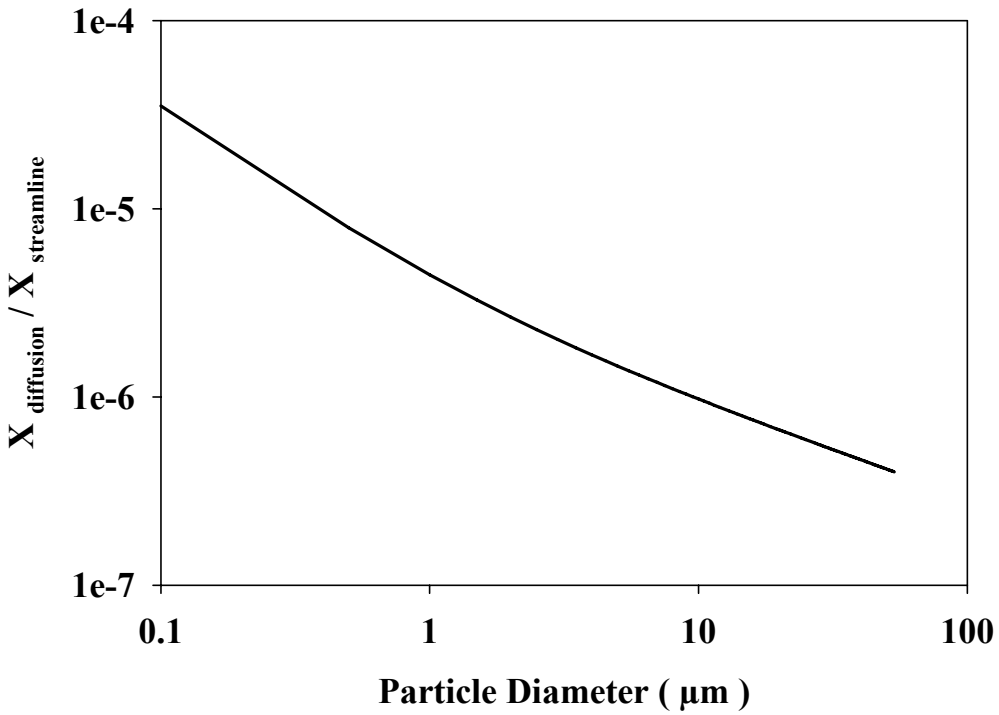

Figure B.3 Ratio of the displacement of the particle through diffusion to the displacement by following the streamlines of the carrier gas for the particle which moves inside the reaction tube.

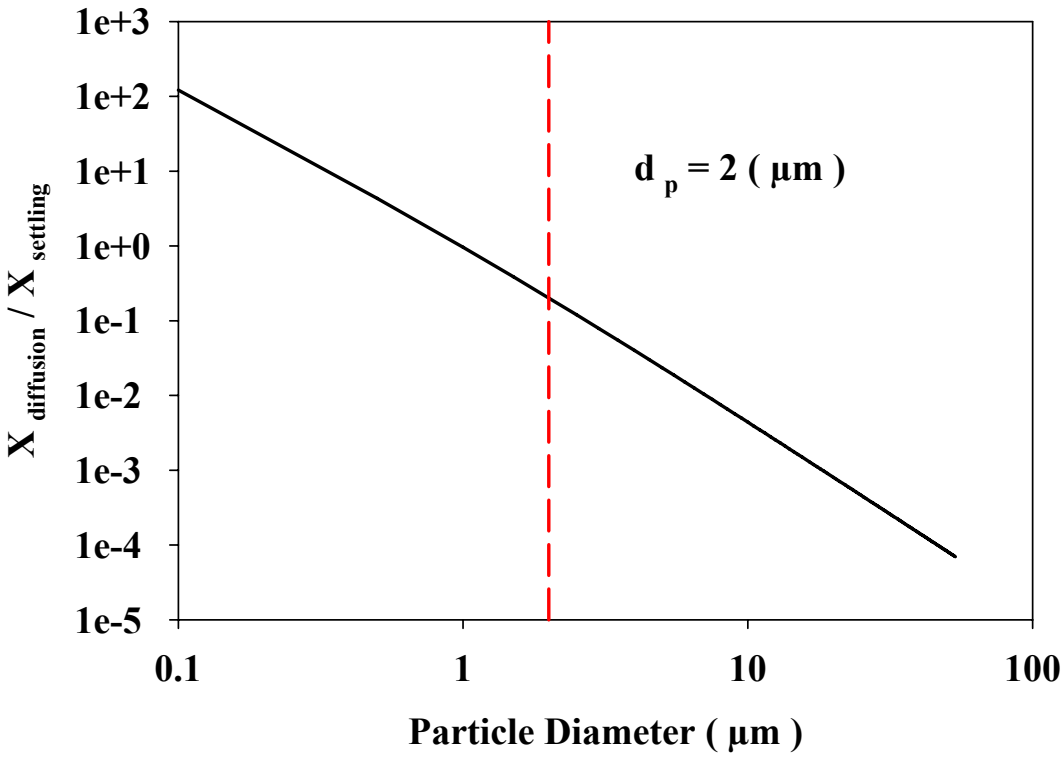

Figure B.4 Ratio of the displacement of the particle through diffusion to displacement by gravitational settling for the particle which moves inside the reaction tube.

B.7 Case Study III: Motion of the particle inside the micro-channels

Figure B.5 illustrates motion of the feed droplest into the micro-channels.The temperature of the fluid inside the micro-channels is assumed to be 300°C, which is the mean temperature for the cold stream. The velocity of the fluid inside the micro-channels is calculated based of the flow rate of the carrier gas in cold inlet of the micro-structured mixer and the total number of the micro-channels in the cold passage of the micro-structured mixers. The velocity of the fluid is 7.6 m/s. Figure B.6 shows that the Stokes number of the feed particles at the entrance to the array of the micro-channels is less than 0.1 when the feed droplet is less than 6 µm. Figure B.7 shows that the contribution of diffusion to motion of the feed droplet at the entreance of the micro-channels is insignificant.Movment of the particles due to gravitational settling at such high velocity was also insignificant.

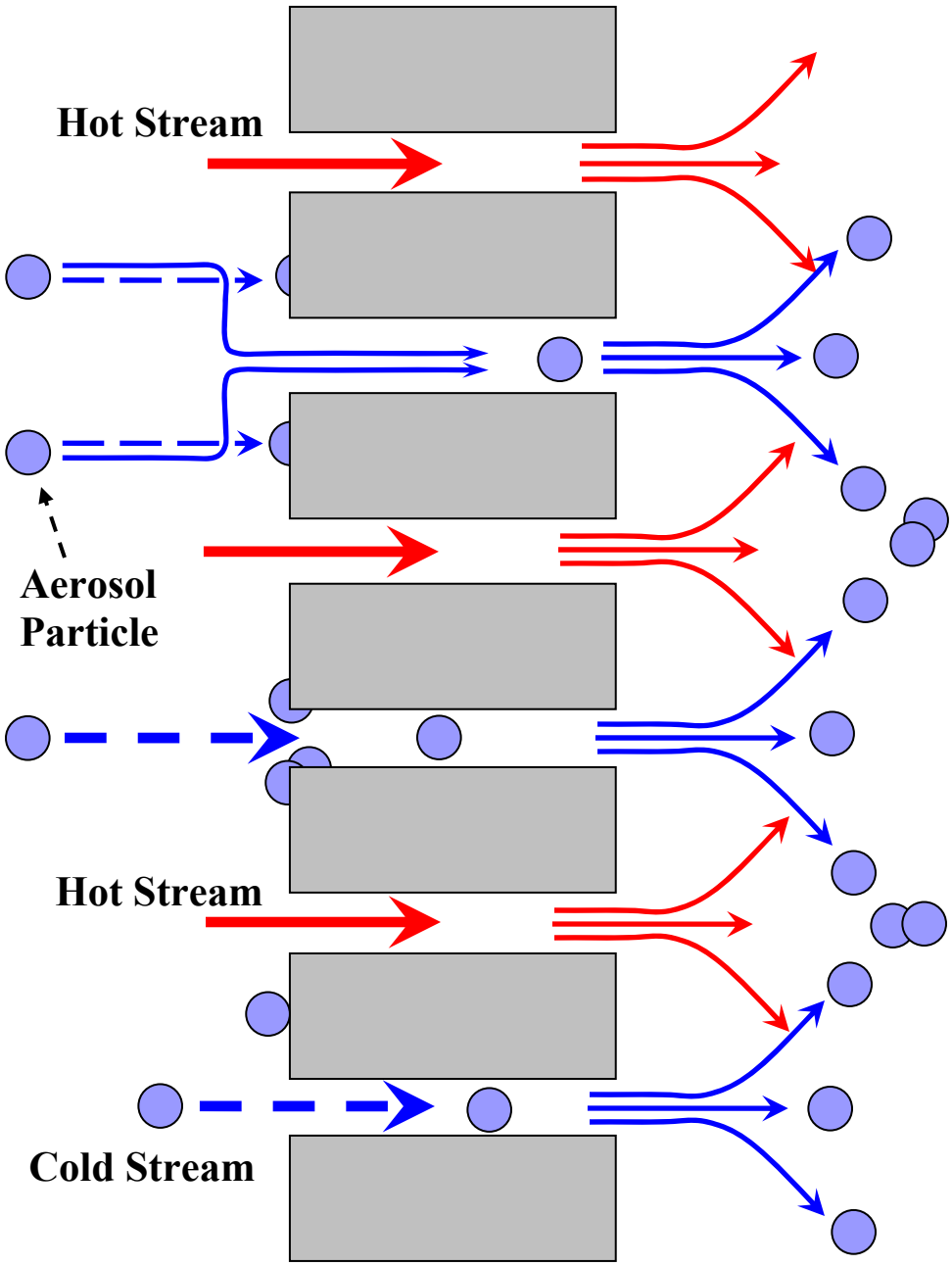

Figure B.5 Flow of the particles through the micro-structured mixer

Figure B.8 shows that for particles smaller than 0.5 μm, the Stokes number is below 0.1, which ensures that these particles follow the streamlines of the carrier gas. Base on the case studies II and III, it can be concluded that the preferred size of the feed particles to pass through the micro-channels are submicron. Because coalescence of the particles immediately starts upon their generation, and continues until they are introduced into the reaction tube and even after, the success of this method can only be verified by experimentation.

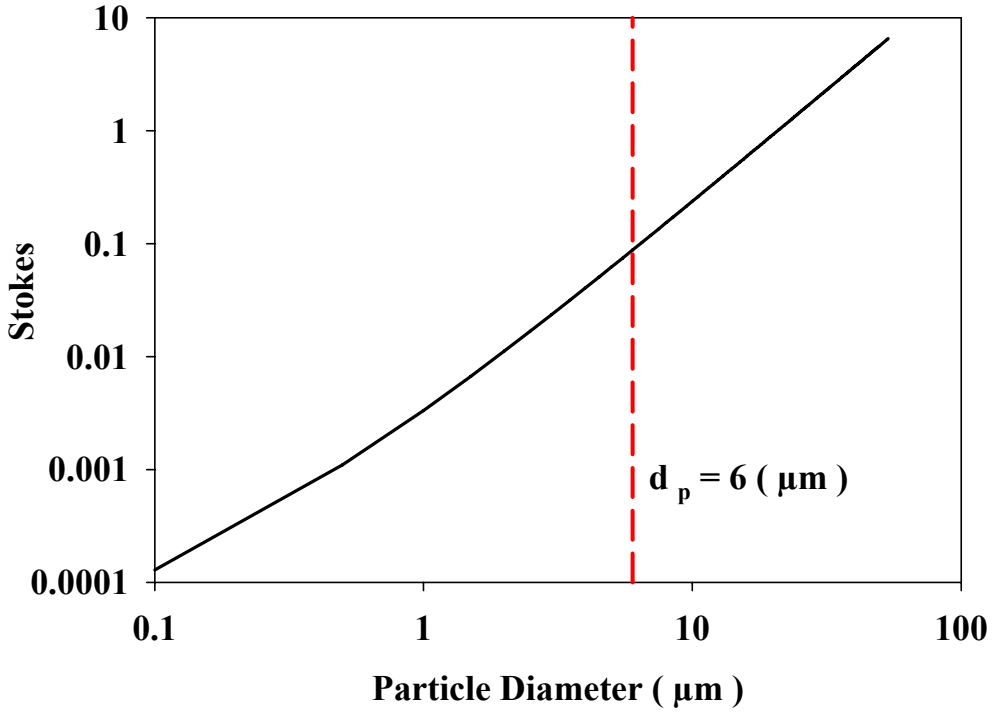

Figure B.6 Stokes number of the feed particles at the entrance to the array of the micro-channels.

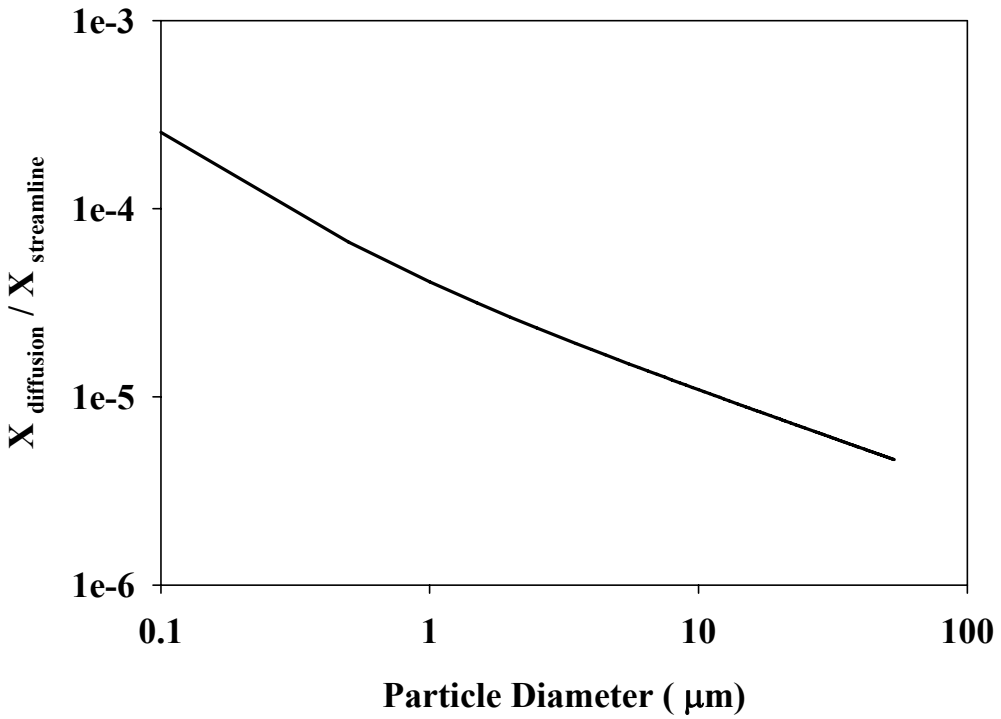

Figure B.7 Ratio of the displacement of the particle through diffusion to the displacement of the particle by following the streamlines of the carrier gas at the entrance to the array of the micro-channels.

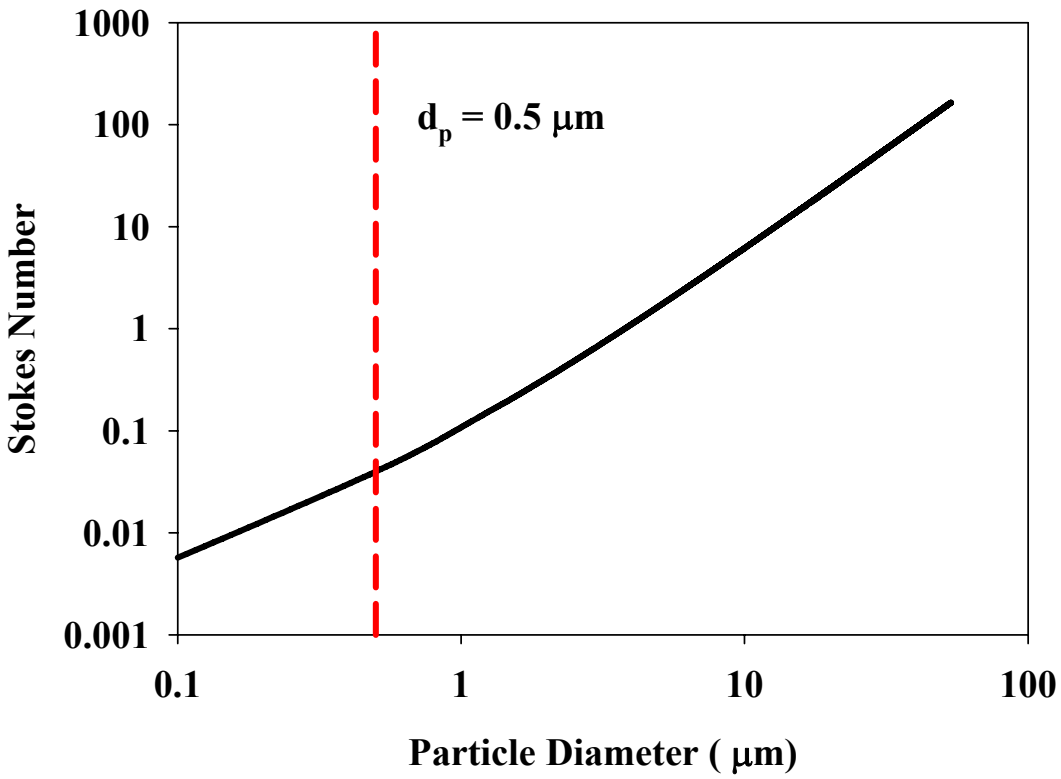

Figure B.8 Stokes number inside the micro-channels of the cold passage of the micro-structured mixer

Appendix C

A Simulation Case Study on Micro-mixing by COMSOL Multiphysics

The temperature profiles of the isothermal reactor were examined in Chapter 4. In this section, micro-mixing of sublayers of two hot and cold streams of helium by a micro-structured mixer is simulated by COMSOL Multiphysics. The case study is based on the actual geometries of the micro-structured mixer which is used in this research. The purpose of this simulation is to estimate the order of magnitude of the required time for thermal equilibrium after mixing of the hot stream of the carrier gas with the cold stream which carriers the reactant.

The governing equations of heat transfer, motion, and continuity are formulated as follows:

Heat balance

$$\nabla.(-k\nabla T) = Q - \rho C_p \mathbf{u}.\nabla T \qquad \text{(C.1)}$$

Non-isothermal flow:

$$\rho \mathbf{u}.\nabla \mathbf{u} = \nabla.[-p\mathbf{I} + \eta(\nabla \mathbf{u} + (\nabla \mathbf{u})^T) - (2\eta/3 - \kappa_{dv})(\nabla.\mathbf{u})\mathbf{I}] + \mathbf{F} \qquad \text{(C.2)}$$

Contiunuity:

$$\nabla.(\rho \mathbf{u}) = 0 \qquad \text{(C.3)}$$

where the variables are as follows:

Q = heat source W/m^3

$\boldsymbol{u}$ = velocity

ρ = density

I = identity matrix

$\boldsymbol{F}$ = body force N/m3

κ_{dv} = Dilational viscosity Pa.s

η = dynamic viscosity Pa.s

The body forces F, and dilation viscosity κ_{dv} are assumed to be zero. The concentration of reactant is insignificant in the carrier gas so the effect of the heat of reaction, or Q, can be neglected. The size of the micro-channels and the distance between two adjacent channels in the simulation are the same as the sizes in the real micro-structured mixer, 200 and 170μm respectively.

The problem is assumed to be two-dimensional. The real micro-structure mixer is three dimensional and there are fins between the micro-channels in each foil. However, this simplification does not affect the purpose of this simulation as far as micro-mixing and heat transfer through conduction between sublayers of fluid at the outlet of the micro-structured mixer is considered as the only mechanism for heat transfer. This simulation does not consider heat transfer to the cold stream by radiation and conduction through the body of the micro-structured mixer. There are 13 sublayers of hot stream which are mixed with 12 sublayers of cold stream. The total flow of the hot and cold stream of helium are 5 and 3 sL/min respectively. The inlet velocities of the fluids in the hot and cold channels are 22.2 m/s and 7.6 m/s accordingly. These velocities are calculated based on the flow rates which are in range with the experiments that are described in Chapter 4 and based on the inlet temperatures to the micro-structured mixer. The worst case study, in which the longest temperature rise time would be calculated, is when there is no heat transfer to the fluids as they pass the micro-channels. In the real operation the micro-structured mixer is not adiabatic. Nevertheless, the assumption of the adiabatic operation will make the estimated thermal equilibrium time longer than the real value which makes a safer approximation.

The thermal equilibrium quality, M_T, is the degree to which the mixture of the two streams has approached to the thermal equilibrium and is defined by equations (C.4) to (C.7) which are defined similar to equations (3.2) to (3.5).

$$M_T = 1 - \frac{S}{S_0} \tag{C.4}$$

$$s = \sqrt{\frac{1}{N-1}\sum_{i=1}^{N}(T_i - \overline{T})^2} \tag{C.5}$$

$$\overline{T} = \frac{1}{N}\sum_{i=1}^{N} T_i \tag{C.6}$$

$$t_T = \frac{L_T}{V_{out}} \tag{C.7}$$

in which S is the standard deviation of N samples and S_0 is the standard deviation referring to the initial state. T_i is the temperature at a certain axial distance from the outlet of the mixer which is measured at different radial positions. $\overline{T}$ is the mean value for these measurements. Comsol Multiphysics version 3.3 is used. The physical property of helium is taken from the library of this software. This software uses finite element method to solve the partial differential equations. The solver was Direct UMFPACK, relative tolerance of 1×10^{-6}, maximum number of iteration 25 and pre-defined elements Lagrange- Quadratic. The convergence of the solver was verified automatically by the software. Figure C.1 demonstrates the discretization of the domain to 3652 triangular elements. The mesh is refined more at outlet of the micro-channels into the reactor.

Since there this is a simulation study, sampling is made from the numerical results of COMSOL Multiphysics for the simulated case. Figure C.2 and Figure C.3 demonstrate the velocity field and temperature distribution at the outlet of the microstructures mixer. Figure C.2 shows that at a short distance from the outlet of the mixer compared with the size of the microchannels, the sublayers start to mix with each other and a fully developed velocity field is achieved in a short distance, which is less than the diameter of the reaction tube. Figure C.3 shows that at a short distance from the outlet of the microstructured mixer, the average temperature comes very close to the equilibrium temperature. Figure C.4 and

Figure C. demonstrate that for the case which is studied, the distance in which the mixed fluids reach 95% of complete thermal equilibrium is 2.5 mm and it takes 0.3 ms to reach this status. This time is consistent with the prediction for thermal equilibrium time when helium is used as the carrier gas in Figure 3.6.

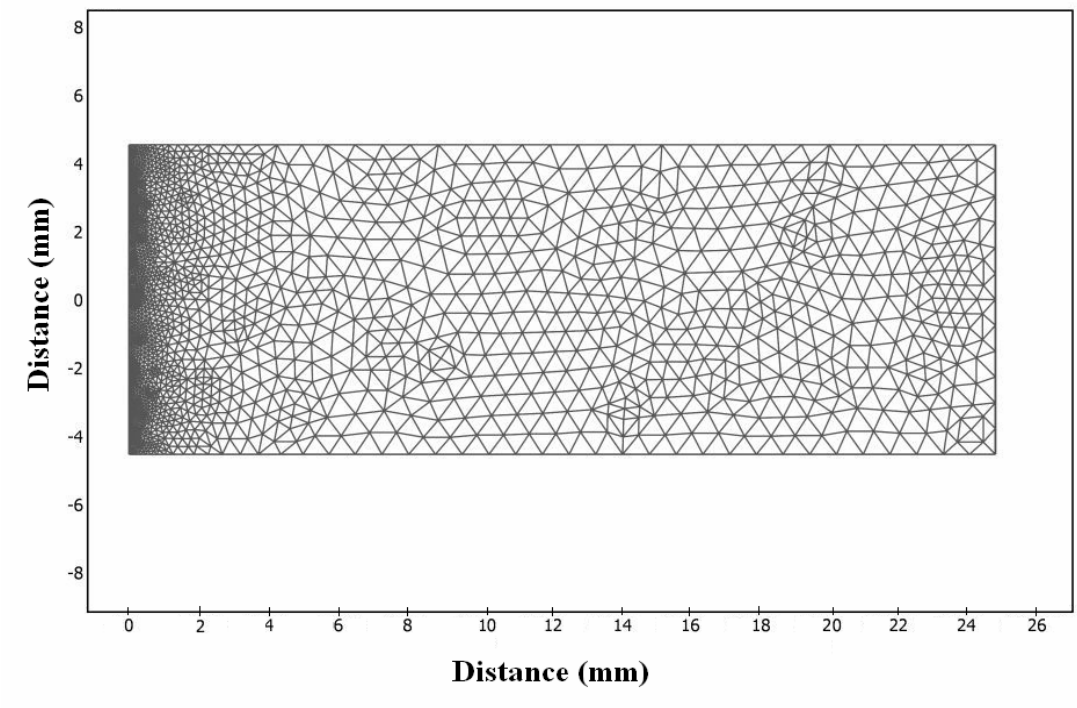

Figure C.1 Discretization of the domain to 3652 triangular elements. The mesh is refined more at outlet of the micro-channels into the reactor.

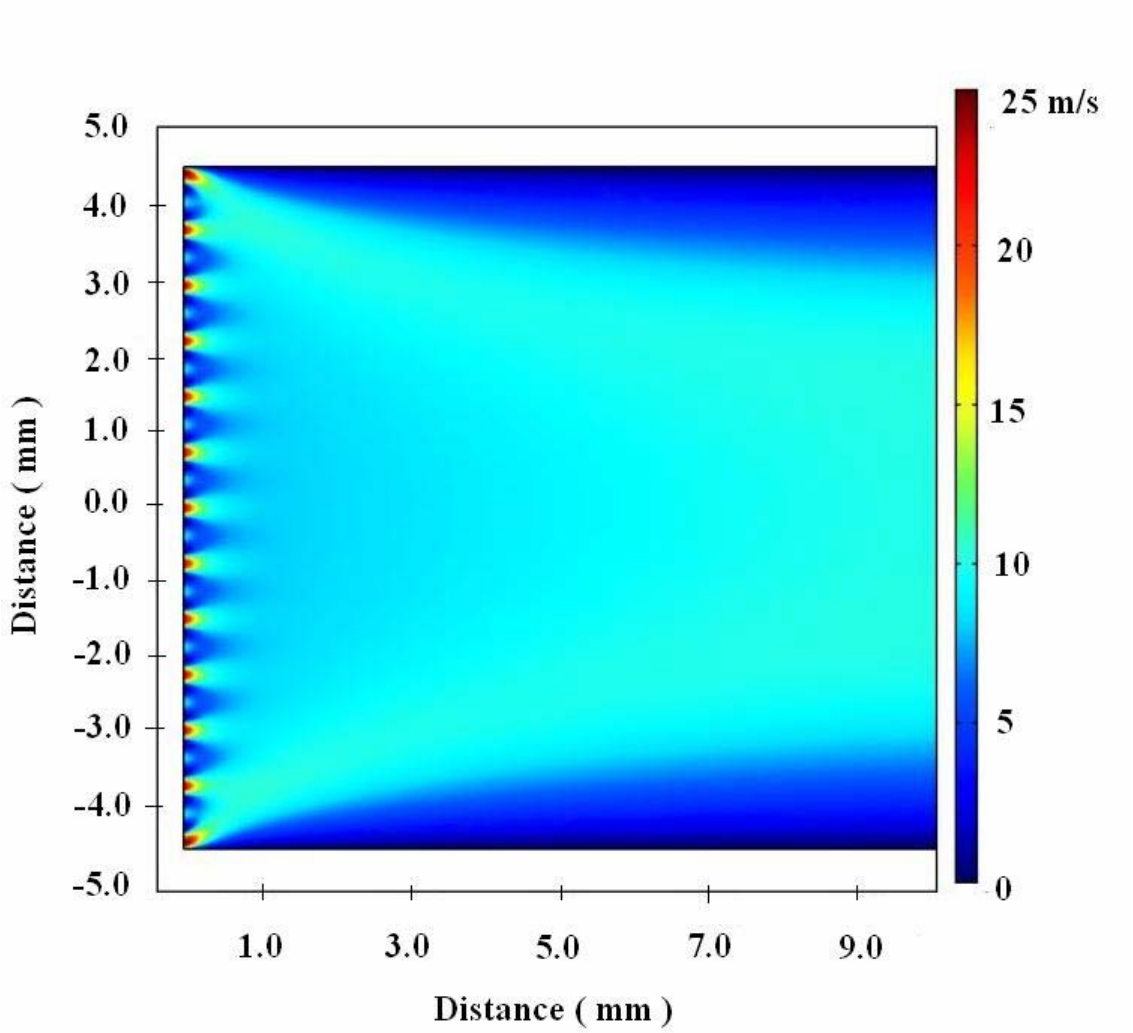

Figure C.2 The velocity field in simulation of the micro-mixing of two streams of hot and cold helium:velocity in hot channels = 22.2 m/s and 7.6 m/s in cold channels , 13 hot channels and 12 cold channels ,cold stream at 300°C and hot stream at 800°C. Size of channels : 200 μm height and the fin between the channels 170 μm. The average velocity in the tube at equilibrium temperature is 8.1 m/s. Equilibrium temperature 605 °C.

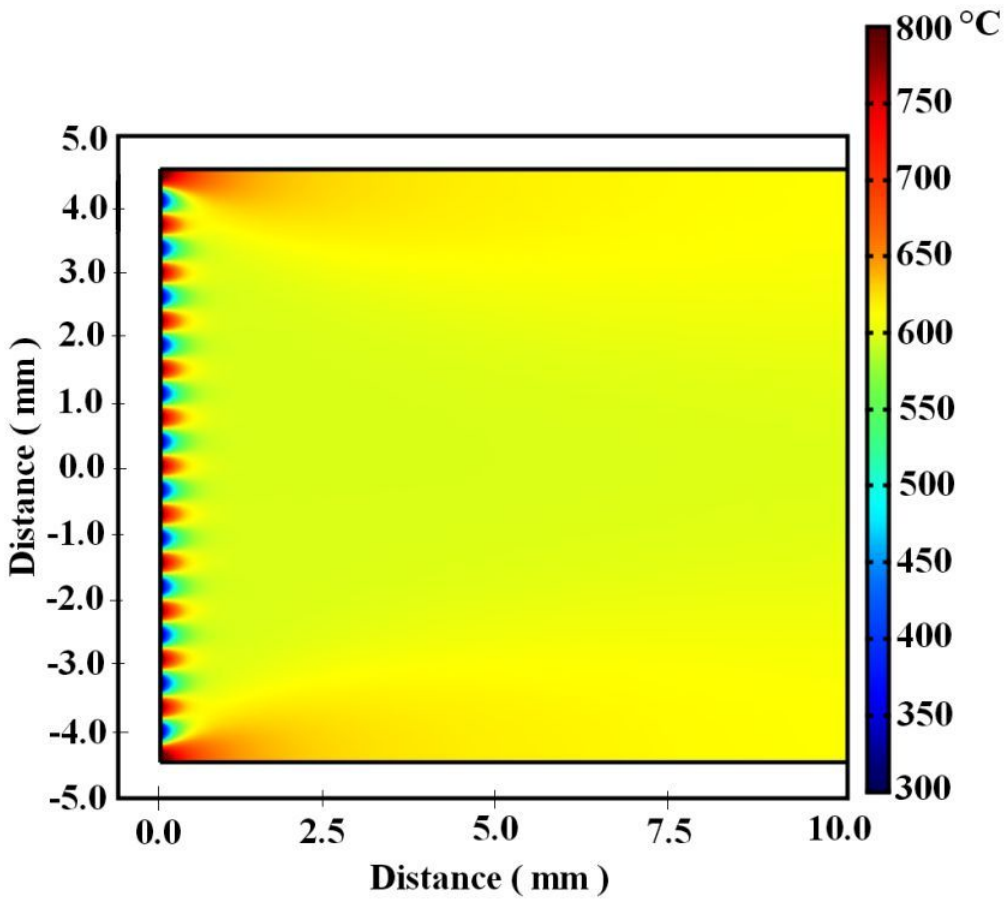

Figure C.3 The temperature distribution in the simulation of the micro-mixing of a hot and cold stream of helium: velocity in hot channels = 22.2 m/s and 7.6 m/s in cold channels, 13 hot channels and 12 cold channels, cold stream at 300 °C and hot stream at 800°C. Size of channels : 200 μm height and the fin between the channels 170 μm. The average velocity in the tube at equilibrium temperature is 8.1 m/s. Equilibrium temperature 605°C.

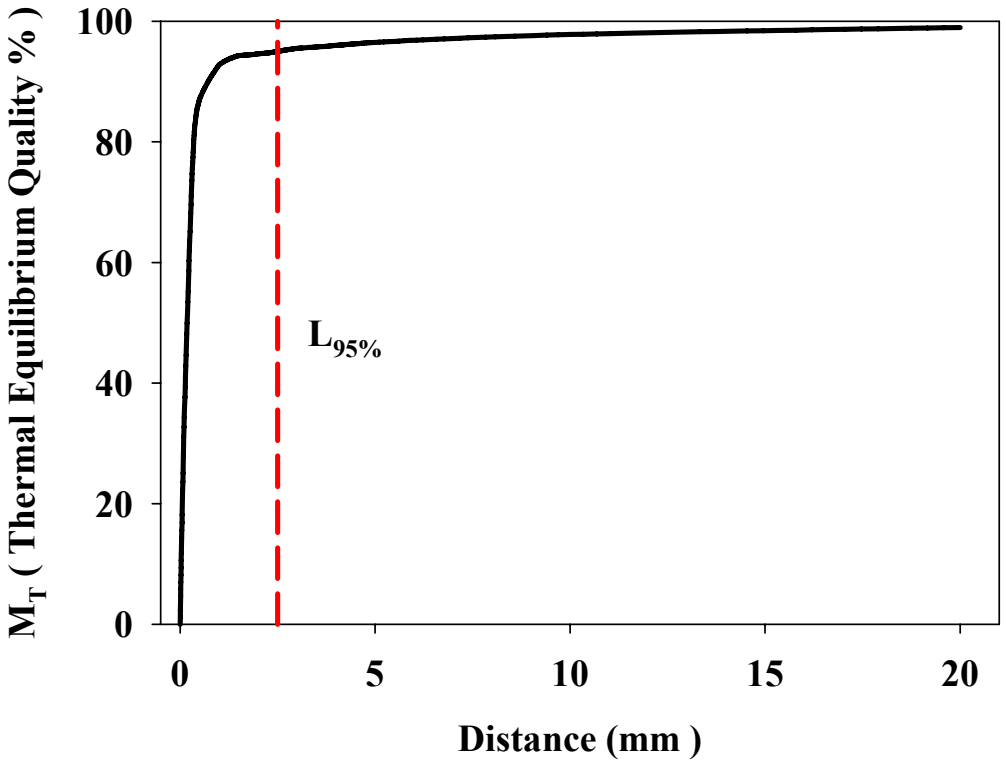

Figure C.4 Thermal equilibrium quality in the case study of the micro-mixing of two streams of hot and cold helium. The distance in direction of the flow to reach 95% of thermal equilibrium, $L_{95\%}$, is 2.5 mm which is a short distance considering the average velocity of 8.1 m/s in the reaction tube

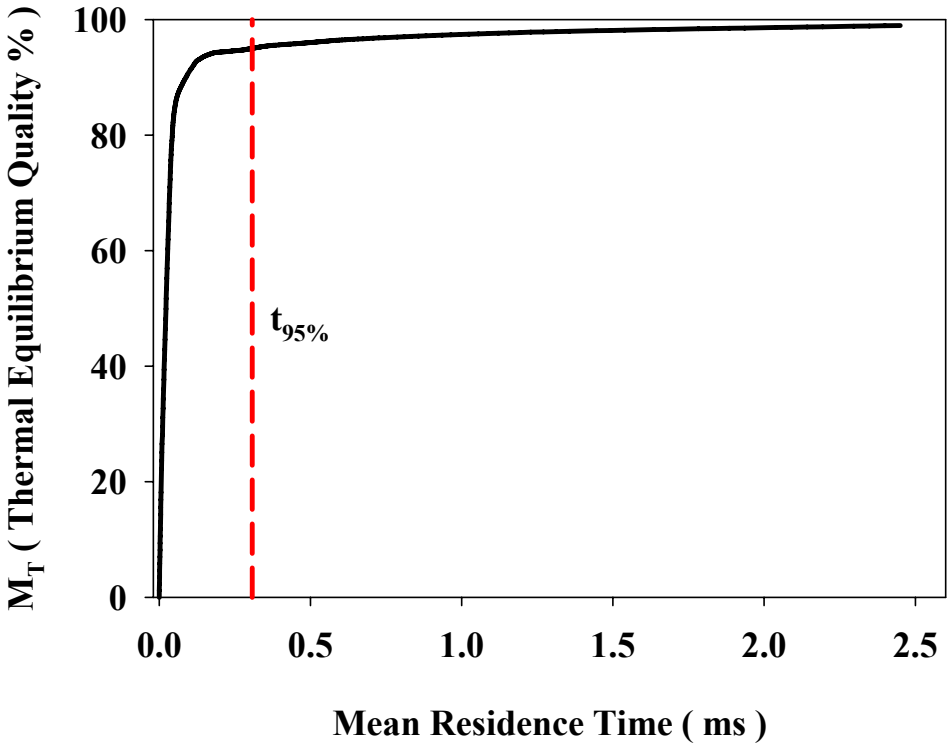

Figure C.5 The case study of the micro-mixing of two streams of hot and cold helium. The time to reach 95% of thermal equilibrium, $t_{95\%}$, is 0.3 ms

Appendix D

Heat Transfer Model for the Non-isothermal Reactor

The tubular continuous flow reactor, which used to study thermal cracking of vacuum residue (Chapter 5), was operated in a non-isothermal condition. The size of the feed particles was approximated to be less than 550 nm. Appendix B showed that such small particles would follow the direction and temperature of the streamlines of the carrier gas. Therefore, the problem of calculation of temperature and mean residence time for the reactant is reduced to calculation of the temperature and velocity distribution of the fluid in the reactor. The temperature of the fluid varies in the radial and axial direction. Different methods can be used to calculate the temperature profile. Finite element and finite volume partial differential equation solvers can be used. These programs however should be combined with the reaction model and an optimizer to calculate the kinetic parameters. The experimental data and the design of the reactor impose uncertainties which cannot be resolved by adopting a very sophisticated numerical model and tools to solve the most general equation of energy and motion for the reactor. In Chapter 6 it was shown that the calculated kinetic parameters are not sensitive to a bias in the reaction temperature, within the uncertainty of the yield data. This insensitivity allows for reasonable simplifying assumption to be made.

D.1 Assumption and sources of uncertainties

The reactor is of a tubular continuous flow type. The atomizer sprays the feed inside the reactor. At the applied operating condition, the minimized deposition of feed on the walls demonstrates the minimization of vortices around the tip of the nozzle and equalization of the velocity field of the spray with the make up gas flow. Therefore, based on the Reynolds number of the flow (Chapter 5), it is assumed an entire undisturbed laminar regime encompasses the whole reactor. It is not assumed that a fully developed velocity and temperature profile is established upon the entry of the fluid inside the reactor. This issue will be

discussed later in section D.4. However, the assumption that the spray cone does not disturb the temperature and velocity profile can supersede the uncertainties, which may arise by ignoring the undeveloped velocity or temperature profile in the absence of the streamlines of the spray. The atomizer and the spray are not considered in the modeling. Therefore, the model considers the total fluid as a laminar flow, which enters a tubular reaction tube with a measured wall temperature profile. The reactor is operated at atmospheric pressure. The reaction is assumed to be operated at constant pressure and the pressure drop along the reactor is negligible. The concentration of feed and products are low enough to neglect the reaction temperature and heat of vaporization of the feed. However, the heat capacity of the solvent is considered in the calculations (section D.6).

D.2 Governing equations for transportation of mass and energy

The reactor is operated in non-isothermal condition. Helium is applied as the carrier gas and the concentration of feed solution is low enough that the fluid can be treated as an ideal gas and a Newtonian fluid. The most general form of the equation of continuity, momentum and energy without any simplifying assumption can be written as the following [54].

The equation of continuity:

$$\frac{D\rho}{Dt} = -\rho(\nabla.\mathbf{u}) \tag{D.8}$$

The equation of motion:

$$\rho\frac{D\mathbf{U}}{Dt} = -\nabla p - [\nabla.\boldsymbol{\tau}] + \rho\mathbf{g} \tag{D.9}$$

For a Newtonian fluid τ can be substituted by its relationship with gradients of velocity and viscosity according to the Newton's law of viscosity.

The equation of energy:

$$\rho C_v \frac{DT}{Dt} = -(\nabla.\, q) - T\left(\frac{\partial p}{\partial T}\right)_\rho (\nabla.u) + \mu\Phi_v \tag{D.10}$$

In which Φ_v is viscous dissipation, which is defined with the following equation:

$$\Phi_v = 2\left[\left(\frac{\partial u_x}{\partial x}\right)^2 + \left(\frac{\partial u_y}{\partial y}\right)^2 + \left(\frac{\partial u_z}{\partial z}\right)^2\right]$$
$$+\left(\frac{\partial u_y}{\partial x} + \frac{\partial u_x}{\partial y}\right)^2 + \left(\frac{\partial u_z}{\partial y} + \frac{\partial u_y}{\partial z}\right)^2 + \left(\frac{\partial u_x}{\partial z} + \frac{\partial u_z}{\partial x}\right)^2$$
$$-\frac{2}{3}\left(\frac{\partial u_x}{\partial x_i} + \frac{\partial u_y}{\partial y} + \frac{\partial u_z}{\partial z}\right)^2$$

(D.11)

Equation (D.10) can be written in dimensionless format as the following:

$$\rho^* C_v^* \left[St\,\frac{\partial T^*}{\partial t^*} + u_i^*\,\frac{\partial T^*}{\partial x_i^*}\right] = -\frac{1}{\mathrm{Re}\,\mathrm{Pr}}(\nabla^*.\,q^*) - Ec\,T^*\left(\frac{\partial p^*}{\partial T^*}\right)_\rho (\nabla^*.u^*) + \frac{Ec}{\mathrm{Re}}\mu^*\,\Phi_v^*$$

(D.12)

The parameters are normalized as the following:

$$x_i^* = \frac{x_i}{D} \tag{D.13}$$

$$u_i^* = \frac{u_i}{u_0} \tag{D.14}$$

$$P^* = \frac{P}{\rho u_0^2} \tag{D.15}$$

$$T^* = \frac{T}{T_w - T_0} \tag{D.16}$$

$$\nabla^*.\,q^* = \frac{\partial}{\partial x_i^*}\left(-k^*\left(\frac{\partial T^*}{\partial x_i^*}\right)\right) \tag{D.17}$$

$$k^* = \frac{k}{k_0} \tag{D.18}$$

$$\rho^* = \frac{\rho}{\rho_0} \tag{D.19}$$

$$k^* = \frac{k}{k_0} \tag{D.20}$$

$$\mu^* = \frac{\mu}{\mu_0} \tag{D.21}$$

Strouhal Number

$$St = \left(\frac{f\, D}{u_0} \right) \tag{D.22}$$

f is vortex shedding frequency (s^{-1}) [81]

Reynolds number:

$$\mathrm{Re} = \left(\frac{\rho_0\ u_0\ D}{\mu_0} \right) \tag{D.23}$$

Prandtl number:

$$\mathrm{Pr} = \left(\frac{\mu_0\ C_{p0}}{k_0} \right) \tag{D.24}$$

Eckert number:

$$Ec = \left(\frac{u_0^{\ 2}}{C_{p0}\,(T_w - T_0)} \right) \tag{D.25}$$

For the operation condition in this research work, Ec number varies in the range of 10^{-7} to 10^{-6} , the order of magnitude of $\frac{Ec}{\mathrm{Re}}$ is 10^{-8} and $\frac{1}{\mathrm{Re}\,\mathrm{Pr}}$ varies in the range of 10^{-3} to 10^{-2} . In addition in equation (D.10)

$$\left(\frac{\partial p^*}{\partial T^*} \right)_{\rho} \approx 0 \tag{D.26}$$

because the change of pressure along the reactor is not significant and the reactor is assumed to be at constant pressure. Therefore, equation (D.12) can be approximated to the following equation:

$$\rho^* C_v^* \left[u_i^* \frac{\partial T^*}{\partial x_i^*} \right] = -\frac{1}{\mathrm{Re}\,\mathrm{Pr}} (\nabla^* .\ q^*) \tag{D.27}$$

D.3 Heat transfer model

The operation is steady state. The symmetry in geometry of the reactor allows the reduction of the problem to two dimensions. The equation of motion and energy cannot be further simplified and the physical properties of the fluid change along the reactor. In order to solve this problem, a partial differential equation solver should be used to solve the equation of motion and energy simultaneously. If the mean temperature of the fluid is calculated in the axial direction , the mathematics of the model can be simplified so that there will be no requirement for a partial differential equation solver.

For a tube with a constant wall temperature, the axial distribution of the mean fluid temperature can be calculated by the heat transfer model which is explained by Incropera and De Witt [55]. In order to apply this model to the case of the reactor under the study in this research with a wall temperature profile, the tube in non-isothermal operation is divided to many segments (Figure D.1). The number of the segments is selected to be large enough so that the wall temperature at each segment can be considered as a constant value. The temperature profile of the wall of the tubular reactor was measured. The wall temperature profile consists of a non-isothermal section starting from the inlet where the fluid enters the tube and then the reaches the furnace temperature at before the middle of the reactor. Therefore, the uncertainty which can be caused by segmentation of the reactor will be limited to almost half of the reactor length.

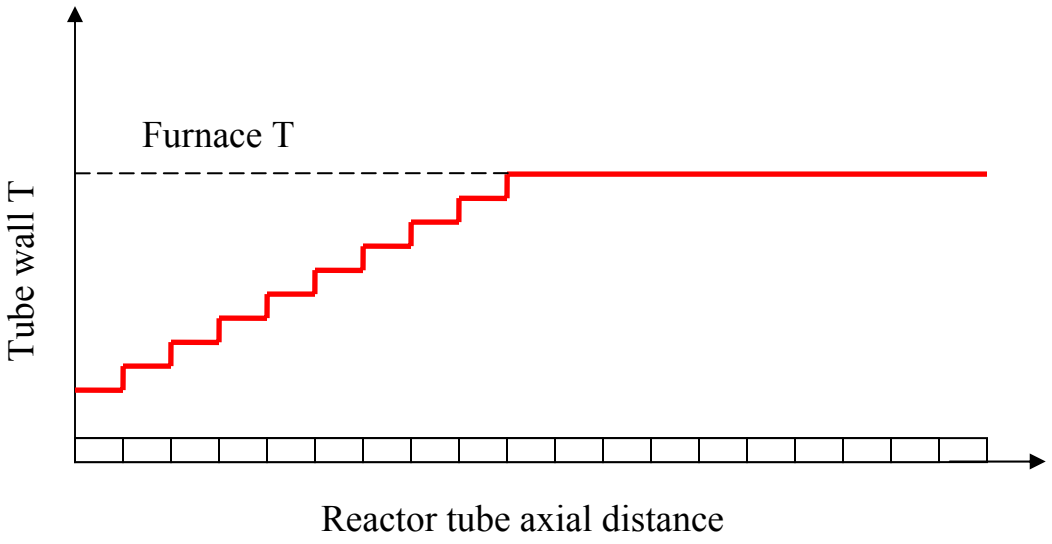

Figure D.1 Segmentation of the non-isothermal reaction tube. Each segment can be considered as a tube with constant surface temperature

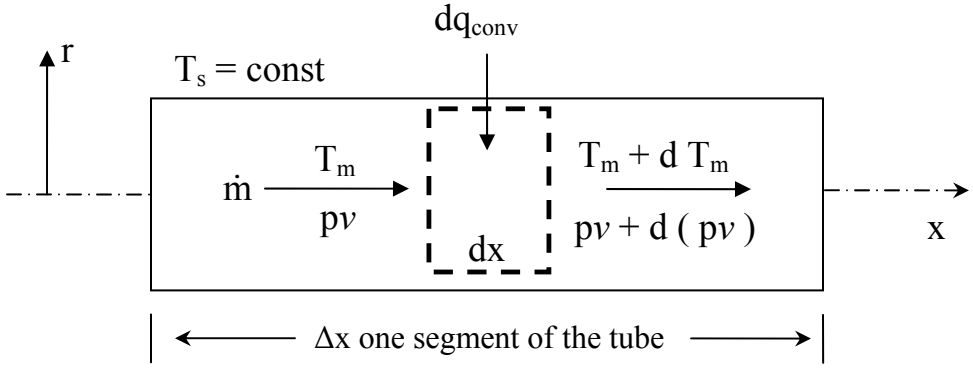

Figure D.2 Each segment of tube can be considered as a tubular flow with constant surface temperature

Figure D.2 demonstrates the energy balance over a control volume inside one of the segments. The change of fluid temperature along each segment is calculated by the following equations:

$$dq_{conv} + \dot{m}(C_v T_m + Pv) - \left[\dot{m}(C_v T_m + Pv) + \dot{m}\frac{d(C_v T_m + pv)}{dx} dx \right] = 0 \qquad (D.28)$$

or

$$dq_{conv} = \dot{m} d(C_V T_m + Pv) \tag{D.29}$$

in which , C_V and C_P are the constant volume and constant pressure heat capacity of the fluid T_m is the mean temperature of the fluid at axial position x , P is pressure of the fluid , v is the special volume of the fluid , $\dot{m}$ is a mass flow rate and q_{conv} is the heat transfer via convection**.**

Equation (D.29) describes the rate of convection of heat to the segment, which is equal to the sum of the rate at which the fluid thermal energy increases and the net rate at which work is done to move the fluid through the control volume. The carrier gas is helium at high temperature and low pressure. The concentration of feed and the products are insignificant (section D.6). The heat capacity of helium is dominant and does not change with temperature. Therefore, by applying ideal gas law:

$$Pv = \frac{R}{MW} T \tag{D.30}$$

and the relationship between the heat capacities of ideal gas at constant pressure and volume :

$$C_p = \frac{R}{MW} + C_V \tag{D.31}$$

equation (D.29) could then be written as :

$$dq_{conv} = \dot{m} C_p dT_m \tag{D.32}$$

Equation (D.32) can be integrated along the segment to give:

$$q_{conv} = \dot{m} C_p (T_{m,o} - T_{m,i}) \tag{D.33}$$

This equation is applied to the fluid flow inside the tubular reactor irrespective of the nature of the thermal condition of the wall or the flow regime. Now by substituting equation (D.34)

$$dq_{conv} = q_s'' \pi D = h\, A\, (T_s - T_m) \qquad \text{(D.34)}$$

in **(D.32)**

$$\frac{dT_m}{dx} = \frac{q_s'' \pi D}{\dot{m} C_p} h\,(T_s - T_m) \qquad \text{(D.35)}$$

equation (D.35) is obtained which describe the change of fluid temperature along the tube (each segment in this study).

When the wall temperature is constant, equation (D.35) can be written as [55]:

$$\frac{T_s - T_{m,o}}{T_s - T_{m,i}} = \exp\left(-\frac{\pi D \Delta x}{\dot{m} C_p} h_{ave}\right) \qquad T_s = \text{Constant} \qquad \text{(D.36)}$$

In equation (D.36) h_{ave} is the average convection heat transfer coefficient which is evaluated at the average temperature, T_{ave}, in each segment:

$$T_{ave} = \frac{T_{m,o} + T_{m,i}}{2} \qquad \text{(D.37)}$$

Equation (D.36) is used to calculate the mean fluid temperature along each segment and hence along the reactor.

D.4 Heat transfer coefficient and the entry region

The flow cannot be considered compressible by assuming that $\nabla.\mathbf{u}=0$, however the term containing $\nabla.\mathbf{u}$ is omitted from equation (D.12) because the gradient of pressure along the reactor is negligible. Therefore, despite the fact that the density changes along the reactor, the change of energy by expansion plays a minimum role in the equation of energy. Kays and Crawford has analytically calculated the Nusselt number for fluid flow inside a tube with constant wall temperature [82]:

$$Nu = 3.658 \qquad (D.38)$$

They assumed that a steady state operation, incompressible flow and fully developed flow regime. In addition, in order to derive equation (D.38) , they assumed that the effect of the viscous dissipation term in the partial differential equation of energy was negligible. Furthermore, they assumed that thermal conductivity of the fluid was constant. This approximation cannot cause a significant error when the reactor is divided to many segments in which the change of temperature is small so that the change in the thermal conductivity is insignificant. The thermal conductivity of helium changes from 0.304 to 0.354 ($W.m^{-1}.K^{-1}$) when temperature ranges from 527 to 727°C. However to assume a velocity profile they considered the fully developed flow regime and incompressibility of the flow. The assumption of incompressibility can be a source of uncertainty as the model was intended to be used for the case of non-isothermal reactor. For the case of this study, the reactor is divided to many segments at which the wall temperature is constant and the rise of the fluid temperature in each segment is not dramatic due to the large number of segments. Therefore, the assumption of incompressibility of flow which was made to derive the value for the Nusselt number can be alleviated.

The equation of Sieder and Tate is proposed to calculate the Nusselt number by considering both the thermal and velocity entry length in the tube [55]:

$$Nu = 1.86\left(\frac{\mathrm{Re}\,\mathrm{Pr}}{L/D}\right)^{1/3}\left(\frac{\mu}{\mu_S}\right)^{0.14} \qquad \text{(D.39)}$$

Equation (D.39) is recommended when

$$\left(\frac{\mathrm{Re}\,\mathrm{Pr}}{L/D}\right)^{1/3}\left(\frac{\mu}{\mu_S}\right)^{0.14} \geq 2 \qquad \text{(D.40)}$$

Below this limit fully developed conditions encompass much of the tube and equation (D.38) can be used. If this model is used , the value of this term ranges between 0.99 to 1.3 which is below 2 so equation (D.38) is considered to be used to calculated the Nusselt number and hence the heat transfer coefficient.

D.5 The heat effect of the reactant and solvent

Heat of reaction, vaporization and heat capacity of the feed and products can be neglected because their concentration in the carrier gas is so low (Table 5.4 and Table D.1). Therefore, only heat capacity of the helium and the solvent were considered in calculation. The heat capacity of toluene at elevated temperature was taken from NIST chemistry web book [56].

Table D.1 Concentration of the gas products at the end of the reaction tube

Experiment	Gas products (mol%)
700-1	5.97E-03
700-2	4.30E-03
750-1	9.91E-03
750-2	1.05E-02
800-1	1.41E-02
800-2	1.24E-02

D.6 Discussion on the sensitivity of the kinematic parameters assumptions

In Chapter 6, it was shown that a 10% bias in measurement of temperature does not change the activation energy and the pre-exponential factor to values which lay outside the range that uncertainty of the yield data. The result of this test is also valid if the bias is assumed to be caused by the adopted mathematical model and through the calculation method. It was also shown for the specific case of thermal cracking of vacuum residue that assumption that the reactor was isothermal gave the kinetic parameters which were in range with the results of non-isothermal model considering the uncertainty of the experimental data. In Chapter 6 the insensitivity of the kinetic parameters to bias in pressure of the reactor was demonstrated. These insensitivities can justify neglecting the radial temperature distribution in favor of reduction of the problem to one dimension. The thermal cracking reaction is considered to be of first order, which means that the rate constant of the reaction does not depend on the conversion, thence it is expected that the impact of neglecting the radial temperature distribution can be compensated by use of a mean axial temperature profile and a mean residence time.

For the energy balance, the assumption of incompressibility of flow does not play a role, but in order to calculate a value for the Nusselt number, both a compressible flow and a fully developed flow regime were assumed. The

uncertainty of the assumption that the spray does not disturb the temperature and velocity profile supersedes any uncertainty due to the impact of the entry region on the fluid. However, the fact that the high tendency of coalescence and deposition of feed on the wall of the reactor and around the tip of the atomization nozzle was significantly reduced at the applied operating condition indicates that this is a reasonable assumption. In addition, it was shown that the operating condition and the physical properties of the fluid are in a range that does not make the equation of Sieder and Tate to be preferred rather than equation (D.38). This means that the effect of thermal and velocity entry lengths is not significant in calculation of the temperature profile along the reactor.

If this model is used; the ratio of the difference of the density along each segment divided by the density at the outlet of that segment varies from 10^{-5} to 10^{-2}. Calculation of Mach number can help to evaluate the assumption of the incompressibility of flow. It is known that if $Ma < 0.3$, the flow can be considered as incompressible [83] . By using this heat transfer model the order of magnitude of Mach number along the entire reactor was calculated to be 10^{-3}. Therefore, the assumption of incompressibility of flow and thence the value of the Nusselt number are reasonable.

Appendix E

Derivation of a Simple Kinetic Model for Toluene Interactions with Vacuum Residue

In Chapter 6 it was shown that the activation energy which was calculated for thermal cracking of vacuum residue gave values which were significantly lower than the activation energy of the *n*-alkanes and extrapolation from the work of previous researchers. It was also shown that the calculated activation energy increased when higher order of reaction was considered, but this change reduced the fitness of the model to the data, indicating that the lumped kinetic model with higher reaction order is not a useful representation. In the following appendix, I show that a simple mechanism for interaction of the solvent with vacuum residue can explain both change of the overall reaction order and the activation energy[§].

Simplified free radical mechanism in absence of the solvent (toluene) can be written as the follows:

Initiation: $$P \xrightarrow{k_1} 2\,R^{\cdot} \qquad \text{(E.1)}$$

Propagation:

Hydrogen abstraction $$R^{\cdot} + P \xrightarrow{k_2} RH + P^{\cdot} \qquad \text{(E.2)}$$

β-Scission $$P^{\cdot} \xrightarrow{k_3} R^{\cdot} + O \qquad \text{(E.3)}$$

Termination: $$R^{\cdot} + P^{\cdot} \xrightarrow{k_4} Products \qquad \text{(E.4)}$$

[§] This model is derived by Professor M.R. Gray

where P and $P^{\cdot}$ are the parent vacuum residue and parent radicals, respectively, $R^{\cdot}$ and RH are smaller radicals and the corresponding cracked products, respectively, and O represents olefins. If cracking takes place in a tubular reactor, then the rate of change of the radicals with mean residence time can be written:

$$\frac{d[R^{\cdot}]}{d\tau} = 2k_1[P] - k_2[R^{\cdot}][P] + k_3[P^{\cdot}] - k_4[R^{\cdot}][P^{\cdot}] \tag{E.5}$$

$$\frac{d[P\cdot]}{d\tau} = k_2[R\cdot][P] - k_3[P\cdot] - k_4[R\cdot][P\cdot] \tag{E.6}$$

The concentration of radicals is small, and will change very little through the course of the reaction. These intermediates will be in a pseudo-steady state, where the concentration of radicals changes more slowly than the reactants, and the rate of change in the concentration of radical species is negligible:

$$\frac{d[P\cdot]}{d\tau} = \frac{d[R\cdot]}{d\tau} \cong 0 \tag{E.7}$$

Solving for the concentration of radicals gives:

$$[R\cdot] = \left[\frac{2k_1k_3}{k_2k_4}\right]^{1/2} \tag{E.8}$$

$$[\mathrm{P}\cdot] = \frac{\mathrm{k}_2[\mathrm{R}\cdot][\mathrm{P}]}{\mathrm{k}_3 + \mathrm{k}_4[\mathrm{R}\cdot]} \cong \frac{\mathrm{k}_2[\mathrm{R}\cdot][\mathrm{P}]}{\mathrm{k}_3} = \left[\frac{2\mathrm{k}_1\mathrm{k}_2}{\mathrm{k}_3\mathrm{k}_4}\right]^{1/2}[\mathrm{P}] \tag{E.9}$$

The disappearance of the parent compound is:

$$-\frac{d[P]}{d\tau} = k_1[P] + k_2[R\cdot][P] \qquad \text{(E.10)}$$

The free radical reaction is a chain reaction, and once the radicals form they go through many cycles of the propagation steps. If the long-chain approximation is applied, then the rate of propagation will be much greater then the rate of initiation, so that $k_2[R\cdot][P] >> k_1[P]$ in Equation (E.10), giving:

$$-\frac{d[P]}{d\tau} = \frac{\mathrm{d[RH]}}{\mathrm{dt}}\tau = \frac{\mathrm{d[O]}}{\mathrm{d}\tau} = \left(2k_1 k_2 k_3 / k_4\right)^{1/2}[P] \qquad \text{(E.11)}$$

In the presence of the toluene as solvent, the molar concentration of toluene is very high and I add the following reactions, where T is toluene:

Hydrogen abstraction :

$$R\cdot + T \xrightarrow{k_2'} RH + T\cdot \qquad \text{(E.12)}$$

$$T\cdot + P \xrightarrow{k_2''} T + P\cdot \qquad \text{(E.13)}$$

Termination:

$$T^{\cdot} + T^{\cdot} \xrightarrow{k_4'} \textit{Products} \tag{E.14}$$

In this case, the termination is assumed to be dominated by the benzyl radicals *[T•]* from the toluene. The equations then become:

$$\frac{d[R\cdot]}{d\tau} = 2k_1[P] - k_2'[R\cdot][T] - k_4[R\cdot][P\cdot] \tag{E.15}$$

$$\frac{d[P\cdot]}{d\tau} = k_2[R\cdot][P] - k_3[P\cdot] + k_2''[P][T\cdot] - k_4[R\cdot][P\cdot] \tag{E.16}$$

$$\frac{d[T\cdot]}{d\tau} = k_2'[R\cdot][T] - k_2''[P][T\cdot] - k_4'[T\cdot]^2 \tag{E.17}$$

Assuming pseudo-steady state of radical concentrations, and that the main termination reaction is(E.14), I obtain:

$$[P\cdot] = \frac{k_2''[P][T\cdot]}{k_3} \tag{E.18}$$

$$[R\cdot] = \frac{2k_1[P] + k_2''[P][T\cdot]}{k_2'[T] + \frac{k_4 k_2''}{k_3}[P][T\cdot]} \cong \frac{2k_1[P] + k_2''[P][T\cdot]}{k_2'[T]} \tag{E.19}$$

$$[T\cdot] = \sqrt{\frac{2k_1[P]}{k_4'}} \tag{E.20}$$

Applying the long-chain approximation, the disappearance of the VR is:

$$-\frac{d[P]}{d\tau} = k_2[R\cdot][P] + k_2''[T\cdot][P] \tag{E.21}$$

Substituting the results from equations (E.19) through (E.20) gives:

$$-\frac{d[P]}{d\tau} = \frac{2k_1k_2}{k_2'[T]^2}[P]^2 + \frac{k_2k_2''}{k_2'[T]}\sqrt{\frac{2k_1}{k_4'}}[P]^{5/2} + k_2''\sqrt{\frac{2k_1}{k_4'}}[P]^{3/2} \tag{E.22}$$

This result arises from a highly simplified model, which gives an indication of trends but which should not be over-interpreted. A comparison of equation (E.22) with equation (E.11) suggests that diluting the vacuum residue with large amounts of toluene will reduce the rate of reaction, increase the apparent order of the reaction, and change the apparent activation energy. As *[T]* becomes large, then equation (E.22) gives:

$$-\frac{d[P]}{d\tau} \approx k_2''\sqrt{\frac{2k_1}{k_4'}}[P]^{3/2} \tag{E.23}$$

The order in this case rises to 3/2 and the activation energy is dominated by the activation energy for reaction (E.13), along with termination reaction of the benzyl radicals (E.14) and the initiation reaction of dissociation of the parent molecule (E.1). All of these changes arise from the addition of new reactions of toluene and the resulting benzyl radicals, with benzyl becoming the dominant radical carrier in the chain reaction.

Appendix F

Statistical Analysis of the Results of Thermal Cracking of Pure n-Hexadecane and its Mixture with Toluene

In Chapter 5, in order to investigate the effect of toluene on suppression of the rate of thermal cracking of n-hexadecane, two sets of experiments were carried out. In set 1 a mixture of pure n-hexadecane was used (molar ratio of toluene/nC_{16} = 115) and in set 2 only pure n-hexadecane was used as the feed. The yield of total gas and yield of the major components were measured. Each experiment in each set was repeated 3 times. In order to conclude that results of these two set of experiments are significantly different a t-test was carried out [73]. The difference could be because of a mechanism like interaction of toluene with the free radical chain of reactions or because of only a random scatter in the data. The purpose of this test is to eliminate the probability that the difference between the mean yield values were due to the uncertainty of the experimental data. The results of this test for confidence limit of 95% are given in Table F.1 to Table F. 7. Y refers to the yield value, S_d is the standard deviation of the set and μ is mean value of the universe for each set. μ is the mean value which could be calculated for the yield if the experiment in each set was carried out in infinite numbers. In this test, the confidence limits for ΔY_{mean} compared with the value of ΔY_{mean}. If the confidence level is larger, then there is a good chance that ΔY_{mean} is zero and thence Δμ is zero. This concept can be clearly demonstrated by equation (F.1).

$$\Delta Y_{mean} - \text{confidence limit} \leq \Delta\mu \leq \Delta Y_{mean} + \text{confidence limit} \qquad \text{(F.1)}$$

If the confidence limit is smaller than ΔY_{mean} then the difference between the mean value of the yields between the two sets are significant.

Table F.1 The result of t-test for yield of methane in thermal cracking of pure n-hexadecane and the mixture of n-hexadecane with toluene (molar ratio of toluene to nC_{16} = 115)

	$Y_{methane}$ (wt%)
nC_{16} + toluene No.1	0.87
nC_{16} + toluene No.2	1.05
nC_{16} + toluene No.3	1.79
Pure nC_{16} No.1	1.48
Pure nC_{16} No.2	1.56
Pure nC_{16} No.3	1.71
nC_{16} + toluene Y_{Mean}	1.24
nC_{16} + toluene S_d	0.49
Pure nC_{16} Y_{Mean}	1.58
Pure nC_{16} S_d	0.12

t-test:	$\Delta\mu = 0$?
Level of Confidence	95%
S_{YMean}	0.29
ΔY_{Mean}	0.34
Confidence Limit	± 0.80
$\Delta\mu$ is insignificant	

Table F. 2 The result of t-test for yield of ethane in thermal cracking of pure n-hexadecane and the mixture of n-hexadecane with toluene (molar ratio of toluene to nC_{16} = 115)

	Y_{ethane} (wt%)
nC_{16} + toluene No.1	0.026
nC_{16} + toluene No.2	0.035
nC_{16} + toluene No.3	0.10
Pure nC_{16} No.1	0.58
Pure nC_{16} No.2	0.61
Pure nC_{16} No.3	0.60
nC_{16} + toluene Y_{Mean}	0.055
nC_{16} + toluene S_d	0.042
Pure nC_{16} Y_{Mean}	0.60
Pure nC_{16} S_d	0.012

t-test:	$\Delta\mu = 0$?
Level of Confidence	95%
S_{YMean}	0.025
ΔY_{Mean}	0.54
Confidence Limit	± 0.071
$\Delta\mu$ is significant	

Table F. 3 The result of t-test for yield of propane in thermal cracking of pure n-hexadecane and the mixture of n-hexadecane with toluene (molar ratio of toluene to nC_{16} = 115)

	$Y_{propane}$(wt%)
nC_{16} + toluene No.1	0.0017
nC_{16} + toluene No.2	0.0093
nC_{16} + toluene No.3	0.093
Pure nC_{16} No.1	0.19
Pure nC_{16} No.2	0.20
Pure nC_{16} No.3	0.20
nC_{16} + toluene Y_{Mean}	0.035
nC_{16} + toluene S_d	0.050
Pure nC_{16} Y_{Mean}	0.20
Pure nC_{16} S_d	0.010

t-test:	$\Delta\mu = 0$?
Level of Confidence	95%
S_{YMean}	0.03
ΔY_{Mean}	0.16
Confidence Limit	± 0.082
$\Delta\mu$ is significant	

Table F.4 The result of t-test for yield of ethene in thermal cracking of pure n-hexadecane and the mixture of n-hexadecane with toluene (molar ratio of toluene to nC_{16} = 115)

	Y_{ethene} (wt%)
nC_{16} + toluene No.1	3.61
nC_{16} + toluene No.2	4.61
nC_{16} + toluene No.3	7.43
Pure nC_{16} No.1	14.86
Pure nC_{16} No.2	15.63
Pure nC_{16} No.3	15.74
nC_{16} + toluene Y_{Mean}	5.22
nC_{16} + toluene S_d	1.98
Pure nC_{16} Y_{Mean}	15.41
Pure nC_{16} S_d	0.48

t-test:	$\Delta\mu = 0$?
Level of Confidence	95%
S_{YMean}	1.18
ΔY_{Mean}	10.19
Confidence Limit	± 3.26
$\Delta\mu$ is significant	

Table F. 5 The result of t-test for yield of propene in thermal cracking of pure n-hexadecane and the mixture of n-hexadecane with toluene (molar ratio of toluene to nC_{16} = 115)

	$Y_{propene}$ (wt%)
nC_{16} + toluene No.1	0.91
nC_{16} + toluene No.2	1.23
nC_{16} + toluene No.3	1.77
Pure nC_{16} No.1	6.36
Pure nC_{16} No.2	6.64
Pure nC_{16} No.3	6.77
nC_{16} + toluene Y_{Mean}	1.30
nC_{16} + toluene S_d	0.44
Pure nC_{16} Y_{Mean}	6.59
Pure nC_{16} S_d	0.21

t-test:	$\Delta\mu = 0$?
Level of Confidence	95%
S_{YMean}	0.28
ΔY_{Mean}	5.28
Confidence Limit	± 0.78
$\Delta\mu$ is significant	

Table F.6 The result of t-test for yield of C_1 to C_3 gases in thermal cracking of pure n-hexadecane and the mixture of n-hexadecane with toluene (molar ratio of toluene to nC_{16} = 115)

	Y_{C1-C3} (wt%)
nC_{16} + toluene No.1	5.43
nC_{16} + toluene No.2	6.94
nC_{16} + toluene No.3	11.19
Pure nC_{16} No.1	23.48
Pure nC_{16} No.2	24.67
Pure nC_{16} No.3	25.03
nC_{16} + toluene Y_{Mean}	7.85
nC_{16} + toluene S_d	2.99
Pure nC_{16} Y_{Mean}	24.40
Pure nC_{16} S_d	0.81

t-test:	$\Delta\mu = 0$?
Level of Confidence	95%
S_{YMean}	1.79
ΔY_{Mean}	16.54
Confidence Limit	± 4.96
$\Delta\mu$ is significant	

Table F. 7 The result of t-test for yield of total gas products in thermal cracking of pure n-hexadecane and the mixture of n-hexadecane with toluene (molar ratio of toluene to nC_{16} = 115)

	$Y_{total\ gas}$ (wt%)
nC_{16} + toluene No.1	6.26
nC_{16} + toluene No.2	8.08
nC_{16} + toluene No.3	13.50
Pure nC_{16} No.1	33.33
Pure nC_{16} No.2	36.73
Pure nC_{16} No.3	41.69
nC_{16} + toluene Y_{Mean}	9.28
nC_{16} + toluene S_d	3.77
Pure nC_{16} Y_{Mean}	37.25
Pure nC_{16} S_d	4.20

t-test:	$\Delta\mu = 0$?
Level of Confidence	95%
S_{YMean}	3.26
ΔY_{Mean}	27.97
Confidence Limit	± 9.04
$\Delta\mu$ is significant	